



Chair of Polymer Processing

Doctoral Thesis



Development of Ceramic Feedstocks for Fused  
Filament Fabrication

Santiago Cano Cano

July 2020

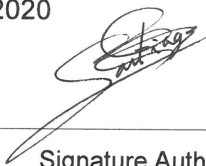
**AFFIDAVIT**

I declare on oath that I wrote this thesis independently, did not use other than the specified sources and aids, and did not otherwise use any unauthorized aids.

I declare that I have read, understood, and complied with the guidelines of the senate of the Montanuniversität Leoben for "Good Scientific Practice".

Furthermore, I declare that the electronic and printed version of the submitted thesis are identical, both, formally and with regard to content.

Date 22.07.2020



---

Signature Author  
Santiago, Cano Cano

## Acknowledgements

I would like to express my deepest gratitude to my supervisor Clemens Holzer for accepting me as his student, for his profound belief in my work, and for his help and guidance through these years. Special thanks to my menthor Gemma Herranz for her continuous support and for encouraging me to look for new challenges.

I cannot begin to express my thanks to Christian Kukla for helping me to see things on a different perspective, for his guidance, for his constructive suggestions and for his invaluable experience. The completion and success of this thesis would not have been possible without the relentless support and insightful advice of Joamin Gonzalez-Gutierrez, who has been always there to patiently listen and help me.

I would like to extend my deepest gratitude to Stephan Schuschnigg for his relentless and unconditional support, and for always finding time to listen and help me. I am deeply indebted to Martin Spoerk and to Janak Sapkota. Thanks to their constructive advice, their support and encouragement I could overtake the big initial challenges of this thesis. I very much appreciate the help of Ivica Duretek in the measurement and analysis of the rheological properties of binders and feedstocks and his continuous guidance in the experimental work through these years.

Many thanks go to the students that helped me to conduct the experimental work throughout all the thesis: Maria Gferrer, Fabian Schuschter, Celina Harecker, Ivan Raguz, Ivan Meyer, Thomas Steinert, Tabea Zirinig and Nikolaus Heindl. I am extremely grateful for the motivation and relentless dedication of Dario Kaylani and Philipp Huber to their Bachelor theses, which were of critical importance to this work.

Through these years I also had great pleasure of working with experts in the different areas related to this thesis. Many thanks to Florian Arbeiter for the help in the analysis of the mechanical properties of feedstocks and binders. The insightful suggestions and assistance of Baris Kaynak and Ali Gooneie in the analysis of the interfacial interactions between powder and binder are greatly appreciated. I very much appreciate the invaluable experience and the unwavering support of Tanja Lube in the measurement and analysis of the defects and mechanical properties of the sintered ceramic parts.

I would also like to acknowledge the assistance of all the colleagues of the Institute of Polymer Processing for all the help through these years and the nice working environment.

Gracias a mis padres Dolores y Santiago y a mi hermano Eugenio por todo el amor, cariño y apoyo incondicional que me habéis dado durante toda mi vida. Aunque hayamos estado separados se que habéis compartido todas mis alegrías y penas durante estos años.

Para ti que aceptaste vivir esta aventura conmigo, que has celebrado como tuyos propios todos mis logros y que me has sostenido, aguantado y escuchado en los malos momentos, no puedo expresar lo suficiente todo mi agradecimiento. Nada de esto habría sido posible sin ti a mi lado, Desirée.

## Abstract

The Fused Filament Fabrication (FFF) of ceramics is a promising technique for the low-cost production of components with complex geometry. The process relies on a thermoplastic binder highly filled with ceramic powder to produce feedstock filaments. Filaments are used to shape parts in the same machines as for FFF of plastics. The binders are removed in the debinding step, and the final parts are obtained after sintering. The use of filaments requires strong, flexible, and low viscous feedstocks, which is a challenge due to the high content of ceramic powder ( $\geq 45$  vol.%). Different FFF feedstocks have been reported in the literature. However, these formulations use a single step of thermal debinding, which requires long thermal cycles to avoid defects. On the contrary, most of the commercially available FFF feedstocks are debound in two steps. A major fraction of the binder is dissolved, creating an open-pore structure to remove the remaining polymers. Currently little information about the binders required for the two-step debinding is publicly available, which hinders the development of new formulations.

The purpose of this thesis was to develop a better understanding of the binders required for the FFF and solvent debinding of ceramics. The properties required for FFF of ceramics and metals were compiled and combined with the requirements for solvent debinding known from the powder injection moulding process. A novel zirconia feedstock was developed using as criteria the morphology, rheological and mechanical properties, and the solvent debinding performance. Two soluble components were necessary for the production of flexible and low viscous feedstocks with no debinding defects. The feedstock morphology had a strong influence on the debinding behaviour since the inhomogeneity leads to defects. Based on these results, a formulation composed of high density polyethylene grafted with acrylic acid, stearic acid, paraffin wax and styrene-ethylene/butylene-styrene copolymer was developed. Incorporating stearic acid reduced the viscosity and facilitated the FFF shaping, but it reduced the strength and flexibility of the filaments. The powder-binder interfacial interactions and adhesion when the binder was grafted with polar groups were also investigated. The improved adhesion for the grafted binder resulted in better powder dispersion and high mechanical properties.

The effect of the processing parameters on the solvent debinding performance was determined for a zirconia feedstock with a binder composed of a grafted polyolefin as backbone and thermoplastic elastomer as soluble binder. Increasing the temperature of the solvent increased the debinding rate but also the defects; incorporating stearic acid in the feedstock reduced the debinding defects; on the contrary, using a swelling inhibitor had little effect.

Finally, the effect of the FFF parameters on the defects and the mechanical properties of the final parts was determined. The changes in the feedstock during shaping, the variability on the filament diameter and the orientation of the extruded roads affected the size and orientation of defects. The FFF defects determined the bending properties

of the sintered parts. Therefore, the loads applied to the ceramic parts during their service have to be considered during the FFF.

The results of this PhD thesis provide a first insight into the binders required for the combination of FFF and solvent debinding. Moreover, the influence of the processing parameters on the processability and final properties were determined. These results can facilitate the development of new binder formulations, improve the understanding of the phenomena occurring during processing ceramics by FFF, and provide new perspectives in the processing of ceramics by other conventional and additive manufacturing technologies based on similar materials.

*Keywords:* Fused filament fabrication; feedstock; highly-filled polymers; solvent debinding, ceramics, zirconia; grafted polymers; infill orientation.

## Kurzfassung

Die extrusionsbasierte additive Fertigung (Fused Filament Fabrication FFF), ist eine vielversprechende Technik zur kostengünstigen Produktion von Komponenten hoher geometrischer Komplexität. Der Prozess basiert auf einem mit keramischen Pulver hochgefüllten, thermoplastischen Binder zur Produktion von Feedstock-Filamenten, die auf denselben Maschinen verwendet wie bei der FFF von Kunststoffen. Die Binder werden in einem Entbinderungsschritt entfernt, und die finalen Bauteile erhält man nach dem Sinterschritt. Für die Filamenten braucht man feste, flexible und niedrig-viskose Feedstocks, was aufgrund des hohen Anteils an keramischem Pulver ( $\geq 45$  vol.%) eine Herausforderung darstellt. Unterschiedliche FFF-Feedstocks wurden bisher in der Literatur behandelt, die jedoch auf einem einzelnen Schritt des thermischen Entbinderns basieren, was zu langen thermische Zyklen zur Vermeidung von Defekten führt. Die meisten kommerziell erhältlichen FFF-Feedstocks werden in zwei Schritten entbindert. Zur Zeit ist wenig Information über die für das zweistufige Entbindern notwendigen Binder vorhanden, damit wird die Entwicklung neuer Formulierungen erschwert.

Das Ziel dieser Dissertation war die Entwicklung eines besseren Verständnisses für die Binder. Die gewünschten Eigenschaften für die FFF von Keramiken und Metallen wurden zusammengefasst und mit den Voraussetzungen für das lösungsmittelbasierte Entbindern, die vom Pulverspritzguss-Prozess bekannt sind, kombiniert. Ein Zirkoniumdioxid-Feedstock wurde nach den Kriterien der Morphologie, rheologischer und mechanischer Eigenschaften und des Verhaltens beim lösungsmittelbasierten Entbindern entwickelt. Zwei lösliche Komponenten waren für die Herstellung flexibler und niedrig-viskoser Feedstocks notwendig. Darauf basierend wurde eine Formulierung aus einem Polyethylen hoher Dichte gepropft mit Acrylsäure, Stearinsäure, Paraffinwachs und Styrol-Ethylen/Butylen-Styrol Copolymer entwickelt. Die Stearinsäure reduzierte die Viskosität und erleichterte die Formgebung durch FFF, erniedrigte aber auch die Festigkeit und Flexibilität der Filamente. Die Wechselwirkungen und Adhäsion an den Grenzflächen zwischen Pulver und mit polaren Gruppen gepropften Binder wurde ebenfalls untersucht. Die verbesserte Adhäsion des gepropften Binders ergab eine bessere Dispersion des Pulvers und hohe mechanische Eigenschaften.

Der Einfluss der Prozessparameter auf das lösungsmittelbasierte Entbindern wurde für einen  $ZrO_2$ -Feedstock mit einem Binder aus gepropften Polyolefin als Backbone und einem thermoplastischen Elastomer als löslichen Binder bestimmt. Die Erhöhung der Temperatur des Lösungsmittels erhöhte die Rate des Entbinderns, aber ebenfalls die Defekte; die Hinzugabe von Stearinsäure zum Feedstock verminderte die Defekte. Die Verwendung eines Quell-Hemmstoffs hatte nur einen geringen Einfluss.

Schließlich wurde der Effekt der FFF-Parameter auf die Eigenschaften der Endprodukte bestimmt. Die Veränderungen im Feedstock während der Formgebung, die Schwankungen des Filamentdurchmessers und die Ausrichtung der extrudierten Stränge beeinflussten die Größe und Orientierung der Defekte. Die FFF-Defekte

bestimmten wiederum die Biegeeigenschaften der gesinterten Teile. Daher müssen die Lasten, die auf die keramischen Teile wirken, bereits während des FFF-Prozesses berücksichtigt werden.

Die Ergebnisse dieser Dissertation bieten einen fundierten Einblick in die Binder, die für die Kombination FFF / lösungsmittelbasiertes Entbindern benötigt werden. Desweiteren wurde der Einfluss der Prozessparameter auf die Verarbeitbarkeit und Eigenschaften der Endprodukte bestimmt. Diese Ergebnisse erleichtern die Entwicklung neuer Binderformulierungen, das Verständnis der Phänomene während der Herstellung von Keramiken mit FFF und eröffnen neue Blickwinkel auf die Herstellung von Keramiken ähnlicher Formulierungen mittels anderer konventioneller und additiver Herstelltechnologien.

*Schlüsselwörter:* Fused filament fabrication; feedstock; hochgefüllte Polymere; lösungsmittelbasierte Entbindern; Keramik; Zirkoniumdioxid; gefropfte Polymere; Infill Orientierung.

# Table of Contents

<b>1</b>	<b>FUNDAMENTALS .....</b>	<b>1</b>
1.1	ADDITIVE MANUFACTURING.....	1
1.1.1	Steps in the AM process .....	2
1.1.2	Classification of AM technologies.....	3
1.2	ADDITIVE MANUFACTURING OF CERAMICS .....	10
1.3	FFF OF CERAMICS AND METALS .....	15
1.3.1	Thermoplastic based manufacturing .....	15
1.3.2	Comparison to other processes .....	18
1.3.3	Materials processed by FFF .....	19
1.4	ZIRCONIA.....	21
<b>2</b>	<b>INTRODUCTION AND OBJECTIVES.....</b>	<b>23</b>
2.1	MOTIVATION AND BACKGROUND.....	23
2.2	HYPOTHESES AND APPROACH .....	24
2.3	OUTLINE OF THE THESIS .....	26
<b>3</b>	<b>DEVELOPMENT OF BINDER FORMULATION .....</b>	<b>28</b>
3.1	STATE OF THE ART.....	28
3.1.1	Binders for FFF .....	28
3.1.2	Binders for solvent debinding.....	32
3.2	INTRODUCTION TO PUBLICATIONS A, B, C AND D.....	35
3.3	PUBLICATION A .....	37
3.4	PUBLICATION B .....	67
3.5	PUBLICATION C .....	75
3.6	PUBLICATION D .....	84
3.7	SUMMARY OF THE BINDER DEVELOPMENT PROCESS .....	108
<b>4</b>	<b>INFLUENCE OF THE SOLVENT DEBINDING PARAMETERS.....</b>	<b>111</b>
4.1	STATE OF THE ART.....	111
4.1.1	Stages and mechanisms of solvent debinding .....	111
4.1.2	Effect of the debinding parameters .....	112
4.1.3	Effect of the powder characteristics.....	114
4.2	INTRODUCTION TO PUBLICATION E .....	116
4.3	PUBLICATION E .....	117
<b>5</b>	<b>DEVELOPMENT AND STUDY OF THE FFF PROCESS.....</b>	<b>131</b>
5.1	STATE OF THE ART.....	131
5.2	INTRODUCTION TO PUBLICATION F .....	134
5.3	PUBLICATION F.....	135
<b>6</b>	<b>CONCLUSIONS AND RESEARCH OUTLOOK.....</b>	<b>163</b>
6.1	CONCLUSIONS .....	163
6.2	RESEARCH OUTLOOK .....	166
<b>7</b>	<b>ACRONYMS .....</b>	<b>168</b>
<b>8</b>	<b>LITERATURE.....</b>	<b>171</b>



# 1 Fundamentals

## 1.1 Additive manufacturing

According to the International Standard ISO/ASTM 52900:2015, "Additive manufacturing is the process of joining materials to make parts from 3D model data, usually layer upon layer, as opposed to subtractive manufacturing and formative manufacturing methodologies" [110]. In general, the initial geometrical representation is a software model, and the parts are created layer by layer, being each one of these layers a thin cross-section of the model.

The first commercial system based on this philosophy dates back to 1987 when the SLA-1 machine from 3D systems was released. Solid objects could be created by the exposure to an ultraviolet laser of a liquid light-sensitive polymer, a technique known as stereolithography [222]. During the first years of development, the main application of AM was the production of prototypes. Since a machine and a CAD model were the only elements required for the production of these prototypes, the cost and time could be considerably reduced by substituting the traditional prototyping techniques [238].

From then on, further research and development in the computer systems, machinery and processes have promoted the expansion of the technology in other areas like the fabrication of tools, dies and moulds. Nevertheless, the main focus of the research and industrial AM communities is the direct fabrication of end-use products [90]. In areas such as the aerospace [139], the automotive [105] and the medical industries [146, 228] the AM processes have a high potential. Other industries such as the textiles, jewellery or furniture could benefit as well from these new technologies [74, 115].

The advantages of using additive manufacturing instead of other production technologies are the following [21, 26, 62, 72, 104, 168, 217]:

- Substantial reduction in the consumption of raw material compared with subtractive manufacturing methods.
- Lower production costs for small batches.
- Recyclability of the waste material, such as powders or resins.
- Processing equipment such as tools, moulds or punches is not needed, which increases the flexibility and reduces the cost.
- The porosity of the final parts can be controlled with the processing conditions.
- New geometrical features are possible, such as internal channels or lattices.
- Assembly operations can be reduced or eliminated by the direct production of assembled systems.
- The production costs are not affected by the complexity of the parts.
- Automated manufacturing.

- Reduction or disappearance of inventories.
- Decentralised production is possible, reducing the costs of the supply chain.
- The flexibility of the production schedule: changes in the production sequence can be done without increasing the cost.
- If the AM design potential is fully exploited, lightweight components can be produced, reducing not only the production cost but the energy consumption and even the CO<sub>2</sub> emissions in the end-use applications [75].

Nevertheless, due to the relative novelty of these processes, still, a set of challenges must be overcome in the future. Nowadays, the main limitations of AM are [21, 26, 62, 72, 104, 168, 217]:

- Higher costs for large productions than other processes, such as injection moulding.
- Limited availability of materials for some AM technologies, e.g. light-sensitivity is required in the LCM polymers for the creation of layers using UV light.
- Despite the number of applications is increasing, there is a lack of specialised designers that could leverage all the design advantages of AM.
- Post-processing operations are required to improve the surface finish.
- The concept of economy of scale (reduction of the unitary production costs with the increase of the production) cannot be applied.
- Lack of standards regulating aspects like the materials properties or quality control [169].
- Limited size of building space.
- Intellectual property rights.

### **1.1.1 Steps in the AM process**

Despite some variations might appear for each particular process, the Additive Manufacturing approach is conducted with the set of steps described by Gibson et al. [78], which can be summarised in:

1. Design and CAD model: Solid or surface models are created using Computer Assisted Design (CAD) software. In contrast to other processes such as Computer Numerical Control (CNC) machining, minimum or no changes must be done in the models to produce by AM.
2. Conversion to STL: The term STL (Standard Tessellation Language) designates the file format used in most of the AM machines. Using a series of triangular faces, the geometry of the part is described in this format. By making the offset of the triangles smaller than the resolution of the machine, geometric problems are avoided.

Nevertheless, STL files cannot include other features of the parts such as units, colour or material. Because of these limitations, a new file format has been adopted for most of the CAD and AM companies, the AMF or Additive Manufacturing File Format. This format increases the features that can be included, reduces the problems of working with STL, and has been already accepted as an ASTM/ISO standard format [111].

3. Transfer to AM equipment and manipulation of the STL file: Features such as the position, orientation or even rescaling of the parts are defined. In other cases, different parts can be built at the same time, for example, by using the same model or combining different ones. In most of the cases, specialised software is used for the visualisation and modification of the models.
4. Machine setup: Different parameters must be modified before starting the printing depending on the technology or machine. Layer thickness and printing rate are examples of them. Additionally, the machine has to be physically prepared for the printing process, e.g. the cleaning, the load of the material, and the stabilisation of the system must be conducted.
5. Building of the parts: The parts are physically created by the formation of cross-sectional layers of material. The first step in the layer formation process is the material deposition. For some AM technologies, the deposited material is directly incorporated into the part. In other cases, the union takes place in a second step by the use of an energy source. Once a layer is created, the next is built over it by the use of a height-adjustable system.
6. Removal and clean-up: In this stage take place operations such as the separation of the part from the building platform, or the removal of the excess material surrounding the part. If support structures are used in the building process, additional work is required. Incorrect manipulation can lead to defects in the parts, so skilled operators are needed.
7. Post-processing: The surface finish of the AM parts is usually defined by the employed layer thickness in the building step. For some special applications, finishing operations such as polishing or even CNC machining are applied. In other cases, the properties of the parts must be improved with thermal or chemical treatments, coatings, or infiltration of other materials.

### **1.1.2 Classification of AM technologies**

Different criteria have been proposed for classifying the AM processes over the years. One of the most common ways divides the technologies according to the physical state of the materials used. E.g. Guo et al. [90] classified the technologies in four categories according to the bulk materials state: liquid, filament/paste, powder or solid sheet.

A combination of two classification methods was proposed by Pham et al. [170] and updated to include the newest technologies by Gibson et al. [78]. The mentioned classification based on the raw material is combined with a second one based on the layer construction method. According to this system, the layer can be created by using 1D Channel, an array of 1D Channels (e.g. by combining various extrusion heads) or even with 2D Channels which expose a whole surface at once.

Looking for an improvement of the communication and dissemination of the AM technologies, a unified classification system was set by the ASTM F42 and ISO TC 261 committees. This new ASTM/ISO standard system divides the AM processes into seven categories [110]:

- Binder Jetting (BJT): These processes are based on the selective deposition of a liquid bonding agent into a powder bed.
- Directed Energy Deposition (DED): The cross-section is formed by the deposition of a material and its simultaneous melting. A focused thermal energy source, e.g. a laser or an electron beam, is used to melt the material.
- Material Extrusion (MEX): In these processes, the material is selectively extruded through a nozzle, producing the cross-section of the part.
- Material Jetting (MJT): Additive Manufacturing processes where droplets of the building material are selectively deposited.
- Powder Bed Fusion (PBF): A powder bed is selectively melted using an energy source, commonly a laser or an electron beam.
- Sheet Lamination (SHL): Processes in which the layers are created by the deposition of sheets of material, and the bonding of them.
- Vat Photopolymerization (VPP): A liquid photopolymer contained in a vat is cured by a selective light-activated polymerisation process.

Next, the main characteristics, advantages and limitations of the different categories are summarised from the description presented by Gibson et al. [78].

### 1.1.2.1 Binder Jetting

It was in the early 1990s when these processes were developed under the name of Three-Dimensional Printing (3DP). Starting from a powder bed, the cross-sectional layer of the part is created by the deposition of a bonding agent. This binder not only joins together the powder particles but also bonds the layer with the previous one.

The creation of the layer starts spreading the powder, usually employing a roller system. The binder is then selectively deposited through a nozzle, forming agglomerates with the powder. Once the layer is built, the building platform moves down, and a new layer of powder is spread. During the building process, the part is surrounded by the unbound powder, helping shape preservation. This unbound powder is removed in the post-processing stage with compressed air.

Powders of polymer, metal and ceramic are commercially available for binder jetting [66]. When comparing the Binder Jetting process with other AM techniques, the first advantage is that productivity can be increased easily by the incorporation of more nozzles in the printing head. The price of the machines is also low when compared to other technologies, like those based on lasers. Different compositions can be easily achieved by the right combination of powders and binder additives. Another significant advantage is that printing with different colours is possible, improving the aesthetic of the parts.

Nevertheless, due to the limitations on the dry powder distribution, low densities can be achieved with Binder Jetting [235]. Low-density results in parts with poor mechanical properties, which must be enhanced by post-processing. Typically the infiltration with a second material is employed.

### 1.1.2.2 Directed Energy Deposition

These processes are based on the simultaneous deposition and melting of the bulk raw material. A focused heat source melts not only the feedstock material but also a part of the substrate. The melted region, known as melt pool, solidifies almost immediately and the material is bonded to the part. After each pass of the deposition system, a track of solid material is formed, and the layers are created by adjacent lines of material.

Even though these processes have been tested for ceramic and polymeric materials, their main application is the production of metallic components. The feeding system can use either powder or wire. When a feeding wire is used, the porosity of the parts is reduced. However, there is a loss of dimensional accuracy, and a subtractive milling system needs to be integrated. Another alternative is the combination of both systems, which increases the deposition efficiency and improves the surface finish [201].

Two main systems can be distinguished for Directed Energy Deposition, the electron beam and the laser based deposition processes. The selection of the heat source depends strongly on the application. I.e. the electron beam was developed by NASA Langley Research Center for the production of components in space [134]. Regarding the laser-based systems, different systems are available, e.g. the Laser Engineered Net Shaping (LENS) developed in the Sandia National Laboratories [79].

Unique advantages can be leveraged with Direct Energy Deposition. The composition can be easily modified in all the directions just by changing the feeding material. For the same reason, composite materials can be produced without any problem [158]. Another advantage is the lack of dimensional limits, only restricted by the machine size [62].

The main limitation is that the melt pools are relatively large, especially when compared to Powder Bed Fusion processes. A large melt pool implies a worse surface finish, less accuracy, and the inability to produce small geometries. Machining operations are frequently used to improve surface quality. Lattice structures and internal channels are neither possible, limiting the design freedom [62].

### 1.1.2.3 Material Extrusion

These processes use the selective extrusion of either a material in a liquid state or a paste, to produce the components. Two different approaches have been developed for controlling the state of the extruded material. The first one is based on a chemical change to produce the solidification. The second one employs the temperature to melt and then extrude the material.

When a chemical change is used, the material can bond either by the addition of a curing agent or a small content of solvent, the reaction with air or by drying. Once the chemical reaction occurs, the material becomes completely solid and stable. An example of these processes is Robocasting, in which an aqueous ceramic paste is extruded [148, 183].

The second approach is based on temperature for controlling the state of the material. Once the liquid material is extruded through the nozzle, it bonds with the substrate and solidifies. The deposited material produces the melting of part of the substrate, resulting in the bonding with it. An innovative and environmentally friendly example of this approach is Freeze-form Extrusion Fabrication (FEF). In this process, parts are produced by the controlled deposition of aqueous pastes which are deposited in a substrate at sub-zero temperatures [130, 147].

Within the Material Extrusion processes, the most common technology is Fused Filament Fabrication (FFF). It was developed in the late 1980s by S. Scott Crump [180] and commercialised by Stratasys under the name Fused Deposition Modeling (FDM) [200]. In FFF, polymers or polymer-based compounds in the form of filaments are processed. The spooled filament is fed in the machine by the action of two counter-rotating rollers. In the machine, the material is introduced in the liquefier region where it melts. The unmelted polymer acts as a piston, pushing the melted fraction and producing its flow through the nozzle. The temperature of extrusion is slightly higher than the melting point of the polymeric material so that it rapidly solidifies and bonds to the substrate once deposited. Thermoplastic polymers and waxes are commonly employed. FFF machines typically operate in three axes. Firstly, one layer is created using the extrusion head, which moves in a plane parallel to the building platform. Once the layer is built, the platform moves down and the next layer can be created. Novel systems have been also developed, going up to eight axis of construction [215]. The main advantage of increasing the number of axes is that the support structures used for some special geometries are no longer required.

The use of filament as feeding material generates restrictions which reduce the range of material that can be used. E.g. the diameter of the filament has to be constant to have a constant mass flow, and it has to be very flexible to be spooled. In order to overcome these limitations, two new feeding systems have been developed, the syringe and the screw extrusion-based MEX. In Figure 1 the schematics of the FFF system (Figure 1a), the syringe based MEX (Figure 1b) and the screw extrusion-based MEX (Figure 1c) are shown.

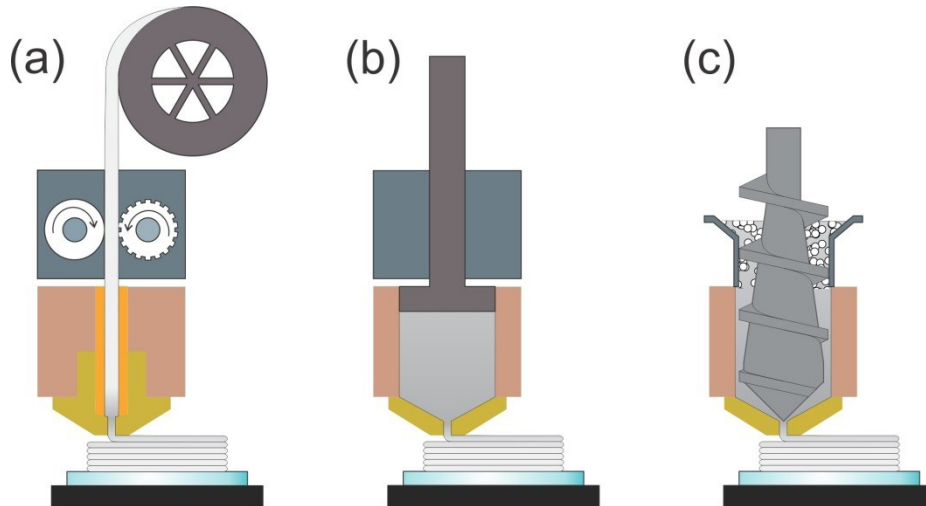


Figure 1: Overview of MEX systems: (a) Filament based MEX (also known as FFF), (b) syringe based MEX, (c) screw extrusion based MEX (adapted from Ref. [212])

In the syringe based system, a piston or a pneumatic system pushes the material instead of a filament. Some advantages of this system are the simplicity of the construction and the use of granules, pastes or suspensions instead of filaments. If the piston is filled with granules, the presence of air interrupts the extrusion, and the material inside the syringe can degrade thermally [212]. Because of this, the process is mostly used in materials that solidify due to a chemical reaction rather than by a thermal process [148, 183].

The extrusion-based process offers more advantages than the syringe based MEX. By using a screw extrusion process, a continuous process can be realised, and a shorter exposure at high temperatures for the polymers, resulting in less thermal degradation [212]. Currently, the first commercial systems for the extrusion of ceramic and metallic feedstocks are available [7].

### 1.1.2.4 Material Jetting

The technology of these processes is very similar to binder jetting, the difference being that in this case, all the building material is deposited from the nozzle as droplets. Solidscape introduced the first machine able to create 3D objects by the inkjet printing of melted wax in 1994 [222]. Wax polymers were the material commonly employed in the first generation of machines, with applications such as prototyping and patterns for investment casting.

Acrylic photopolymers have been introduced in the last years to the industrial processes. In this case, droplets of liquid monomer are deposited and then polymerised using UV light.

In the scientific field, the processing by Material Jetting of a broader range of materials has been tested. Ceramic parts have been produced by the droplet deposition of aqueous ceramic pastes [58] and polymer-ceramic compounds [59]. For metals, the main approach is the deposition of droplets of melted metal. Thus, only metals with low melting temperature can be used. That is why most of the work is focused on the electronic industry for applications such as soldering or the formation of electronic connections.

Since the philosophy of this technology is very similar to that of Binder Jetting, the same advantages can be found. E.g. multiple nozzles can be easily incorporated to increase productivity. Further benefits include better surface finish and dimensional accuracy than those of Binder Jetting, and the possibility to create multi-material parts.

The main limitation of Material Jetting is the limited range of materials commercially available. When ceramic slurries or polymer compounds with metal or ceramic powders are used, the low viscosity required is another limiting factor.

### 1.1.2.5 Powder Bed Fusion

As the name indicates, these technologies are based on the selective melting of a powder bed by the use of one or more thermal sources. The process starts with the deposition of a powder layer with a thickness of around 0.1 mm. This layer is levelled afterwards by the action of a counter-rotating roller. A focused energy source is then employed to fuse the powder particles and join them, thus forming a cross-section of the final part. Once the layer is completed, the building platform lowers down, and the next layer of powder is deposited.

Thermoplastic polymers such as polyamides, polystyrene-based materials, thermoplastic elastomers (TPE), or Polyether Ether Ketone (PEEK) are commercially available for Powder Bed Fusion. Processing of metals is also possible, provided that the metal can be welded. Stainless and tool steels, titanium alloys, nickel-based alloys, aluminium alloys, and cobalt-chrome alloys are processed in the industry. Regarding the ceramic materials, despite numerous materials such as aluminium or calcium hydroxyapatite have been tested, the high melting temperatures make the processing difficult.

To prevent the warping of the parts during the building process, and to reduce the power required to fuse the powder, the raw material and the powder in the bed are maintained at an elevated temperature, just below the melting point. A protective atmosphere is also used to avoid degradation or oxidation of the material.

The fusion of the powder particles can be performed with different methods, being those based on the sintering or the melting of the particles the most common. A laser or an electron beam are used as thermal sources. Techniques such as Selective Laser Melting (SLM) or Selective Laser Sintering (SLS) are well known and applied in the industry [62].

Considerable advantages can be leveraged with Powder Bed Fusion processes. The unmelted powders can be recycled without problems, saving costs [159]. These powders act as support material for the parts; thus, geometrical features such as internal cooling channels are possible, and the removal and cleaning of the parts are considerably easier.



Nevertheless, the shrinkage in the production of metal components makes necessary the use of support structures to avoid warping. The surface finish and dimensional accuracy are worse than those of processes such as stereolithography. These parameters can be improved by the use of smaller powder, thus increasing the cost. Another primary limitation is the high cost of the equipment.

### 1.1.2.6 Sheet Lamination

These technologies are based in the direct deposition of a whole layer of material at once, which is bonded to the part. The bonding can be done either by the use of an adhesive, a thermal process, clamping the layers, or by ultrasonic welding.

The cross-section of the parts is created by cutting a sheet of the building material, either by a knife, a laser, or a machining centre. The cutting can be done after the bonding to the substrate, or before it. If the cutting is done before the bonding, internal features and small channels can be produced. Another significant advantage is the reduction in pressure control in the cutting step. However, these processes have been tested mostly at the research level.

Polymer [171], metal [31], ceramic [135] and composite [202] parts have been produced and studied with Sheet Lamination. Paper has also been widely used for these technologies, with the Laminated Object Manufacturing (LOM) system of Helysis being one of the first systems developed [78]. Currently, machines working with standard A4 paper can be acquired in the market [145].

Since all the material of one layer is deposited at once, the fabrication speed is higher than other AM processes [90]. When machining or knife systems are used for cutting, the machine costs are also lower than in other techniques.

Nevertheless, the surface finish is determined by the thickness of the sheet used. Thus, it is challenging to attain good surface finish [90]. Another disadvantage is the high anisotropy in the properties when adhesives are used for the bonding of the parts.

### 1.1.2.7 Vat Photopolymerization

Stereolithography (SLA), a Vat Photopolymerization process, was the first AM technology commercialised back in the 1980s. The method used is the curing of a liquid photopolymer contained in a vat by a selective light-activated polymerisation process. Ultraviolet (UV) light is commonly employed to activate the process, but other radiation sources such as electron beams or visible light can be used with some polymers.

The traditional machine configuration consists of a laser beam and scanning galvanometers to create the parts in a point-wise manner. Once a layer is built, the building platform in which the part is placed descends and the next later of uncured polymer is deposited.

New processes based on mask projection can produce entire layers. An example of it is using a Digital Micromirror Device (DMD). In this technology, a large radiation beam, with a lower price than a laser beam, is used. Thus, a cheaper and faster process is attained [90].

Another novel process is the Two-photon polymerisation, in which the photopolymer is cured in a point-wise manner in the intersection of two laser beams. High-performance systems with resolutions down to 100 nm and building speed up to 5 m/s have been developed [209].

The range of materials which can be processed by Vat Photopolymerization is considerably smaller than those of other processes. Two main types of photopolymer resins are employed: epoxy and acrylic resins. The epoxy polymers have lower shrinkage and enable the production of harder and stronger parts. However, the photopolymerisation is slower, and the epoxy parts are more brittle than the acrylic parts. Thus, the conventional approach is to combine both resins.

The production of ceramic [101] and metallic [15] parts is also possible by Vat Photopolymerization. In this case, a suspension highly filled with powder is cured, the polymer is then removed by thermal degradation, and the ceramic or metal parts are finally sintered. Yet, the powders that can be processed are limited. The main reason for it is that the powder cannot absorb the curing light; thus, it is recommended that white or bright powders are employed for an efficient process.

Parts with excellent surface finish and high dimensional accuracy can be obtained by Vat Photopolymerization. Using mask projection systems the cost of the equipment is reduced and the process faster, therefore improving the competitiveness of the process. On the other hand, the materials are expensive, and few can be processed, thus limiting the application [104].

### **1.2 Additive manufacturing of ceramics**

Except for some polymer-derived ceramics, mostly based on silicon [47], the processing of ceramic materials requires the use of raw material in the shape of powder. Independently of the technology, the powder must be mixed with inorganic and or organic additives which facilitate and enable its shaping [175]. Once the components are shaped, the organic additives, from either synthetic or natural origin, are removed before sintering. Since the inorganic additives cannot be eliminated and remain in the parts, their use is limited to the applications in which they do not deteriorate the properties of the final part after sintering. In the sintering step, the densification of the parts by different mechanisms occurs, leading to parts with the desired microstructure and porosity [175]. In this section, an overview of the main conventional and AM techniques for shaping ceramic components is presented. In further sections, the overall shaping, debinding and sintering process is presented for the FFF process.

Table 1 summarises the most common ceramic shaping methods and the geometries attainable in the green body (after shaping) with each of them. Due to the high costs required for machining ceramic components, which can go up to 30 - 50% of the process costs, each of these technologies has been optimised to produce near-net-shape of a specific type of components [150].

Table 1: Classification of the conventional ceramic shaping methods [150, 175]

<b>Forming method</b>	<b>Feed material</b>	<b>Green body</b>
<b>(Semi-) dry pressing</b>		
Uniaxial pressing	Powder or free-flowing granules	Small and simple shapes
Isostatic pressing	Powder or fragile granules	Larger, more intricate shapes
<b>Wet-shaping</b>		
(Pressure) Slip casting	Free-flowing slurry with low binder content	Thin and intricate shapes
Tape casting	Free-flowing slurry with high binder content	Thin sheets
<b>(Thermo)Plastic shaping</b>		
Extrusion	Moist mixture of powder and binder solution	Elongated shapes with uniform cross-section
	Granulated mixture of powder and polymeric binder	
Ceramic Injection Moulding	Granulated mixture of powder and polymeric binder	Small intricate shapes

The mechanical compaction by pressing of dry or semidry powders enables the shaping of large series of components with relatively simple shapes. A minimal amount of additive is required to lubricate during pressing and to maintain the shape of the green components. These components can be latterly machined, but with a high waste of material [150]. In the uniaxial pressing method, the non-uniform pressure applied to the powder can result in density variations in the green body [175]. Nevertheless, such variations have been significantly reduced by the further development of the pressing tools and the isostatic pressing process [28, 150, 175].

A more uniform density is obtained in the wet-shaping techniques [175], also known as colloidal processing techniques [131]. The feed material is a liquid suspension in which organic additives such as plasticisers or polymers are required to adapt the rheological behaviour and increase the strength of the green components [131]. The only exception are the clay-based ceramics, in which the aqueous suspension possess enough plasticity without the need of processing additives [131]. In the slip-casting of clays and porcelains, an aqueous suspension is poured into a plaster mould with the desired shape. The porous mould absorbs the water and a solid layer of powder is formed; following the residual suspensions is removed, and the parts further processed [28, 150]. In the pressure slip

casting process, porous polymer moulds are employed, and by the application of pressure, the formation of the solid layer is accelerated [28, 150]. The tape casting process enables the shaping of sheets of different thickness as finished products or as semi-products that can be processed by laminating, punching or by the SHL of ceramics [150]. A step forward is the use of colloidal systems that allow the transition from a liquid suspension to a stiff structure without the need for drying the components [191]. This transformation can occur by the formation of a cross-linked organic network as occurs in the gel-casting process, or by the formation of a colloidal gel, which is the case of the direct coagulation casting [131].

The plastic shaping methods rely in the plastic deformation of a powder-additive mixture to shape the green components [175]. In ceramic extrusion, a paste composed of powder, solvent and additive is extruded through a nozzle by the action of a piston or screw [175]. A variation of this process is the thermoplastic extrusion of ceramics, in which the solvent and additive are substituted by a multi-component binder system resulting in lower friction and less powder-binder separation [46]. Despite the high efficiency of the extrusion processes, the shapes available with them are limited since the shape in the z-direction is fixed [150]. When high productivity of complex-shaped ceramic components with small and medium size is required, the Ceramic Injection Moulding (CIM) process is the preferred option [150]. In the CIM process, a thermoplastic compound highly filled with ceramic powder is molten and injected into a mould in a process similar to the injection moulding of plastics [76, 153]. Due to the abrasion of the ceramic powder, special coatings of hard materials are required [188]. In fact, due to the high tooling costs, the CIM process is only feasible for large series of products [76, 153].

In general terms, all the conventional processes for the shaping of ceramics shown in Table 1 need tooling, either sacrificial or permanent. The layer-by-layer shape generation in the AM of ceramics eliminates tooling, and thus all the costs and time required for the production of tools [140]. This cost reduction makes economically feasible the production of a short series of ceramic components, which would be too expensive to produce by conventional methods [140, 150, 207]. Furthermore, the AM technologies enable the production of new complex geometries that could not be produced by conventional methods. These new geometry possibilities can, for example, enhance the performance of components such as heat exchangers [167, 186], catalysts [60] or microfluidic devices [150], or be used for the production of components with a functionally graded porosity for medical applications [82, 148].

Nevertheless, it must be stated that the AM technologies will not replace the conventional shaping processes, due to the high productivity of the second [150]. On the contrary, AM technologies can expand the range of applications of ceramic materials and serve as perfectly complementary techniques to well established conventional processes such as CIM [140, 150, 151]. In Table 2, the main applications expected for AM ceramic components according to the annual report of SmarTech Analysis [194] are summarised.

Table 2: Expected applications for AM ceramics with the number indicating the expected demand (1 highest and 6 lowest) (adapted from [194]).

	<b>Field</b>	<b>Applications</b>	<b>Materials</b>
<b>1</b>	<b>Industrial manufacturing and tooling</b>	Industrial cores and moulds, tools	Silica (sand), quartz, beads, cements
<b>2</b>	<b>Electronics and optics</b>	Sensors, manifolds, custom assemblies, antenna components, substrates, x-ray tubes, gyrotron components, nozzles, seals	Zirconia, alumina, silicon carbide
<b>3</b>	<b>Aerospace and defence</b>	Thermal and armour components, sensors, seals, fuel injectors, nozzles, satellite parts, manifolds, subassemblies	Zirconia, alumina, silicon nitride, silicon carbide, boron carbide
<b>4</b>	<b>Biomedical and dental</b>	Bone grafting, bone grafting, spinal implants, dental replacements, medical tools	TCP, HA/HAP, zirconia
<b>5</b>	<b>Automotive and rail</b>	Sensors, powertrain elements, fluid control, interior parts, valves, seals, heat exchangers, brushes, inverters, discs, ball bearings, fuel injectors, seals	Zirconia, alumina, silicon carbide
<b>5</b>	<b>Consumer products</b>	Sculptures, vases, tableware, furniture, architectural items, tiles	Clay, terracotta, glass
<b>6</b>	<b>Energy and maritime</b>	Ship building parts, substrates, propulsion parts, fluid control parts, ball bearings, grinding media, valves, seals, pump products	Zirconia, alumina, silicon carbide

Over the last decades, the AM of ceramics has been studied for all the processes described in section 1.1.2. Nevertheless, the high thermal gradient in the Directed Energy Deposition (DED) and Powder Bed Fusion (PBF) processes results in residual stresses and defects such as cracks and distortions. Moreover, the coarse surface finish and porosity of the parts limit their areas of application [41]. The Sheet Lamination (SHL) of ceramics could benefit from the use of tape casted ceramics as raw materials [150]. However, most of the studies for the ceramics SHL were conducted years ago, and only for components with simple geometries

such as gears [41]. Due to different reasons, the most relevant technologies for the AM of ceramics are the Vat Photopolymerization (VPP), Binder Jetting (BJT), Material Jetting (MJT) and Material Extrusion (MEX) technologies [194].

The VPP technologies are the most advanced processes for the AM of technical ceramics [41, 194]. High density and high mechanical properties can be obtained with these processes [92, 187]. Moreover, the parts produced by VPP have the highest dimensional accuracy and the lowest surface roughness of all the AM technologies [41, 241]. The VPP of ceramics employs photocurable resins filled with a high content of ceramic particles. The parts are formed by the selective curing of the polymeric resin, based in a laser beam or the digital light projection [194]. The limitations of this technology are the low speed of the shaping process [41] and the maximum thickness of the parts that can be produced [241]. Since the binders are photo-cured polymers, they can be only removed by thermal decomposition, and several days are required for the debinding of parts with a wall thickness of about 1 cm [241].

If a high shaping speed or large-sized parts are the desired criteria, the BJT of ceramics is the best option [241]. In this process, a binder is selectively deposited on a ceramic powder bed to obtain the green parts, which must be treated to increase their strength before debinding and sintering [61]. Due to the use of a powder bed, the green parts are very porous, and an additional step of infiltration or isostatic pressing is required to increase the density [41, 241]. Currently, the main applications of the BJT of ceramics are the production of low-cost parts or parts with large size, like large mould and foundry cores [194].

Inkjet printing is the most common process for the MJT of ceramics [41]. In this process, droplets of ceramic inks are selectively deposited to produce the parts. The ceramic inks are composed of a solvent, additives and ceramic powder; as the ink is deposited, the solvent evaporates, and dense green parts are obtained [241]. The process enables the production of small single- and multi-material components with well controllable material gradients [241]. Due to these reasons, there is a great interest in the application of this technology in the fields of microelectronics and energy devices [41].

The MEX of ceramics can employ the two approaches described in section 1.1.2.3 to control the state of the deposited material. If a ceramic ink or gel is extruded, the drying of the solvent and/or a physical transformation such as gelation ensure the preservation of the shape [241]. These MEX processes are commonly known as direct ink writing [41]. For the formulations with a higher content of solvent, the parts must be immersed in an oil bath to prevent non-uniform drying during shaping; however, due to the low content of organics, an additional debinding step is not necessary [148]. Direct ink writing is the most common method for the AM of porous ceramic structures for applications such as piezoelectric components, catalyst carriers and tissue engineering [41, 148]. The second approach to control the state of the extruded material is the melting and solidification of a thermoplastic binder highly filled with ceramic powder. This compound is known as feedstock and can be in the shape of pellets or filaments. If a screw-based MEX system is used (Figure 1b) the same pellets as for the CIM process can be employed [7]. In general terms, it can be stated that the MEX of ceramics enables the production of multi-material components, has a higher shaping speed than other techniques such as VPP and requires low investment costs for the shaping equipment [41, 53]. However, the parts produced by MEX have a poor surface

quality and the defects generated during shaping make the production of dense monolithic parts difficult [41, 241]. In the next section, a more detailed description of the filament-based MEX of ceramics, also known as FFF of ceramics, is presented.

### **1.3 FFF of ceramics and metals**

#### **1.3.1 Thermoplastic based manufacturing**

In the thermoplastic-based manufacturing of ceramics and metals, a thermoplastic binder compound highly filled with powder of the final material is employed. I.e. the binder acts as a carrier, which additionally provides mechanical interlocking to the network formed by the particles. Powder injection moulding and the thermoplastic extrusion of ceramics are examples of this approach that are well implemented in the industry. In general terms, the process consists of four stages: compounding, shaping, debinding, and sintering. Next, the stages of the process are described, focusing on the characteristics of the filament-based FFF.

##### 1.3.1.1 Compounding

In the compounding stage, the feedstocks used as raw material are produced by mixing the powder with the different components of the binder. Thus, before this stage, the selection of the powders and polymers must be undertaken. In order to attain the requirements of the different processes, multicomponent binders are employed in all the technologies. In the FFF technology, thermoplastic polymers are used in the binder system. Since the shape of these polymers can be easily changed by melting the material, filaments can be firstly produced with the compounds and then extruded to the desired shape. Besides, recycling is possible, reducing the cost of the process. In section 3.1, a discussion of the state-of-the-art for the FFF binders is available.

Once selected the materials, the compounding is carried out. The polymer is melted, and the shear action must produce the breakdown of the particles clusters, as well as the dispersion and distribution of the powder in the binder in a homogeneous mixture [153]. Two types of equipment can be employed for compounding. Roller mixers, also known as kneaders, produce the material in batches. For a continuous production of material, shear rollers or co-rotating twin-screw extruders are used. The main advantages of the batch mixing equipment are the lower cost of the equipment and the possibility to produce a small quantity of material [63]. Also, the mixing torque can be measured over time and be used as an indicator of the feedstock homogeneity [100]. Nevertheless, the productivity and shear applied with the batch mixing techniques are lower than for the shear rollers and twin-screw extruders.

##### 1.3.1.2 Shaping

After the compounding, the shaping stage is carried out. For some technologies such as Powder Injection Moulding or Vat Photopolymerization, the feedstock or suspension can be directly used to produce the parts. As the technique used in this project was the filament-

based FFF, in which filaments must be first produced from the feedstock, the shaping process and requirements are described for this process.

For the production of filaments in the stage of material development, the use of special setups is usual. E.g. small quantities of filaments can be produced by employing a capillary rheometer, in which a piston forces the flow of the material through a capillary. Then the extruded material is pulled by a conveyor belt to produce the filament [4, 125, 213]. Nevertheless, for the mass production of filaments, single- or twin-screw extruders are the equipment commonly used. Other devices such as pulling and winding units and elements for cooling or measuring the filament diameter are also necessary [1, 116, 193].

The produced filaments are used in the shaping stage, in which the parts are created layer by layer using the FFF technology (Figure 2). First, the filament is driven into the extrusion head by two counter-rotating wheels. Once introduced, the polymer fraction is melted in the liquefier, and acts as a carrier of the ceramic or metallic particles. Finally, the feedstock is extruded through the nozzle and deposited in the part as a melted strand.

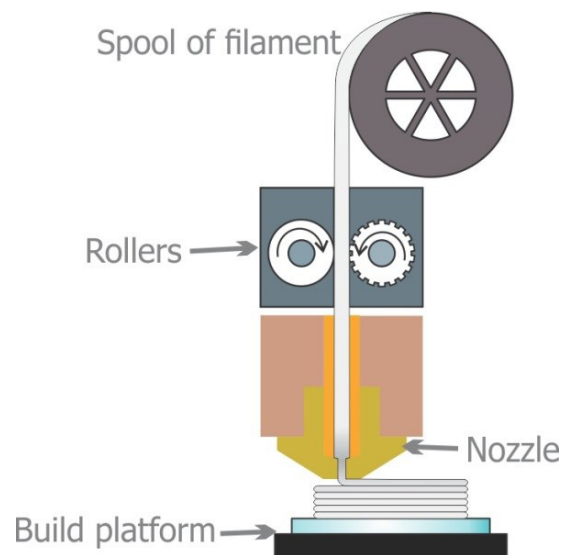


Figure 2: Schematics of the FFF shaping system

In general terms, the outcome of the shaping stage in the powder-binder technologies are the so-called „green parts“. In these parts, the polymeric binder is responsible for the shape retention of the parts, providing the stiffness needed in the following stages of the process.

### 1.3.1.3 Debinding

Debinding is one of the longest steps of the process. After moulding, the shape of the parts is maintained by the binder system, which provides a mechanical interlocking to the network formed by the particles. The paths that the binder has to follow in this network when it is removed are very tortuous, and the pore structure is characterised by its capillary pressure or resistance to fluid flow. This capillary pressure also produces the union between the particles. Besides, no damage to the parts should occur when the binder goes through the network [76]. The resulting part after debinding is called brown part [160].

The main techniques of debinding can be classified into three groups [76]:



**Thermal debinding:** Binders are removed by thermal mobilisation. The most commonly used process is to dissociate the polymer molecules into smaller molecules producing degradation of the binder. A protective atmosphere prevents the oxidation of the part and removes the products of decomposition. A variation of this method is wicking extraction, in which the parts are buried in a porous substrate (usually alumina), that absorbs the melted polymers. This process is faster but can produce a higher number of defects.

**Solvent debinding:** Used for binders which are partially soluble in substances such as hexane, heptane or water. The parts are put in contact with the solvent, leaving an open pore structure as the fluid penetrates the parts from the surface. The solvent can be in a liquid or vaporous state. When the debinding is carried out at high pressure, it is called a supercritical process.

**Catalytic debinding:** Polyoxymethylene (POM), also known as polyacetal, is decomposed by the action of an acid catalyst. The process is faster and less harmful for the parts than the previous ones, but corrosion of some metallic parts and high contamination are its drawbacks. BASF Catamold system, the most employed commercial feedstock for PIM, is based on this system.

For a fast and progressive debinding, multicomponent systems are employed. A primary binder, with low molecular weight, is responsible for reducing the viscosity of the feedstocks and is removed in the first stage, leaving an open pore structure. On the other hand, the backbone or secondary binder retains the shape and provides rigidity to the parts until it is removed in the second stage. Additives such as dispersants, plasticisers, stabilisers and intermolecular-lubricants are also very common. These additives can be removed along with the primary binder or in the second stage [64].

A single step thermal debinding has been the traditionally employed method, because of its simplicity and the need for lower investment costs. Nevertheless, the binder softens, and defects can be generated by internal vapour pressures derived from its degradation [49]. To avoid this, the process needs to be carried out at gradual heating rates, to ensure a progressive degradation of the different polymers, which generates long and energetically inefficient processes [76].

Nowadays, more efficient processes are performed in two steps, one for each of the principal components of the binder. A solvent or catalytic debinding technique is employed in the primary debinding, producing an open pore structure from the surface to the inner region of the parts. The remaining binders are thermally removed in the secondary debinding, using the existent pores. The advantages of this method are a faster process, better dimensional control than a single thermal step debinding [13] and the reduction of defects such as warpage [42]. Additionally, this technique permits the production of parts with larger sections as has been demonstrated not only for PIM [135] but also for the production of large diameter-rods by extrusion [136].

### 1.3.1.4 Sintering

Sintering can be defined as the solid-state densification process in which particles are bonded together through diffusion and other atomic-scale mass transport mechanisms. By

this densification process, the brown parts are transformed into final compact parts, with relative densities up to 98 %. Both the microstructure and the properties of these final parts depend on parameters such as the heating and cooling rates, the time the sample remains at the sintering temperature, and the atmosphere at which the process is performed [196].

One of the main driving forces of the process is the reduction of the surface energy by the decrease of the surface area. When the temperature is high enough to reach the diffusion activation energy, the formation of cohesive bonds between the particles in contact begins. These bonds, known as necks, grow until the particles are completely united, and the porosity in the parts is considerably reduced. The small particle size implies a high surface area, which facilitates the process. Another primary mechanism is the difference of surface vapour pressure. In the concave bonds, the pressure is smaller than in the rest of the surface, with a convex shape. This pressure difference enhances the diffusion of atoms during the initial stages of sintering [37].

The sintering process is divided into different stages. In the case of spherical particles, which is the simplest situation, three stages can be considered [76]:

- Initial stage: The porous structure is open and interconnected. As the temperature increases, the bonds start to form in the contact points between the particles. The necks formation causes small rearrangements in the particles packing due to small displacements and rotations.
- Intermediate stage: As the temperature increases during the heating cycle, the necks grow due to different mass transport mechanisms. These mechanisms are surface diffusion, evaporation-condensation, grain boundary diffusion, lattice diffusion, viscous flow, and plastic flow. The porosity of the part decreases, and the densification is notorious.
- Final stage: At the end of the process, the densification rate decreases. The pores reach their minimum size, have a round shape and are isolated. If the sintering time is excessively long, the grain size of the material starts to increase, resulting in a decrease of the mechanical properties.

### **1.3.2 Comparison to other processes**

The simplicity and low cost of the FFF equipment have promoted its use and expansion at industrial and end-user level for the production of polymeric parts. On this manner, the existing knowledge on FFF and its popularity can promote its expansion and application for the production of metal and ceramic materials. Moreover, the whole system for shaping, debinding and sintering can currently be purchased for a few thousands of euros [53].

The debinding and sintering processes are well known for well-established technologies such as PIM, which can facilitate the implementation of FFF as a complementary production route in the development of new products, in the production of small batches of parts, in the customisation of mass-produced components and in the production of tooling [151, 214].

The many properties required in the feedstocks for the production of filaments constitute a technical barrier and is one of the main factors hindering the expansion of the FFF process for the production of metallic and ceramic materials [25]. Moreover, high dimensional

tolerance of the filaments is required to have a continuous flow of material and avoid failures during shaping with FFF [25, 78], which increases the price of the feedstock [152]. The screw based MEX processes using feedstock pellets [7, 18, 50, 212] can help to solve these problems and reduce the cost of the feedstock production [152]. Nevertheless, further improvements are required for the optimisation and control of the material flow [18, 84].

Support structures are required in FFF for the generation of shapes such as overhangs or bridges, which requires a second material being extruded and an additional step of support removal. Nevertheless, 5- and 6-axis machines have been designed by modification of the FFF systems or their combination with robotic arm systems [173]. These modifications reduce the need for support structures and enable the production of new geometries.

The shaping by the extrusion of strands results in high surface roughness for FFF parts as compared to other AM processes [54, 81, 152]. Since the surface roughness is inversely proportional to the layer thickness and thus to the nozzle diameter, the use of nozzles with small diameters improves the surface quality as thinner layers can be used [156]. The surface roughness can also be reduced by the thermo-mechanical treatment of the green parts [30]. The resolution attainable by FFF is also limited by the nozzle geometry and is lower than for other technologies such as Vat Photopolymerisation, Material or Binder Jetting [78, 152, 241]. Conversely, the build chamber of the FFF machines can be larger than for other processes, which enables the shaping of larger green parts [151]. Moreover, the combination of various materials in a single component is facilitated, since various nozzles can be easily incorporated in a single machine [113].

Debinding is one of the most critical steps of the FFF process. If a single step of thermal debinding is conducted, long and expensive thermal cycles are required to avoid defects in the parts. Whereas thermal debinding is the only alternative for techniques such as ceramic Vat Photopolymerisation [241], binders for solvent and catalytic debinding have been developed for FFF (Table 5). The use of a two-step debinding process enables the production of thicker components [137, 152] in a short and cost-efficient process [152].

### **1.3.3 Materials processed by FFF**

The size of the powders, which is not a single size but a distribution of sizes, is one of the limiting factors for processing for FFF. Although there is no lower limit, submicron particles have a high tendency to agglomerate and require a de-agglomeration and coating treatment [144, 208, 225]. On the other side, the powder must be small enough to avoid the clogging of the nozzle during FFF [19, 24] and powders with  $D_{90} \leq 22 \mu\text{m}$  are usually preferred. Kukla et al. [125] investigated the effect of the particle size on the processing of feedstocks with 55 vol% of 316L. The feedstock with larger particles ( $D_{50} \sim 8.6 \mu\text{m}$ ) had lower flexibility, stiffness and viscosity than the one with smaller particle size ( $D_{50} \sim 5.5 \mu\text{m}$ ). Despite the reduction of the viscosity, the reduction in stiffness resulted in buckling for the feedstock with larger particles and failure in the shaping by FFF [125]. The properties and processing of the feedstock are also influenced by the morphology of the powder. Using spherical powders results in a higher packing density and higher flowability [97]. Nevertheless, irregularly-shaped powders can also be produced by FFF. Irregular powders offer the

advantages of better shape retention and lower cost than the spherical powders produced by gas atomization [97].

The maximum powder content in a feedstock processable by FFF depends not only on the geometry but also on its surface chemistry and the powder-binder interaction [84]. Gonzalez-Gutierrez et al. compared the mechanical properties of filaments with the same binder system but two types of powders [84, 85]. For the filaments with ceramic and irregular  $\text{SrFe}_{12}\text{O}_{19}$  powder, the strength and flexibility were much lower than those of filaments with 316L powder with spherical and larger particles. For both materials, more brittle and fragile filaments were obtained for high powder contents. Nevertheless, filaments with up to 60 vol% could be processed by FFF for the 316L powder, whereas the filaments with  $\text{SrFe}_{12}\text{O}_{19}$  could be only processed for contents lower than 55 vol% [84, 85]. Nötzel et al. [156] compared the shaping by FFF of alumina feedstocks with different powder content. Increasing the powder content increased the viscosity, and small nozzles could only be used for solid contents lower than 50 vol% [156].

Similarly to Powder Injection Moulding, FFF can produce components with a wide variety of metallic and ceramic materials [84, 176]. Silicon nitride [3, 5, 112], alumina [49, 89, 91, 156, 163], lead zirconate titanate [5, 113, 143], mullite [10, 162], fused silica [5, 12, 162], titanium dioxide [162], zirconia [1, 77], and tricalcium phosphate [88] are examples of ceramics that have been produced by FFF. The FFF of metals such as the precipitation hardening stainless steel 17-4PH [83, 86, 225], the austenitic stainless steel 316L [30, 86, 126, 180], the titanium alloy Ti6Al4V [124, 239], the rare earth magnetic alloy NdFeB [123], pure copper [55] and a new tungsten-chromium alloy [24] has been reported in the literature. Metal-ceramic composites such as hard metals (tungsten carbide with a cobalt matrix) [20, 129] and cermets (carbides and nitrides of titanium and other elements in cobalt and/or nickel matrix) [129] can also be produced by FFF. The AM of such composites by methods employing a powder bed would be a challenging task due to two factors. When unbound powders are used, the powders of the hard-phase and the matrix separate in the powder bed, complicating the reuse [129]. Furthermore, sintering or melting the powders with an energy source would result in inhomogeneity in the composition and loss of the metallic matrix [129, 233].

The FFF of multi-material components has also been investigated since it would improve the part's performance and make it possible to combine various functionalities in a single part. In order to combine two or more materials, binders with similar composition must be employed to ensure a good strand bonding when shaping the parts and a similar debinding behaviour [120]. Nevertheless, the co-sintering of the materials is the most challenging task. A similar thermal expansion coefficient and similar shrinkage evolution during sintering are critical [1]. Piezoelectric components combining soft and hard lead zirconate titanate have been produced by Jafari et al. [113]. Brennan et al. [27] reported the fabrication of multi-material actuators composed of electrostrictive and piezoelectric ceramics. Furthermore, the combination of stainless steel and zirconia to combine electrical conductivity and insulation properties in infrared heaters has been demonstrated by Abel et al. [1].

Table 3 summarizes the metallic and ceramic materials that can be commercially purchased in filaments and sintered. As can be observed, the stainless steels 316L and 17-4PH are the

most commonly offered metals, followed by copper. Alumina and zirconia are the most common ceramics. Since one of the main applications for FFF currently is the production of tooling, other metals such as the tool steels and the Inconel alloy 625 are also offered by the company Markforged. All the producers shown in Table 3 have also other materials available with special orders or under development. Therefore, it can be expected that the number of commercial FFF filaments of metallic and ceramic materials increases considerably in the next years.

Table 3: Main distributors of filaments for the FFF of metals and ceramics.

Company	Metallic filaments	Ceramic filaments	Debinding	Source
The Virtual Foundry	316L Bronze Cu High C iron	-	Wick (Carbon paste) + Thermal	[204]
BASF	316L	-	Catalytic + Thermal	[16]
Spectrum SiCeram Emery oleochemicals	-	Silicon nitride Alumina Zirconia Porcelain	Solvent + Thermal	[197]
Nanoe	316L	White zirconia Black zirconia Alumina	Solvent (Acetone) + Thermal	[53]
Markforged	17-4 PH Cu Inconel 625 Tool steels (D2, H2 and H13)	As support material	Solvent + Thermal	[141]
XERION	17-4 PH 316L	Alumina Zirconia	Solvent + Thermal	[227]

## 1.4 Zirconia

Zirconia ( $ZrO_2$ ) is the ceramic oxide of zirconium, a strong metal with properties similar to titanium [56]. Zirconia is not present as a pure oxide in nature, and the two main natural sources of zirconium are the minerals baddeleyite ( $ZrO_2$ ) and zircon (zirconium silicate,  $ZrO_2 \cdot SiO_2$ ,  $ZrSiO_4$ ) [23, 142]. To obtain zirconia from these minerals decomposition processes such as chlorination and thermal decomposition, alkaline oxide decomposition and thermal decomposition in plasma are used [23].

Pure zirconia can have three forms depending on the temperature: monoclinic, tetragonal and cubic. Monoclinic zirconia is stable at temperatures up to 1170 °C, at which it transforms to tetragonal zirconia. The cubic zirconia is formed at temperatures higher than 2370 °C. These transformations are reversible, and at the end of cooling the monoclinic zirconia is formed. Due to the higher density of tetragonal zirconia, the monoclinic-to-tetragonal

transformation is accompanied by a small shrinkage, and in the reverse transformation there is an expansion of 3 to 5 vol.% [23].

The change in volume caused by the tetragonal-to-monoclinic transformation limits the use of zirconia under frequent temperature changes and results in cracks and flaws in sintered zirconia. In order to avoid these defects, stabilization oxides such as CaO, MgO, CeO<sub>2</sub> and Y<sub>2</sub>O<sub>3</sub> are used to maintain the tetragonal and cubic phases at room temperature after sintering. Fully stabilized zirconia is obtained with high contents of stabilizers, whereas partially stabilized zirconia is obtained at lower contents. The partially stabilized zirconia is a combination of tetragonal and cubic forms, which requires small particle sizes to avoid the transformation of the tetragonal to monoclinic form [23, 142]. The tetragonal phase in the partially stabilized zirconia remains metastable at ambient temperature [142]. If the stress field in front of a propagating crack is large enough, the tetragonal grains in the vicinity of the crack undergo a tetragonal-to-monoclinic transformation. The volume expansion associated with the transformation induces compressive loads in the tip of the crack, increasing the resistance of the material to the crack propagation [23, 142].

Due to the transformation toughening and the good biocompatibility of zirconia, partially stabilized zirconia is widely used in dentistry [56, 142] and the production of prostheses such as femoral heads, knees and acetabular components for hip replacements [23]. The high ionic conductivity of zirconia, especially when it is stabilized with yttria, has promoted its application as electrolyte in solid oxide fuel cells and electrochemical sensors [23]. Another major application of zirconia is as thermal barrier coating for the protection of metallic materials at high temperatures; the low thermal conductivity of yttria stabilized zirconia and its coefficient of thermal expansion similar to that of the metal substrate make this material an excellent option for these barrier coatings [23].

Zirconia partially stabilized with 3 mol.% yttria has been the powder employed through all the investigations of this PhD thesis. The main reason to select this material was its similar thermal expansion coefficient and sintering behaviour to those of stainless steels, which makes the FFF of multi-material parts combining electrical conductivity and insulating properties possible, as demonstrated in previous works to this thesis [1].

## 2 Introduction and objectives

### 2.1 Motivation and background

Over the last decades, Additive Manufacturing (AM) has aroused the attention of the industry and the consumers. These technologies have opened the door for the production of components with extraordinarily complex geometries, as well as expanded the flexibility for producing highly personalised products and components without the need for expensive tooling.

Significant progress has been attained in the commercialisation of AM methods for polymers, not only at an industrial scale but also for the end-user production. On the other hand, the production of ceramic and metallic components is restricted to the industrial field, due to the need for more specialised equipment. Laser or electron beam AM techniques are the preferred option for metals; however, the equipment is considerably expensive, and the application to ceramics is limited to porous structures due to the high melting temperature. The alternatives are those technologies that use a polymeric system as a carrier, known as a binder, which enables the shaping of ceramic and/or metal powders. The binder is then removed, and the components are sintered to attain almost full density. Within these technologies, we can find Fused Filament Fabrication (FFF), a technology well-known for polymers. For FFF there are no restrictions for the selection of the metallic or ceramic material, which enables a broad range of applications. Besides, the cost of the FFF equipment is considerably lower than the one required for other AM technologies.

The main limitation of the FFF technology is the form of the employed raw material, a spooled filament. Since the polymer system is highly loaded with the ceramic or metallic powder, the mechanical properties of the polymers are critical. Not only the polymers must be very flexible and strong to be spooled as filaments, but they must be stiff enough to feed the extrusion system. The bonding between the extruded roads in each layer and the adhesion between the extruded layers is another major issue. In addition, the particles must be homogeneously distributed in the polymeric matrix. Research has been conducted for the development of binders for FFF [4, 143], and the production of metallic and ceramic parts has been tested [113, 225].

To remove the binder, it is subjected to a thermal degradation step, the so-called thermal debinding. During the thermal debinding process, the polymer decomposes in the whole volume in the parts. Therefore, gases are formed in the parts that can end up in severe defects and bloating. To avoid these defects, slow heating rates are employed, and this step is characterised by long runtimes and large amounts of energy consumption [13].

A more efficient debinding process is based on the dissolution of the major part of the polymeric components in a solvent. After solvent debinding, a porous structure is created in the parts, which can be used in the next step for the thermal degradation of the rest of the polymers [13]. The reduction of energy consumption in the thermal debinding step makes the FFF process more efficient and increases its competitiveness. Another advantage of solvent debinding is that parts with larger sections can be created, thanks to the reduction of the internal stresses during debinding and the progressive removal of the polymers [137].

This two-step debinding process is used in most of the commercial feedstocks for FFF, and the first studies have been reported in the literature [67, 122]. However, the current information of the type of binder components required for the combination of FFF and solvent debinding is limited as most of the developed systems remain confidential.

Considering the described situation, the main objective of this thesis was to develop a better understanding of the feedstock formulations required for the combination of the FFF of ceramics with a more efficient debinding stage. A novel formulation for the FFF and solvent debinding of zirconia components was developed systematically. The type of components necessary to meet the requirements for the process were defined, and their influence on the properties and processing of the feedstock was determined. The second focus was on the influence of the processing parameters on the processability of the feedstocks for FFF and solvent debinding and the impact on the final parts. For those investigations, a binder formulation previously developed in the Institute of Polymer Processing was employed [122].

## 2.2 Hypotheses and Approach

Based on the current state of the art and the problems described in the previous section, a series of hypotheses were proposed at the beginning of this thesis. It was believed that further development in the processing of ceramics by FFF and solvent debinding could be achieved based on the following hypotheses:

1. **By the right combination of binder components, a high strength, stiffness and flexibility, as well as low viscosity could be obtained as required for FFF.**
2. Solvent debinding requires two types of components. First, a major fraction of the binder must be leached with a solvent. The rest, known as backbone, must maintain the shape of the parts during the process and be removed in the subsequent thermal debinding step. **The combination of the right soluble binders and backbones should enable the use of solvent debinding in FFF.**
3. **The use of a polymer grafted with polar groups as backbone should result in an improvement of the adhesion to the polar surface of the zirconia powder.** A high powder-binder adhesion should result in a more homogeneous feedstock, with lower viscosity and with higher mechanical properties.
4. **The parameters employed in the solvent debinding of FFF feedstocks should determine the debinding rate and the apparition of defects.**
5. **The defects caused during the shaping step in the FFF of ceramics and their effect on the properties of the final parts could be reduced by the proper adjustment of the parameters during shaping.**

The hypotheses 1, 2 and 3 concern the systematic development of a novel feedstock formulation for the FFF and solvent debinding of zirconia. The characterisation of several binders and feedstock formulations was conducted by different methods to validate these hypotheses. The viscosity of binders and feedstocks was characterised by rotational and



high-pressure capillary rheology respectively. Tensile tests on the filaments enabled the determination of the strength, stiffness and flexibility of the compounds. The debinding performance was measured regarding the mass loss and the apparition of defects using immersion tests on cyclohexane. Finally, the interaction of the different binder components with the powder and between themselves was studied by scanning electron microscopy (SEM), differential scanning calorimetry (DSC), thermogravimetric analyses (TGA) and attenuated total reflectance spectroscopy (ATR). In the investigations concerning hypothesis 3, the molecular dynamics (MD) simulations of Dr. Ali Gooneie from the Empa–Swiss Federal Laboratories for Materials Science and Technology, enabled a better understanding of the interfacial interactions occurring between the zirconia powder and the binder. The work conducted in all these studies has been published in two peer-reviewed journal articles and two peer-reviewed conference articles (designated as publications A [34], B [33], C [118] and D [35]).

In parallel to the investigations of feedstock development, the study of the influence of the solvent debinding parameters was investigated for a zirconia feedstock with a binder system previously developed [122]. To validate hypothesis 4, a series of immersion tests in cyclohexane with different debinding parameters were conducted. The solvent debinding performance was characterised in terms of mass loss, the apparition of defects and dimensional variations of the parts. The investigation was conducted by Mr. Dario Kaylani in his bachelor thesis, and the conceptualisation, supervision and analysis of results were conducted by the author of this thesis. The results of this investigation have been published in a peer-reviewed journal article (designated as publication E [119]).

The binder system developed in [122] was also employed in the investigations concerning hypothesis 5. In the last part of the thesis, the effect on the final properties of the FFF shaping parameters, and more specifically of the deposition path of the extruder, was investigated. Bars with three different deposition path directions were shaped by FFF, debound and sintered. The final properties were characterised by means of three-point bending tests, and the defects and porosity distribution were identified and evaluated by different types of microscopy. Additionally, the rheological and mechanical properties of the zirconia feedstock filaments and their thermal degradation behaviour were characterised by the techniques previously mentioned. This investigation was partly conducted by Mr. Philipp Huber in his bachelor thesis, by Prof. Tanja Lube and by the DYPAM group led by Prof. Gemma Herranz. The author of this thesis coordinated the work and participated in all the matters of this investigation. The results of this investigation have been published in a peer-reviewed journal article (designated as publication F [36]).

Figure 3 shows an overview of the aspects of the FFF of ceramics process investigated in this thesis, the information obtained in each processing step and the characterisation techniques employed in the different investigations. The focus of each publication is also indicated with the letter used to designate it (A to F).

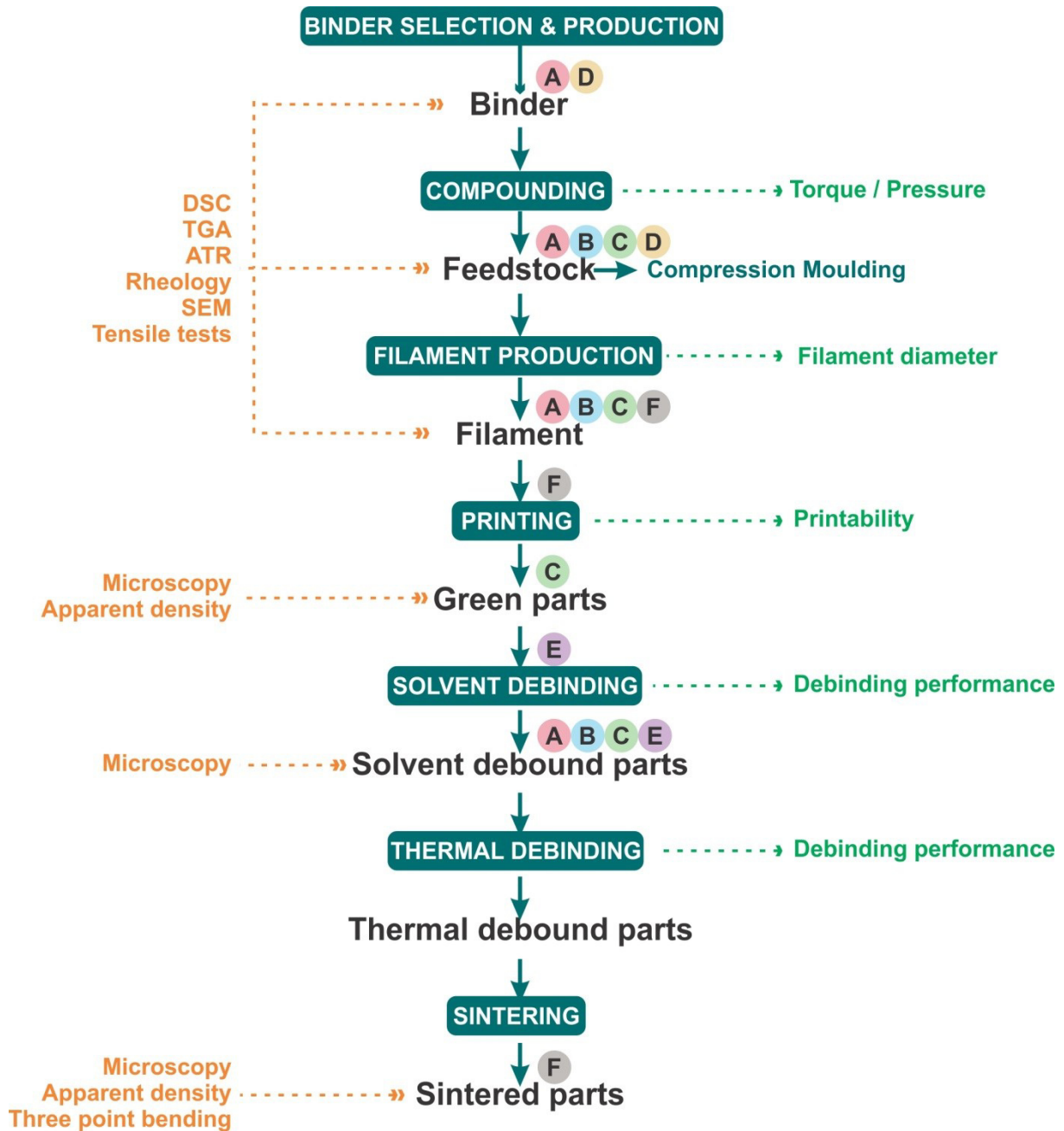


Figure 3: Areas of the Fused Filament Fabrication investigated in this thesis and employed characterisation techniques. The focus of each publication is indicated with its designation letter (A to F).

## 2.3 Outline of the Thesis

This PhD thesis is organised as a compilation of the publications in each of the three topics investigated. Table 4 summarises the publications in each of the research topics and the letters used to designate the publications through the entire thesis. The text of the original publications has been included with only minor format changes to adapt it to the format of this document.

The thesis comprises 6 sections. In section 1, the motivation, background, objectives, and hypotheses have been described. Section 2 presents an overview of the additive manufacturing and ceramic processing fields, the position of FFF as a ceramic processing method, and a brief description of the nature and applications of zirconia. Sections 3 to 5 are dedicated to each of the topics of investigation and are the core of the thesis. In each section, the state-of-the-art is presented, followed by an introduction to link the publications with the thesis objectives and hypotheses. Since section 3 is composed of four different publications, an additional subsection with the summary of the feedstock development process is included. Finally, the conclusions of this thesis, the contributions of the conducted investigations to the research field of ceramic FFF and the research outlook are presented in section 6.

Table 4: Summary of the publications in the main topics of investigation of this PhD thesis. The letter (A to F) used to designate each publication is indicated.

---

<b>Development of novel ceramic feedstock for FFF and solvent debinding</b>	
A	<u>Cano, S.</u> ; Gonzalez-Gutierrez, J.; Sapkota, J.; Spoerk, M.; Arbeiter, F.; Schuschnigg, S.; Holzer, C.; Kukla, C.: Additive manufacturing of zirconia parts by fused filament fabrication and solvent debinding: Selection of binder formulation, <i>Additive Manufacturing</i> 26, 2019, pp. 117–128.
B	<u>Cano, S.</u> ; Cajner, H.; Gonzalez-Gutierrez, J.; Sapkota, J.; Kukla, C.; Arbeiter, F.; Schuschnigg, S.; Holzer, C.: Optimization of material properties for highly-filled thermoplastic polymers used in fused filament fabrication of ceramics, <i>AIP Conference Proceedings</i> 2065, 2019.
C	Kukla, C.; <u>Cano, S.</u> ; Holzer, C.; Gonzalez-Gutierrez, J.: Influence of stearic acid in feedstocks for FFF and PIM, In: EPMA (Ed.), <i>Euro PM2019 Proceedings</i> , European Powder Metallurgy Association (EMPA), Shrewsbury, UK, 2019.
D	<u>Cano, S.</u> ; Gooneie, A.; Kukla, C.; Rieß, G.; Holzer, C.; Gonzalez-Gutierrez, J.: Modification of Interfacial Interactions in Ceramic-Polymer Nanocomposites by Grafting: Morphology and Properties for Powder Injection Molding and Additive Manufacturing, <i>Applied Sciences</i> 10 (4), 2020, 1471.

---

<b>Influence of the solvent debinding parameters on the debinding performance</b>	
E	Kukla, C.; <u>Cano, S.</u> ; Kaylani, D.; Schuschnigg, S.; Holzer, C.; Gonzalez-Gutierrez, J.: Debinding behaviour of feedstock for material extrusion additive manufacturing of zirconia, <i>Powder Metallurgy</i> 62 (3), 2019, pp. 196–204.

---

<b>Influence of the FFF shaping parameters on the properties of the final zirconia parts</b>	
F	<u>Cano, S.</u> ; Lube, T.; Huber, P.; Gallego, A.; Naranjo, J.A.; Berges, C.; Schuschnigg, S.; Herranz, G.; Kukla, C.; Holzer, C.; Gonzalez-Gutierrez, J.: Influence of the infill orientation on the properties of zirconia parts produced by Fused Filament Fabrication, <i>Materials</i> 13 (14), 2020, 3158.

---

## 3 Development of binder formulation

### 3.1 State of the art

#### 3.1.1 Binders for FFF

Agarwala et al. presented the first study on the development of binders for the FFF of  $\text{Si}_3\text{N}_4$  [4]. The process, presented one year earlier by these authors as the Fused Deposition of Ceramics (FDC), was based on the Stratasys FDM technology [6]. In order to process a feedstock by FFF, the characteristics of the process must be considered [4]. The material is molten and solidified during compounding, filament production, and shaping FFF. Therefore, the binder must be composed mostly of thermoplastic polymers.

In the FFF machines, the material is supplied as a continuous filament wound in a spool. Thus, it must possess enough flexibility to enable the spooling, the storage and transport of the spools and for feeding the machine without fracture. High tensile strength is also required for the production of filaments and feeding during shaping. Once the filament is in the machine, two counter-rotating rollers drive it into a liquefier where it melts before being extruded through the nozzle. The solid filament must transmit the force from the rollers and produce the flow of the molten material, which requires a high stiffness to avoid buckling between the rollers and the liquefier. If the material has a high resistance to flow, the force generated by the rollers might not be sufficient to extrude the material, causing the grinding of the filament or the slippage in the contact area. Therefore, a low viscosity is critical for the success of the process. Excellent adhesion between the first layer of extruded material and the build platform is necessary to avoid the separation during shaping. Nevertheless, it should not be excessively strong in order to not damage the components during extraction. The good bonding between the extruded strands and a low viscosity also contribute to reducing the voids and the porosity in the green parts [198]. Finally, the material must have a small shrinkage to avoid internal stresses in the parts that would result in warpage or separation from the building platform [199]. In Figure 4, all the requirements for FFF are summarised.

In addition to all the requirements for FFF, the binder components need to have excellent compatibility to ensure a homogeneous mixture. A high powder content is required in the feedstock to reduce the shrinkage during the sintering phase and reach high densification in the final part [40]. Thus, good bonding between the binder and the powder is desired to facilitate the dispersion of particles and to avoid the powder-binder separation. Moreover, a homogeneous distribution of the binder components in the feedstock is necessary. If the separation between the powder and the binder or any of its components occurs, there is a heterogeneous deposition in the material during shaping which results in defects in the final parts [67, 126]. Finally, the binder must leave no residue and defects after debinding.

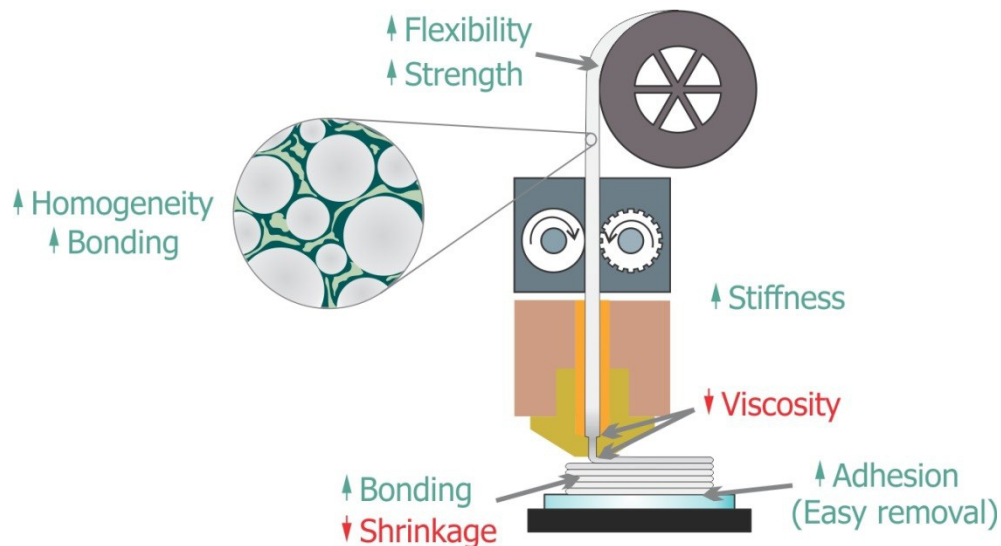


Figure 4: Requirements for the binders systems in FFF

Since it is not possible to attain all the requirements with one single polymer, multicomponent binders are employed. In many cases, a thermoplastic polymer with a good combination of stiffness and flexibility constitutes the major component [6, 68, 88, 122, 143, 162, 166]. Elastomers and plasticizers are commonly employed to improve further the flexibility [4, 138, 143, 162]. Incorporating a polymer with high tackiness as “tackifier” helps to improve the powder-binder adhesion and the bonding between layers [4, 52, 143, 162, 180]. Different types of waxes have also been incorporated frequently to reduce the viscosity of the feedstocks [4, 6, 138, 143, 156, 162, 166]. Finally, the additives help to improve the dispersion of the powder further or reduce the viscosity of the compounds. Stearic acid (SA) is the most common additive and is been incorporated either in the compounding phase [68, 88, 156] or in a prior step of powder milling and coating [144, 225]. In Table 5, a summary of the binder components reported in the literature is shown. Although most of the commercial FFF feedstocks are based in a two-step debinding approach (Table 3), little information is available in the literature regarding the feedstocks for catalytic or solvent debinding. Most of the studies use thermal debinding as the only debinding technique, sometimes in combination with wick debinding. The catalytic debinding of FFF feedstocks has been patented by BASF for a feedstock consisting of polyoxymethylene as the major component and polyolefins and other polymers as backbone and additives [154]. Because of this patent, no studies are dealing with the development of feedstocks for FFF and catalytic debinding. The amount of studies dealing with FFF feedstocks for solvent debinding is also limited, as shown in Table 5.

Table 5: Composition of FFF feedstocks reported in the literature.

Debinding	Binder			Powder	Ref.
	Main component/s	Secondary component/s	Additives		
Thermal	PA	-	Plasticizer Dispersant	316L	[180]
Thermal	ABS	-	-	Al <sub>2</sub> O <sub>3</sub>	[157]
Thermal	EVA	-	SA	TCP	[88]
Thermal	PW	POM	-	316L	[126]
Wick + Thermal	Wax Polymer	Elastomer Tackifier	--	Si <sub>3</sub> N <sub>4</sub>	[3]
Wick + Thermal	Tackifier	Elastomer Wax Polymer	Oleic acid coating	Si <sub>3</sub> N <sub>4</sub>	[4]
Wick + Thermal	Amorphous polyolefin	Tackifier Wax Plasticizer	-	PZT-5H	[143]
Wick + Thermal	Amorphous polyolefin	Tackifier Wax Plasticizer	SA coating	PZT-5H	[144]
Wick + Thermal	PP	Elastomer Plasticizer Tackifier Wax	-	Mixtures of ceramics	[162]
Wick + Thermal	EVA	-	SA	Al <sub>2</sub> O <sub>3</sub>	[49]
Heptane + Thermal	EVA	MA grafted PP	PW as plasticizer SA as surfactant	Al <sub>2</sub> O <sub>3</sub>	[68]
Cyclohexane + Thermal	TPE	Grafted polyolefin	-	316L	[122]
n-hexane + Thermal	PW	LDPE	SA Release agents	Al <sub>2</sub> O <sub>3</sub>	[156]

To reach the right trade-off of properties, the specific concentration of each binder component must be thoroughly adjusted. Round-die capillary rheology tests are the traditional method to determine the viscosity of the feedstocks [121], and the ones closer to the real FFF extrusion process [213].

Three methods are usually used to determine the mechanical properties of the FFF feedstocks (flexibility, strength and stiffness). The minimum bend radius of the filament determines the flexibility of the material [68, 88, 138]. Feedstocks with a low bend radius have high flexibility and are more suitable for spooling without fracture. Tensile tests using normalized specimens [143] or filaments [122, 199] can be used to determine the flexibility, strength and stiffness of the material. Using the maximum strain of the filament in the elastic

deformation region and the corresponding stress, flexibility, and strength can be respectively inferred. In addition, the stiffness of the material can be estimated with tensile tests using the secant modulus of the filament. Nevertheless, the best method to determine the stiffness of the feedstocks and thus, the resistance to buckling is the mechanical testing of small pieces of filament under compression [179, 213].

As was previously stated, both the viscosity and the stiffness of the feedstock determine the tendency to buckle. According to Venkataram et al. [213], the filament buckles when the extrusion pressure ( $\Delta P'$ ) exceeds the critical buckling stress of the material ( $\sigma_{cr}$ ). Assuming that the critical stress is equal to the buckling stress by Euler's criterion [21] and that there is a linear scaling factor correlating the pressure drop in the capillary rheometer [14] with the one during shaping by FFF, the filaments buckles when:

$$E/\eta_a < \frac{32Ql(L/R)^2}{\pi^3 r^4 k} \quad (1)$$

Where  $E$  is the elastic modulus of the material,  $R$  is the radius of the filament,  $Q$  is the volumetric flow,  $\eta_a$  is the apparent viscosity, and  $r$  and  $l$  are the radius and length of the capillary employed in the rheometer. By compression tests on the filaments and apparent viscosity measurements on feedstocks with different binders and powders, Venkataram et al. [213] concluded that the buckling of the filaments would occur when the  $E/\eta_a$  parameter is below the experimental critical range of  $3 \times 10^5$  to  $5 \times 10^5 \text{ s}^{-1}$  in the typical range of shear rates for FFF ( $100$  to  $200 \text{ s}^{-1}$ ) [213]. Similar work was conducted by Rangajaran et al. [179] for a  $\text{Si}_3\text{N}_4$  feedstock containing 55 vol% of powder. These authors assumed that the parameter defining the relation between the pressure measured in the capillary rheometer and the pressure in the FFF nozzle is proportional to the diameter difference in both devices and equal to 1.1 [179].

The thermal stability and degradation of the binder components is another aspect to be considered in the development of new binders. Lombardi et al. [138] employed Differential Scanning Calorimetry (DSC) to determine the stability of a  $\text{Si}_3\text{N}_4$  feedstock. The ageing of the wax in the feedstock at room temperature could be detected in the increase of the melting point and crystallinity and resulted in an increase of the minimum bend radius of the filament (i.e. in a flexibility decrease) [138].

The Thermogravimetric Analyses (TGA) of the binder components and the feedstock measure the mass loss over the temperature in a controlled atmosphere. Therefore, they are commonly used to program the temperature cycles in thermal debinding [13]. TGAs can also be used to select the polymers most suitable to undertake thermal debinding progressively without damaging the parts. For instance, Pekin et al. [165] employed TGAs under air and  $\text{N}_2$  to measure the degradation of microcrystalline wax and Ethylene Vinyl Acetate (EVA) of different molecular weights as candidates for the FFF of alumina. For the microcrystalline wax, an easy and controlled thermal debinding could be conducted; whereas it is difficult to have a controlled removal for the EVA with high molecular weight [165]. The problems in the thermal degradation of EVA have also been reported for the FFF feedstock developed by Gorjan et al. [88]. During the thermal decomposition of the binder, a dense layer partially cross-linked polymer formed in the surface of the parts and hindered the evacuation of gases, resulting in defects during debinding [88]. These problems could only be solved by the use

of long thermal debinding cycles and the use of wick debinding, as reported by the authors in a second study [49].

#### **3.1.2 Binders for solvent debinding**

Through the years, different binder systems have been developed for the debinding with solvents. Depending on the solvent used, the binders can be classified in those which can be removed with organic solvents, and those soluble in water. Following, the state-of-the art in the development of binders for solvent debinding for powder injection moulding is presented. Despite the feedstocks shown in Table 5 are available for FFF, the focus of those studies was on other aspects of the FFF process rather than the binder requirements for solvent debinding.

##### 3.1.2.1 Binders for debinding in water

The water debinding process was initially developed by Rivers in 1978 for binders based on methylcellulose or polyvinyl alcohol [181]. During the years, different polymers have been studied as the water-soluble component of the binder [182]: Polyethylene Glycol (PEG), Polyvinylpyrrolidone (PVP), Isobutylene and Maleic Anhydride (ISOBAM), Polyvinyl Alcohol (PVA), Polyacrylic Acid (PAA) or Poly(2-ethyl-2-oxazoline). The use of alternative substances, such as tapioca starch, has been reported as well [2].

Among all the water-soluble polymers, PEG is well known as a very safe chemical and is widely used in the food and medical industry [230]. Different backbone polymers have been combined with PEG to find a suitable binder system e.g. Polypropylene (PP) [38, 128, 184, 206, 211], Polyethylene (PE) wax [229, 230], Linear Density Polyethylene (LDPE) [94], Polyvinyl Butyral (PVB) [117, 203], Poly(Methyl Methacrylate) (PMMA) [39, 44, 96, 137], Cellulose Acetate Butyrate (CAB) [99, 164] or mixtures of different waxes for a processing at lower temperature [94, 95].

When comparing the compositions of the binders from the literature, the maximum volume fraction of PEG in the composition is approximately 70 vol.% for most of the backbones. The exception is the systems based in PMMA, for which PEG concentrations up to 90 vol.% have been reported by Omar et al. [161]. In their study, Omar et al. proved that despite the debinding rate is improved by increasing the PEG fraction, the mechanical properties of the feedstock, and thus of the green parts, are reduced.

The influence of the PEG molecular weight in all the stages of the process has been extensively studied. Park et al. combined CAB with PEGs of different molecular weight for the MIM of two stainless steel powders. The solvent debinding was performed in distilled water at room temperature for 12 hours. The increase of the PEG molecular weight produced the increase of the swelling and the cracks in the parts. According to the authors, the difference was caused because of the size of the PEG crystals. PEGs with higher molecular weight have big crystals, and a bigger area is exposed to the solvent, increasing the swelling [164]. Hayat et al. performed a similar study with titanium feedstocks containing PMMA and PEGs of different molecular weights. The water debinding at 50 °C and different times was performed. The increase of PEG molecular weight produced not only the increase of the



swelling but also the reduction of the debinding rate in water. The cause of both phenomena might be the reduction of the diffusion of the dissolved molecules with a bigger size. Since the water penetrates faster in the parts, the sample expands, and the cracks appear [96].

For the rest of the systems, most of the compositions have been protected by patents [218]. For example, binders based on Polyvinyl Alcohol (PVOH) together with polyolefins such as PE or PP were patented by Xiaoming Yang et al. for the use in feedstocks with at least 70 wt.% of metal or ceramic powder [231].

#### 3.1.2.2 Binders for debinding in organic solvents

The wax-based systems are the most common for the debinding in organic solvents. The one-component binders developed by Wiech [221] were the first of this kind. The debinding was a long and complicated process, in which the parts were first heated up to the flow point of the polymer; then a solvent in vapour state was introduced to remove most of the organic components; finally, the solvent condensed and the parts were immersed in the liquid solvent. Depending on the geometry and thickness of the green parts, the time required for effective removal of the binder could go up to a few days.

Since then, a whole set of different polymers have been studied, predominantly for the debinding by immersion in a liquid solvent. Paraffin Wax (PW) has been one of the preferred binder components, due to its proper flow ability, low melt temperature and reactivity with many organic solvents [32]. Heptane [98, 102, 106, 160, 174, 220, 242], hexane [32, 236] and isooctane [236] are examples of the solvents which used for debinding PW.

The influence of the PW density in the debinding stage was studied by Westcot et al., who compared two paraffin waxes with different densities. The dissolution of the higher density PW was slower, as well as the diffusion of the swollen dissolved molecules. Since the extraction of the swollen molecules takes longer, the forces that they exert in the rest of the polymers are more prominent, and the dimensional changes during the process are more brusque [220].

The standard backbones for the wax-based systems are polyolefins such as PP [32, 106, 160], PE [98, 102, 103, 149, 174], EVA [236, 237] and combinations of them [220, 242], since they are not affected by most of the solvents and can preserve the shape of the parts during the process.

Comparative studies of feedstocks containing PW and different backbones have been performed. E.g. Lin et al. compared PP versus LDPE as the backbone in the debinding in heptane of feedstocks containing PW and Stearic Acid (SA). PP was the best option due to the smaller dimensional changes during the immersion in the solvent [133]. The effect of the density of the polyethylene was studied by Huang et al., who after comparing feedstocks with low and high density polyethylene, obtained worse dimensional stability results in the solvent debinding of LDPE feedstocks [103]. Similar results have been obtained by Zhao et al. [240] for zirconia feedstocks for injection moulding with different fractions of LDPE and HDPE in the backbone. The increase of the LDPE fraction resulted in cracks due to the large swelling of this polymer. However, the solvent debinding rate increased with the increase of

the LDPE fraction in the feedstock, which according to these authors was produced by the lower entanglement of the polymer molecules [240].

The influence of the backbone content in the solvent debinding was studied by Westcot et al. [220]. A higher swelling was observed for those feedstocks with more backbone content. The backbones, PP and LDPE, were not dissolved by heptane, but it produced their swelling. The reason was the increase of the swelled polymer which cannot be dissolved, which additionally reduced the volume of the porosity that the dissolved polymer uses to diffuse out of the specimens [220]. Nevertheless, the backbone content must be high enough to ensure the presence of an interconnected backbone-powder structure as reported by Wen et al. [219]. In the zirconia injection moulding feedstocks evaluated by these authors with different backbone contents, a minimum of 30 wt.% of backbone was required to avoid the apparition of cracks.

The incorporation of additives can improve the solvent debinding behaviour in wax-based systems. Setasuwon et al. [189] reported the increase of the debinding rate in petroleum ether when a fraction of the PW was substituted by palm oil; this improvement was attributed to the faster dissolution of the palm oil [189]. However, the incorporation of non-soluble additives can also improve the debinding rate. For instance, Ye et al. [234] reported the increase of the debinding rate when the PW in strontium ferrite feedstocks was partly substituted by microcrystalline wax. Despite the microcrystalline wax was not soluble in the n-heptane employed as a solvent, its incorporation resulted in an improvement of the homogeneity and thus in an increase of the debinding rate [234]. The coating of the powder with silane results in the same homogenization effect, as demonstrated by Deng et al. for zirconia feedstocks [57].

Besides PW, other polymers are used as the primary component. E.g. Palm stearin, the solid fraction of the crystallization of palm oil [132], has been successfully used with PE in the solvent debinding of feedstocks in heptane [22, 93, 216]. Other examples of alternative binders include restaurant waste fats and oils [109] and thermoplastic rice starch [8].

## 3.2 Introduction to publications A, B, C and D

The work in publications A, B, C and D covers the main part of this thesis, the development of a novel binder formulation for the fused filament fabrication and solvent debinding of zirconia parts. Three hypotheses were proposed in this regard based on the state-of-the-art:

1. ***By the right combination of binder components, a high strength, stiffness and flexibility, as well as low viscosity could be obtained as required for FFF.***
2. *Solvent debinding requires two types of components. First, a major fraction of the binder must be leached with a solvent. The rest, known as backbone, must maintain the shape of the parts during the process and be removed in the subsequent thermal debinding step. **The combination of the right soluble binders and backbones should enable the use of solvent debinding in FFF.***
3. ***The use of a polymer grafted with polar groups as backbone should result in an improvement of the adhesion to the polar surface of the zirconia powder. A high powder-binder adhesion should result in a more homogeneous feedstock, with lower viscosity and with higher mechanical properties.***

The first step conducted was the pre-selection of the best candidates for the binder components. In the pre-selection process, many different polymers were selected based on their mechanical properties and chemical resistance as backbones or their solubility as major binder components. Polymers soluble in different organic solvents and water were selected. In total, more than 100 binder and feedstock formulations were investigated looking for the combination of high strength and flexibility, low viscosity and no defects during solvent debinding. As a result of the pre-selection process, high density polyethylene grafted with acrylic acid was selected as the backbone and stearic acid as a surfactant to improve the powder dispersion. For the major binder fraction soluble in cyclohexane, an amorphous polyolefin and a styrene-ethylene/butylene-styrene copolymer were chosen as possible components due to their flexibility. Paraffin wax and paraffinic extender oil were selected as a possible second soluble binder due to their low viscosity and low swelling during dissolution.

In the work presented in publication A, a detailed investigation was conducted for the selection of the soluble binder components based on the properties required for FFF and solvent debinding. Unfilled binder systems and feedstocks of zirconia were evaluated to get a better understanding of the binder-binder and powder-binder interactions. The selected soluble binders resulted in a feedstock with a proper combination of mechanical properties, low viscosity and no debinding defects.

Once the binder components were selected, two investigations were conducted. The first investigation, presented in publication B, was the statistical analysis of the effect of the main binder components fractions on the feedstock properties. The second investigation was presented in publication C and was focused on the effect that the SA incorporation could have on the feedstock properties and its processability by FFF and solvent debinding.

Publication D focuses on hypothesis number 3, i.e. in the study of the high density polyethylene grafted with acrylic acid used as backbone. The use of a grafted polyolefin as

the backbone in FFF soluble feedstocks [68, 87, 122] and PIM feedstocks [223] is known to improve the powder dispersion and reduce the defects of the components. However, no detailed investigation has been conducted so far on the phenomena causing these improvements. In publication D, a first step was taken in understanding the interfacial interactions between the powder and the grafted backbone and the effect on the feedstock properties for the processing by FFF.

### 3.3 Publication A

#### ***Additive manufacturing of zirconia parts by fused filament fabrication and solvent debinding: Selection of binder formulation***

Santiago Cano<sup>a\*</sup>, Joamin Gonzalez-Gutierrez<sup>a</sup>, Janak Sapkota<sup>a</sup>, Martin Spoerk<sup>a</sup>, Florian Arbeiter<sup>b</sup>, Stephan Schuschnigg<sup>a</sup>, Clemens Holzer<sup>a</sup>, Christian Kukla<sup>c</sup>

**Additive Manufacturing, 26 (2019) 117-128**

doi: 10.1016/j.addma.2019.01.001

Received: 29.11.2018

Revised: 07.01.2019

Accepted: 07.01.2019

Available online: 28.01.2019

#### **ABSTRACT**

The material extrusion additive manufacturing technique known as fused filament fabrication (FFF) is an interesting method to fabricate complex ceramic parts whereby feedstocks containing thermoplastic binders and ceramic powders are printed and the resulting parts are subjected to debinding and sintering. A limiting factor of this process is the debinding step, usually done thermally. Long thermal cycles are required to avoid defects such as cracks and blisters caused by trapped pyrolysis products. The current study addresses this issue by developing a novel FFF binder formulation for the production of zirconia parts with an intermediate solvent debinding step. Different unfilled binder systems were evaluated considering the mechanical and rheological properties required for the FFF process together with the solvent debinding performance of the parts. Subsequently, the same compounds were used in feedstocks filled with 47 vol.% of zirconia powder, and the resulting morphology was studied. Finally, the most promising formulation, containing zirconia, styrene-ethylene/butylene-styrene copolymer, paraffin wax, stearic acid, and acrylic acid-grafted high density polyethylene was successfully processed by FFF. After solvent debinding, 55.4 wt.% of the binder was dissolved in cyclohexane, creating an interconnected porosity of 29 vol.% that allowed a successful thermal debinding and subsequent pre-sintering.

*Keywords:* Fused filament fabrication; material extrusion; highly-filled polymers; solvent debinding; zirconia.

## 1. Introduction

The rapid developments of additive manufacturing (AM) have enabled the transition from a rapid prototyping technique to a broad technology capable of making three dimensional (3D) objects via layer-wise assembling of components from computer-aided-design (CAD) data. One of these processes is the material extrusion additive manufacturing technique known as fused filament fabrication (FFF), in which polymer-based compounds in the shape of filaments are extruded and deposited in a layer-wise manner to create 3D objects [1]. With comparably low investment costs required, FFF facilitates the cost-effective and flexible production of customized parts with intricate designs. The production of ceramic and metallic objects by FFF is also possible, as demonstrated for silicon nitride [1,2], alumina [3,4], lead zirconate titanate [5,6], mullite [7], fused silica [8,9], stainless steel [10,11], zirconia [12], neodymium-iron-boron [13], or titanium [14] components. In general, there are no restrictions concerning the selection of the ceramic or metallic material, which enables a broad range of potential applications such as the production of multi-material multilayer piezoelectric transducers [6] or components combining electrical insulating and conductive properties [12]. For a detailed comparison of FFF to other AM techniques for producing metals and ceramics, several overviews can be found in the literature, such as [15–19].

In order to produce ceramic or metallic parts by FFF, thermoplastic compounds are highly-filled (ca. 50 vol.%) with ceramic or metallic powder to produce a feedstock, which is extruded to filaments. The polymeric components in the feedstock (also known as binder) act as a carrier of the powder and enable the shaping of parts. Once the parts are produced by FFF, the polymers are removed in the so-called debinding step. Subsequently, the components are sintered to attain densities comparable to those fabricated via conventional approaches [2].

The required properties of the feedstocks and, thus, of the binders are determined by the characteristics of the FFF process [5,19–24]. Binders and powders need a good compatibility to ensure homogeneity in mixing and to avoid phase separation during processing. The flexibility and strength of the resulting filament should be sufficient to spool/de-spool the filament for its storage and printing. Concurrently, appropriate stiffness of the filament is needed to avoid buckling during printing. The viscosity of the feedstock should be low enough to enable the flow through the printing nozzle with minimum resistance to reduce the backup pressure. For highly-filled polymeric compounds this is quite challenging to achieve, especially for submicron powders due to the high tendency for particle agglomeration, which increases the resistance to flow [25]. In addition, the adhesion to the building platform must be good enough to avoid separation during shaping, but should not be excessively strong in order not to damage the components during the extraction from the build platform [26–28]. A good bonding between the deposited strands is required to achieve good properties of the produced part [1,5,29,30]. Furthermore, the thermoplastic binder should be easily removable without defects [31,32]. All these requirements form a technical obstacle and therefore hinder the expansion of the FFF process for the production of ceramic and metallic components.

To meet all the requirements of the process, different multi-component binder compositions have been proposed in literature [5,33,34]. In addition to the main binder, other

components such as elastomers, tackifiers, waxes or plasticizers must be included to attain a good balance of properties. In all these cases, the removal of the binder system was conducted in a single step thermal debinding cycle, in which the polymers evaporate and/or decompose. Nevertheless, the decomposition occurs in the entire volume of the component, generating trapped residual gases that can lead to internal stresses and defects [31,32]. One alternative to this approach is the use of a prior step of catalytic debinding [35], which is limited to polyoxymethylene based binders. Another alternative is the dissolution of the major fraction of the binder in either organic solvent or water. This generates an open-pore structure, in which the powder is held together by the component known as backbone. The backbone is then removed in a second step of thermal debinding, in which the thermal decomposition gases can be easily evacuated using the existing porosity [36,37]. The production of metallic components by FFF through a two-step debinding process has been demonstrated [11] and is commercially available [38]. However, little information about the binder recipes employed for such combinations is publically available, and a detailed understanding of the type of thermoplastic-based binders required for the production of ceramic components by FFF and solvent debinding is missing.

Hence, this study presents the development process of a novel formulation for the FFF and solvent debinding of zirconia parts. A better understanding of the soluble binder components' selection process is developed based on the influence of these components on the mechanical and rheological properties as well as on the capability to conduct a defect-free solvent debinding step. Finally, the processability of the developed feedstock is demonstrated by shaping components of different geometries by FFF, together with the debinding and pre-sintering of the printed parts to obtain zirconia components.

## 2. Materials and methods

### 2.1. Materials and selection criteria

Tetragonal zirconia ( $ZrO_2$ ) (TZ-3YS-E, partially stabilized with 3 mol% yttria ( $Y_2O_3$ ), Tosoh Europe B.V., The Netherlands), supplied as spray dried granules with an average particle size of 90 nm and a specific surface area of  $7 \pm 2 \text{ m}^2 \cdot \text{g}^{-1}$ , was the powder used to produce the ceramic feedstocks. Fig. 1 depicts the scanning electron microscopy (SEM) image of the powder, as provided by the supplier without a binder.

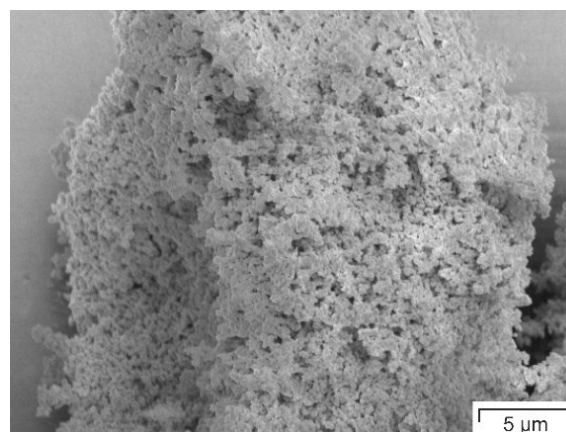


Fig. 1. SEM of the zirconia powder partially stabilized with yttria.

Based on previous studies dealing with the development of binders for FFF [5,19,33,34,39], multicomponent binders were designed in order to meet all the processing requirements. The systems were composed of a backbone, a surfactant, and a major fraction of soluble binder. Due to the poor strength of the powder network and the swelling occurring during the dissolution of polymers [40], the backbone is necessary to maintain the shape of the parts during the dissolution of the rest of the components. Thus, a good chemical resistance and low swelling during solvent immersion are required for the backbone [41,42]. In addition, a good adhesion to the powder surface is desired in order to improve its dispersion. For powders with polar surfaces, improved adhesion can be attained by the use of binders grafted with polar reactive groups [43]. The attenuated total reflection Fourier-transform infrared spectrogram of the zirconia powder (the detailed curve is presented in Fig. S1 in the supporting information) revealed a maximum peak intensity at  $3355\text{ cm}^{-1}$ , confirming the polar -OH groups on its surface [44]. Hence, the acrylic acid-grafted high density polyethylene SCONA TPPE 2400 (AA-HDPE, BYK-Chemie GmbH, Germany) was selected as a backbone in order to improve the mechanical properties required for FFF and the powder dispersion. Since the zirconia powder has a large surface area and a tendency to agglomerate [45], stearic acid (SA, Merck Schuchardt OHG, Germany) was incorporated as a surfactant to facilitate particle dispersion in the binder and prevent re-agglomeration [44,46].

The selection of the soluble components was based on a first set of screening experiments that fulfilled the requirements for FFF (i.e. high flexibility, strength and stiffness, and moderately low viscosity) and solvent debinding, as they showed good solubility in cyclohexane. The amorphous polyolefin Aerafin 180 (APO, Eastman Chemical Company, USA) and the styrene-ethylene/butylene-styrene copolymer MD1653 (SEBS, Kraton Polymers Nederland B.V., The Netherlands) were chosen as possible main soluble binders. The incorporation of a second soluble component with a low viscosity and swelling during the dissolution was also tested. The paraffin wax Sasolwax 6403 (PW, Sasol Limited, South Africa) and the highly paraffinic extender oil Risella X 430 (EO, Shell Oil Company, USA) were selected to this end.

The effect of the soluble component 1 (SEBS or APO) and the soluble component 2 (PW or EO) on the properties was studied based on the unfilled binder formulations summarized in Table 1. Since the objective was the selection of the soluble binders and not the optimization of the whole system, the concentration of the different types of components was fixed and kept constant in all the formulations to avoid the performance of an excessive number of experiments which would be impossible to realize within the scope of this work. Through the whole manuscript, the nomenclature used to name the unfilled compounds consists of two parts: X/Y, in which X refers either to SEBS or to APO; and Y indicates, which low viscosity component (No (no low viscosity component), PW or EO) was used. The ability of the binder components to bind to and disperse the powder were evaluated in feedstocks with 47 vol.% zirconia powder and the binder systems from Table 1. For the composite feedstocks a Z was included in the nomenclature to indicate the presence of zirconia powder. For more details on the composition of feedstocks please refer to Table S1 in the supplementary information.

Table 1. Composition of the polymeric binders in volumetric percentage. APO and SEBS refer to the amorphous polyolefin and styrene-ethylene-butylene copolymer, respectively. 'No' refers to the binder systems without a second soluble component, whereas PW and EO refer



to the binder systems with paraffin wax and highly paraffinic extender oil, respectively. AA-HDPE refers to the acrylic-acid grafted high density polyethylene and SA to the stearic acid.

	<b>Backbone</b>	<b>Surfactant</b>	<b>Soluble comp. 1</b>		<b>Soluble comp. 2</b>	
	<b>AA-HDPE</b>	<b>SA</b>	<b>APO</b>	<b>SEBS</b>	<b>PW</b>	<b>EO</b>
<b>APO/No</b>	35	10	55	-	-	-
<b>APO/PW</b>	35	10	27.5	-	27.5	-
<b>APO/EO</b>	35	10	27.5	-	-	27.5
<b>SEBS/No</b>	35	10	-	55	-	-
<b>SEBS/PW</b>	35	10	-	27.5	27.5	-
<b>SEBS/EO</b>	35	10	-	27.5	-	27.5

## 2.2. Preparation of compounds

All the binders were prepared in an internal mixer fitted with counter rotating roller rotors with a mixing chamber volume of 300 cm<sup>3</sup> (HAAKE Rheomix R3000p, Thermo Fisher Scientific Inc., USA). Mixing was performed at 160 °C and 60 rpm. The compounding sequence for the binders can be found in Table 2. The mixing was continued for the total mixing time of 30 min. Due to the smaller quantity available of the powders, a similar mixer system (Plasti-Corder PL2000, Brabender GmbH & Co. KG, Germany), but with a smaller volume of the mixing chamber (38 cm<sup>3</sup>), was employed to produce the feedstocks. Prior to the compounding, the zirconia powder was dried in the vacuum oven Binder VD 23 (Binder GmbH, Germany) at 180 °C for 1 hour to reduce the moisture content and, hence, subsequent agglomerations during mixing [25]. Subsequently, the method described in Table 2 was employed for the production of the feedstocks. The mixed compounds were extracted from the chamber in the molten state, cooled down to room temperature and granulated using the cutting mill Retsch SM200 (Retsch GmbH, Germany) equipped with a sieve with 4×4 mm<sup>2</sup> square perforations.

Table 2. Compounding sequence for producing the binders and feedstocks.

<b>Binder compounding</b>		<b>Feedstock compounding</b>	
<b>Time (min)</b>	<b>Operation</b>	<b>Time (min)</b>	<b>Operation</b>
0	Adding backbone and surfactant	0	Adding powder and surfactant
5	Adding soluble component 1 and 2	5	Adding backbone
30	Extraction	10	Adding soluble component 1 and 2
		75	Extraction

#### 2.3. Filament production

The filaments of the binders were produced using the filter test single screw extruder FT-E20T-MP-IS (Dr. Collin GmbH, Germany). Tests were performed at a screw speed of 30 rpm and at temperatures from 120 to 140 °C (from solid conveyor zone to the extrusion die). A round die with a diameter of 1.9 mm and a length of 10 mm was used in all cases. The extruded material was then cooled down in a water bath at room temperature and wound onto spools using an in-house manufactured spooling device. The laser-measurement device Diagnostic Laser 2000 (SIKORA AG, Germany) was placed after the water bath to determine the diameter and ovality of the filament.

Since the amount of feedstock material produced was much smaller than that of the binder systems, the feedstock filaments were produced in the high pressure capillary rheometer Rheograph 2002 (Göttfert Werkstoff-Prüfmaschinen GmbH, Germany) with a die of 1.75 mm in diameter and 30 mm in length. The extrusion temperature was set to 150 °C and the piston (diameter 15 mm) speed to  $1 \text{ mm}\cdot\text{s}^{-1}$ . The extrudate was cooled down to room temperature as it was transported on a polytetrafluoroethylene (PTFE) conveyor belt.

#### 2.4. Rheological evaluation

The rheological evaluation of the binder systems was conducted using the rotational rheometer MCR 501 (Anton Paar GmbH, Austria). The measurements were performed under nitrogen atmosphere to avoid a possible degradation of the material. Parallel-plates with a diameter of 25 mm and a gap of 1 mm were used in oscillation measurements in a rate-controlled mode. Oscillatory measurements were used in order to increase the range of shear rates that are measurable without leading to melt fracture or sample expulsion, which can occur when measurements are performed in constant rotational mode. First, strain-sweep measurements were conducted at a constant angular frequency of  $1 \text{ rad}\cdot\text{s}^{-1}$  to determine the linear viscoelastic region of the material and to prevent the damage of the elastic structure of the material [47]. Using the information from these tests, a strain value of 1 % was used during the dynamic rheological tests (i.e. frequency sweep) at angular frequencies from 0.1 to  $500 \text{ rad}\cdot\text{s}^{-1}$ . All the tests were conducted at a temperature of 150 °C, and three repetitions were carried out for each material.

For the feedstocks, the apparent viscosity was measured during the filament production in the high pressure capillary rheometer Rheograph 2002. The speed of  $1 \text{ mm}\cdot\text{s}^{-1}$  led to a shear rate at the walls of the die of  $215 \text{ s}^{-1}$ . The reasons for using the capillary rheology method instead of oscillatory rotational rheology are twofold. Firstly, for highly filled polymers, the shear rates that can be measured are limited to shear rates smaller than  $100 \text{ s}^{-1}$  [46]. Thus, the viscosity values obtained are non-applicable to the FFF process. Secondly, the different binders cause different normal forces in the rotational rheometer for the feedstocks investigated. When a higher initial normal force is applied to the feedstock, the number of particle interactions increases. Thus, the measured viscosity values are artificially increased and therefore it makes a direct comparison irrelevant [46]. Additionally, during the capillary rheology process the feedstock is forced to flow through a die, which is a comparable situation to the transportation of the feedstock through the FFF nozzle [5].

#### **2.5. Tensile tests**

The mechanical properties of the compounds were measured by means of tensile tests on the filaments. By this approach the ability of the materials being processed by FFF can be inferred [22,48]. Straight filament specimens with a length of 100 mm were tested on the universal testing machine Zwick Z001 (Zwick GmbH & Co.KG, Germany) with a 1 kN load cell and pneumatic grips. An initial gauge length of 50 mm was set for all the measurements. The tests were performed at standardized conditions (23 °C and 50 % relative humidity), at a speed of 10 mm·min<sup>-1</sup> until the rupture of the specimen. At least five repetitions per material were performed. Since specimens were not tapered in the center, special care was taken to avoid premature fracture at the grip area.

#### **2.6. Solvent debinding**

The specimens for the solvent debinding were produced by compression molding, which was used to compare the solubility of the binder components at the first stage of the binder development, before checking the processability by FFF. Cylindrical specimens with a height of 5 mm and a diameter of 8 mm were produced in the hydraulic vacuum press P200PV (Dr. Collin GmbH, Germany). Prior to the pressing, the materials were pre-compressed by hand at room temperature and PTFE seals were used to avoid leakage of the material. The filled mold was pre-heated at 160 °C during 40 min at a pressure of 1 bar, compressed at 50 bar during 5 min and finally cooled down to room temperature at a pressure of 50 bar [49].

Once the specimens were produced, the solvent debinding performance was evaluated using cyclohexane (Carl Roth GmbH & Co. KG, Germany) as a solvent. A glass desiccator enclosed within an oil bath unit with a temperature control (Memmert GmbH, Germany) was used. The solvent was refluxed with a Dimroth condenser attached to the lid to prevent the evaporation of the solvent. The specimens were placed in holders of known mass and the total mass was measured. Then they were immersed in pre-heated cyclohexane at 60 °C for 6 hours, with 12 ml of solvent per gram of binder or feedstock material. After 6 hours in the solvent, the specimens were dried in the vacuum drying oven Binder VD 23 (Binder GmbH, Germany) at 80 °C for at least 2 hours. The final mass was measured to evaluate the percentage of leached binder. At least four specimens were measured per formulation at a given time.

#### **2.7. Morphology analyses**

The morphology of the filaments of the zirconia feedstocks was studied by scanning electron microscopy (SEM, Tescan Vega II, Tescan Brno, s.r.o., Czech Republic) to determine the capability of the binders to disperse the zirconia powder. The cryo-fractured surface was analyzed for the extruded filaments as well as for those immersed in cyclohexane at room temperature for 18 hours. The analyses were performed on gold sputtered (100 s at 20 mA) specimens at 5 kV using secondary electrons.

## 2.8. Production upscaling and printing trials

Once the most promising formulation was selected that met the requirements for both FFF and solvent debinding, the upscaling of the feedstock production and the printing was performed. Two batches of the feedstock (ca. 720 g each) were pre-compounded for 30 min in the HAAKE Rheomix R3000p using the same procedure as described above (Table 2). The pre-compounded feedstocks were later filled in the co-rotating extruder Leistritz ZSE 18 HP-48D (Leistritz Extrusionstechnik GmbH, Germany), which ensured a better dispersion and distribution of the filler particles in the binder system. The pre-compounded feedstock was added at a rate of  $6 \text{ kg}\cdot\text{h}^{-1}$  and the screw speed was set to 600 rpm. Extrusion temperatures from 165 to 175 °C were used, and the extruded material was collected and pelletized (Reduction Engineering GmbH, Germany). The filaments for FFF were produced using the same filter test single screw extruder FT-E20T-MP-IS as for the binder, but for the zirconia composites it was equipped with a round die with a diameter of 1.75 mm and a length of 10 mm. The screw rotation was lowered to 25 rpm, and the extrusion temperatures were between 155 and 160 °C. The extruded material was transported with a PTFE conveyor belt, on which it cooled down to room temperature by natural convection. The diameter and ovality of the filaments were recorded using the Diagnostic Laser 2000 device.

Using these filaments, four different CAD models were printed: 4 point bending bars, a watch case [50], a monolithic catalyzer, and the holder for a thermocouple used during the filament production. The Cura slicer software was used for the generation of the G-code. The parts were produced by means of the Duplicator i3 v2 (Wanhao, USA) FFF machine. A brass nozzle of 0.6 mm in diameter coated with TwinClad® was used for the printing at a temperature of 190 °C. In Table 3 the printing parameters employed for each of the test specimens are summarized. The layer thickness was set to 225  $\mu\text{m}$  in all the geometries, except in the thermocouple holder, for which a layer thickness of 100  $\mu\text{m}$  was used to achieve a better surface finish. A paper tape glued to a glass mirror set to 80 °C was used as the build platform. For the production of the watch case, support structures were produced with the feedstock using a low infill and later removed manually. For more details about the printing process, please refer to Table S2 in the supporting information.

Table 3. Printer settings for each of the demonstrators.

	<b>4 Point bending bars</b>	<b>Watch case</b>	<b>Monolithic catalyzer</b>	<b>Holder for thermocouple</b>
<b>Layer thickness (mm)</b>	0.23	0.23	0.23	0.1
<b>Number of perimeters</b>	1	1	2	2
<b>Infill (%)</b>	180	110	100	100
<b>Infill orientation (° C)</b>	0	±45	-	±45
<b>Printing speed perimeter (<math>\text{mm}\cdot\text{s}^{-1}</math>)</b>	24	10	16.25	12.5
<b>Printing speed infill (<math>\text{mm}\cdot\text{s}^{-1}</math>)</b>	12	10	-	12.5

The solvent debinding of the FFF specimens was then conducted as described above (section 2.6) with a cyclohexane volume of 700 ml. To ensure the formation of an interconnected porosity in the solvent-debound parts, and to facilitate the subsequent thermal debinding, an immersion time of 24 hours was employed. The thermal debinding and pre-sintering of the specimens was conducted under air in the muffle furnace Nabertherm LT 40/11/B180 (Nabertherm GmbH, Germany). In Fig. 2, the thermal cycle employed is shown, including the progressive thermal debinding up to 600 °C and a pre-sintering step at 1050 °C. The parts were then left in the furnace to cool down by natural convection to room temperature. Due to the limitations of the furnace used, a higher sintering temperature could not be employed.

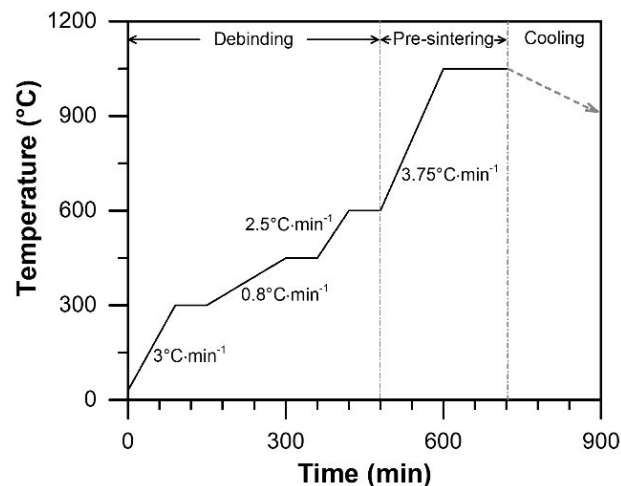


Fig. 2. Thermal debinding and pre-sintering cycle applied for the printed specimens starting at room temperature. Once the cycle was finished, the parts were left in the furnace to cool down by natural convection to room temperature.

### 3. Statistical analysis

Similarly to Refs. [51–53], a one-way analysis of variance followed by Tukey's post hoc tests (with a confidence level of 0.05) were used to determine whether the differences in the viscosity, tensile properties and leached binder values of the different compounds are statistically significant. The software Minitab 17 (Minitab Inc., USA) was used for the analyses. The results in the graphs were reported using the mean and standard deviation.

## 4. Results and discussion

### 4.1. Evaluation of the binders

The first part of this study focuses on the evaluation of the unfilled binder systems to determine the properties of each material combination prior to the feedstock evaluation. This approach enables a better understanding of the compatibility of the binder components and resulting properties, as demonstrated by McNulty et al. [5] for the development of FFF binders and by Herranz et al. [54] for PIM binders. Nevertheless, the results of the present study must be considered together with those of the feedstock characterization, since the incorporation of the powder drastically changes the rheological behavior of the compounds [54] as well as the mechanical properties of the FFF filaments [24].

#### 4.1.1. Rheological behavior of binders

The viscosity of the compound plays a critical role during the extrusion of the material in FFF, in which the filament must act as a piston to produce the flow of the molten compound [19]. In Fig. 3 a comparison of the viscosity curves for the investigated binder systems is depicted. Shear thinning behavior was detected for all the compounds at high angular frequencies, and a clear influence of the composition can be observed. Comparing the two compounds with only one soluble component, SEBS/No showed considerably and significantly higher complex viscosity values than those of APO/No, due to the higher viscosity of SEBS compared to APO [55]. A high viscosity implies a greater risk for clogging and a higher stiffness in the material to avoid filament buckling or slipping on the rollers [20,21].

In the systems with either PW or EO, the complex viscosity was significantly lower than for those with only one soluble component. At angular frequencies higher than  $100 \text{ rad}\cdot\text{s}^{-1}$ , a significant viscosity reduction (as can be observed by the Tukey grouping in Fig. 3) between 57% and 65% was measured for APO/PW and APO/EO compared to the viscosity of APO/No. In fact, APO/PW and APO/EO had the lowest values of the tested binders and no significant differences existed among them as both were grouped with the same letter in the Tukey tests (d in Fig. 3). For SEBS/EO and SEBS/PW, the viscosity decreased by 82% and 90%, respectively, compared to SEBS/No. No significant differences could be found between SEBS/PW and SEBS/EO (both were grouped with b in Fig. 3). Similar reductions in the viscosity have been reported in previous studies when incorporating PW to HDPE [54] and EO to SEBS [56] compounds.

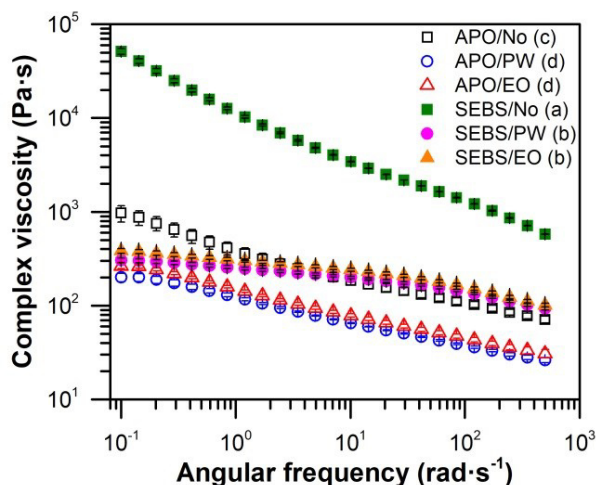


Fig. 3. Shear viscosity as a function of the angular frequency for the investigated binder systems measured at  $150 \text{ }^\circ\text{C}$ . Groups sharing the same superscript letter (a, b, c or d) are not significantly different (Tukey post hoc tests,  $P < 0.05$ ).

#### 4.1.2. Mechanical properties of binders

Besides the viscosity, the mechanical properties of the compounds are crucial to determine the most suitable formulation for FFF. Fig. 4 summarizes the mechanical properties employed for the evaluation of the binders investigated. The detailed stress-strain curves of the binders are presented in Fig. S2 in the supporting information. Since no plastic

deformation should occur during the FFF process [22,23], the stress at yield and the strain at yield were the parameters used to evaluate the strength and flexibility for the compound with pronounced yielding behavior (SEBS/No (Fig. S2)). For the other binders, the ultimate tensile stress (UTS), and the strain at UTS were used, since these materials fractured shortly after showing these values without pronounced yielding. The secant modulus was used to evaluate the stiffness and was calculated for all the compounds in the strain range between 0.1 and 0.3% in order to avoid the initial stage, in which the slight curvature of the specimens (due to the processing and handling the material) could influence the results. Ideally, the three properties (stress, strain and secant modulus) should be high enough to ensure that the filaments are processable by FFF [19,22–24,33].

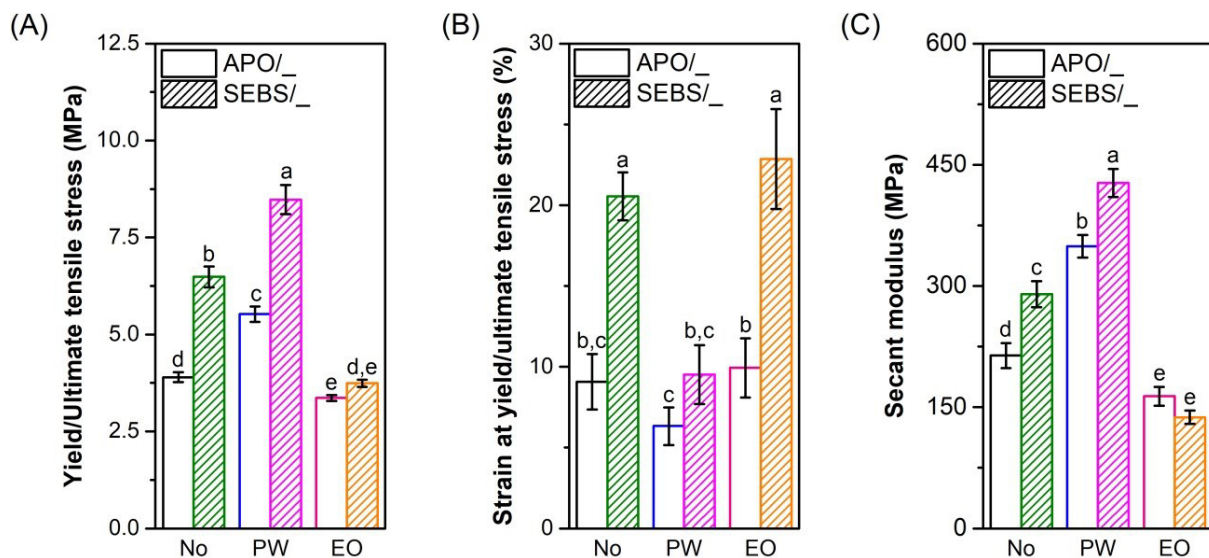


Fig. 4. Tensile properties of filaments made from the binders: (A) Yield or ultimate tensile stress, (B) strain at yield or at the ultimate tensile stress, and (C) secant modulus. Groups sharing the same superscript letter (a, b, c, d or e) are not significantly different (Tukey post hoc tests,  $P < 0.05$ ).

As can be observed in Fig. 4, the binder SEBS/No shows significantly higher values for all the evaluated parameters than the binder APO/No. The measured difference is most probably caused by the higher mechanical properties of the SEBS than the APO, as observed by Kim et al. [55] for binary compounds with both polymers. Similarly, higher ultimate tensile stress and secant modulus are obtained for SEBS/PW than for APO/PW. When comparing SEBS/PW with SEBS/No and APO/PW with APO/No, a significantly higher secant modulus (Fig. 4C) and a higher UTS or yield stress (Fig. 4A) was measured for the compounds with PW, which could be attributed to an increase of the crystallinity of the other components by the wax [57,58]. Nevertheless, the corresponding strain values for SEBS/No were lower than those of SEBS/PW (Fig. 4B). This reduction is due to the poor mechanical properties of the wax, which disperses in the amorphous phases of the rest of the components and acts as defect points [57,59]. The incorporation of the EO resulted in an increase of the mean strain values for the compounds APO/EO and SEBS/EO compared to those formulations without EO (Fig. 4B). Nevertheless, no significant difference exists (same letters in Fig. 4B) due to the high variability of these values. Both the stresses (Fig. 4A) and the secant moduli (Fig. 4C) of the

filaments with EO were significantly lower than those of the compounds without EO. These phenomena could be caused by the plasticization effect that the EO causes in the backbone (AA-HDPE) and the other soluble component (SEBS or APO) [60], as has been reported for combinations of oil with SEBS and PP [61].

#### **4.1.3. Solvent debinding of binders**

To evaluate the solvent debinding behavior of the binders, the phenomena that happen during the process must be considered. At the beginning of the immersion, the solvent gets in contact with the binder molecules, which subsequently swell. If the attraction forces between polymer and solvent are higher than the polymer intermolecular forces, the dissolution of the polymer occurs [40,62]. Consequently, the dissolved molecules are taken out by capillary forces and diffusion [63]. As stated in section 2.1, the major fraction of the polymeric binder was constituted of materials soluble in cyclohexane. According to previous studies and the technical information provided by the suppliers, the APO [64], SEBS [65,66], PW [67], EO [66], and SA [67] are the components soluble in cyclohexane. Although high density polyethylene is insoluble in cyclohexane [40], the interaction with the solvent can produce swelling in its amorphous phases [42]. The swelling of both the backbone and the soluble components results in a dimensional variation of the samples, and therefore must be kept as low as possible.

The percentage of leached binder and the defects found in the part after debinding are depicted in Fig. 5 and Fig. 6, respectively. Both results must be evaluated carefully and combined, since the defects in the parts affect their mass loss. The highest percentage of leached binder was measured for SEBS/No (Fig. 5). Nevertheless, large cracks were observed for this material (Fig. 6d), which is produced by the large swelling of the compound components [42,68]. The cracks facilitate the penetration of the solvent to the core of the specimen and, thus, promote a larger mass loss. For the binder APO/No a smaller quantity of binder was removed compared to SEBS/No (Fig. 5), and small cracks could be observed in the surface (Fig. 6a). Large pores appeared also in the surface of the APO/No cylinders, which number and size increased for APO/PW (Fig. 6B) and APO/EO (Fig. 6C). An uneven distribution of the binder components in the specimens might be the reason for the large pores [69]. This separation would result in areas rich in soluble binder, which leach out during solvent debinding. In absence of enough content of backbone, it distorts in a porous morphology. Since pieces of binders were observed floating when removing the specimens out of the solvent, this supports the hypothesis of the inhomogeneity in the specimens. In spite of the loss of big pieces, the leached binder fraction for APO/PW and APO/EO were among the lowest measured values (Fig. 5). Similar defects were observed for the specimens with the binder SEBS/EO (Fig. 6F), which had a lower leached binder fraction than the original SEBS/No (Fig. 5). Even though SEBS/PW had an even lower leached binder fraction than SEBS/EO, the specimens with the first showed a small and homogeneously distributed porosity (Fig. 6E). Moreover, it was the only binder without visible defects after debinding.



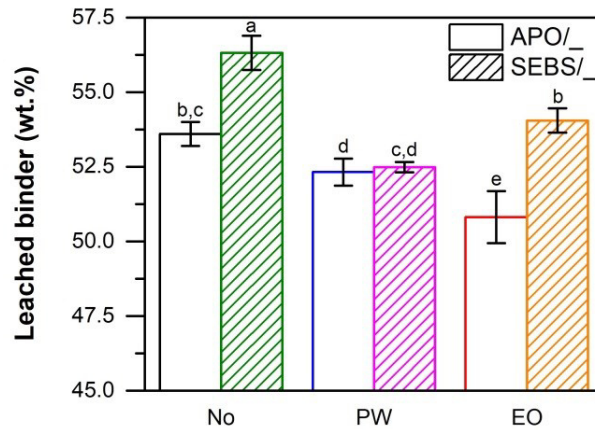


Fig. 5. Percentage of leached binder after solvent debinding for the investigated binder components. Groups sharing the same superscript letter (a, b, c, d or e) are not significantly different (Tukey post hoc tests,  $P < 0.05$ ).

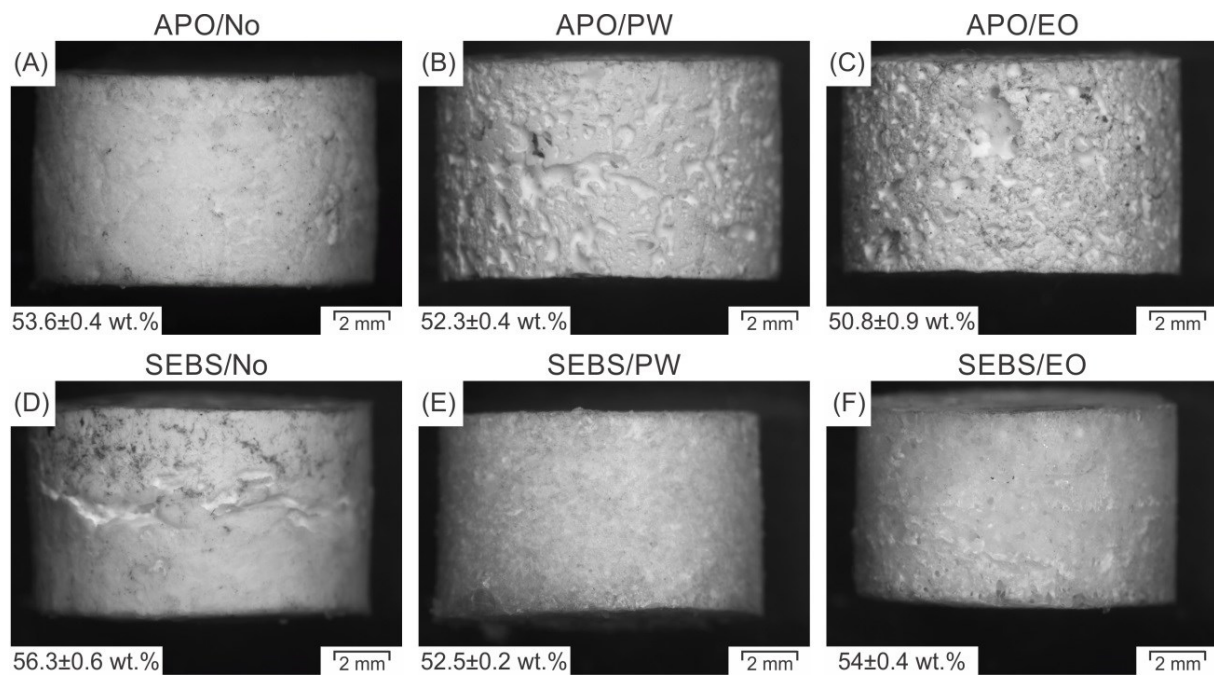


Fig. 6. Specimens after solvent debinding of the binders (A) APO/No, (B) APO/PW, (C) APO/EO, (D) SEBS/No, (E) SEBS/PW, and (F) SEBS/EO. The percentage of leached binder after solvent debinding is indicated in the bottom left corner of each photograph.

The combination of the mechanical properties of the filament and the viscosity of the binder indicates that a possible candidate for the binder system is the compound SEBS/PW, since it exhibits a good balance of mechanical properties, while having a low viscosity. After the solvent debinding experiments, it can be concluded that SEBS/PW is the best possible binder, as no defects were observed. Nevertheless, in order to investigate the influence of the filler particles on these properties, feedstock materials were prepared with all the binder systems.

## 4.2. Evaluation of the feedstocks

### 4.2.1. Rheological behavior of the feedstocks

Fig. 7 depicts the apparent viscosity measured during the production of the feedstock filaments at a shear rate at the walls of  $215 \text{ s}^{-1}$ . It can be seen that all values are significantly different among each other since the group letters obtained by the Tukey post hoc tests are all different for each value compared. The feedstock SEBS/No/Z showed the significantly highest viscosity value with more than twice the viscosity of APO/No/Z (Fig. 7). Although the apparent viscosity of SEBS/No/Z is similar to those of other filled materials produced by FFF [70], the high resistance to flow could result in weak bonding between the extruded strands, which could affect the mechanical properties of the final part [29]. After the partial substitution of the SEBS by a second soluble component in SEBS/PW/Z and SEBS/EO/Z, the viscosity was reduced by approximately 56 % for both feedstocks. Similarly, the viscosity was reduced by 42 % for APO/PW/Z and 47 % for APO/EO/Z compared to APO/No/Z.

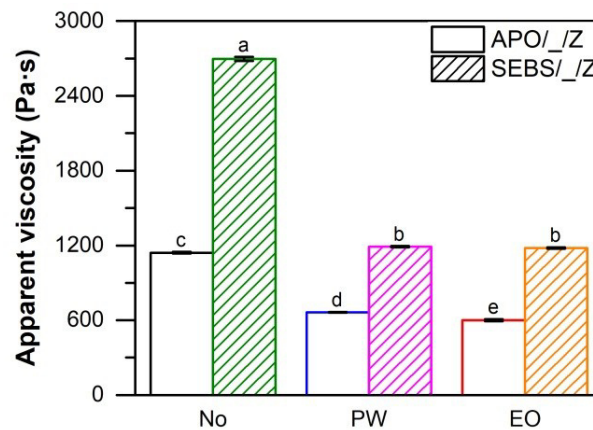


Fig. 7. Apparent viscosity as a function of the feedstock components during the production of filaments at  $150 \text{ }^{\circ}\text{C}$  at a shear rate of  $215 \text{ s}^{-1}$ . Groups sharing the same superscript letter (a, b, c, d or e) are not significantly different (Tukey post hoc tests,  $P < 0.05$ ).

### 4.2.2. Mechanical properties of the feedstocks

The mechanical properties of the feedstocks were measured by tensile tests on the feedstock filaments, similarly to the binders above. Feedstock filaments showed no yielding during testing, and the ultimate tensile strain and its corresponding strain value coincide with the stress and strain at break values, respectively (for the strain-stress curves please refer to the supporting information Fig. S3). When comparing the properties of the filled filaments, the feedstock SEBS/No/Z showed significantly higher stiffness, strength, and flexibility than APO/No/Z (Fig. 8), similarly to the trends for the corresponding binders (Fig. 4). Interestingly, unlike the binder systems (Fig. 4), no significant difference exists between the values of APO/No/Z and APO/PW/Z (as both have the same letters in the Tukey groups in Fig. 8), and the filaments of SEBS/No/Z were stronger and stiffer than those of SEBS/PW/Z (Fig. 8). On the contrary to the considerably lower flexibility for the binders with PW than for those without it (Fig. 4B), the maximum strain of the feedstocks is insignificantly different from

each other (same letter in Fig. 8A). The properties of the feedstocks with EO changed in the same manner as in the binders (Fig. 4). Despite the flexibility of the compounds is increased for APO/EO/Z and SEBS/EO/Z compared to APO/No/Z and SEBS/No/Z, the difference is not significant due to the high variability of the results (same letter in the Tukey groups in Fig. 8B). Additionally, the compounds with EO have the significantly lowest strength (Fig. 8A) and stiffness (Fig. 8C) of all the evaluated compounds.

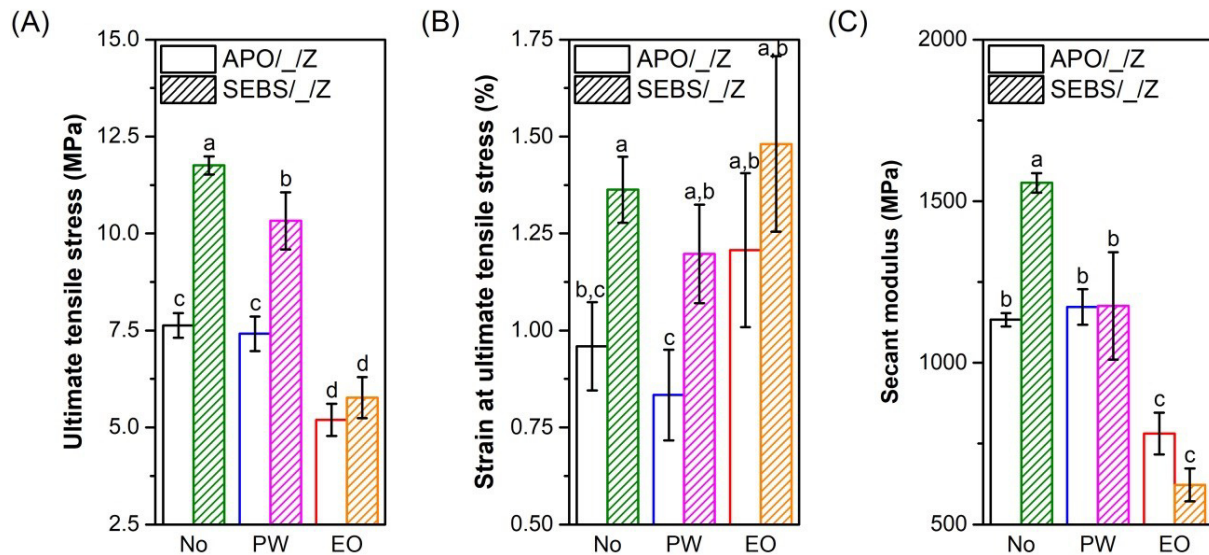


Fig. 8. Tensile properties of the filaments made from the feedstocks: (A) Ultimate tensile stress, (B) strain at the ultimate tensile stress, and (C) secant modulus. Groups sharing the same superscript letter (a, b, c or d) are not significantly different (Tukey post hoc tests,  $P < 0.05$ ).

#### 4.2.3. Solvent debinding of the feedstocks

The percentage of leached binder and the defects found after solvent debinding of the feedstocks are shown in Fig. 9 and Fig. 10, respectively. A slight decrease in the percentage of leached binder was detected compared to the binders (Fig. 5). For the binders, the AA-HDPE was the only component not dissolving, but for the feedstocks a high volume of the specimens is occupied by the insoluble zirconia particles. An intricate network of backbone and powder is formed in the green structure and the diffusion of the dissolved products out of the specimens is hindered, and so is the overall debinding rate [63,71]. As the swollen molecules of the dissolved polymers cannot be easily evacuated through the network, the overall swelling of the specimens increases [63], generating the defects observed in Fig. 10. The highest drop of leached binder occurs for the feedstocks with only one soluble component; APO/No/Z had a leached binder reduction of  $\sim 6$  wt.% compared to APO/No; and SEBS/No/Z had a reduction of  $\sim 5$  wt.% compared to SEBS/No. For the rest of the formulations minor differences ( $< 1.5$  wt.%) were found. In this manner, the large cracks observed for SEBS/No (Fig. 6D) together with the reduction of the debinding rate resulted in total loss of shape for SEBS/No/Z (Fig. 10D). Large cracks were observed as well for APO/No/Z (Fig. 10A), which nevertheless had the significantly lowest leached binder of all the tested feedstocks (different letter in the Tukey's groups Fig. 10). The use of a polymer

with a large tackiness like the APO [72] results in an excessive adhesion to the powder, which hinders the dissolution process [73]. In general, there is a high variability in the percentage of leached binder, as indicated by a large standard deviation and the Tukey grouping in Fig. 9. The high variability might be caused by the different surface of individual specimens and numerous cracks that varied the solvent penetration phenomena. Fig. 10 shows that the inclusion of EO or PW in the feedstock not only results in a low viscosity (Fig. 7), but also is an effective way to reduce defects in the samples. The addition of these soluble components decreases the swelling of the overall specimen and, hence, reduces the internal stresses [73]. In principle, the EO compounds should show smaller cracks than those with PW, since the EO is liquid at the test temperature. Thus, it should have a faster dissolution and mobility than the PW [74,75], which is only partially molten at 60 °C, at which the test is conducted (see Fig. S4). Surprisingly, there are no significant differences in the type of defects found in the specimens of APO/PW/Z (Fig. 10B) and APO/EO/Z (Fig. 10E), whereas the opposite trend is observed for the SEBS feedstocks. Feedstock SEBS/EO/Z (Fig. 10F) had considerably larger defects compared to those of feedstock SEBS/PW/Z (Fig. 10E), which has the smallest cracks of all the tested feedstocks. As a result, the combination of SEBS with PW is the most effective for the reduction of defects, even though it has not been possible to obtain completely defect-free compression molded specimens.

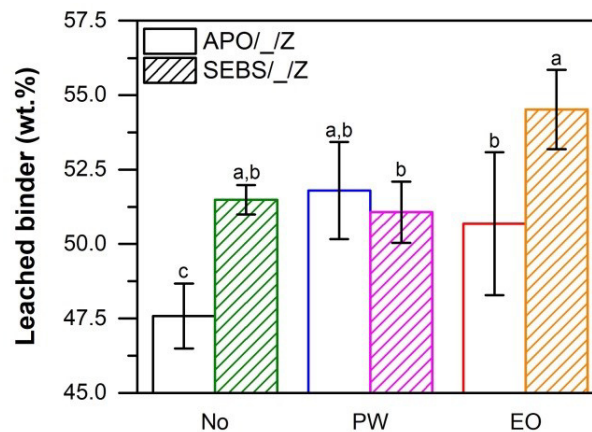


Fig. 9. Percentage of leached binder in the feedstock as a function of the binder components. Groups sharing the same superscript letter (a, b, or c) are not significantly different (Tukey post hoc tests,  $P < 0.05$ ).

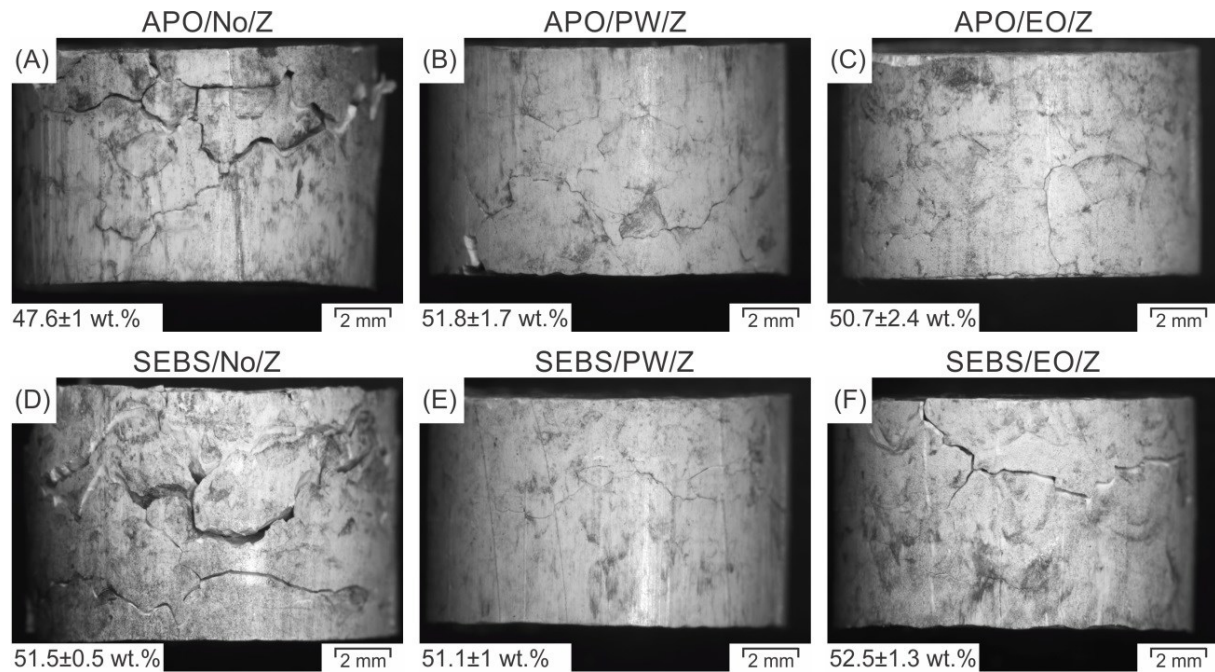


Fig. 10. Specimens after solvent debinding of feedstocks (A) APO/No/Z, (B) APO/PW/Z, (C) APO/EO/Z, (D) SEBS/No/Z, (E) SEBS/PW/Z, and (F) SEBS/EO/Z. The percentage of leached binder after solvent debinding is indicated in the bottom left corner of each photograph.

#### 4.2.4. Morphology of the feedstocks

The morphology of the filaments before and after leaching the soluble component is depicted in Fig. 11. For feedstock SEBS/No/Z with only SEBS as a soluble component, a large fraction of platelets rich in binder could be observed prior to debinding (Fig. 11G). However, after solvent debinding, it showed a structure with a uniform distribution of powder held by the AA-HDPE (Fig. 11J) similar to those of other solvent-debound feedstocks [76,77]. This suggests that the phase-separated platelets could be mostly composed of the soluble component (in this case SEBS), which does not bond with the powder and/or the AA-HDPE. Similar phase separation and partial compatibility has been reported for HDPE and SEBS blends, resulting in inhomogeneous microstructures [78,79]. Compared to SEBS/No/Z, APO/No/Z showed a smaller concentration of platelets before the immersion in the solvent (Fig. 11A). A platelet-free morphology was also observed for APO/No/Z after solvent debinding (Fig. 11D). Since the APO used in this study is based on propylene, it can be assumed, based on previous studies [80], that the compatibility of the APO with the AA-HDPE is poor as well, and the platelets are composed of APO, which dissolves in cyclohexane.

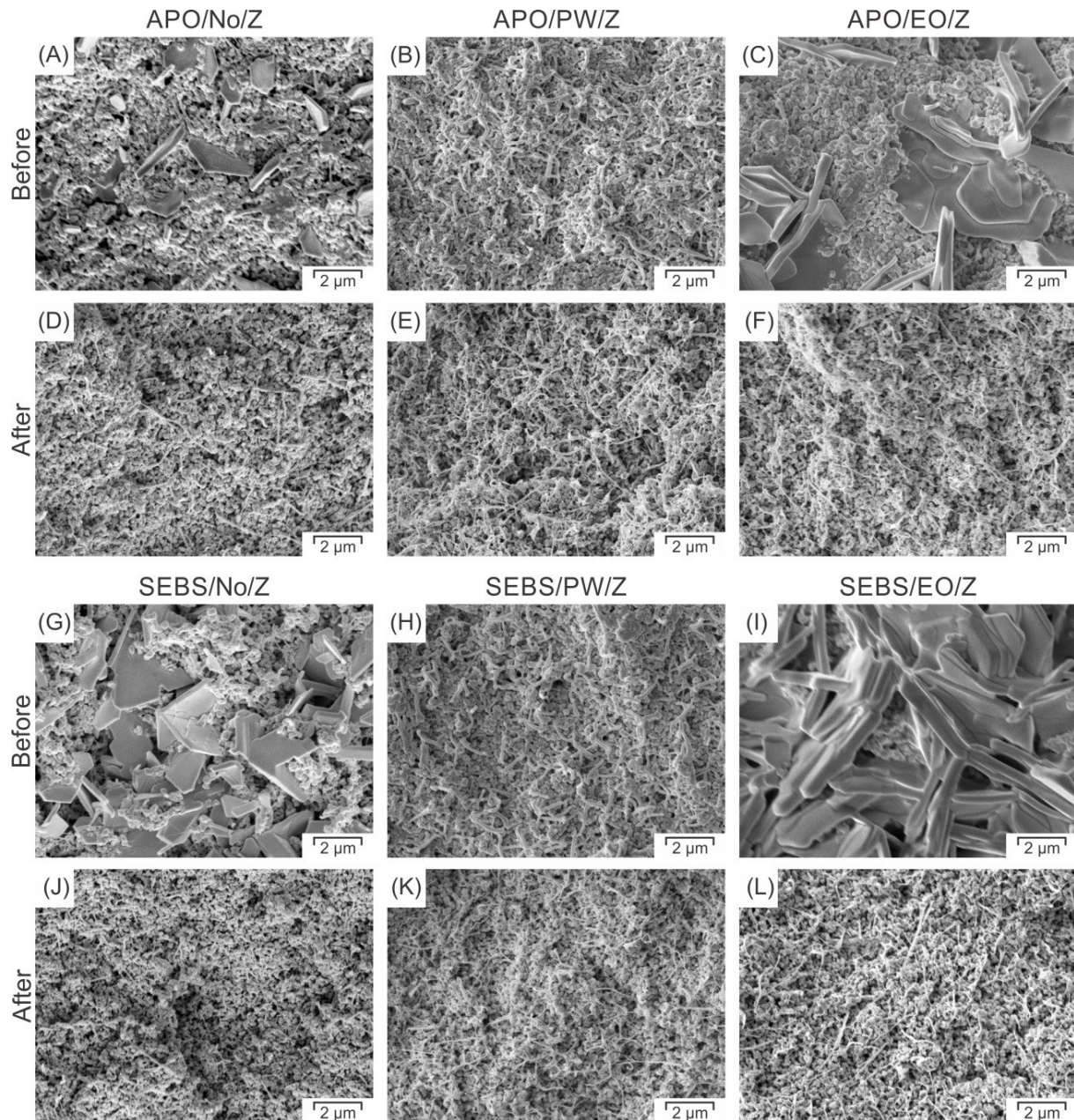


Fig. 11. Morphology of the cryo-fractured filaments of APO/No/Z (A, D), APO/PW/Z (B, E), APO/EO/Z (C, F), SEBS/No/Z (G, J), SEBS/PW/Z (H, K), and SEBS/EO/Z (I, L) before and after solvent debinding.

Incorporating the second soluble component (PW or EO) in the feedstocks produced two completely different morphologies. A large increase in the concentration and size of the platelets could be observed for APO/EO/Z (Fig. 11C) compared to APO/No/Z (Fig. 11A) and for SEBS/EO/Z (Fig. 11I) compared to SEBS/No/Z (Fig. 11G). This effect is especially pronounced for the compound containing SEBS, which might be caused by the preferential distribution of the EO in the elastomeric phase than in the AA-HDPE used as backbone [60]. As neither APO/EO/Z (Fig. 11F) nor SEBS/EO/Z (Fig. 11L) show platelets after the solvent debinding step, it can be stated that they are constituted once more by the soluble components (e.g. EO and APO or SEBS, respectively).

On the contrary, APO/PW/Z (Fig. 11B) and SEBS/PW/Z (Fig. 11H) showed a platelet-free microstructure and homogeneous microstructure before solvent debinding. Therefore, the wax seems to improve the coating of the powder and the homogenization of the dispersion in the 'green' microstructure. The APO or SEBS is removed together with the PW during the debinding process, leaving an interconnected microstructure of powder and backbone (Fig. 11E and Fig. 11K).

The defects observed in the feedstocks after solvent debinding (Fig. 10) seem to be strongly correlated with the morphology of the compounds before that process (Fig. 11). Although the compounds with PW or EO had smaller defects than the compounds without PW or EO, the EO feedstocks have larger defects than those containing PW (Fig. 10). The large concentration of platelets of soluble binder might be the major cause of this difference, since the initial swelling of the binder is larger in the platelets than in the rest of the material. Therefore, there is a concentration of stress, which promotes the propagation of cracks in the specimens.

#### **4.3. Selection of the formulation and upscaling**

Considering the previous results, the formulation that had the best combination of properties is SEBS/PW/Z. The SEBS must be incorporated to attain the mechanical strength and strain required for the production and spooling of the filament as well as the stiffness needed to extrude the material in the FFF printer (Fig. 4 and Fig. 8). Yet, SEBS/No/Z has a poor dispersion of the powder, a high viscosity and large defects in the specimens during its dissolution. To overcome and eliminate these problems, the incorporation of the PW has proven to be the best solution, as both SEBS/PW and SEBS/PW/Z revealed a homogeneous powder distribution, low viscosity, and the smallest defects after the solvent debinding trials on compression-molded specimens.

The filaments produced in the upscaling stage with the selected feedstock SEBS/PW/Z were subsequently used for the production of parts with complex geometry by FFF (Fig. 12). Compared to our experience with conventional FFF materials, a more careful handling of the feedstock filaments and feeding to the FFF machine was required due to the brittle nature of the highly-filled material. The brittleness of the material also complicated the defect-free removal of the specimens from the build platform. Fig. 12C exemplarily shows a typical delamination of the first deposited layer due to the brittleness of the produced part. Therefore, the adjustment of the fraction of the different binder components must be conducted in future steps in order to facilitate the processing and improve the quality of the parts. Another type of defect observed was an incomplete infill as the one in Fig. 12C and Fig. 12D, with voids between the deposited strands. The optimization of the FFF processing parameters and the adaptation of the slicing software to the highly filled materials could solve this problem, as has been discussed in [6,12].

The produced specimens were then immersed in cyclohexane with no defects (Fig. 12) and an average of  $55.4 \pm 0.5$  wt. % binder removed from the specimens, which is equivalent to a porosity of 29.4 %. According to Fan et al. [81], a minimum porosity of 14% is required for the formation of an interconnected pore structure reaching the center of the specimens. This structure can later enable the easy evacuation of the gas molecules generated during

thermal debinding. Despite the powder and feedstock composition were different for the study of Fan et al. [81], the large porosity value of the tested parts (more than double of the required porosity) was considered sufficient for further processing (i.e. thermal backbone elimination and sintering).

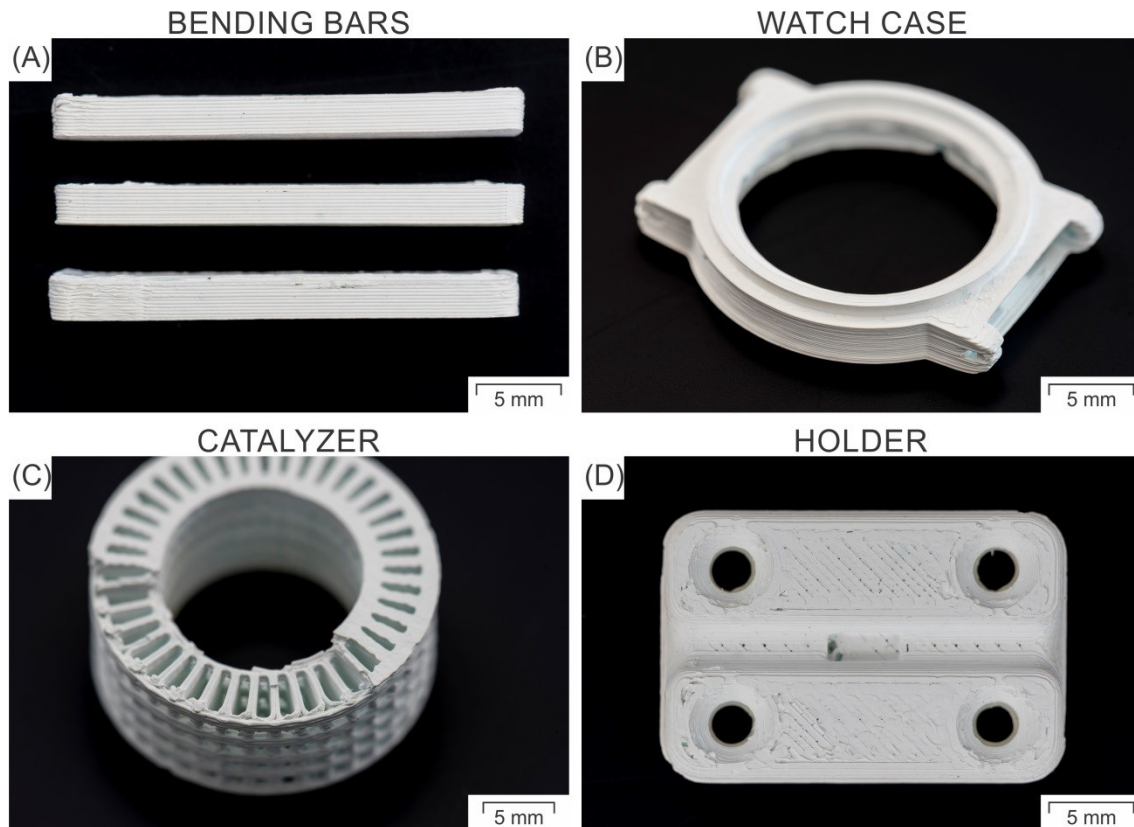


Fig. 12. Specimens produced by FFF of the most promising feedstock SEBS/PW/Z after pre-sintering: (A) bending bars, (B) watch case, (C) catalyzer, and (D) holder.

No cracks were observed in the solvent-debound specimens, as compared to the cylinders of Fig. 10E. This could be attributed to two different factors: (i) the mixing in a twin screw compounder increases the homogeneity of the feedstock components, which causes a more uniform swelling, and the formation of a homogeneous porous network; and (ii) the specimens produced by compression molding are less porous than the specimens produced by FFF, more pores in FFF parts can help to alleviate the formation of cracks. However, these hypotheses are to be tested in future investigations. Finally, the solvent-debound specimens were placed in the muffle furnace for thermal debinding and pre-sintering. The rest of the binder could be removed out of the parts and as can be observed in Fig. 12, no defects appeared in this step. Considering that all the steps up to the initial stages of sintering could be conducted with SEBS/PW/Z, it can be stated that the developed feedstock is suitable for the combination of FFF with a two-step debinding process.

## 5. Conclusion

A new binder for the production of zirconia specimens by fused filament fabrication (FFF) and solvent debinding was developed. The design of a multicomponent binder along with the selection of its soluble components was the major focus of the present work. An amorphous



polyolefin (APO) and a styrene-ethylene/butylene-ethylene copolymer (SEBS) were tested as single soluble components. The incorporation of paraffin wax (PW) or extender oil (EO) as second soluble component was also evaluated. Stearic acid (SA) and acrylic acid-grafted high density polyethylene (AA-HDPE) were employed in all the formulations. The content of the different components was kept constant. The mechanical and rheological properties, the solvent debinding behavior, and the dispersion of the powder were the parameters evaluated for the binders and the feedstocks.

The binder system containing SEBS and PW had the significantly highest ultimate tensile strength and secant modulus, a low viscosity, and also no defects after solvent debinding. The incorporation of zirconia powder increased the viscosity, strength, and stiffness of the compounds, while drastically reducing the flexibility. The dispersion of the powder and homogeneity of the feedstocks turned out to be the major aspects determining the required properties for FFF. Although the formulations solely containing SEBS had the most promising mechanical properties, the incorporation of PW as a low-viscous and soluble component was necessary to reduce the viscosity and the amount of defects that are present after solvent debinding. Therefore, the formulation SEBS/PW/Z was selected and its performance on the FFF and solvent debinding process was evaluated. The filament made of SEBS/PW/Z could be processed by FFF and the printed parts had no visible defects after debinding and pre-sintering.

Hence, these investigations offer an insight into the structure-property relation needed to make processable filaments of zirconia feedstocks for FFF combined with solvent and thermal debinding and sintering, and thus can be the basis for the applicability of this manufacturing strategy for other ceramic materials. In future studies, it is expected to demonstrate the successful reduction of the thermal debinding time as well as the production of fully dense parts by further developing the thermal debinding and sintering steps. The mechanical properties of the sintered parts as well as their morphology are also the matter of future investigations.

### **Acknowledgements**

This research was performed under the European project CerAMufacturing and the Austria-China bilateral cooperation project FlexiFactory3Dp. The CerAMufacturing project has received the financial support of the European Commission in the frame of the FoF Horizon 2020 with financial agreement 678503. FlexiFactory3Dp has received funding from the Austrian Research Promotion Agency under the program Production of the Future, Grant Agreement No. 860385.

The authors thank Baris Kaynak from the Institute of Chemistry of Polymeric Materials, Montanuniversitaet Leoben, and Axel Mueller-Koehn from the Fraunhofer IKTS Dresden for the characterization of the zirconia powder and fruitful discussions. Special thanks go to Thomas Lucyshyn for the help with the statistical analysis of the results. Thanks go to Ivan Raguž, Rudolf Schatzer, Maria Gfrerrer, Fabian Schuster, and Celina Harecker for their help during the experimental work. The authors want to thank the companies BYK-Chemie GmbH, Eastman Chemical Company, and Kraton Polymers Nederland B.V. for kindly donating the materials.

## Supplementary Information

Table S1. Composition of the feedstocks in volumetric percentage. In all the composites 47 vol.% of tetragonal zirconia, partially stabilized with yttria, (TZ-3YS-E) powder was used. APO and SEBS refer to the amorphous polyolefin and styrene-ethylene-butylene copolymer, respectively. 'No' refers to the binder systems without a second soluble component, whereas PW and EO refer to the binder systems with paraffin wax and highly paraffinic extender oil, respectively. AA-HDPE refers to the acrylic acid-grafted high density polyethylene and SA to the stearic acid used as surfactant.

	Backbone		Soluble comp. 1		Soluble comp. 2		Surfactant	TZ-3YS-E Powder
	AA-HDPE	APO	SEBS	PW	EO	SA	Z	
APO/No/Z	18.55	29.15	-	-	-	5.3	47	
APO/PW/Z	18.55	14.575	-	14.575	-	5.3	47	
APO/EO/Z	18.55	14.575	-	-	14.575	5.3	47	
SEBS/No/Z	18.55	-	29.15	-	-	5.3	47	
SEBS/PW/Z	18.55	-	14.575	14.575	-	5.3	47	
SEBS/EO/Z	18.55	-	14.575	-	14.575	5.3	47	

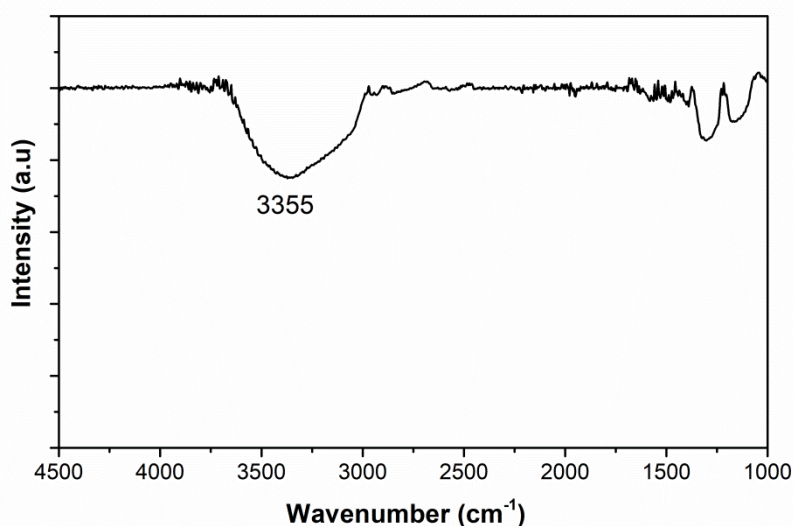


Fig. S1. Infrared absorption spectrum of the zirconia powder. The intensity peak at a wavenumber of  $3355\text{ cm}^{-1}$  for the surface -OH groups is marked. ATR spectroscopy was performed with a Vertex 70 spectrometer (Bruker, Germany). 128 scans were accumulated with a resolution of  $4\text{ cm}^{-1}$ .

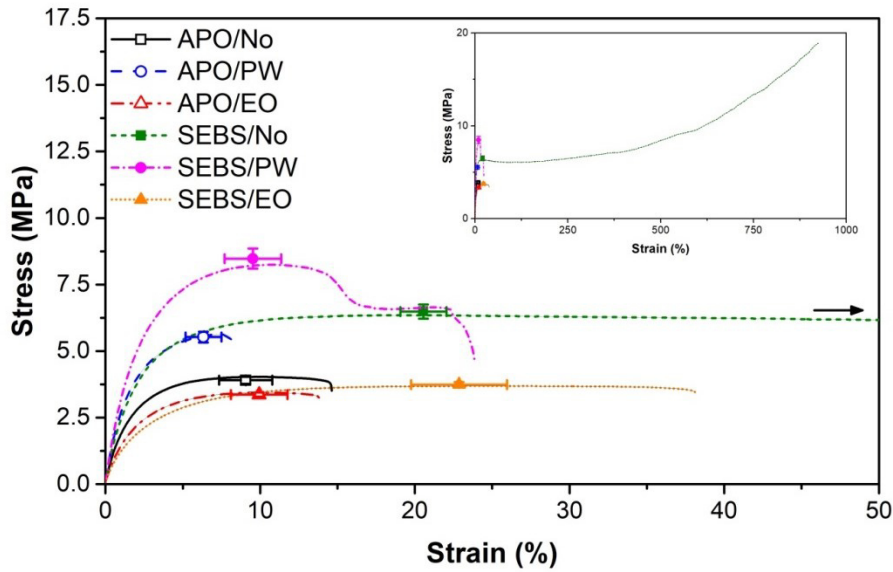


Fig. S2. Representative stress-strain curves of the investigated binders. The mean and standard deviation for the yield stress/ultimate tensile stress and the strain at yield/ultimate tensile stress are marked by symbols and error bars. For reasons of clarity, only the first 50 % of strain are represented. On the top right, the same stress-strain curves are given for the full strain to visualize the elasticity of the compound B/SEBS/No.

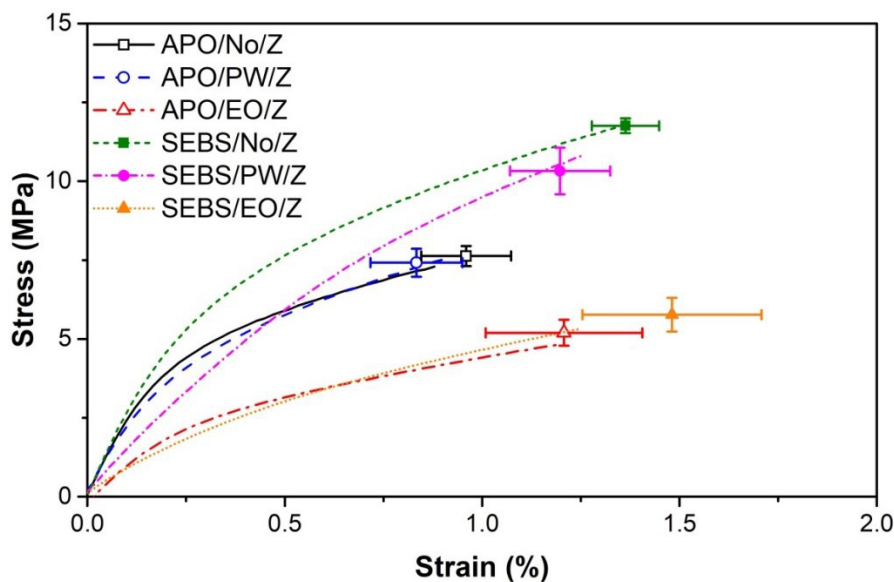


Fig. S3. Representative strain-stress of the feedstocks. The mean and standard deviation for the ultimate tensile stress and the strain at ultimate tensile stress are marked by symbols and error bars.

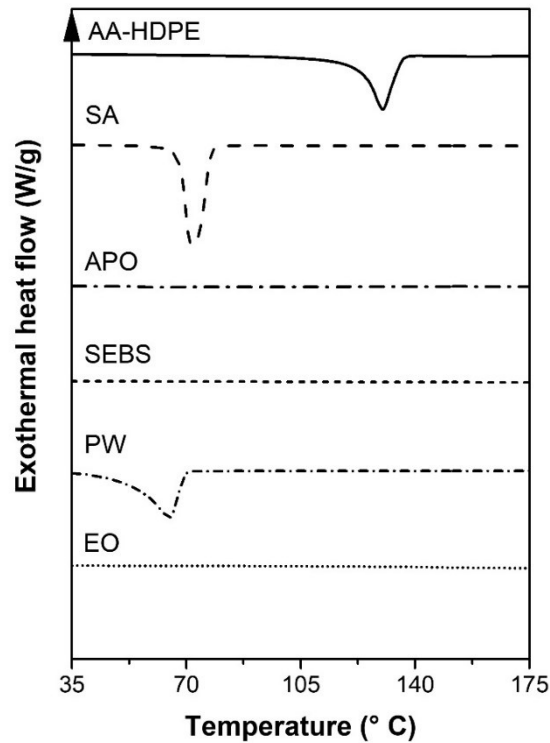


Fig. S4. Differential Scanning Calorimetry (DSC) thermograms from the second heating cycle of the evaluated binder components. The measurements were conducted under nitrogen atmosphere on a Mettler Toledo DSC 1 equipped with a gas controller GC 200 (Mettler Toledo GmbH, Switzerland). Three specimens were investigated per material. Heat-cool-heat runs, with the heating and cooling rate set to  $10 \text{ K}\cdot\text{min}^{-1}$ , respectively, were performed in temperatures between 30 and 180 °C.

## References

- [1] M.K. Agarwala, V.R. Jamalabad, N.A. Langrana, A. Safari, P.J. Whalen, S.C. Danforth, Structural quality of parts processed by fused deposition, *Rapid Prototyping Journal* 2 (4) (1996) 4–19. <https://doi.org/10.1108/13552549610732034>.
- [2] S. Iyer, J. McIntosh, A. Bandyopadhyay, N. Langrana, A. Safari, S.C. Danforth, R.B. Clancy, C. Gasdaska, P.J. Whalen, Microstructural Characterization and Mechanical Properties of Si<sub>3</sub>N<sub>4</sub> Formed by Fused Deposition of Ceramics, *Int J Applied Ceramic Technology* 5 (2) (2008) 127–137. <https://doi.org/10.1111/j.1744-7402.2008.02193.x>.
- [3] E.A. Griffin, S. McMillin, Selective Laser Sintering and Fused Deposition Modeling Processes for Functional Ceramic Parts, in: *Proceedings of the Solid Freeform Fabrication Symposium*, Austin, Texas, 1995.
- [4] D. Nötzel, R. Eickhoff, T. Hanemann, Fused Filament Fabrication of Small Ceramic Components, *Materials* 11 (8) (2018) 1463. <https://doi.org/10.3390/ma11081463>.
- [5] T.F. McNulty, F. Mohammadi, A. Bandyopadhyay, D.J. Shanefield, S.C. Danforth, A. Safari, Development of a binder formulation for fused deposition of ceramics, *Rapid Prototyping Journal* 4 (4) (1998) 144–150. <https://doi.org/10.1108/13552549810239012>.

- [6] M.A. Jafari, W. Han, F. Mohammadi, A. Safari, S.C. Danforth, N. Langrana, A novel system for fused deposition of advanced multiple ceramics, *Rapid Prototyping Journal* 6 (3) (2000) 161–175. <https://doi.org/10.1108/13552540010337047>.
- [7] R. Atisivan, S. Bose, A. Bandyopadhyay, Porous Mullite Preforms via Fused Deposition, *Journal of the American Ceramic Society* 84 (1) (2001) 221–223. <https://doi.org/10.1111/j.1151-2916.2001.tb00635.x>.
- [8] M.K. Agarwala, R. van Weeren, A. Bandyopadhyay, P.J. Whalen, A. Safari, S.C. Danforth, Fused Deposition of Ceramics and Metals: An Overview, in: *Proceedings of the Solid Freeform Fabrication Symposium, Austin, Texas, United States of America, 1996*.
- [9] A. Bandyopadhyay, K. Das, J. Marusich, S. Onagoruwa, Application of fused deposition in controlled microstructure metal-ceramic composites, *Rapid Prototyping Journal* 12 (3) (2006) 121–128. <https://doi.org/10.1108/13552540610670690>.
- [10] G. Wu, N.A. Langrana, R. Sadanji, S. Danforth, Solid freeform fabrication of metal components using fused deposition of metals, *Materials & Design* 23 (1) (2002) 97–105. [https://doi.org/10.1016/S0261-3069\(01\)00079-6](https://doi.org/10.1016/S0261-3069(01)00079-6).
- [11] J. Gonzalez-Gutierrez, D. Godec, C. Kukla, T. Schlauf, C. Burkhardt, C. Holzer, Shaping, Debinding and Sintering of Steel Components via Fused Filament Fabrication, in: *CIM 2017 Computer Integrated Manufacturing and High Speed Machining, Zadar, Croatia, Croatian Association of Production Engineering, Zagreb, Croatia, 2017*, pp. 99–104.
- [12] J. Abel, U. Scheithauer, S. Hampel, S. Cano, A. Müller-Köhn, A. Günther, C. Kukla, T. Moritz, Fused Filament Fabrication (FFF) of metal-ceramic components, *Journal of Visualized Experiments (In press)*. <https://doi.org/>.
- [13] C. Kukla, J. Gonzalez-Gutierrez, C. Burkhardt, O. Weber, C. Holzer, The Production of Magnets by FFF - Fused Filament Fabrication, in: *Euro PM2017 Proceedings, Milan, Italy, EPMA, Bellstone, 2017*, pp. 1–6.
- [14] C. Kukla, J. Gonzalez-Gutierrez, S. Cano, S. Hampel, C. Burkhardt, T. Moritz, C. Holzer, Fused Filament Fabrication (FFF) of PIM Feedstocks, in: *Actas del VI Congreso Nacional de Pulvimetalurgia y I Congreso Iberoamericano de Pulvimetalurgia, Ciudad Real, Castilla La Mancha, Spain, 1st ed., Asociación ManchaArte, 2017*, pp. 1–6.
- [15] J. Deckers, J. Vleugels, J.P. Kruth, Additive Manufacturing of Ceramics: A Review, *Journal of Ceramic Science and Technology* 5 (4) (2014) 245–260. <https://doi.org/>.
- [16] S. Bose, S. Vahabzadeh, D. Ke, A. Bandyopadhyay, Additive Manufacturing of Ceramics (2015) 143–184. <https://doi.org/10.1201/b18893-6>.
- [17] A. Zocca, P. Colombo, C.M. Gomes, J. Günster, D.J. Green, Additive Manufacturing of Ceramics: Issues, Potentialities, and Opportunities, *J. Am. Ceram. Soc.* 98 (7) (2015) 1983–2001. <https://doi.org/10.1111/jace.13700>.
- [18] Y. He, Y. Wu, J.-z. Fu, Q. Gao, J.-j. Qiu, Developments of 3D Printing Microfluidics and Applications in Chemistry and Biology: A Review, *Electroanalysis* 28 (8) (2016) 1658–1678. <https://doi.org/10.1002/elan.201600043>.

- [19] J. Gonzalez-Gutierrez, S. Cano, S. Schuschnigg, C. Kukla, J. Sapkota, C. Holzer, Additive Manufacturing of Metallic and Ceramic Components by the Material Extrusion of Highly-Filled Polymers: A Review and Future Perspectives, *Materials* 11 (5) (2018). <https://doi.org/10.3390/ma11050840>.
- [20] N. Venkataraman, S. Rangarajan, M.J. Matthewson, B. Harper, A. Safari, S.C. Danforth, G. Wu, N. Langrana, S.I. Guceri, A. Yardimci, Feedstock material property – process relationships in fused deposition of ceramics (FDC), *Rapid Prototyping Journal* 6 (4) (2000) 244–253. <https://doi.org/10.1108/13552540010373344>.
- [21] S. Rangarajan, G. Qi, N. Venkataraman, A. Safari, S.C. Danforth, Powder Processing, Rheology, and Mechanical Properties of Feedstock for Fused Deposition of Si<sub>3</sub>N<sub>4</sub> Ceramics, *Journal of the American Ceramic Society* 83 (7) (2000) 1663–1669. <https://doi.org/10.1111/j.1151-2916.2000.tb01446.x>.
- [22] M. Spoerk, J. Sapkota, G. Weingrill, T. Fischinger, F. Arbeiter, C. Holzer, Shrinkage and Warpage Optimization of Expanded-Perlite-Filled Polypropylene Composites in Extrusion-Based Additive Manufacturing, *Macromol. Mater. Eng.* 12 (2017) 1700143. <https://doi.org/10.1002/mame.201700143>.
- [23] E.L. Gilmer, D. Miller, C.A. Chatham, C. Zawaski, J.J. Fallon, A. Pekkanen, T.E. Long, C.B. Williams, M.J. Bortner, Model analysis of feedstock behavior in fused filament fabrication: Enabling rapid materials screening, *Polymer* (2017). <https://doi.org/10.1016/j.polymer.2017.11.068>.
- [24] M. Spoerk, C. Savandaiah, F. Arbeiter, J. Sapkota, C. Holzer, Optimization of mechanical properties of glass-spheres-filled polypropylene composites for extrusion-based additive manufacturing, *Polym. Compos.* 83 (2017) 768. <https://doi.org/10.1002/pc.24701>.
- [25] B.C. Mutsuddy, R.G. Ford, *Ceramic injection moulding*, Chapman & Hall, London, 1995.
- [26] M. Spoerk, J. Gonzalez-Gutierrez, J. Sapkota, S. Schuschnigg, C. Holzer, Effect of the printing bed temperature on the adhesion of parts produced by fused filament fabrication, *Plastics, Rubber and Composites* 47 (1) (2018) 17–24. <https://doi.org/10.1080/14658011.2017.1399531>.
- [27] O.S. Carneiro, A.F. Silva, R. Gomes, Fused deposition modeling with polypropylene, *Materials & Design* 83 (2015) 768–776. <https://doi.org/10.1016/j.matdes.2015.06.053>.
- [28] M. Spoerk, J. Gonzalez-Gutierrez, C. Lichal, H. Cajner, G. Berger, S. Schuschnigg, L. Cardon, C. Holzer, Optimisation of the Adhesion of Polypropylene-Based Materials during Extrusion-Based Additive Manufacturing, *Polymers* 10 (5) (2018) 490. <https://doi.org/10.3390/polym10050490>.
- [29] M. Spoerk, F. Arbeiter, H. Cajner, J. Sapkota, C. Holzer, Parametric optimization of intra- and inter-layer strengths in parts produced by extrusion-based additive manufacturing of poly(lactic acid), *J. Appl. Polym. Sci.* 134 (41) (2017) 45401. <https://doi.org/10.1002/app.45401>.
- [30] M.H. Khaliq, R. Gomes, C. Fernandes, J. Nóbrega, O.S. Carneiro, L.L. Ferrás, On the use of high viscosity polymers in the fused filament fabrication process, *Rapid Prototyping Journal* 23 (4) (2017) 727–735. <https://doi.org/10.1108/RPJ-02-2016-0027>.

- [31]S. Pekin, J. Bukowski, A. Zangvil, A Study on Weight Loss Rate Controlled Binder Removal From Parts Produced by FDC, in: Proceedings of the Solid Freeform Fabrication Symposium, Austin, Texas, 1998.
- [32]S. Banerjee, C.J. Joens, Debinding and sintering of metal injection molding (MIM) components, in: D.F. Heaney (Ed.), Handbook of metal injection molding, Woodhead Publishing, Cambridge UK, Philadelphia PA, 2012, pp. 133–180.
- [33]M.K. Agarwala, R. van Weeren, A. Bandyopadhyay, A. Safari, S.C. Danforth, W.R. Priedeman, Filament Feed Materials for Fused Deposition Processing of Ceramics and Metals, in: Proceedings of the Solid Freeform Fabrication Symposium, Austin, Texas, United States of America, 1996.
- [34]S. Onagoruwa, S. Bose, A. Bandyopadhyay, Fused Deposition of Ceramics (FDC) and Composites, in: Proceedings of the Solid Freeform Fabrication Symposium, Austin, Texas, United States of America, 2001.
- [35]N. Nestle, M. Hermant, K. Schimdt (BASF, SE) WO 2016/012486 A1, 22.07.
- [36]K.-S. Hwang, H.K. Lin, S.C. Lee, Thermal, Solvent, and Vacuum Debinding Mechanisms of PIM Compacts, *Materials and Manufacturing Processes* 12 (4) (1997) 593–608. <https://doi.org/10.1080/10426919708935169>.
- [37]K. Sharmin, I. Schoegl, Optimization of binder removal for ceramic microfabrication via polymer co-extrusion, *Ceramics International* 40 (3) (2014) 3939–3946. <https://doi.org/10.1016/j.ceramint.2013.08.039>.
- [38]Desktop Metal Inc, Prototype and mass produce with the same alloys, available at <https://www.desktopmetal.com/products/materials/> (accessed 29 March 2018).
- [39]C. Kukla, I. Duretek, S. Schuschnigg, J. Gonzalez-Gutierrez, C. Holzer, Properties for PIM Feedstocks Used in Fused Filament Fabrication, in: World PM2016 Proceedings, Hamburg, Germany, EPMA, 2016.
- [40]J.A. Brydson, *Plastics materials*, 7th ed., Butterworth-Heinemann, Boston, 1999.
- [41]H.-K. Lin, K.-S. Hwang, In situ dimensional changes of powder injection-molded compacts during solvent debinding, *Acta Materialia* 46 (12) (1998) 4303–4309. [https://doi.org/10.1016/S1359-6454\(98\)00093-7](https://doi.org/10.1016/S1359-6454(98)00093-7).
- [42]J. Wen, Z. Xie, W. Cao, X. Yang, Effects of different backbone binders on the characteristics of zirconia parts using wax-based binder system via ceramic injection molding, *J Adv Ceram* (2016). <https://doi.org/10.1007/s40145-016-0205-1>.
- [43]P. Wongpanit, S. Khanthasri, S. Puengboonsri, A. Manonukul, Effects of acrylic acid-grafted HDPE in HDPE-based binder on properties after injection and debinding in metal injection molding, *Materials Chemistry and Physics* 147 (1-2) (2014) 238–246. <https://doi.org/10.1016/j.matchemphys.2014.04.035>.
- [44]W. Liu, Z. Xie, X. Yang, Y. Wu, C. Jia, T. Bo, L. Wang, Surface Modification Mechanism of Stearic Acid to Zirconia Powders Induced by Ball Milling for Water-Based Injection Molding, *Journal of the American Ceramic Society* 94 (5) (2011) 1327–1330. <https://doi.org/10.1111/j.1551-2916.2011.04475.x>.

- [45]W.J. Tseng, D.-M. Liu, C.-K. Hsu, Influence of stearic acid on suspension structure and green microstructure of injection-molded zirconia ceramics, *Ceramics International* 25 (2) (1999) 191–195. [https://doi.org/10.1016/S0272-8842\(98\)00024-8](https://doi.org/10.1016/S0272-8842(98)00024-8).
- [46]C. Kukla, S. Cano, D. Kaylani, S. Schuschnigg, C. Holzer, J. Gonzalez-Gutierrez, Debinding behaviour of feedstock for material extrusion additive manufacturing of zirconia, *Powder Metallurgy under revision* (2018). <https://doi.org/>.
- [47]C. Kukla, I. Duretek, J. Gonzalez-Gutierrez, C. Holzer, Rheology of PIM feedstocks, *Metal Powder Report* 72 (1) (2017) 39–44. <https://doi.org/10.1016/j.mprp.2016.03.003>.
- [48]N. Aliheidari, R. Tripuraneni, C. Hohimer, J. Christ, A. Ameli, S. Nadimpalli, The impact of nozzle and bed temperatures on the fracture resistance of FDM printed materials, in: *Proc. SPIE 10165, Behavior and Mechanics of Multifunctional Materials and Composites 2017*, 2017, p. 1016512.
- [49]D. Kaylani, *Untersuchung des Löslichkeitsverhaltens von hochgefüllten Pulver-Kunststoff-Compounds*. Bachelor Thesis, Leoben, Austria, 2017.
- [50]Casio MQ24 watch case model, available at <https://www.thingiverse.com/thing:3000693> (accessed 18 August 2018).
- [51]M. Niepraschk, C. Rahiotis, T.G. Bradley, T. Eliades, G. Eliades, Effect of various curing lights on the degree of cure of orthodontic adhesives, *American journal of orthodontics and dentofacial orthopedics official publication of the American Association of Orthodontists, its constituent societies, and the American Board of Orthodontics* 132 (3) (2007) 382–384. <https://doi.org/10.1016/j.ajodo.2007.04.029>.
- [52]T.A. Hamza, S.F. Rosenstiel, M.M. Elhosary, R.M. Ibraheem, The effect of fiber reinforcement on the fracture toughness and flexural strength of provisional restorative resins, *The Journal of Prosthetic Dentistry* 91 (3) (2004) 258–264. <https://doi.org/10.1016/j.prosdent.2004.01.005>.
- [53]M. Guazzato, K. Proos, L. Quach, M.V. Swain, Strength, reliability and mode of fracture of bilayered porcelain/zirconia (Y-TZP) dental ceramics, *Biomaterials* 25 (20) (2004) 5045–5052. <https://doi.org/10.1016/j.biomaterials.2004.02.036>.
- [54]G. Herranz, B. Levenfeld, A. Várez, J.M. Torralba, Development of new feedstock formulation based on high density polyethylene for MIM of M2 high speed steels, *Powder Metallurgy* 48 (2) (2005) 134–138. <https://doi.org/10.1179/003258905X37828>.
- [55]J.-H. Kim, H.-G. Kim, J.-C. Lim, K.-S. Cho, K.-E. Min, Thermal properties and adhesion strength of amorphous poly( $\alpha$ -olefins)/styrene-ethylene-butylene copolymer/terpene hot-melt adhesive, *J. Appl. Polym. Sci.* 124 (4) (2012) 3312–3319. <https://doi.org/10.1002/app.35244>.
- [56]J.K. Kim, M.A. Paglicawan, S.H. Lee, M. Balasubramanian, Influence of Hydrocarbon Oils on the Physical Gelation of Poly(styrene-*b*-(ethylene-co-butylene)-*b*-styrene) (SEBS) Triblock Copolymers, *Journal of Elastomers & Plastics* 39 (2) (2007) 133–150. <https://doi.org/10.1177/0095244306067694>.



- [57] M.E. Mngomezulu, A.S. Luyt, I. Krupa, Structure and properties of phase-change materials based on high-density polyethylene, hard Fischer-Tropsch paraffin wax, and wood flour, *Polym Compos* 32 (8) (2011) 1155–1163. <https://doi.org/10.1002/pc.21134>.
- [58] H.S. Mpanza, A.S. Luyt, Comparison of different waxes as processing agents for low-density polyethylene, *Polymer Testing* 25 (4) (2006) 436–442. <https://doi.org/10.1016/j.polymertesting.2006.01.008>.
- [59] J.A. Molefi, A.S. Luyt, I. Krupa, Comparison of LDPE, LLDPE and HDPE as matrices for phase change materials based on a soft Fischer–Tropsch paraffin wax, *Thermochimica Acta* 500 (1-2) (2010) 88–92. <https://doi.org/10.1016/j.tca.2010.01.002>.
- [60] W. Sengers, M. Wübbenhorst, S.J. Picken, A.D. Gotsis, Distribution of oil in olefinic thermoplastic elastomer blends, *Polymer* 46 (17) (2005) 6391–6401. <https://doi.org/10.1016/j.polymer.2005.04.094>.
- [61] N. Vennemann, J. Huendorf, C. Kummerloewe, Phasenmorphologie und Relaxationsverhalten von SEBS/PP-Blends, *Kautschuk Gummi Kunststoffe* 54 (2001) 362–367. <https://doi.org/>.
- [62] S.T. Lin, R.M. German, Extraction Debinding of Injection Molded Parts by Condensed Solvent, *International Journal of Powder Metallurgy* 21 (5) (1989) 19–24. <https://doi.org/>.
- [63] E.J. Westcot, C. Binet Andrandall, R.M. German, In situ dimensional change, mass loss and mechanisms for solvent debinding of powder injection moulded components, *Powder Metallurgy* 46 (1) (2003) 61–67. <https://doi.org/10.1179/003258903225010442>.
- [64] Eastman Chemical Company, EASTOFLEX Amorphous Polyolefins.
- [65] G. Ovejero, P. Pérez, M.D. Romero, I. Díaz, E. Díez, SEBS triblock copolymer-Solvent interaction parameters from inverse gas chromatography measurements, *European Polymer Journal* 45 (2) (2009) 590–594. <https://doi.org/>.
- [66] J.H. Laurer, R. Bukovnik, R.J. Spontak, Morphological Characteristics of SEBS Thermoplastic Elastomer Gels, *Macromolecules* 29 (17) (1996) 5760–5762. <https://doi.org/10.1021/ma9607271>.
- [67] M.T. Zaky, F.S. Soliman, A.S. Farag, Influence of paraffin wax characteristics on the formulation of wax-based binders and their debinding from green molded parts using two comparative techniques, *Journal of Materials Processing Technology* 209 (18-19) (2009) 5981–5989. <https://doi.org/10.1016/j.jmatprotec.2009.07.018>.
- [68] S. Li, B. Huang, Y. Li, X. Qu, S. Liu, J. Fan, A new type of binder for metal injection molding, *Journal of Materials Processing Technology* 137 (1-3) (2003) 70–73. [https://doi.org/10.1016/S0924-0136\(02\)01069-5](https://doi.org/10.1016/S0924-0136(02)01069-5).
- [69] I. Krupa, G. Miková, A.S. Luyt, Polypropylene as a potential matrix for the creation of shape stabilized phase change materials, *European Polymer Journal* 43 (3) (2007) 895–907. <https://doi.org/10.1016/j.eurpolymj.2006.12.019>.
- [70] V. Kishore, X. Chen, C. Ajinjeru, A.A. Hassen, J. Lindahl, J. Failla, J. Kunc, C. Duty, Additive Manufacturing of High Performance Semicrystalline Thermoplastics and Their

Composites, in: Proceedings of the Solid Freeform Fabrication Symposium, Austin, Texas, United States of America, 2016.

- [71] K.S. Hwang, Y.M. Hsieh, Comparative study of pore structure evolution during solvent and thermal debinding of powder injection molded parts, *MMTA* 27 (2) (1996) 245–253. <https://doi.org/10.1007/BF02648403>.
- [72] M.D. Kanderski, L.A. Svenningsen, D.M. Strelow, C. Zhang, M.A. Gibes, B. Wang (Bostik Inc) US7262251B2, 2007.
- [73] M.D. Hayat, G. Wen, M.F. Zulkifli, P. Cao, Effect of PEG molecular weight on rheological properties of Ti-MIM feedstocks and water debinding behaviour, *Powder Technology* 270 (2015) 296–301. <https://doi.org/10.1016/j.powtec.2014.10.035>.
- [74] W. Liu, X. Yang, Z. Xie, C. Jia, L. Wang, Novel fabrication of injection-moulded ceramic parts with large section via partially water-debinding method, *Journal of the European Ceramic Society* 32 (10) (2012) 2187–2191. <https://doi.org/10.1016/j.jeurceramsoc.2012.03.005>.
- [75] S. Lee, W. Jeung, Anisotropic injection molding of strontium ferrite powder using a PP/PEG binder system, *Journal of Magnetism and Magnetic Materials* 226-230 (2001) 1400–1402. [https://doi.org/10.1016/S0304-8853\(00\)00960-4](https://doi.org/10.1016/S0304-8853(00)00960-4).
- [76] J. Hidalgo, C. Abajo, A. Jiménez-Morales, J.M. Torralba, Effect of a binder system on the low-pressure powder injection moulding of water-soluble zircon feedstocks, *Journal of the European Ceramic Society* 33 (15-16) (2013) 3185–3194. <https://doi.org/10.1016/j.jeurceramsoc.2013.06.027>.
- [77] Y. Ye, L. Qiao, J. Zheng, Y. Ying, W. Li, J. Yu, S. Che, L. Jiang, Effect of microcrystalline wax on the solvent debinding of the Sr-ferrite ceramics prepared by powder injection molding, *Journal of the European Ceramic Society* 37 (5) (2017) 2105–2114. <https://doi.org/10.1016/j.jeurceramsoc.2016.12.026>.
- [78] X. Yu, Z. Zheng, J. Lu, X. Wang, Morphology and mechanical properties of styrene–ethylene/butylene–styrene triblock copolymer/high-density polyethylene composites, *J. Appl. Polym. Sci.* 107 (2) (2008) 726–731. <https://doi.org/10.1002/app.26967>.
- [79] E. Helal, N.R. Demarquette, E. David, M.F. Frechette, Polyethylene/styrenic block copolymer blends: Morphology and dielectric properties, in: 2014 IEEE Conference on Electrical Insulation and Dielectric Phenomena (CEIDP), Des Moines, IA, IEEE, Piscataway, NJ, 2014, pp. 767–770.
- [80] R.E. Robertson, D.R. Paul, Stress–strain behavior of polyolefin blends, *J. Appl. Polym. Sci.* 17 (8) (1973) 2579–2595. <https://doi.org/10.1002/app.1973.070170823>.
- [81] Y.L. Fan, K.-S. Hwang, S.H. Wu, Y.C. Liao, Minimum Amount of Binder Removal Required during Solvent Debinding of Powder-Injection-Molded Compacts, *Metall and Mat Trans A* 40 (4) (2009) 768–779. <https://doi.org/10.1007/s11661-008-9760-6>.

## 3.4 Publication B

### ***Optimization of Material Properties for Highly-Filled Thermoplastic Polymers used in Fused Filament Fabrication of Ceramics***

Santiago Cano\*, Hrvoje Cajner, Joamin Gonzalez-Gutierrez, Janak Sapkota, Christian Kukla, Florian Arbeiter, Stephan Schuschnigg, Clemens Holzer

**AIP Conference Proceedings, 2065 (2019) 030058-1–030058-5**

**Proceedings of 34th International Conference of Polymer Processing Society (PPS-34)- 2018, Taipei, Taiwan, 21-25.05.2018**

doi: 10.1063/1.5088316

Available online: 06.02.2019

#### **ABSTRACT**

Fused Filament Fabrication (FFF) is a material extrusion based additive manufacturing technique that enables the processing of thermoplastic filaments, which are selectively extruded and deposited in a layer-wise manner to create three-dimensional objects. Filaments of polymer-based compounds highly-filled with ceramic powders (ca. 40-60 vol.%), known as feedstocks, can be processed by means of FFF to shape ceramic parts. Such parts are then debound in order to remove the polymer from the feedstock. A highly porous structure is obtained, which is sintered at high temperatures to produce dense ceramic components. The use of highly-filled polymers constitutes a processing challenge, due to their high viscosity that complicates the fabrication by FFF. The material properties of compounds filled with zirconia (ca. 47 vol%) were optimized by the incorporation of an additional low viscosity component. It was observed that by adding the low viscosity component, the mechanical properties (flexibility, strength and stiffness) and feedstock viscosity are suitable for the production of filaments and the FFF process. Furthermore, the low viscosity component further promotes the defect-free removal of the major polymer fraction by leaching with a solvent.

*Keywords:* Additive manufacturing; fused filament fabrication; highly-filled polymers; zirconia; binder; feedstock.

## Introduction

The low investment required for the printers, the wide range of available materials and the possibility to combine various materials have consolidated Fused Filament Fabrication (FFF) as the most common additive manufacturing technique for thermoplastic polymers and thermoplastic-based composites. In the FFF process filaments are driven by the action of two (or more) counter-rotating elements into a liquefier where the material melts and is selectively extruded through a nozzle to create parts in a layer-by-layer manner. This principle can be employed for the flexible production of ceramic components with customized and intricate design. In the FFF of ceramics, a polymeric compound (known as binder) acts as a carrier of a high load of ceramic powder (ca. 40-60 vol.%) and facilitates the production of filaments and the subsequent shaping of the parts. The next step is the removal of the polymeric components in the debinding process by dissolution in a solvent and/or thermal decomposition, followed by the sintering of the powders to obtain the final ceramic part [1].

One major obstacle for the FFF of ceramics is the production of filaments with the necessary mechanical properties [1–3]. For instance, the filament must be strong and flexible enough to be spooled/de-spooled when being produced and for feeding the printer without breaking. A high stiffness is also required to avoid buckling and to transfer the force from the rollers to the molten material. Another big challenge to address is the high viscosity of the filled compounds (known as feedstocks). A high viscosity implies a higher resistance to flow through the FFF nozzle and therefore higher stiffness in the solid material to produce the flow [2,3].

A new binder formulation for the FFF of zirconia with a solvent and thermal debinding process was developed in our previous investigation [4]. Compounds with different binders soluble in cyclohexane were produced and the rheological and mechanical properties, as well as the solvent debinding behavior were tested. The formulation with styrene-ethylene/butylene-styrene copolymer (SEBS) as soluble component had the best strength, stiffness and flexibility. Nevertheless, the feedstock had a high viscosity and large cracks appeared during debinding. The partial substitution of the SEBS by paraffin wax (PW) could reduce effectively the viscosity and the defects. Moreover, the wax contributed to the homogenization of the feedstock microstructure and the dispersion of the zirconia powder. The drawback of the PW incorporation was the reduction of the strength, stiffness and flexibility of the feedstock filaments, making necessary a careful handling and processing of the filaments to avoid breakage [4].

In this paper, the optimization of the material properties by the adjustment of the fractions of the binder components is presented. The objective of this study was the improvement of the mechanical properties of the compounds while maintaining a low viscosity and a minimum number of defects after solvent debinding. In the design of experiments the contents of the binder components were the varying factors in different formulations in order to determine their specific effect on the feedstock properties.

## Experimental procedure

Zirconium oxide containing 3 mol% of yttrium oxide (TZ-3YS-E, Tosoh Europe B.V., The Netherlands) was the ceramic powder employed in the feedstocks in a content of 47 vol%. The composition of the different binders was selected considering the process limitations and using the software Design Expert 10.0 (Stat-Ease, Inc., United States of America) in the design of experiments (DOE). A grafted polyolefin (gP, BYK-Chemie GmbH, Germany) was used as backbone. The minimum backbone fraction was limited to 35 vol% of the total binder content to maintain the strength of the parts during solvent debinding; and the maximum content was kept to 50 vol% of the binder since the insoluble backbone will hinder the diffusion of the dissolved products. A fixed fraction of surfactant (S, Merck Schuchardt OHG, Germany) was always used to facilitate the powder dispersion. The soluble binders were SEBS (Kraton Polymers Nederland B.V., The Netherlands) incorporated as flexible component, and PW (Sasol Limited, South Africa) as the low viscosity component. Since the objective is to improve the strength, flexibility and stiffness of the filaments, the fraction of PW in the compounds was always equal or smaller than the SEBS fraction. For the quantification of the influence of the binder components on the properties, regression models were calculated using the statistical software. The evaluated factors are the contents of the three main components, denoted by their acronyms. When evaluating the results, it must be considered that the models here reported are only valid in the range of compositions delimited by the constraints above. In all the cases the square root transformation was applied to provide homoscedasticity of variance and to ensure that the residuals remained normally distributed.

The compounds were prepared in an internal mixer (Plasti-Corder PL2000, Brabender GmbH & Co. KG, Germany) with counter rotating roller rotors. Prior to compounding, the zirconia powder was dried in a vacuum oven Binder VD 23 (Binder GmbH, Germany) at 180 °C for 1 hour to reduce the moisture content and, hence, subsequent agglomerations during mixing [5]. The mixing chamber was pre-heated to 160 °C and the mixing was conducted at 60 rpm during 75 min. First, the powder and the dispersant were introduced in the chamber, after 5 min the backbone was incorporated and after 5 min the base binder and the lubricant were added. At the end of the compounding the material was extracted and cooled down to room temperature. The material was then granulated in a cutting mill Retsch SM200 (Retsch GmbH, Germany) equipped with a sieve with 4x4 mm<sup>2</sup> squared perforations.

Feedstock filaments were produced at 150 °C in a high pressure capillary rheometer Rheograph 2002 (Göttfert Werkstoff-Prüfmaschinen GmbH, Germany). A die of 30 mm in length and 1.75 mm in diameter was employed. The feedstock was filled in the cylinder and left for 5 minutes to ensure the binder melting and the temperature homogenization. Then the piston moved at a speed of 1 mm/s and the extrudate was collected on a polytetrafluoroethylene (PTFE) conveyor belt where it cooled down. The pressure at the entrance of the die was measured during the process to calculate the apparent viscosity of the feedstock at one shear rate.

The mechanical properties of the filaments were evaluated with tensile tests to determine the processability by FFF [6,7]. A universal testing machine Zwick Z001 (Zwick GmbH & Co. KG, Germany) with a 1 kN load cell and pneumatic grips was employed. At least 5

straight specimens with a length of 100 mm were evaluated per material. The initial gauge length was set to 50 mm. The tests were performed at a speed of 10 mm/min until rupture at standardized conditions (23 °C and 50% relative humidity).

Compression molded cylinders with a diameter of 8 mm and a height of 5 mm were used to compare the solvent debinding behavior of the different compounds. The specimens were produced in a mold with PTFE seals and inside a hydraulic vacuum press P200PV (Dr. Collin GmbH, Germany). The mold was filled and heated to 160 °C at 1 bar during 40 min. Following 50 bars of pressure during 5 min enabled the compaction of the material, which was then cooled down to 30 °C at 50 bars. Five cylinders of each feedstock were immersed during 6 hours in cyclohexane at 60 °C. An oil bath unit (Mettmert GmbH, Germany) was used to control the temperature. The specimens and the solvent were placed in glass desiccators with Dimroth condensers attached to the lid to prevent the solvent evaporation. In all the cases 20 ml of solvent were employed per gram of feedstock. After 6 hours in the solvent the specimens were extracted and dried at 80 °C for 2 hours in a vacuum drying oven (Binder VD 23, Binder GmbH, Germany). The initial and final mass was measured gravimetrically to determine the mass loss.

## Results and discussion

The capillary rheology measurement is one of the most useful tools to determine the processability of the compounds by FFF due to the similarity with the FFF nozzle [2,3]. In our case the average apparent viscosity ( $\eta_a$ ) recorded during the filament production at an apparent shear rate of  $215 \text{ s}^{-1}$  was used to determine the influence of the binder components on the flow behavior. The regression model (1) (with response surface plot in Fig. 1a) indicates a linear dependence of the apparent viscosity on the three factors. Increasing the gP and SEBS increased the viscosity as observed for binary mixtures of wax with polyolefins [8]. Nevertheless, the SEBS has largest effect on the viscosity increase. Similarly to our previous study [4], the incorporation of PW is necessary to decrease the feedstock viscosity and enable the flow through the FFF nozzle with less required stiffness [2,3]. The high  $R^2$  value of 0.985 and normal distribution of residuals (Fig. 1b) indicate the adequacy of the obtained model in the range of compositions studied.

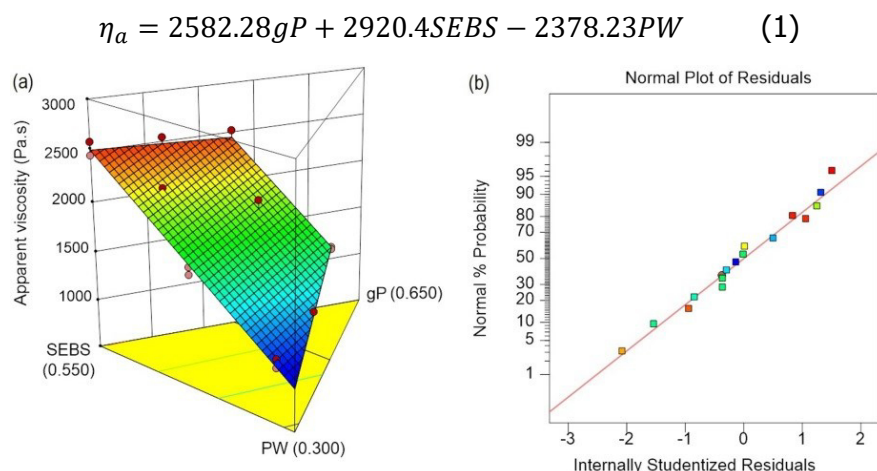


Figure 1. Response surface plot of the regression model (a) and normal probability plot (b) of the apparent viscosity.

Tensile tests were conducted on the filaments to determine their strength, flexibility and stiffness. The stress at break ( $\sigma_b$ ) of the filaments was used to determine the filaments strength. The effect of the evaluated factors in  $\sigma_b$  is calculated in the regression equation (2) and Fig. 2a depicts the response surface plot of the regression model. The  $R^2$  value is 0.69, which cannot be considered high enough for obtaining a precise prediction of the  $\sigma_b$  value with the calculated model. The high scattering of the  $\sigma_b$  results might be caused by two phenomena. For brittle filaments such as the ones tested, a processing induced curvature of the specimen before testing generates additional bending stresses that lead to an earlier fracture at the beginning of the tensile tests. Despite taking special care to collect straight specimens during the filament production, the slightest curvature resulting from handling the specimens will affect the results. In addition, the used zirconia powder has a high tendency to agglomerate due to its small size [5]. An agglomerate in the filament constitutes a weak point in which the fracture will occur preferentially. Nevertheless, the model can provide important information about how each factor affects the strength. No component had a detrimental effect on  $\sigma_b$ , and the highest values were measured for compounds with high gP. The use of the grafted polyolefin improves the adhesion with the powder [9], increasing the strength of the material [10]. Despite the poor strength of the PW, its incorporation produces a higher increase in  $\sigma_b$  than the SEBS. The reasons might be that at the concentrations here investigated, the PW can increase the crystallinity of the rest of the components [11] and improve the microstructure homogeneity [4].

$$\sigma_b^2 = 519.05gP + 4.53SEBS + 28.91PW \quad (2)$$

The strain at break ( $\varepsilon_b$ ) of the filaments was used to determine their flexibility. In the regression model (3) and in its response surface plot (depicted in Fig. 2b) the effect of the evaluated factors in the  $\varepsilon_b$  can be observed. The higher sensitivity of the strain values to the phenomena previously mentioned resulted in a  $R^2$  of 0.53. Nevertheless the residuals remained normally distributed as shown in Fig. 2e. In general terms, it can be stated that the individual effect of the PW is a decrease of strain values, which is in accordance with the results of similar studies [8]. Even though gP and SEBS increase the strain values slightly, the highest increase is obtained for the interaction of SEBS and PW. This interaction could be caused by the combined effect of the good flexibility of the compounds with SEBS, and the improvement of the homogeneity when incorporating the PW [4]. When combining both soluble components in the right proportion, high strain values could be obtained.

$$\varepsilon_b^{1.35} = 2.69gP + 3.55SEBS - 15.99PW + 61.08SEBS \cdot PW \quad (3)$$

The stiffness of the filaments was determined by means of the secant modulus (SM) calculated in the strain range between 0.1 and 0.3%. These values were chosen in order to reduce the effect of the specimen's curvature on the results. The effect of the evaluated factors in the SM can be observed in the regression equation (4). Fig. 2c depicts the response surface plot of the regression model. The residuals are normally distributed (Fig. 2f) and the  $R^2$  value is 0.745, which is the highest value of the models for the mechanical properties. The individual effects of the components show the decrease of the filaments stiffness with the increase of all of them, especially with SEBS. Nevertheless, a large improvement is obtained by the interaction of gP with both SEBS and PW.

$$SM^{1.5} = (-1.56gP - 2.65SEBS - 1.61PW + 13.44gP \cdot SEBS + 11.3gP \cdot PW)10^5 \quad (4)$$

### 3. Development of binder formulation

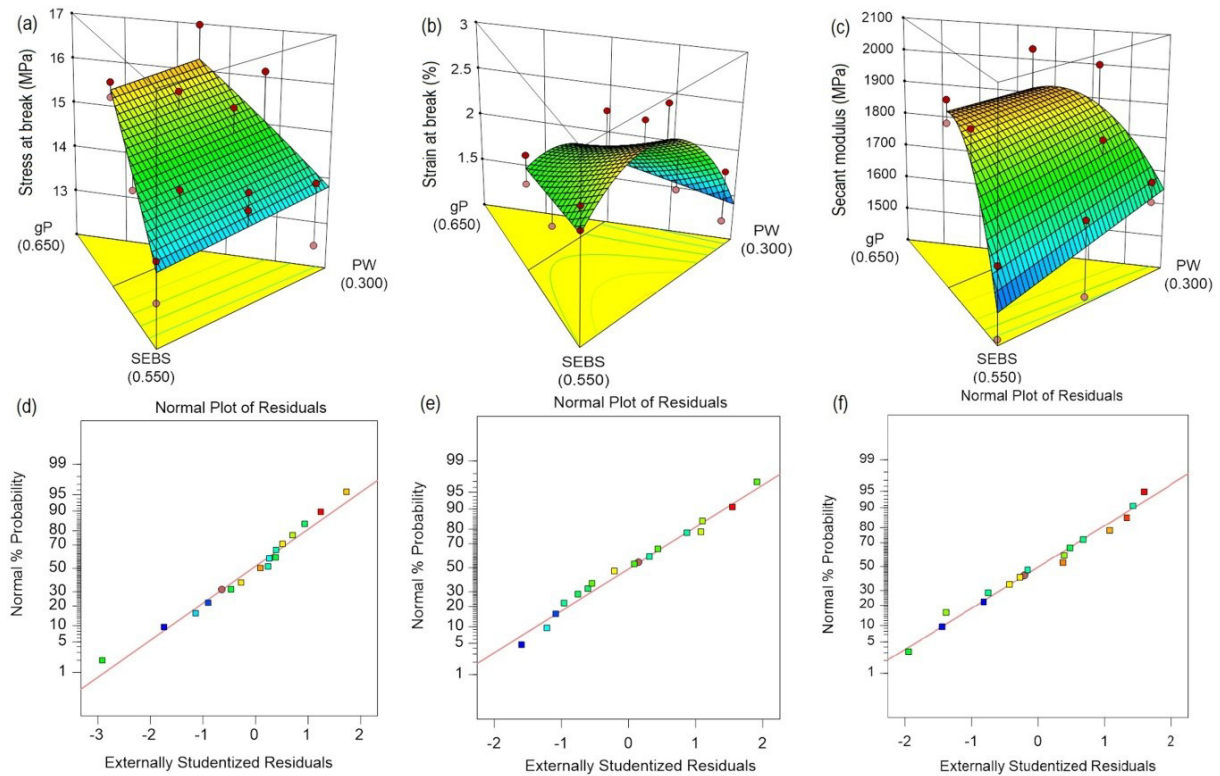


Figure 2. Response surface plot of the regression model of the stress at break (a), the strain at break (b) and the secant modulus (c). Normal probability plot of the stress at break (d), the strain at break (e) and the secant modulus (f).

The loss of soluble binder (LSB) was calculated with the assumption that no powder or backbone was lost during debinding. At the end of the tests, cracks appeared on the specimens with different sizes depending on the composition (Fig. 3a). Therefore the LSB results must be carefully evaluated considering the different cracking of the parts. Like in the previous models, the square root transformation was applied for the LSB analysis in order to provide homoscedasticity of variance and to ensure that the residuals remained normally distributed (Fig. 3b). In the regression equation (5) the effect of the evaluated factors in the inverse of LSB is calculated. The response surface plot of the regression model is depicted in Fig. 3c. In this case the  $R^2$  of the experimental model is 0.798. As can be expected, increasing the gP produces a large decrease in the LSB since the insoluble backbone creates a physical barrier that hinders the diffusion of the dissolved polymers out of the specimens, which is the limiting factor during solvent debinding [12]. The increase of SEBS has the higher effect on LSB, nevertheless is due to the large cracks observed for these feedstocks (Fig. 3a) since the solvent penetrates easily through the cracks to the core of the specimen and the dissolved products are easily removed. The incorporation of the PW proved to be best option for the increase of LSB and for the reduction of the defects as a result a better homogeneity of the compounds [4].

$$LSB^{-1} = (21.9gP + 7.51SEBS + 10.93PW) \cdot 10^{-3} \quad (5)$$



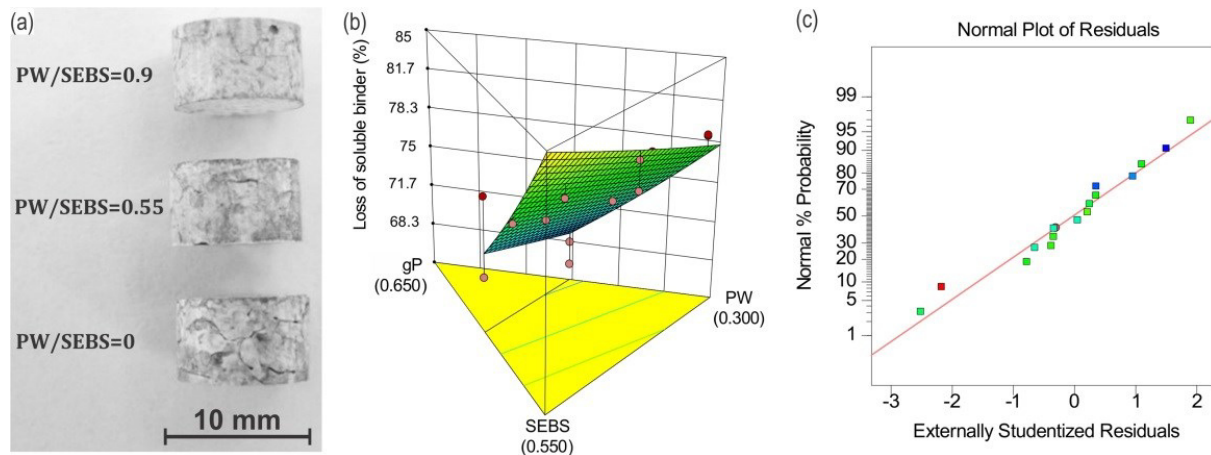


Figure 3. Cracks observed in specimens with the same gP content, but different PW/SEBS ratio (a). Response surface plot of the regression model (b) and normal probability plot (c) of the loss of soluble binder.

## Conclusions

The effect of the fractions of the binder components in the properties of FFF feedstocks has been statistically determined. Increasing the content of gP and SEBS improves the mechanical properties of the filaments. Nevertheless both components increase the viscosity and make the defect-free solvent debinding more difficult. The incorporation of PW reduces the feedstocks viscosity and the defects while improving the debinding rate. Thus, intermediate contents of backbone and ratios  $1 \geq \text{PW/SEBS} \geq 0.6$  should be employed for the best combination of properties. Based on these results the feedstock with the best properties combination has been selected and a detailed investigation on the whole FFF process of zirconia is ongoing.

## Acknowledgements

This research was performed under the project CerAMufacturing with the financial support of the European Commission in the frame of the FoF Horizon 2020 with financial agreement 678503.

## References

1. M. K. Agarwala, V. R. Jamalabad, N. A. Langrana, A. Safari, P. J. Whalen, and S. C. Danforth, *Rapid Prototyping Journal* **2**, 4 (1996).
2. S. Rangarajan, G. Qi, N. Venkataraman, A. Safari, and S. C. Danforth, *Journal of the American Ceramic Society* **83**, 1663 (2000).
3. N. Venkataraman, S. Rangarajan, M. J. Matthewson, B. Harper, A. Safari, S. C. Danforth, G. Wu, N. Langrana, S. I. Guceri, and A. Yardimci, *Rapid Prototyping Journal* **6**, 244 (2000).
4. S. Cano, J. Gonzalez-Gutierrez, J. Sapkota, M. Spoerk, F. Arbeiter, C. Holzer, and C. Kukla (Submitted).

5. B. C. Mutsuddy and R. G. Ford, *Ceramic injection moulding* (Chapman & Hall, London, 1995).
6. N. Aliheidari, R. Tripuraneni, C. Hohimer, J. Christ, A. Ameli, and S. Nadimpalli, "The impact of nozzle and bed temperatures on the fracture resistance of FDM printed materials," in *Proc. SPIE 10165, Behavior and Mechanics of Multifunctional Materials and Composites 2017*, edited by N. C. Goulbourne (2017), p. 1016512.
7. M. Spoerk, J. Sapkota, G. Weingrill, T. Fischinger, F. Arbeiter, and C. Holzer, *Macromol. Mater. Eng.* **12**, 1700143 (2017).
8. M. E. Sotomayor, I. Krupa, A. Várez, and B. Levenfeld, *Renewable Energy* **68**, 140 (2014).
9. P. Wongpanit, S. Khanthasri, S. Puengboonsri, and A. Manonukul, *Materials Chemistry and Physics* **147**, 238 (2014).
10. M. Alexandre and P. Dubois, *Materials Science and Engineering: R: Reports* **28**, 1 (2000).
11. H.S. Mpanza and A. S. Luyt, *Polymer Testing* **25**, 436 (2006).
12. M. A. Omar, H. A. Davies, P. F. Messer, and B. Ellis, *Journal of Materials Processing Technology* **113**, 477 (2001).

## 3.5 Publication C

### ***Influence of stearic acid in feedstocks for FFF and PIM***

Kukla C., Cano S., Holzer C., Gonzalez-Gutierrez J.

© European Powder Metallurgy Association (EPMA). First published in the Euro PM2019 Congress Proceedings, Maastricht, Netherlands, 13-16.10.19

ISBN: 978-1-899072-51-4

Available online: 16.10.2019

#### **ABSTRACT**

Material extrusion additive manufacturing with filaments is also known as Fused Filament Fabrication (FFF). FFF is a versatile and popular technology that, when combined with debinding and sintering, can be used for the fabrication of functional metal and/or ceramic parts similar to Powder Injection Moulding (PIM). In order to produce filaments that are processable by FFF, a complex binder system is needed. The binder is generally composed of the main binder component, the backbone and additives. One popular additive in feedstocks for FFF or PIM is stearic acid (SA), since the use of SA is an effective way to reduce the viscosity, improve the feedstocks homogeneity and increase the solvent debinding rate. In this investigation, the incorporation of SA into a binder system comprised of acrylic acid-grafted high density polyethylene, paraffin wax and styrene-ethylene/butylene-styrene copolymer has been studied. The effect of the SA on the viscosity, mechanical properties, debinding rate and processing by FFF for zirconia feedstocks is presented.

## Introduction

Metallic and ceramic components can be produced by the material extrusion process known as Fused Filament Fabrication (FFF). In the FFF of metals and ceramics, a polymeric binder is used to carry a high fraction of metallic or ceramic powder, obtaining the so-called feedstock. The feedstock is used to produce filaments which are then processed in a conventional FFF process to shape the parts, which must be debound and sintered similarly to the well-established process of Powder Injection Moulding (PIM). Like in PIM, FFF powders of different sizes and shapes can be employed and a wide range of materials can be processed [1]. Moreover, the same feedstocks can be employed for both processes, making possible their combination or the use of FFF as a prototyping method for PIM.

In order to be processed as filaments by FFF, the feedstocks must meet many rheological and mechanical requirements [2–4]. One of the main factors affecting the properties of the feedstocks and their processability by FFF is the wetting and adhesion of the polymeric binder to the powder surface. A poor adhesion in particulate filled polymers leads to the separation of both types of materials and to inhomogeneities in the mixture, resulting in a high viscosity and in poor mechanical properties [5–7]. Since the polymers commonly employed as binders in PIM and FFF are highly non-polar, and the powder surface is characterized by a high polarity, additives are incorporated to improve the interaction of both materials.

Stearic acid (SA) is the most common additive for the processing of metals and ceramics by PIM. The polar carbonyl group (C=O) in this fatty acid [7] facilitates the wetting and adhesion of the binder to the polar surface of the powders. Therefore, SA has been added as surfactant to improve the feedstock homogeneity and reduce the viscosity in both PIM [7–9] and FFF feedstocks [3,4]. In this study, the effect of SA on the properties of zirconia feedstocks developed in our previous study [2] is evaluated and correlated to the processability by FFF and solvent debinding.

## Experimental

### Materials

TZ-3YS-E (Tosoh Europe B.V., The Netherlands) with 3 mol% of yttria, a specific surface area of  $7 \pm 2 \text{ m}^2/\text{g}$  and a particle size of  $d_{50} = 0.09 \mu\text{m}$  was the zirconia powder selected. A multicomponent binder developed in our previous study [2] comprised of acrylic acid-grafted high density polyethylene (AA-HDPE), paraffin wax (PW) and styrene-ethylene/butylene-styrene copolymer (SEBS) was used. The compositions shown in Table 1 were compared. In order to determine the effect of the stearic acid (SA), the relative content of the AA-HDPE, PW and SEBS was constant in both feedstocks.

Table 1. Composition of the feedstocks in volumetric percentage. The stearic acid content in the feedstock is used to name and to differentiate between both mixtures.

	<b>AA-HDPE</b>	<b>SEBS</b>	<b>PW</b>	<b>SA</b>	<b>Z</b>
5.3% SA	18.55	14.58	14.58	5.3	47
0% SA	20.61	16.19	16.19	0	47

#### **Compounding and filament production**

The binder mixture consisting of AA-HDPE+PW+SEBS was produced in a co-rotating twin screw extruder (Werner & Plfeiderer GmbH, Germany). The compounding was conducted at a speed of 100 rpm with a temperature profile from the hopper to the nozzle of 75 to 170 °C. The material was collected in a metal conveyor belt, cooled using air ventilators and pelletized (Reduction Engineering GmbH, Germany).

Following, the feedstocks were produced in the co-rotating twin screw extruder Leistritz ZSE 18 HP-48D (Leistritz Extrusionstechnik GmbH, Germany). The binder was introduced by a first gravimetric feeder and in a second gravimetric feeder the zirconia powder was fed together with the stearic acid. The binder was added at a rate of 6 kg·h<sup>-1</sup> and the powder at an according speed to have the right powder content. The screw speed was set to 600 rpm. Extrusion temperatures from 165 to 175 °C were used, and the extruded material was collected with the same metal conveyor belt and pelletized.

For the production of filaments at laboratory-scale, single screw extruder FT-E20T-MP-IS (Dr. Collin GmbH, Germany) was used. The round die had a diameter of 1.75 mm and a length of 20 mm. The rotation speed was set to 30 rpm and the temperature profile went from 170 °C at the feeding zone to 200 °C at the die. The extruded filament was cooled on a conveyor belt by air and then wound using a winding unit developed in-house.

#### **Rheology**

The apparent viscosity of the feedstocks was measured using the high pressure capillary rheometer Rheograph 2002 (Göttfert Werkstoff-Prüfmaschinen GmbH, Germany) at 230 °C and apparent shear rates from 75 to 750 s<sup>-1</sup>. A round die with a diameter of 1 mm and a length of 30 mm was employed.

#### **Tensile tests**

The mechanical properties of the filaments were measured by means of tensile tests. Straight filaments with a length of 100 mm were tested on the universal testing machine Zwick Z001 (Zwick GmbH & Co.KG, Germany) with a 1 kN load cell and pneumatic grips. The initial gauge length was 50 mm for all the measurements. The tests were performed until rupture at a speed of 10 mm·min<sup>-1</sup> at standardized conditions (23 °C and 50 % relative humidity). At least five repetitions per material were performed.

#### **Morphology evaluation**

The cryo-fracture surface of the extruded filaments with the zirconia feedstocks was studied by scanning electron microscopy (SEM, Tescan Vega II, Tescan Brno, s.r.o., Czech Republic). The analyses were performed on gold sputtered (100 s at 20 mA) specimens at 5 kV using secondary electrons.

#### **Fused Filament Fabrication**

Using these filaments, six cuboids of dimensions 15x15x5 mm<sup>3</sup> were produced by FFF. The slicer software Slic3r Prusa Edition was used for the generation of the G-code. The parts were produced by means of the Duplicator i3 v2 (Wanhao, USA) FFF machine. A brass nozzle of 0.6 mm in diameter coated with TwinClad® was used for the printing at a temperature of 230 °C. In the first layer, the printing speed was 5 mm·s<sup>-1</sup> and in the rest of the layers 10 mm s<sup>-1</sup>. The layer thickness was set to 225 µm and a concentric infill was employed. The building platform was a hairspray coated glass mirror set to 80 °C.

#### **Solvent debinding**

The solvent debinding of components with different geometries was performed using cyclohexane. In order to determine the effect of the SA in solvent debinding, the following specimens were tested: straight filaments with a length of 50 mm and a diameter of 1.75 mm; compression moulded discs with a height of 2 mm and a diameter of 25 mm; the FFF cuboids with dimensions 15x15x5 mm<sup>3</sup> and compression moulded cylinders with a height of 5 mm and diameter of 8 mm [2].

A glass desiccator enclosed within an oil bath unit with a temperature control (Memmert GmbH, Germany) was used. The solvent was refluxed with a Dimroth condenser attached to the lid to prevent the evaporation of the solvent. The specimens were immersed in pre-heated cyclohexane at 60 °C for 6 hours, with 12 ml of solvent per gram of feedstock. After 6 hours in the solvent, the specimens were left to dry at room temperature overnight. The final mass was measured to evaluate the percentage of leached binder.

## **Results and Discussion**

#### **Rheological characterization**

In Figure 1 the apparent viscosity of the feedstocks with 5.3 % and 0 % of SA is shown. The use of SA in the feedstock results in a lower apparent viscosity in the whole range of shear rates evaluated, the difference is becoming more pronounced at higher shear rates (48 %) compared to 25 % at the lowest shear rate. The reduction of the viscosity with the increase of SA can be explained by its effect as lubricant as well as surfactant, improving the wetting of the powder and its dispersion in the feedstock [3,5,7,8]. A lower viscosity and an improved powder dispersion result in an improved processability and give the possibility to increase the powder content in the feedstock, as demonstrated for PIM [8,9].

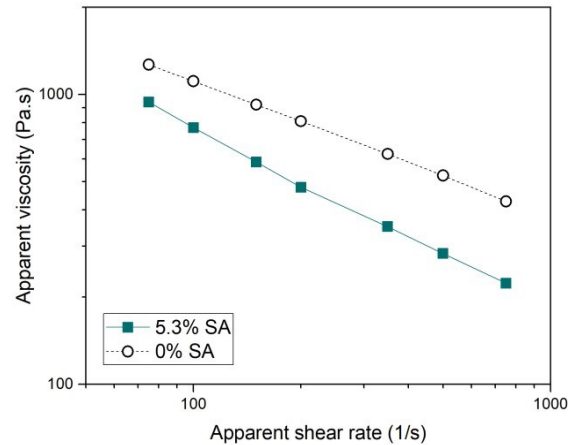


Figure 1: Apparent viscosity at 230 °C for the two feedstocks.

### Mechanical testing

The representative strain-stress curves shown in Figure 2 for the two feedstocks show the reduction of the mechanical properties of the filaments with the incorporation of SA. For the 0 % SA feedstock the strength at break was 39 % higher than for the 5.3 % SA feedstock and the stiffness (determined by the secant modulus between 0.1 and 0.3%) was 9 % higher in the feedstock with no SA. Furthermore, the elongation at break of the 0 % SA filaments was twice the one measured for the 5.3 % SA filaments.

The decrease of the mechanical properties with the incorporation of SA is in principle unexpected, since the improvement of the filler dispersion should result in an increase of the mechanical properties [5]. Nevertheless, the SA is not the only polar organic component in the feedstocks, since the backbone employed is an acrylic acid grafted HDPE [2]. For polymer nanocomposites, it is well known that the use of macromolecules (such as the acrylic acid HDPE) results in higher mechanical properties than the small molecules (such as the SA) due to the stronger interface entanglements with the rest of the polymer matrix [6]. Therefore, the use of SA in the feedstock might result in a reduction of the AA-HDPE effect on the mechanical properties and thus complicates the handling of the filaments without fracture.

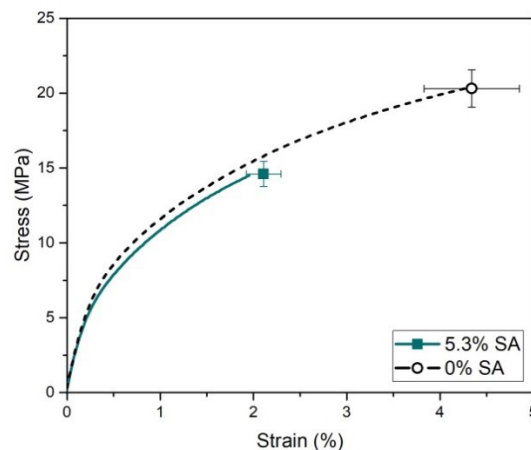


Figure 2: Representative strain-stress curves and average yield stress and strain at break of filaments produced with the two feedstocks.

#### **Morphology**

The cryo-fracture surfaces of green filaments of the evaluated feedstocks are shown in Figure 3. The 5.3% SA feedstock filament has a homogeneous microstructure with small porosity, whereas large pores characterize the 0 % SA feedstock morphology. The improvement in the homogeneity for filled polymers with the incorporation of SA is well-known, as it is produced by the improvement of the powder dispersion and the lubricating effect of the SA [5,7]. With exception of the pores, no inhomogeneity can be observed in the feedstocks produced by the separation of the binder components (as we observed in [2]).

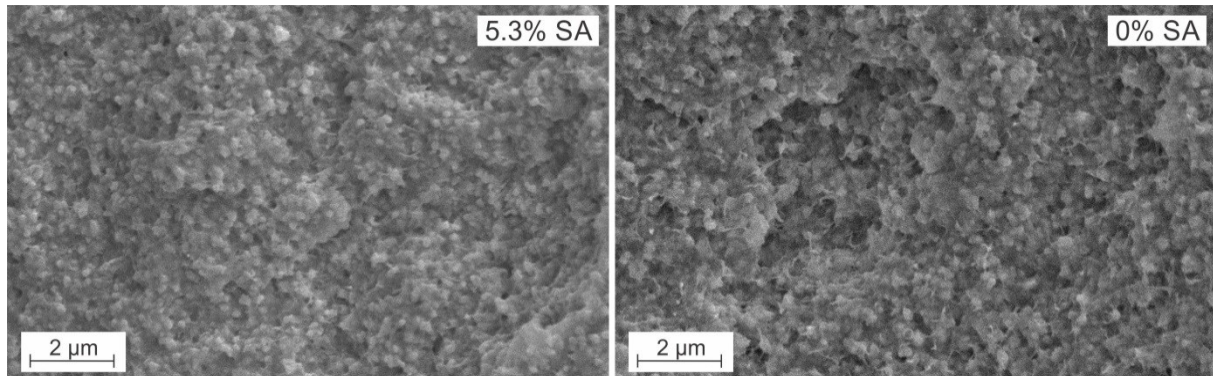


Figure 3: Scanning Electron Microscopy of the cryo-fracture surface of filaments produced with the two feedstocks.

#### **FFF processing**

Figure 4 shows examples of the cuboids produced with the 5.3 % and 0 % SA feedstocks and the average mass of the produced specimens. Due to the reduction in viscosity when using SA, more material was extruded for the 5.3 % SA than for the 0 % SA feedstock. The insufficient extrusion of material combined with a high viscosity, which reduces the cross flow of material for closing the gaps in the parts [10], resulted in parts with underfilled sections for the 0 % SA feedstock. Moreover, the incorporation of SA resulted in a better bonding between the extruded layers for the 5.3 % SA feedstock, which did not show the interlayer cracks observed for the 0 % SA feedstock. Nevertheless, the increase of the extrusion temperature might help to reduce the viscosity of the 0 % SA feedstock and to solve these defects.



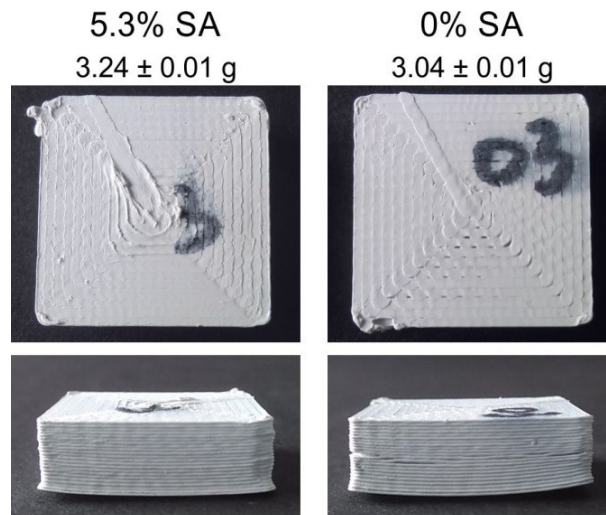


Figure 4: Exemplary FFF cuboids with dimensions  $15 \times 15 \times 5 \text{ mm}^3$  produced with the two feedstocks and average mass of the printed parts.

### Solvent debinding

In Figure 5 the leached soluble binder in wt% is plotted as a function of the surface area to volume ratio ( $A_s/V$ ). As expected, the increase of the  $A_s/V$  ratio resulted in a faster debinding, due to the reduction of the diffusion length [11]. As we observed in our previous study [4], the incorporation of SA resulted in an increase of the solvent debinding performance. This might be the result of either the lower molecular weight of the SA compared to the other soluble components, and/or the improvement of the powder dispersion [4]. The only exception in the described trends is the FFF cuboids produced with the 0% SA feedstock. The reason for such deviation might be the porosity of the parts produced with this feedstock, which can be observed in Figure 4. The gaps between the deposited strands in the parts facilitate the penetration of the solvent into the components, as well as the diffusion of the dissolved products out of the specimens.

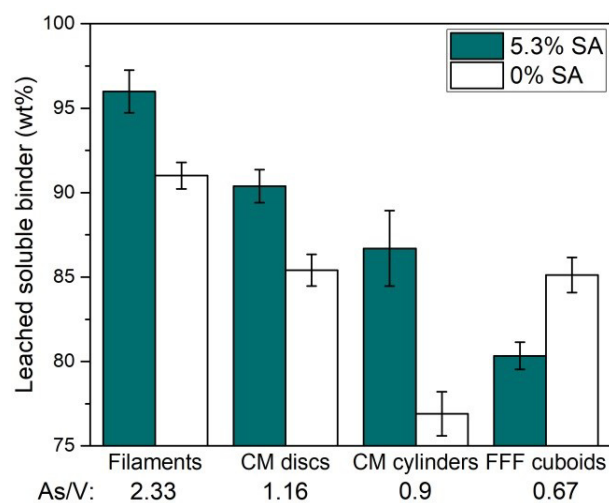


Figure 5: Leached soluble binder of components with different area of the surface/volume ratio: filaments (2.33), compression moulded (CM) discs (1.16) and cylinders (0.9) and FFF cuboids (0.67).

## Conclusion

The use of stearic acid in zirconia feedstocks for FFF is an effective way to reduce the viscosity, improve the feedstocks homogeneity and increase the solvent debinding rate. The reduction in the viscosity is a key factor to attain dense FFF green parts without the interlayer cracks observed for the feedstock without SA. However, the feedstock filaments with SA also have reduced mechanical properties, which results in a more difficult handling of the filaments and complicates a continuous winding of the material. As the filament without SA has considerably higher mechanical properties, further FFF trials with different processing parameters (especially higher extrusion temperatures) must be conducted to attain defect free FFF green parts. In addition, lower quantities of SA could be investigated in order to improve the viscosity and debinding rate without lowering the mechanical properties too much.

## Acknowledgement

This research was performed under the Austria-China bilateral cooperation project FlexiFactory3Dp. The FlexiFactory3Dp project has received funding from the Austrian Research Promotion Agency under the program Production of the Future, Grant Agreement No. 860385.

## References

- [1] J. Gonzalez-Gutierrez, S. Cano, S. Schuschnigg, C. Kukla, J. Sapkota, C. Holzer, Additive Manufacturing of Metallic and Ceramic Components by the Material Extrusion of Highly-Filled Polymers: A Review and Future Perspectives, *Materials* 11 (2018).
- [2] S. Cano, J. Gonzalez-Gutierrez, J. Sapkota, M. Spoerk, F. Arbeiter, S. Schuschnigg, C. Holzer, C. Kukla, Additive manufacturing of zirconia parts by fused filament fabrication and solvent debinding: Selection of binder formulation, *Additive Manufacturing* 26 (2019) 117–128.
- [3] L. Gorjan, L. Reiff, A. Liersch, F. Clemens, Ethylene vinyl acetate as a binder for additive manufacturing of tricalcium phosphate bio-ceramics, *Ceramics International* 44 (2018) 15817–15823.
- [4] C. Kukla, S. Cano, D. Kaylani, S. Schuschnigg, C. Holzer, J. Gonzalez-Gutierrez, Debinding behaviour of feedstock for material extrusion additive manufacturing of zirconia, *Powder Metallurgy*, accepted (2019).
- [5] C. Del Angel, A.B. Morales, F. Navarro-Pardo, T. Lozano, P.G. Lafleur, S. Sanchez-Valdes, G. Martinez-Colunga, E. Ramirez-Vargas, S. Alonso, R. Zitzumbo, Mechanical and rheological properties of polypropylene/bentonite composites with stearic acid as an interface modifier, *J. Appl. Polym. Sci.* 132 (2015) n/a-n/a.
- [6] L. Dányádi, J. Móczó, B. Pukánszky, Effect of various surface modifications of wood flour on the properties of PP/wood composites, *Composites Part A: Applied Science and Manufacturing* 41 (2010) 199–206.
- [7] M.-C. Auscher, R. Fulchiron, N. Fougereuse, T. Périé, P. Cassagnau, Zirconia based feedstocks: Influence of particle surface modification on the rheological properties, *Ceramics International* 43 (2017) 16950–16956.

- [8] Y.-m. Li, X.-q. LIU, F.-h. LUO, J.-l. YUE, Effects of surfactant on properties of MIM feedstock, *Transactions of Nonferrous Metals Society of China* 17 (2007) 1–8.
- [9] T. Hanemann, R. Heldele, T. Mueller, J. Hausselt, Influence of Stearic Acid Concentration on the Processing of ZrO<sub>2</sub>-Containing Feedstocks Suitable for Micropowder Injection Molding, *International Journal of Applied Ceramic Technology* 8 (2011) 865–872.
- [10] M. Spoerk, F. Arbeiter, H. Cajner, J. Sapkota, C. Holzer, Parametric optimization of intra- and inter-layer strengths in parts produced by extrusion-based additive manufacturing of poly(lactic acid), *J. Appl. Polym. Sci.* 134 (2017) 45401.
- [11] T.S. Shivashankar, R.M. German, Effective Length Scale for Predicting Solvent-Debinding Times of Components Produced by Powder Injection Molding, *Journal of the American Ceramic Society* 82 (1999) 1146–1152.

## 3.6 Publication D

### ***Modification of Interfacial Interactions in Ceramic-Polymer Nanocomposites by Grafting: Morphology and Properties for Powder Injection Molding and Additive Manufacturing***

Santiago Cano, Ali Gooneie, Christian Kukla, Gisbert Rieß, Clemens Holzer and Joamin Gonzalez-Gutierrez

**Applied Sciences, 10 (2020) 1471**

**Special Issue *Material Development for Additive Manufacturing and Injection Moulding*, Special Issue Editors Joamin Gonzalez-Gutierrez and Christian Kukla**

doi: 10.3390/app10041471

Received: 05.02.2020

Revised: 18.02.2020

Accepted: 18.02.2020

Available online: 21.02.2020

#### **ABSTRACT**

The adhesion of the polymer to ceramic nanoparticles is a key aspect in the manufacturing of ceramic parts by additive manufacturing and injection molding, due to poor separation results in separation during processing. The purpose of this research is to investigate, by means of molecular dynamics simulations and experimental methods, the role of improved interfacial interactions by acrylic acid grafting-high density polyethylene on the adhesion to zirconia nanoparticles and on the composite properties. The polymer grafting results in high adhesion to the nanoparticles, increases the nanoparticles dispersion and improves the viscoelastic and mechanical properties required for additive manufacturing and injection molding.

*Keywords:* interfacial interactions; rheological properties; mechanical properties; nanocomposites; ceramics; powder injection molding; fused filament fabrication; grafted polymers; molecular dynamics simulation.

## 1. Introduction

The composites of thermoplastic polymers with ceramic nanoparticles are used in numerous fields such as medicine [1–3], electronics [4] or flame retardancy applications [3,5]. Moreover, highly filled ceramic-polymer nanocomposites are used for the manufacturing of ceramic parts by processes such as powder injection molding (PIM) [6–9] and fused filament fabrication (FFF) [10–12]. In these processes, the polymer acts as a carrier that enables the shaping of complex parts by injection molding or layer-by-layer extrusion into three dimensional objects. Once the parts are shaped, the polymer is removed in the debinding step. Finally, the parts are sintered to obtain ceramic components with high density.

Polymer nanocomposites are complex systems, whose properties are determined by the properties of the components, the composition, the interfacial interactions and the morphology of the composite [13–15]. The adhesion and wetting of the polymer matrix to the surface of the powder [9,16] is a critical aspect since a poor adhesion will lead to the separation of both materials during processing, resulting in a weak interface and poor macroscopic properties [16,17]. The powder–binder separation is especially detrimental for the highly-filled composites used in PIM and FFF, since it leads to failure of the process by, for example, filaments with poor mechanical properties which cannot be processed in the FFF machines [11] or by inhomogeneity in the composition of parts with complex geometry in PIM [17,18]. The interaction between the polymers and the ceramic filler is greatly influenced by the polarity of both types of material. In PIM and FFF, multicomponent polymeric blends are used. A major fraction of the polymer blend has low viscosity for PIM, while for FFF not only low viscosity but also flexibility is required. The second major component of the blend, known as the backbone, is in many cases a polyolefin such as polyethylene or polypropylene, which is removed in the last step before sintering and thus must have a high adhesion to the powder. However, polyolefins are non-polar, whereas the surface of the inorganic particles is characterized by a high polarity. Therefore, different strategies have been developed to improve the adhesion and the interfacial interaction between both types of materials.

To improve the adhesion between the polymer and the ceramic, one approach includes the coating of the nanoparticles with a coupling agent such as silane [13] or with a fatty acid such as stearic or oleic acid [6,7,10], which can also be incorporated as a surfactant [8,19]. Fatty acids and stearic acid have been extensively used in PIM and FFF as they improve the dispersion of the particles and reduce the viscosity of the composites [6–8,10,19]. Nonetheless, these low molecular weight polymers are very unstable and degrade if processed at high temperatures or long times [7]. Moreover, short molecules such as the fatty acids do not have strong entanglements with the rest of the polymeric components, which result in poor mechanical properties [13]. Another strategy is the use of polymers grafted with a polar component such as maleic anhydride or acrylic acid, which can be incorporated as a backbone [12,20] or as a compatibilizer [5,21–28]. The improvement of the adhesion to the filler with the use of grafted polymers results in a better dispersion of the filler [27,28] and in an increase in the mechanical properties [5,21–28]. Despite these efforts, a systematic investigation of interfacial interactions is still necessary to understand their effects on the properties of the feedstocks. Here, we aim to address this subject by

means of various experiments as well as atomistic insights from molecular dynamics simulations.

In this study, we focus on the effects of interfacial interactions on feedstock properties by grafting of polyethylene with acrylic acid and modifying its adhesion to ceramic zirconia nanoparticles. The resulting composite morphology and properties for the processing by FFF and PIM are addressed. Molecular dynamic simulations are employed to calculate the binding energies between polyethylene with different grafting densities and zirconia. These results are combined with the experimental characterization of composites produced with two commercial grades of high-density polyethylene (HDPE) and yttria-stabilized zirconia powder. One of the HDPE grades is ungrafted, whereas the other is grafted with acrylic acid. The experimental investigation of the adhesion is conducted with the interfacial tension calculated from contact angle measurements and with the infrared spectra of the polymers and filler materials. The results of these experiments are linked to the dispersion of the particles in the nanocomposites and to the viscoelastic and mechanical properties.

## 2. Materials and Methods

### 2.1. Molecular Dynamics Simulation

Computational simulation methods such as atomistic molecular dynamics (MD), Monte Carlo (MC) and dissipative particle dynamics (DPD) are useful tools in the study of the polymer-filler adhesion and the characterization of the interface between both materials [15,29–34]. Moreover, MD simulations have been employed to study the interface between ceramic oxide fillers and polymer chains with grafted maleic anhydride or acrylic acid (AA) [30]. The MD simulations provide detailed atomistic information about the increase in the work of adhesion and the change of the distribution of the polymer at the interface of the composites with grafting [30,33].

MD simulations were employed for the study of the interfacial interactions between zirconia and polyethylene grafted with different contents of acrylic acid: 0, 5 and 30 mol%. Table 1 summarizes the nomenclature used for the different systems in the MD simulations. The bonded and non-bonded interactions were mapped with the optimized atomistic field COMPASS. The simulations were carried out using the Forcite module of the Materials Studio software (BIOVIA Materials Studio 2017 R2, San Diego, CA, USA). Fifty polyethylene chains ( $C_{120}H_{242}$ ) were used in each simulation run. For the polyethylene grafted with acrylic acid, additional side groups were included. The geometries of the polymer chains were initially optimized with energy and force convergence criteria of  $0.0001 \text{ kcal}\cdot\text{mol}^{-1}$  and  $0.005 \text{ kcal}\cdot\text{mol}^{-1}\cdot\text{\AA}^{-1}$ , respectively. The polyethylene chains were in contact with a zirconia block with dimensions  $L_x = L_y \approx 35.85 \text{ \AA}$  and  $L_z \approx 8.87 \text{ \AA}$ . An orthogonal simulation cell with dimensions  $L_x = L_y \approx 35.85 \text{ \AA}$  and a xyz Cartesian coordinate system was employed. A vacuum space with a length of  $500 \text{ \AA}$  was put on top of the polymer in the z-direction. Consequently, the total  $L_z$  was equal to  $635.46 \text{ \AA}$ . The simulations were run in the NVT ensemble at 443 K for 200 ps with a 0.1 fs time step. The binding energies were calculated and averaged over the final 50 ps of the simulations.

Table 1. Materials studied in the molecular dynamics (MD) simulations and nomenclature.

	<b>Polymer</b>	<b>Acrylic Acid Content (mol%)</b>
PE	PE	0
5AAPE	AA-PE	5
30AAPE	AA-PE	30

## 2.2. Materials

Tetragonal zirconia ( $ZrO_2$ ) (TZ-3YS-E, partially stabilized with 3 mol% yttria ( $Y_2O_3$ ), Tosoh Europe B.V., Amsterdam, The Netherlands), supplied as spray dried granules with an average particle size of 90 nm and a specific surface area of  $7 \pm 2 \text{ m}^2/\text{g}$ , was the filler used. Figure 1 depicts the scanning electron microscopy (SEM) image of the powder. The commercial acrylic acid-grafted high-density polyethylene SCONA TPPE 2400 (AAHDPE, BYK-Chemie GmbH, Wesel, Germany) employed in our previous study [12] was the functionalized polymer. According to the supplier [35], the material contains a minimum of 5 mol% of acrylic acid and has a melt volume rate (MVR) ranging from 9 to 20  $\text{cm}^3/10 \text{ min}$  (190 °C, 2.16 kg). Due to the importance of the viscosity for the processing of polymer nanocomposites, the non-grafted high-density polyethylene was selected based on its MVR. Therefore, the high-density polyethylene CG9620 (HDPE, Borealis AG, Vienna, Austria) was selected as it had a melt flow rate (MFR) of 12 g/10 min (MVR $\sim$ 12.47  $\text{cm}^3/10 \text{ min}$ , 190 °C, 2.16 kg). Using the two polymers and the zirconia powder, the compounds shown in Table 2 were compared.

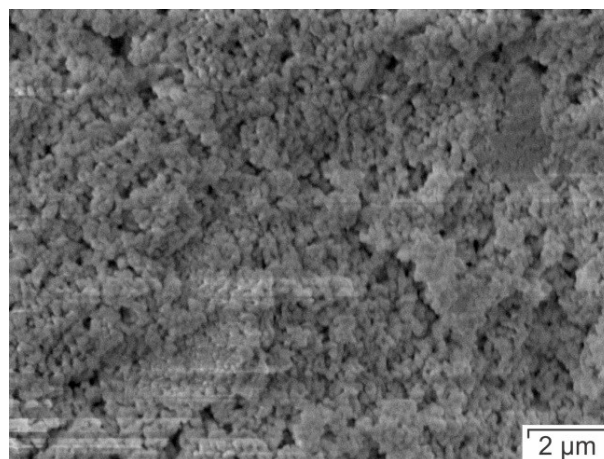


Figure 1. SEM of the zirconia powder partially stabilized with yttria.

Table 2. Compounds prepared and nomenclature.

	<b>Polymer</b>	<b>Acrylic Acid Content (mol%)</b>	<b>Zirconia Content (vol%)</b>
HDPE00	HDPE	0	0
HDPE30	HDPE	0	30
AAHDPE00	AA-HDPE	>5	0
AAHDPE30	AA-HDPE	>5	30

### 2.3. Preparation of the Compounds

All the materials were processed in an internal mixer fitted with counter rotating roller rotors with a mixing chamber volume of 300 cm<sup>3</sup> (HAAKE Rheomix R3000p, Thermo Fisher Scientific Inc., Waltham, MA, USA). Mixing was performed at 160 °C and 60 rpm. The compounding of the nanocomposites started with the filling of the polymer, and after 3 min the powder was added in 5 batches with 5 min after each addition to ensure the stabilization of the torque and thus a proper dispersion. The mixing was continued for a total time of 60 min. The molten compounds were extracted from the chamber and cooled down to room temperature. Following, they were granulated using the cutting mill Retsch SM200 (Retsch GmbH, Haan, Germany) equipped with a sieve with 4 × 4 mm<sup>2</sup> square shaped perforations. The non-filled systems were processed using the same method in order to avoid the influence of the thermo-mechanical processing step.

### 2.4. Calculation of the Interfacial Tension by Contact Angle Measurements

The contact angle measurements of the unfilled polymers (HDPE00 and AAHDPE00) were conducted using compression molded plates. A plate of each material was produced in the hydraulic vacuum press P200PV (Dr. Collin GmbH, Maitenbeth, Germany). A steel frame with a thickness of 2 mm and flat polytetrafluoroethylene (PTFE) plates were used during the pressing. New PTFE plates were used for each material in order to obtain the same surface roughness, as this is known to influence the contact angle measurements [36]. The compression molding started with the pre-heating of the material at 180 °C during 10 min at a pressure of 1 bar, followed by the compression at 50 bar during 10 min and finally by the cooling down to 30 °C at a pressure of 50 bar.

The contact angle measurements were conducted at room temperature with the goniometer Krüss DSA100 (Krüss GmbH, Hamburg, Germany) using deionized water and diiodomethane as the test liquids. Fifteen repetitions were performed per combination of polymer and liquid. For the zirconia, we used the contact angle values measured by González-Martín et al. [37] for plates of pure zirconia, tetragonal zirconia stabilized with yttria and zirconia with 3% of yttria. The contact angle values were employed for the determination of the surface energy components of each material using the Owens, Wendt, Rabel and Kaelble (OWRK) method [38–40]:



$$\frac{(1+\cos \theta) \cdot (\sigma_l^P + \sigma_l^D)}{2 \cdot \sqrt{\sigma_l^D}} = \sqrt{\sigma_m^P} \cdot \sqrt{\frac{\sigma_l^P}{\sigma_l^D}} + \sqrt{\sigma_m^D} \quad (1)$$

where  $\theta$  is the contact angle between the evaluated material (zirconia, AAHDPE or HDPE) and the test liquid;  $\sigma_l^P$  and  $\sigma_l^D$  are the polar and disperse fractions of the surface energy test liquids, respectively, both known;  $\sigma_m^P$  is the polar fraction of the material surface energy, which is calculated as the slope of the fitted line; and  $\sigma_m^D$  is the disperse fraction of the material surface energy, calculated as the intercept between the fitted line and the axis. The interfacial tension between the zirconia and each polymer was calculated [41,42] with the equation:

$$\gamma_{zp} = \sigma_z^P + \sigma_z^D + \sigma_p^P + \sigma_p^D - 2 \cdot \left( \sqrt{\sigma_z^D \cdot \sigma_p^D} + \sqrt{\sigma_z^P \cdot \sigma_p^P} \right), \quad (2)$$

in which the subscript  $z$  refers to the zirconia and the subscript  $p$  to the polymer (HDPE or AAHDPE).

## 2.5. Attenuated Total Reflection Spectroscopy

The infrared absorption spectra of the zirconia powder, the polymers and the compounds were measured by attenuated total reflection spectroscopy (ATR). ATR spectroscopy was performed using a Vertex 70 spectrometer (Bruker, Ettlingen, Germany) at room temperature. A total of 128 scans were accumulated with a resolution of  $4 \text{ cm}^{-1}$ .

## 2.6. Rheological Evaluation

The viscoelastic properties of the neat polymers and the composite materials were evaluated with high-pressure capillary and rotational rheology tests. The high-pressure capillary rheology provides a good understanding of the processability of the materials by FFF or PIM, whereas a more fundamental understanding of the dispersion, structure and interactions between the polymer and filler can be obtained with the rotational rheology tests [43].

The high-pressure capillary rheology was conducted in the capillary rheometer Rheograph 2002 (Göttfert Werkstoff-Prüfmaschinen GmbH, Buchen, Germany) at  $160 \text{ }^\circ\text{C}$  and apparent shear rates from  $75$  to  $2000 \text{ s}^{-1}$ . Round dies with a diameter of  $1 \text{ mm}$  and three lengths ( $10 \text{ mm}$ ,  $20 \text{ mm}$  and  $30 \text{ mm}$ ) were employed. Three measurements were conducted with each die and material to ensure the repeatability of the results. The true shear rate and the true shear stress were calculated with the Weissenberg-Rabinowitsch [44] and the Bagley [45] corrections respectively.

Oscillatory rotational rheology tests were conducted in the rotational rheometer MCR 501 (Anton Paar GmbH, Graz, Austria) using parallel plates with a diameter of  $25 \text{ mm}$ . The tests were conducted using discs with a diameter of  $25 \text{ mm}$  and  $2 \text{ mm}$  height; the disc specimens were prepared in a vacuum press with the same procedure as the specimens for contact angle measurements. The oxidation of the material was avoided using an enclosed chamber under a constant nitrogen flow. After the melting of the material, the specimen was compressed to  $0.2 \text{ mm}$  by taking down the upper plate and the test was started using the automatic control of the normal force to  $0 \text{ N}$ . The range of evaluated angular frequencies

ranged from 0.1 to 500 rad/s using a strain value of 0.1% as the amplitude of oscillation. Three repetitions were conducted per material.

#### **2.7. Morphology Analyses**

The morphology of the filled materials was studied by scanning electron microscopy (SEM, Tescan Vega II, Tescan Brno, s.r.o., Brno, Czech Republic) of the cryo-fractured surface of the material extruded in the capillary rheometer. The analyses were performed on gold sputtered (100 s at 20 mA) specimens at 5 kV using secondary electrons.

#### **2.8. Tensile Tests**

The mechanical properties of the materials were measured by means of tensile tests on straight filaments with a diameter of 1.75 mm and a length of 100 mm. This method enables the rapid screening and comparison of similar materials processed under the same conditions [12,46]. The filaments were produced in the Rheograph 2002 at 160 °C using a round die with a 30 mm length and 1.75 mm diameter. The tests were conducted on the universal testing machine Zwick Z001 (Zwick GmbH & Co.KG, Ulm, Germany) with a 1 kN load cell and pneumatic grips. The initial gauge length was set to 50 mm and standardized conditions (23 °C and 50% relative humidity) were used. The tests were conducted at speed of 10 mm·min<sup>-1</sup> until the rupture of the specimen. Five repetitions were performed per material.

#### **2.9. Differential Scanning Calorimetry**

The crystallinity of the different polymers and composites was obtained using Differential Scanning Calorimetry (DSC) tests. The measurements were conducted under nitrogen atmosphere on a Mettler Toledo DSC 1 equipped with a gas controller GC 200 (Mettler Toledo GmbH, Vienna, Austria). Heat-cool-heat runs, with the heating and cooling rate set to 10 K·min<sup>-1</sup>, respectively, were performed in temperatures between 30 and 190 °C. The normalized enthalpy in cooling was obtained with integral of the crystallization peak for each test. Following this, the crystallinity was calculated as the ratio between the normalized enthalpy in cooling and the normalized enthalpy in cooling for the 100% crystalline polyethylene (293.6 J·g<sup>-1</sup>). Five specimens were investigated per material.

### **3. Results and Discussion**

#### **3.1. MD Simulations**

Figure 2 shows the equilibrium structures of the different polyethylene types on the zirconia surface at the end of the simulation. In all the cases, the polymer chains closer to the zirconia surface are highly oriented parallel to the oxide surface and they get flattened. In the simulated structures of 5AAPE (Figure 2b) and 30AAPE (Figure 2c), the oxygen atoms of the acrylic acid tend to be adsorbed by the zirconia's oxygen atoms and align perpendicular to the surface. The alignment and flattening of the polymer in parallel to metallic and ceramic surfaces has been also observed in other MD simulations [29–31,33]. Considering that the substrate contains oxygen atoms, the oxygen atoms in the polymeric chains localize close to the substrate in order to improve the interactions with the substrate crystalline

surface [30]. This phenomenon can be observed in the structures shown in Figure 2 in which the carboxyl groups (C=O) of all the acrylic acid monomers of the chains are in contact with the zirconia surface. Considering that the oxygen plays the most important role in the surface energy of zirconia [37], we evaluated the adhesion of the three types of PE with the zirconia surface by means of the binding energy.

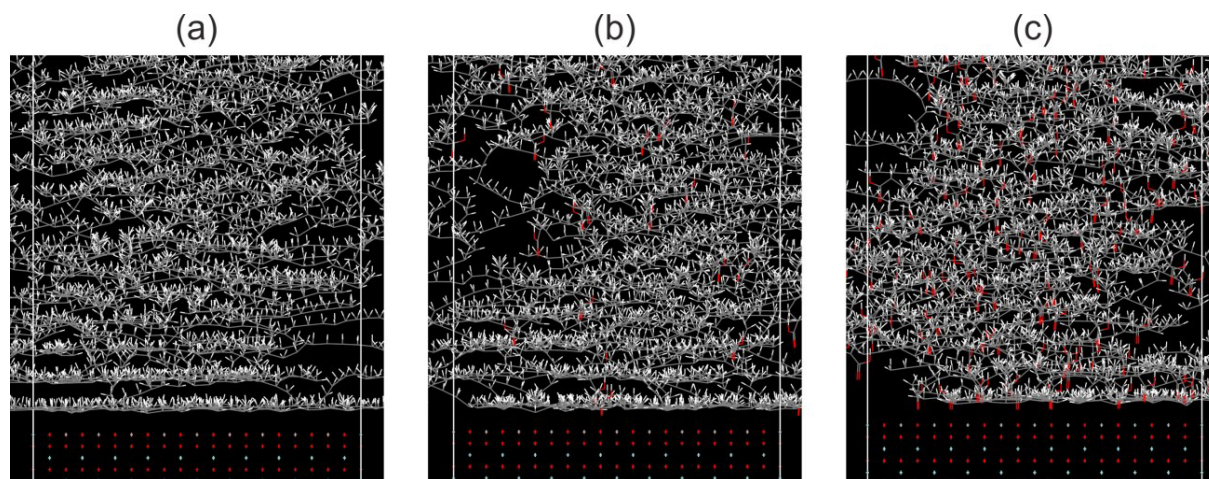


Figure 2. The equilibrium structures of (a) polyethylene (PE), (b) polyethylene grafted with 5 mol% of acrylic acid (5AAPE), and (c) polyethylene grafted with 30 mol% of acrylic acid (30AAPE) on top of a zirconia surface. The colors represent the atoms as follows: O: red, C: grey, H: white, Zr: cyan.

The binding energy between two joined materials is directly correlated to the adhesion between them [47]. Table 3 summarizes the binding energy values, with a higher absolute value indicating a better adhesion to the zirconia surface. The binding energy to zirconia is slightly higher for the 5AAPE than for the PE. This difference becomes larger for the 30AAPE, whose binding energy to the zirconia is 78% higher than that of PE. The higher affinity between the polar acrylic acid and the oxide surface and the adsorption of the oxygen atoms of the polymer on the ceramic oxide surface (Figure 2) are responsible for the higher adhesion between polymer and filler [30,33]. Moreover, the binding energy values show that the increase in the grafting level of the polymer can greatly enhance the adhesion between the polymer chains and ceramic nanoparticles.

Table 3. Binding energy of the polymers to the zirconia substrate.

Polymer	$E_{\text{binding}} (10^5 \text{ kcal}\cdot\text{mol}^{-1})$
PE	-4.2997
5AAPE	-4.8202
30AAPE	-7.6500

### 3.2. Calculation of the Interfacial Tension by Contact Angle Measurements

Table 4 summarizes the contact angle values measured for compression molded plates of the high-density polyethylene with and without acrylic acid grafting in the virgin and processed state. For the powder, the contact angle values shown in Table 4 are those measured by González-Martín et al. [37] for pure zirconia, tetragonal yttria stabilized zirconia and zirconia with 5 mol% of yttria.

According to the results of Decker et al. [47] and Cao et al. [48] with HDPE surface-grafted with acrylic acid, there is a large decrease in the contact angle of water onto the HDPE, even with low contents of AA in the surface [48]. Despite 5 mol% of AA being used in our study, only a slight difference exists between the values for AAHDPE00 and for HDPE00 (Table 4). Such disagreement might arise from the different distribution of the acrylic acid in the samples here employed [49]. For Decker et al. [47] and Cao et al. [48], all the AA was grafted and concentrated on the surface of the polymer. In our case, the commercial AAHPDE was used to produce the plates employed in the measurements. Therefore, after kneading and pressing, the polar and hydrophilic AA might be in the bulk of the compression molded plates rather than in the surface, and the polar chains might also be oriented towards the bulk and not to the surface.

Using the contact angle values and Equation (1), the surface free energy values reported in Table 4 were obtained. The surface energy and its components were higher for the AAHDPE00 than for the HDPE00. Due to the small differences in the contact angle values, the difference in the  $\sigma^P$  of both materials is not as pronounced as expected [47]. Nevertheless, when comparing the values of both components, the  $\sigma^P$  of AAHDPE00 is 62% higher than the one of HDPE00, whereas the  $\sigma^D$  difference is only of 2%. Thus, it can be stated that the polarity of the AAHDPE00 is higher than the one of HDPE00.

Table 4. Contact angle with water ( $\theta_w$ ) and diiodomethane ( $\theta_D$ ) measured for the polymers and values for zirconia as reported by González-Martín et al. [37]. The precision of all the contact angle measurements was within  $\pm 2^\circ$ . Polar ( $\sigma^P$ ) and disperse ( $\sigma^D$ ) components of the surface energy ( $\sigma^T$ ) calculated with Equation (1).

Material	Contact Angle (°)		Surface Energy (mN/m)		
	$\theta_w$	$\theta_D$	$\sigma^D$	$\sigma^P$	$\sigma^T$
<b>AAHDPE00</b>	97	53	32.6	0.55	33.14
<b>HDPE00</b>	99.3	54.2	31.9	0.34	32.24
<b>ZrO<sub>2</sub></b>	71.8	40.9	39.15	6.75	45.9
<b>Tetragonal Y<sub>2</sub>O<sub>3</sub> stabilized ZrO<sub>2</sub></b>	74	47	35.93	6.67	42.6
<b>3%Y<sub>2</sub>O<sub>3</sub>-ZrO<sub>2</sub></b>	66.4	40	39.61	9.14	48.75

Following this, the interfacial tension between the AAHDPE00 and HDPE00 with the different types of zirconia was calculated with Equation (2) and with the surface energy values from

Table 4. The interfacial tension is dependent on the surface energy and the polarity of the materials in contact, and it is inversely proportional to the adhesion between those materials [38,50]. In Table 5, the interfacial tension values between the different material combinations are shown. The interfacial tension of the AAHDPE00 with the three types of zirconia was lower than for the HDPE00. Consequently, a better adhesion to the zirconia can be expected for the AAHDPE than for the HDPE. The increase in the adhesion for the grafted polymer is in agreement with the trend observed in the MD simulation, which showed the increase in the binding energy with the increase in the acrylic acid in the polymer and the orientation of the acrylic acid towards the oxygen of the pure zirconia surface. The lower interfacial tension for the AAHDPE00 might be also produced by the presence of polar hydroxyl ( $-OH$ ) groups on the surface of the zirconia plates employed by González-Martín et al. [37]. To determine whether the powder employed in our study contained hydroxyl groups, attenuated total reflection spectroscopy was conducted.

Table 5. Calculated interfacial tension between the two types of polymers and different zirconia types.

Material	Interfacial Tension (mN/m)		
	ZrO <sub>2</sub>	Tetragonal Y <sub>2</sub> O <sub>3</sub> Stabilized ZrO <sub>2</sub>	3%Y <sub>2</sub> O <sub>3</sub> -ZrO <sub>2</sub>
<b>AAHDPE00</b>	3.74	3.46	5.53
<b>HDPE00</b>	4.43	4.12	6.37

### 3.3. Attenuated Total Reflection Spectroscopy

Figure 3 shows the infrared spectra obtained for the powder, polymers and composites. The zirconia's peak at  $3355\text{ cm}^{-1}$  corresponds to the hydroxyl groups ( $-OH$ ) bound to the powder surface [7,51–53]. Both unfilled polymers (HDPE00 and AAHDPE00) showed the characteristic polyethylene CH peaks at  $1470$ ,  $2847$  and  $2916\text{ cm}^{-1}$  [53,54]. For AAHDPE00 additional peaks were observed at  $1167$ ,  $1246$  and  $1700\text{ cm}^{-1}$ . The strong peak at  $1700\text{ cm}^{-1}$  corresponds to the stretching vibration of the carboxyl ( $C=O$ ) in the acrylic acid group ( $-COOH$ ) [48,55].

The reduction in the peaks' intensity for the composites (Figure 3) is produced by the incorporation of the zirconia as a second component. No new peaks appeared due to the chemisorption of the acrylic acid onto the zirconia surface [55] or to the formation of ester links between the carboxyl ( $C=O$ ) in the acid and the  $-OH$  groups in the zirconia [24,56,57]. However, the  $C=O$  peak of the AAHDPE has a slight shift of approximately  $2\text{ cm}^{-1}$  after incorporating the powder (Figure 3). The other peaks remained exactly at the same frequencies. The shift of the carboxyl group could be produced by the formation of hydrogen bonds with the hydroxyl groups in the powder oxide surface [58,59] and even with the zirconium dioxide [59] itself. The hydrogen bonding with the oxide would be in agreement with the orientation of the acrylic acid towards the oxygen in the zirconia surface and the high adhesion for the grafted polymers observed in the MD simulations (see Figure 3b,c).

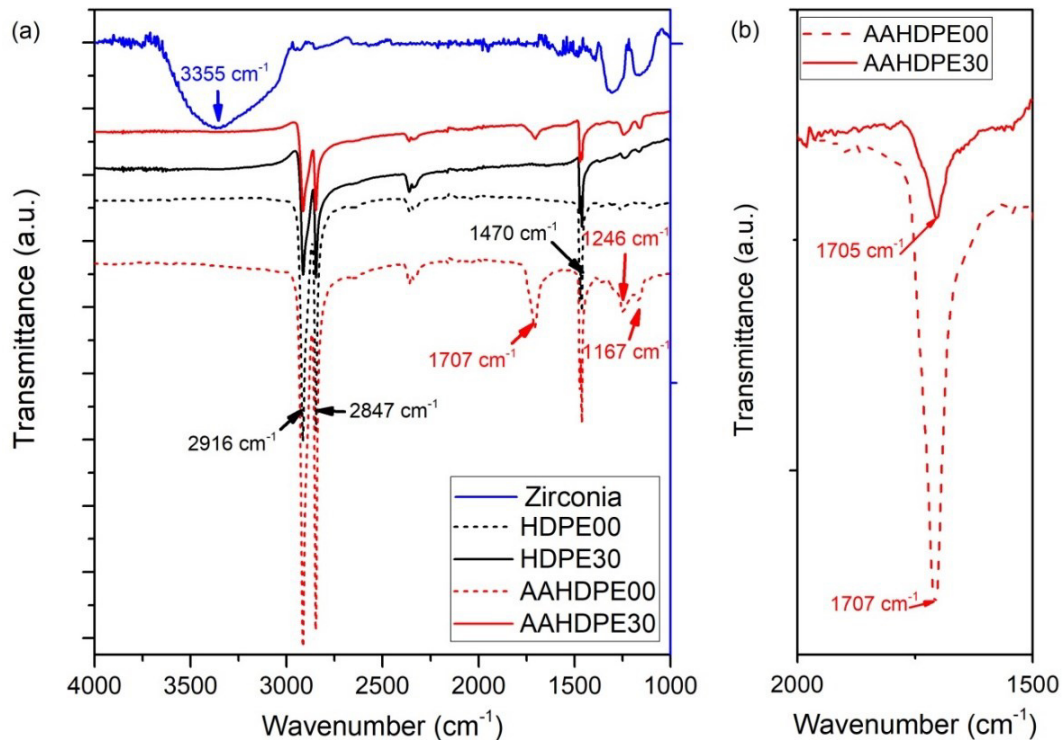


Figure 3. (a) Infrared absorption spectrum of the HDPE00, HDPE30, AAHDPE00 and AAHDPE30 with the main peaks of the pure components in different colors; (b) Magnification of the infrared absorption spectrum for the AAHDPE00 and AAHDPE30 in the 2000–1500  $\text{cm}^{-1}$  range with the carboxyl peak for the polymer and the composite.

### 3.4. Morphology

The cryo-fracture surface of the two composites, shown in Figure 4, shows the large differences between the morphology of both composites. HDPE30 showed large agglomerates of particles, which are heterogeneously distributed in the polymeric matrix. Contrarily, the zirconia powder is homogeneously distributed in AAHDPE30 without large agglomerates (Figure 4). The differences in the morphologies of both composites can be explained by their different adhesion with the zirconia powder as observed in the binding energy values obtained in the MD simulations at melt temperature (see Section 3.1) and in the interfacial tension values at room temperature (see Section 3.2). The poor adhesion between the non-polar HDPE chains and the zirconia's surface cannot overcome the attractive forces existing between the submicron particles of zirconia, which promote their agglomeration [60]. Furthermore, the hydrogen bonding between the hydroxyl groups in the surface of the powder (see Section 3.3) results in strong powder agglomerates [27,28,61,62]. The use of grafted polymers as compatibilizers [27] has proven to be an effective solution in the reduction in the hydrogen bonding of the hydroxyl groups in silica nanoparticles. Thus, the combination of a high adhesion to the oxide surface and the hydrogen bonding of the acrylic acid with the hydroxyl groups on the powder surface are the responsible factors for the better powder dispersion in AAHDPE30 than in HDPE30.

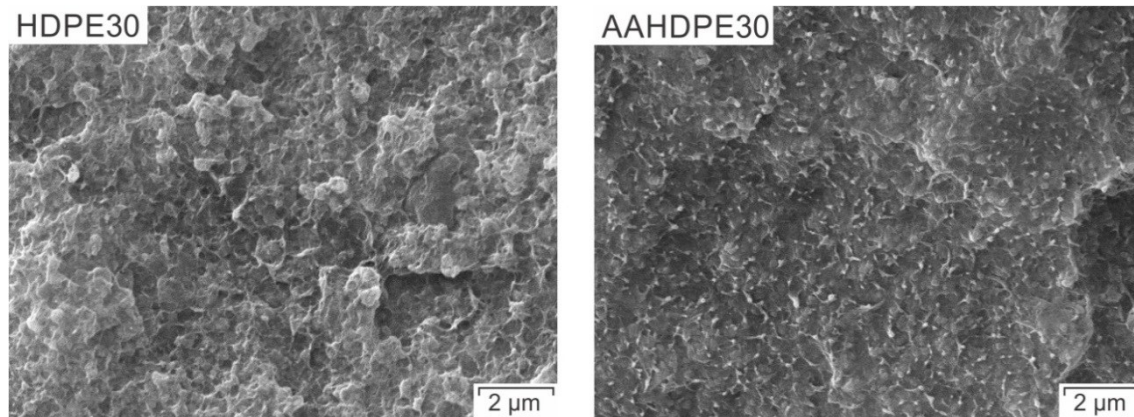


Figure 4. Morphology of the strands produced in the capillary rheometer and cryo-fractured of the compounds of HDPE and AAHDPE filled with 30 vol% of zirconia.

### 3.5. Viscoelastic Properties

Figure 5 shows the viscosity measured in a high-pressure capillary rheometer for the different materials. The measurements in the capillary rheometers are strongly related with the processing of the materials by FFF or PIM, since in both processes the material is forced to flow through a narrow nozzle at high shear rates [63]. As can be observed in Figure 5, the shear viscosity of AAHDPE00 is slightly lower than the one of HDPE00 in the range of shear rates evaluated ( $80$  to  $1000\text{ s}^{-1}$ ). On the contrary, the viscosity of AAHDPE30 is higher than that measured for HDPE30, especially at shear rates below  $500\text{ s}^{-1}$ . Since the effect of the network of particles and polymer plays a more important role at lower shear rates, rotational rheology tests between  $0.1\text{ rad s}^{-1}$  and  $500\text{ rad s}^{-1}$  were conducted.

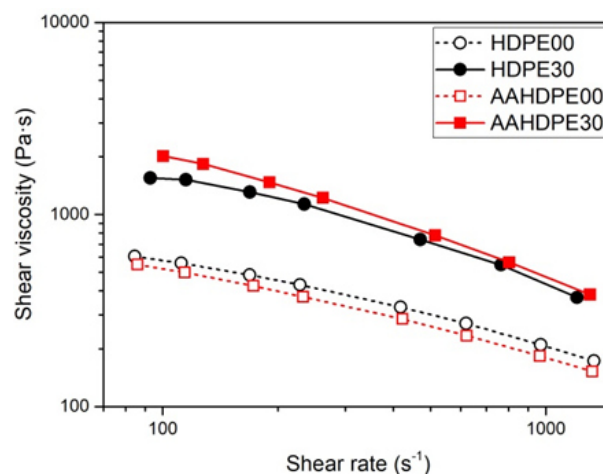


Figure 5. Shear viscosity curves as a function of shear rate measured in a round die capillary rheometer at  $160\text{ }^{\circ}\text{C}$  for HDPE00, HDPE30, AAHDPE00 and AAHDPE30. Lines are included to facilitate the visualization of the results.

In Figure 6a, it can be observed that the complex viscosity of AAHDPE00 is slightly higher than the one of HDPE00 at low angular frequencies ( $<1\text{ rad}\cdot\text{s}^{-1}$ ), whereas HDPE00 is higher in the rest of the angular frequencies. HDPE00 shows a Newtonian plateau at low angular frequencies, whereas AAHDPE00 exhibits a pseudoplastic behavior in the range of angular frequencies evaluated. The increase in viscosity in the low shear region and the

pseudoplastic behavior have been reported for long chain branched polyethylene [64,65] as well as for polyethylene grafted with polar groups such as maleic anhydride, glycidyl methacrylate and acrylic monomers [66,67] or silane [68]. Thus, the differences in the complex viscosity of AAHDPE00 and HDPE might be caused by the branching and partial crosslinking of the poly (acrylic acid) employed in the polymer grafting, which results in a more effective entanglement [67]; the hydrogen bonding between the carboxylic acid in the acrylic acid promotes this behavior [67]. The branching [65] or partial crosslinking [68] of the grafted polyethylene might also be the cause of the trend in the storage modulus (Figure 6b). At low angular frequencies, the  $G'$  of AAHDPE00 is higher than that of HDPE00, whereas the storage modulus of HDPE00 is slightly higher at high angular frequencies. This theory is further supported by the results observed in the loss factor of the unfilled polymers shown in Figure 6c. The slope of the loss factor is negative for HDPE00 in the whole range of angular frequencies evaluated. On the contrary, a positive slope is observed at low frequencies for the AAHDPE00, which is associated with an elastic behavior [68]. Considering the results of the mentioned studies and the trend observed in the complex viscosity (Figure 6), it can be stated that the chain entanglement or crosslinking and the reaction between the acrylic acid monomers in AAHDPE00 are the causes of the big difference in the viscoelastic properties at low angular frequencies for the unfilled polymers.

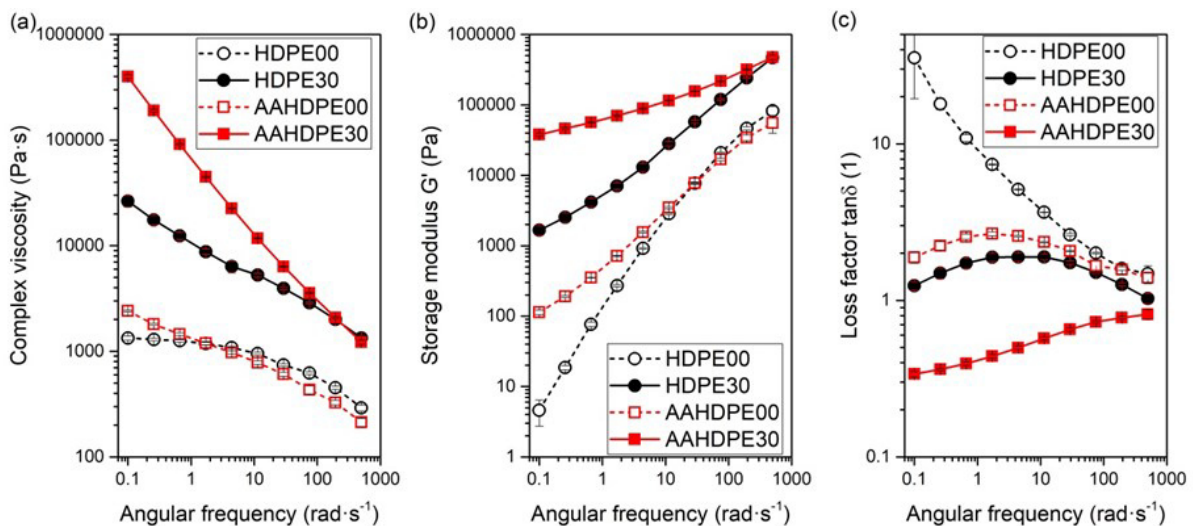


Figure 6. Viscoelastic properties as a function of angular frequency measured in parallel plate rotational rheometer at 160 °C for HDPE00, HDPE30, AAHDPE00 and AAHDPE30: (a) Complex viscosity, (b) Storage modulus and (c) Loss factor. Lines are included to facilitate the visualization of the results.

In the case of the highly filled systems, the complex viscosity of AAHDPE30 is much higher than the one of HDPE30 at low shear rates (Figure 6a). It is known that, at low frequencies, the particle–particle interaction and the network of particles have the main effect on the viscoelastic properties of polymer nanocomposites [43]. As was observed in Figure 4, there are no agglomerates in AAHDPE30, whereas HDPE30 has large agglomerates. Thus, the high viscosity of AAHDPE30 is not produced by the powder’s agglomerates. On the contrary, the decrease in agglomerates results in an increase in the particle surface area in contact with the polymer melt, thus increasing the viscosity [43,69–71]. Additionally, the higher adhesion to the powder for the AAHDPE than for the HDPE (observed in the MD simulations at high



temperature in Section 3.1) and the hydrogen bonding between the zirconia OH groups and the acrylic acid CO groups (observed in the ATR analyses in Section 3.3) promote the higher viscosity of AAHDPE30 [71–74]. A high work of adhesion results in a thicker layer of polymer absorbed in the particles [72]. At low shear rates, the effective particle size of the particles is larger due to the entanglement of the absorbed molecules with the rest of the polymer. At high shear rates, the polymer molecules disentangle and orient [72]. The breakup of this network results in a more pronounced shear thinning of AAHDPE30 as compared to HDPE30 in Figure 6 [43]. As can be observed in Figure 6b, the formation of a polymer-filler network due to the improvement of the powder dispersion and the increase in the adhesion also affects the values of the storage modulus [43]. The polymer molecules adsorbed on one particle interact with the chains adsorbed on the near particles and with the free and mobile polymer, resulting in a decrease in the mobility and in an increase in the elasticity for AAHDPE30 as compared to HDPE30 [14,75].

The elastic behavior of the AAHDPE30 can also be observed in its loss factor values, which are smaller than 1 for all the evaluated angular frequencies (Figure 6c). Moreover, the loss factor of AAHDPE30 has a positive slope in all the evaluated shear rates, which corresponds to a pseudo solid behavior. On the contrary, the loss factor of HDPE30 is always higher than 1 and the positive slope only appears at low angular frequencies (Figure 6c). For similar filled polymers, a positive slope and low values of the loss factors can be attributed to a high filler dispersion [76], which is in line with the differences in the morphology of AAHDPE30 and HDPE30.

### 3.6. Tensile Properties

The mechanical properties of the compounds used in FFF are of vital importance [11,12,77]. Sufficient strength and flexibility are required to spool and de-spool the filament for its production and for printing. Moreover, the filaments must be stiff enough to avoid buckling during printing. Furthermore, high strength and stiffness are also required in the PIM process for the de-molding and handling of the parts [78]. Therefore, tensile tests were conducted on filaments produced with all the evaluated compounds. This method enables a rapid screening and comparison of similar materials processed under the same conditions [12,46].

Figure 7 shows representative strain–stress curves of filaments of the materials evaluated, together with the average ultimate tensile strength ( $UTS$ ) and the corresponding average strain value ( $\varepsilon_{UTS}$ ). The secant modulus ( $E_S$ ) was calculated in the strain range between 0.1% and 0.3% in order to avoid the initial stage of the test, in which the slight curvature of the specimens (due to the processing and handling of the filaments) could influence the results. Table 6 summarizes the average and standard deviation values for the three parameters.

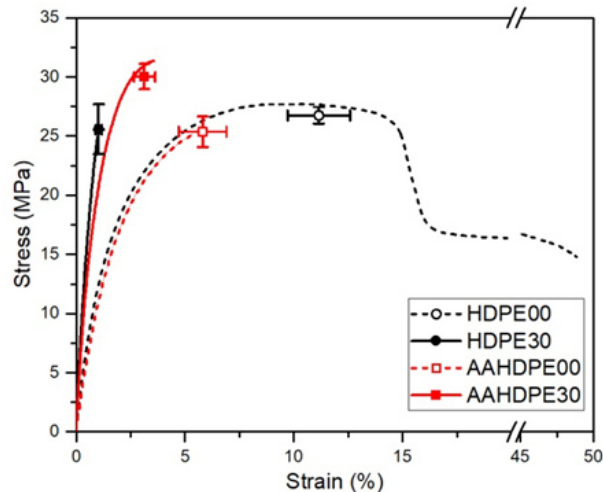


Figure 7. Strain–stress curves for HDPE00, HDPE30, AAHDPE00 and AAHDPE30. The average ultimate tensile stress and its corresponding strain are plotted for all the compounds.

Even though the flowability of the unfilled polyethylene was the only parameter employed to select the two types of high density polyethylene (see Section 2.2), no significant differences existed in the  $UTS$  and  $E_S$  of HDPE00 and AAHDPE00 (Table 6). In fact, the  $\epsilon_{UTS}$  was the only parameter significantly different between HDPE00 and AAHDPE00 (Figure 7) with the non-grafted polymer having a significantly larger value. The incorporation of the particles should result in an increase in the strength and stiffness of the composites [21–23,27,74]. This behavior is observed for AAHDPE30 with an increase of 18% in  $UTS$  and 98% in  $E_S$  with respect to the values of AAHDPE00 (Table 6). In the case of HDPE30, the  $E_S$  is 137% higher than the values of HDPE00, whereas no significant difference in the  $UTS$  was found between HDPE00 and HDPE30 (Table 6). The presence of the zirconia particle results in a decrease in the  $\epsilon_{UTS}$  of 91% in HDPE30 compared to HDPE00 and of 46% in AAHDPE30 compared to AAHDPE00 (Table 6). The decrease in the  $\epsilon_{UTS}$  is produced by the restriction of movement of the polymer by the rigid particles which do not elongate, resulting in a reduction in the ductility of the material [21–23,27,74].

When comparing the properties of the nanocomposites, the  $E_S$  of HDPE30 is significantly higher than that of AAHDPE30 (Table 6). The secant modulus, calculated in the strain range from 0.1% to 0.3%, is highly dependent on the polymer structure and factors such as the crystallinity. In order to determine the crystallinity, Differential Scanning Calorimetry (DSC) tests were conducted on five samples of each material. The crystallinity of HDPE00 is  $76.21\% \pm 2.16\%$  and increases to  $77.65\% \pm 0.31\%$  for HDPE30. For AAHDPE00 the crystallinity is  $63.42\% \pm 1.52\%$  and decreases to  $57.92\% \pm 0.85\%$  for AAHDPE30. In polymer nanocomposites with a semicrystalline polymeric matrix, the nanoparticle surface can act as a heterogeneous nucleating site [14]. Smaller nanoparticles are less able to act as nucleating agents than larger fillers [14, 79]. Additionally, the improvement of the dispersion of adhesion reduces the mobility of the crystallisable chain segments [68,80]. Therefore, the high dispersion and adhesion to the zirconia results in a lower crystallinity of the matrix in AAHDPE30 than in HDPE30 and consequently in a lower secant modulus [80].

The  $UTS$  of AAHDPE30 is significantly higher than the  $UTS$  of HDPE30 (Figure 7). Furthermore, the  $\epsilon_{UTS}$  of AAHDPE30 is three times higher than the one measured for

HDPE30 (Table 6). Such behavior can be attributed to the higher adhesion of the AAHDPE than the HDPE to the zirconia surface, which seems to have a big effect in the high strain region. A high adhesion results in a strong polymer-filler interface and thus in a more effective transfer of load from the polymer matrix to the solid particles [21–23,27,74]. Moreover, the high dispersion of the powder in AAHDPE30 compared to HDPE30 (Figure 4) contributes to difference in the mechanical properties. In polymer composites, defects such as agglomerates or cavities result in a concentration of stresses around those points and eventually the failure of the material in those areas [16,22,23,27]. Thus, it can be concluded that the acrylic acid-grafting of the HDPE results in composites with a higher strength and flexibility by the combination of a strong polymer-filler interface and the reduction in the filler agglomerates.

Table 6. Average and standard deviation of the ultimate tensile strength (UTS), strain at UTS ( $\epsilon_{UTS}$ ) and secant modulus ( $E_s$ ) values for the HDPE00, HDPE30, AAHDPE00 and AAHDPE30.

	<b>HDPE00</b>	<b>HDPE30</b>	<b>AAHDPE00</b>	<b>AAHDPE30</b>
<b>UTS (MPa)</b>	26.75 ± 0.7	25.56 ± 2.1	25.37 ± 1.3	30.01 ± 1.07
<b><math>\epsilon_{UTS}</math> (%)</b>	11.15 ± 1.43	1.03 ± 0.13	5.81 ± 1.1	3.13 ± 0.49
<b><math>E_s</math> (GPa)</b>	1.44 ± 0.05	3.41 ± 0.13	1.33 ± 0.15	2.64 ± 0.09

#### 4. Conclusions

The effect of grafting polyethylene with acrylic acid on the interfacial interactions in zirconia nanocomposites for FFF and PIM has been investigated by MD simulations and experimental methods. The MD simulations show the increase in the adhesion to pure zirconia when polyethylene is grafted with acrylic acid, and the orientation of the acrylic acid side groups towards the oxygen in the zirconia. These results have been compared to the experimental characterization of a commercial acrylic acid grafted high density polyethylene and a comparable ungrafted high-density polyethylene and the nanocomposites of both materials with zirconia. The higher polarity of the acrylic acid-grafted high-density polyethylene compared to a similar ungrafted polymer has been observed in their interface with different zirconia surfaces. Moreover, the shift of the carboxyl group peak in the composite with acrylic acid grafted high density polyethylene demonstrates the formation of hydrogen bonds of the acrylic acid with the hydroxyl groups and the oxide in the powder surface.

The increase in adhesion to the powder in the acrylic acid-grafted polyethylene produced by the increase in polarity, the improved interaction with the oxygen in the zirconia surface and the hydrogen bonding to the hydroxyl groups in the powder strongly affect the morphology and properties of the nanocomposites. All these effects result in an improvement in the dispersion of the powder in the polymer matrix in the nanocomposite with the acrylic acid grafted polyethylene. The combination of a higher adhesion between the matrix and filler and better powder dispersion for the acrylic acid grafted polyethylene than for the ungrafted one greatly affects the viscoelastic and mechanical properties of the nanocomposite. The restriction of the polymer chains movement and the formation of a polymer-filler network in

the nanocomposite with grafted acrylic acid results in higher viscosity and higher storage modulus than for the ungrafted system, especially at lower shear rates. Furthermore, the reduction of the powder agglomerates that act as defect points and the improvement of the adhesion to the powder provide a higher strength and flexibility for the nanocomposite with grafted acrylic acid than for the one not containing it.

These findings offer insight into the interfacial interactions and the improvement of the adhesion between polymer and filler in ceramic nanocomposites for FFF and PIM by the grafting of the backbone polymer with polar groups. It is shown that these modifications result in an improvement of the quality of the nanocomposite by increasing the filler dispersion and the improving the properties required for its processing. In future studies, the effect of the backbone grafting on the properties and processability of feedstocks for FFF and PIM with multicomponent binder systems will be evaluated.

**Author Contributions:** Conceptualization, S.C., A.G., C.K. and J.G.-G.; Investigation, S.C. and A.G.; Formal Analysis, S.C., A.G. and J.G.-G.; Writing-Original Draft, S.C.; Writing-Review & Editing, S.C., A.G., C.K., G.R., C.H. and J.G.-G.; Visualization, S.C.; Supervision, C.K. and C.H.; Project Administration, C.K. and J.G.-G.; Funding Acquisition, C.K. and J.G.-G. All authors have read and agreed to the published version of the manuscript.

**Corrections:** The content of grafted acrylic acid was reported in mol% due to a mistake in the writing of Publication D. However, the correct units are wt%. This mistake affects the content of acrylic acid in the polyethylene chains in the Molecular Dynamic simulations, which actually contained 0, 5 and 30 wt% of acrylic acid. It also affects the minimum content of acrylic acid in the grafted high density polyethylene SCONA TPPE 2400, which actually contains  $\geq 5$  wt%. A request has been sent to *Applied Sciences* on the 21<sup>st</sup> of July of 2020 in order to publish a correction.

**Funding:** This research was performed under the European project CerAMufacturing and the Austria-China bilateral cooperation projects FlexiFactory3Dp and 3DMultiMat. The CerAMufacturing project has received the financial support of the European Commission in the frame of the FoF Horizon 2020 with financial agreement 678503. FlexiFactory3Dp and 3DMultiMat has received funding from the Austrian Research Promotion Agency under the program Production of the Future, Grant Agreements No. 860385 and No. 875650. Dr. Ali Gooneie was supported by the Empa Internal Research Call 2018 in the framework of the "ALLFIN" project.

**Acknowledgments:** The authors greatly appreciate Baris Kaynak, Janak Sapkota and Martin Spoerk for their assistance and the discussions in the planning and testing. The help of Florian Arbeiter in the analysis of the results of the tensile tests is also greatly appreciated. Thanks go to BYK-Chemie GmbH and Borealis AG for kindly donating the polyethylene grades.

**Conflicts of Interest:** The authors declare no conflict of interest. The funders had no role in the design of the study; in the collection, analyses, or interpretation of data; in the writing of the manuscript, or in the decision to publish the results.

## References

1. Dziadek, M.; Stodolak-Zych, E.; Cholewa-Kowalska, K. Biodegradable ceramic-polymer composites for biomedical applications: A review. *Mater. Sci. Eng. C Mater. Biol. Appl.* **2017**, *71*, 1175–1191, doi:10.1016/j.msec.2016.10.014.
2. Park, H.-J.; Kwak, S.-Y.; Kwak, S. Wear-Resistant Ultra High Molecular Weight Polyethylene/Zirconia Composites Prepared by in situ Ziegler-Natta Polymerization. *Macromol. Chem. Phys.* **2005**, *206*, 945–950, doi:10.1002/macp.200400350.
3. Paul, D.R.; Robeson, L.M. Polymer nanotechnology: Nanocomposites. *Polymer* **2008**, *49*, 3187–3204, doi:10.1016/j.polymer.2008.04.017.
4. Zhan, C.; Yu, G.; Lu, Y.; Wang, L.; Wujcik, E.; Wei, S. Conductive polymer nanocomposites: A critical review of modern advanced devices. *J. Mater. Chem. C* **2017**, *5*, 1569–1585, doi:10.1039/C6TC04269D.
5. Hippi, U.; Mattila, J.; Korhonen, M.; Seppälä, J.V. Compatibilization of polyethylene/aluminum hydroxide (PE/ATH) and polyethylene/magnesium hydroxide (PE/MH) composites with functionalized polyethylenes. *Polymer* **2003**, *44*, 1193–1201, doi:10.1016/S0032-3861(02)00856-X.
6. Wen, J.-x.; Zhu, T.-b.; Xie, Z.-p.; Cao, W.-b.; Liu, W. A strategy to obtain a high-density and high-strength zirconia ceramic via ceramic injection molding by the modification of oleic acid. *Int. J. Miner. Metall. Mater.* **2017**, *24*, 718–725, doi:10.1007/s12613-017-1455-9.
7. Auscher, M.-C.; Fulchiron, R.; Fougereuse, N.; Périé, T.; Cassagnau, P. Zirconia based feedstocks: Influence of particle surface modification on the rheological properties. *Ceram. Int.* **2017**, *43*, 16950–16956, doi:10.1016/j.ceramint.2017.09.100.
8. Hanemann, T.; Heldele, R.; Mueller, T.; Hausselt, J. Influence of Stearic Acid Concentration on the Processing of ZrO<sub>2</sub>-Containing Feedstocks Suitable for Micropowder Injection Molding. *Int. J. Appl. Ceram. Technol.* **2011**, *8*, 865–872, doi:10.1111/j.1744-7402.2010.02519.x.
9. Lin, S.T.; German, R.M. Interaction between binder and powder in injection moulding of alumina. *J. Mater. Sci.* **1994**, *29*, 5207–5212, doi:10.1007/BF01151118.
10. McNulty, T.F.; Shanefield, D.J.; Danforth, S.C.; Safari, A. Dispersion of Lead Zirconate Titanate for Fused Deposition of Ceramics. *J. Am. Ceram. Soc.* **1999**, *82*, 1757–1760, doi:10.1111/j.1151-2916.1999.tb01996.x.
11. Gonzalez-Gutierrez, J.; Cano, S.; Schuschnigg, S.; Kukla, C.; Sapkota, J.; Holzer, C. Additive Manufacturing of Metallic and Ceramic Components by the Material Extrusion of Highly-Filled Polymers: A Review and Future Perspectives: A Review and Future Perspectives. *Materials* **2018**, *11*, doi:10.3390/ma11050840.
12. Cano, S.; Gonzalez-Gutierrez, J.; Sapkota, J.; Spoerk, M.; Arbeiter, F.; Schuschnigg, S.; Holzer, C.; Kukla, C. Additive manufacturing of zirconia parts by fused filament fabrication and solvent debinding: Selection of binder formulation. *Addit. Manuf.* **2019**, *26*, 117–128, doi:10.1016/j.addma.2019.01.001.

13. Rong, M.Z.; Zhang, M.Q.; Ruan, W.H. Surface modification of nanoscale fillers for improving properties of polymer nanocomposites: A review. *Mater. Sci. Technol.* **2006**, *22*, 787–796, doi:10.1179/174328406X101247.
14. Li, Y.; Huang, Y.; Krentz, T.; Natarajan, B.; Neely, T.; Schadler, L.S. Polymer Nanocomposite Interfaces: The Hidden Lever for Optimizing Performance in Spherical Nanofilled Polymers. In *Interface/Interphase in Polymer Nanocomposites*, Netravali, A.N., Mittal, K.L., Eds.; John Wiley & Sons, Inc.: Hoboken, NJ, USA, 2016; pp 1–69.
15. Gooneie, A.; Hufenus, R. Polymeric Solvation Shells around Nanotubes: Mesoscopic Simulation of Interfaces in Nanochannels. *Macromolecules* **2019**, *52*, 8803–8813, doi:10.1021/acs.macromol.9b01657.
16. Drelich, J.; Miller, J.D. Critical review of wetting and adhesion phenomena in the preparation of polymer-mineral composites. *Miner. Metall. Process.* **1995**, *12*, 197–204.
17. Jenni, M.; Schimmer, L.; Zauner, R.; Stampfl, J.; Morris, J. Quantitative study of powder binder separation of feedstocks. *Powder Inject. Mould. Int.* **2008**, *2*, 50–55.
18. Mannschatz, A.; Höhn, S.; Moritz, T. Powder-binder separation in injection moulded green parts. *J. Eur. Ceram. Soc.* **2010**, *30*, 2827–2832, doi:10.1016/j.jeurceramsoc.2010.02.020.
19. Gorjan, L.; Reiff, L.; Liersch, A.; Clemens, F. Ethylene vinyl acetate as a binder for additive manufacturing of tricalcium phosphate bio-ceramics. *Ceram. Int.* **2018**, *44*, 15817–15823, doi:10.1016/j.ceramint.2018.05.260.
20. Fan, N.C.; Chen, Y.Y.; Wei, W.C.J.; Liu, B.H.; Wang, A.B.; Luo, R.C. Porous Al<sub>2</sub>O<sub>3</sub> catalyst carrier by 3D additive manufacturing for syngas reforming. *J. Ceram. Process. Res.* **2017**, *18*, 676–682.
21. Xu, Y.; Fang, Z.; Tong, L. On promoting intercalation and exfoliation of bentonite in high-density polyethylene by grafting acrylic acid. *J. Appl. Polym. Sci.* **2005**, *96*, 2429–2434, doi:10.1002/app.21708.
22. Bula, K.; Jesionowski, T. Effect of Polyethylene Functionalization on Mechanical Properties and Morphology of PE/SiO<sub>2</sub> Composites. *Compos. Interfaces* **2010**, *17*, 603–614, doi:10.1163/092764410X513332.
23. Hoang, T.; Truc, T.A.; Thanh, D.T.M.; Chinh, N.T.; Tham, D.Q.; Trang, N.T.T.; Vu Giang, N.; Lam, V.D. Tensile, rheological properties, thermal stability, and morphology of ethylene vinyl acetate copolymer/silica nanocomposites using EVA-g-maleic anhydride. *J. Compos. Mater.* **2014**, *48*, 505–511, doi:10.1177/0021998313476319.
24. Wang, Y.; Yeh, F.-C.; Lai, S.-M.; Chan, H.-C.; Shen, H.-F. Effectiveness of functionalized polyolefins as compatibilizers for polyethylene/wood flour composites. *Polym. Eng. Sci.* **2003**, *43*, 933–945, doi:10.1002/pen.10077.
25. Minkova, L.; Peneva, Y.; Tashev, E.; Filippi, S.; Pracella, M.; Magagnini, P. Thermal properties and microhardness of HDPE/clay nanocomposites compatibilized by

- different functionalized polyethylenes. *Polym. Test.* **2009**, *28*, 528–533, doi:10.1016/j.polymertesting.2009.04.001.
26. Wongpanit, P.; Khanthsri, S.; Puengboonsri, S.; Manonukul, A. Effects of acrylic acid-grafted HDPE in HDPE-based binder on properties after injection and debinding in metal injection molding. *Mater. Chem. Phys.* **2014**, *147*, 238–246, doi:10.1016/j.matchemphys.2014.04.035.
27. Bikiaris, D.N.; Vassiliou, A.; Pavlidou, E.; Karayannidis, G.P. Compatibilisation effect of PP-g-MA copolymer on iPP/SiO<sub>2</sub> nanocomposites prepared by melt mixing. *Eur. Polym. J.* **2005**, *41*, 1965–1978, doi:10.1016/j.eurpolymj.2005.03.008.
28. Zhu, A.; Cai, A.; Yu, Z.; Zhou, W. Film characterization of poly(styrene-butylacrylate-acrylic acid)-silica nanocomposite. *J. Colloid Interface Sci.* **2008**, *322*, 51–58, doi:10.1016/j.jcis.2008.02.014.
29. Eslami, H.; Rahimi, M.; Müller-Plathe, F. Molecular Dynamics Simulation of a Silica Nanoparticle in Oligomeric Poly(methyl methacrylate): A Model System for Studying the Interphase Thickness in a Polymer–Nanocomposite via Different Properties. *Macromolecules* **2013**, *46*, 8680–8692, doi:10.1021/ma401443v.
30. Anastassiou, A.; Mavrantzas, V.G. Molecular Structure and Work of Adhesion of Poly(n-butyl acrylate) and Poly(n-butyl acrylate-co-acrylic acid) on  $\alpha$ -Quartz,  $\alpha$ -Ferric Oxide, and  $\alpha$ -Ferrite from Detailed Molecular Dynamics Simulations. *Macromolecules* **2015**, *48*, 8262–8284, doi:10.1021/acs.macromol.5b01469.
31. Gooneie, A.; Gonzalez-Gutierrez, J.; Holzer, C. Atomistic Modelling of Confined Polypropylene Chains between Ferric Oxide Substrates at Melt Temperature. *Polymers* **2016**, *8*, 361, doi:10.3390/polym8100361.
32. Gooneie, A.; Schuschnigg, S.; Holzer, C. A Review of Multiscale Computational Methods in Polymeric Materials. *Polymers* **2017**, *9*, 16, doi:10.3390/polym9010016.
33. Kisin, S.; Božović Vukić, J.; van der Varst, P.G.T.; With, G.d.; Koning, C.E. Estimating the Polymer–Metal Work of Adhesion from Molecular Dynamics Simulations. *Chem. Mater.* **2007**, *19*, 903–907, doi:10.1021/cm0621702.
34. Gooneie, A.; Holzer, C. Reinforced local heterogeneities in interfacial tension distribution in polymer blends by incorporating carbon nanotubes. *Polymer* **2017**, *125*, 90–101, doi:10.1016/j.polymer.2017.07.077.
35. BYK-Chemie GmbH. *Technical Data Sheet SCONA TPPE 2400 GAHD*; BYK-Chemie GmbH: Wesel, Germany, 2017.
36. Kubiak, K.J.; Wilson, M.C.T.; Mathia, T.G.; Carval, P. Wettability versus roughness of engineering surfaces. *Wear* **2011**, *271*, 523–528, doi:10.1016/j.wear.2010.03.029.
37. González-Martín, M.L.; Labajos-Broncano, L.; Jańczuk, B.; Bruque, J.M. Wettability and surface free energy of zirconia ceramics and their constituents. *J. Mater. Sci.* **1999**, *34*, 5923–5926, doi:10.1023/A:1004767914895.
38. Owens, D.K.; Wendt, R.C. Estimation of the surface free energy of polymers. *J. Appl. Polym. Sci.* **1969**, *13*, 1741–1747, doi:10.1002/app.1969.070130815.

39. Kaelble, D.H. Dispersion-Polar Surface Tension Properties of Organic Solids. *J. Adhes.* **1970**, *2*, 66–81, doi:10.1080/0021846708544582.
40. Rabel, W. Einige Aspekte der Benetzungstheorie und ihre Anwendung auf die Untersuchung und Veränderung der Oberflächeneigenschaften von Polymeren. *Farbe und Lack* **1971**, *77*, 997–1005.
41. Spoerk, M.; Gonzalez-Gutierrez, J.; Lichal, C.; Cajner, H.; Berger, G.R.; Schuschnigg, S.; Cardon, L.; Holzer, C. Optimisation of the Adhesion of Polypropylene-Based Materials during Extrusion-Based Additive Manufacturing. *Polymers* **2018**, *10*, 490, doi:10.3390/polym10050490.
42. Berger, G.R.; Steffel, C.; Friesenbichler, W. A study on the role of wetting parameters on friction in injection moulding. *IJMPT* **2016**, *52*, 193, doi:10.1504/IJMPT.2016.073632.
43. Rueda, M.M.; Auscher, M.-C.; Fulchiron, R.; Périé, T.; Martin, G.; Sonntag, P.; Cassagnau, P. Rheology and applications of highly filled polymers: A review of current understanding. *Prog. Polym. Sci.* **2017**, *66*, 22–53, doi:10.1016/j.progpolymsci.2016.12.007.
44. Rabinowitsch, B. Über die Viskosität und Elastizität von Solen. *Z. für Phys. Chem.* **1929**, *145*, 1–26, doi:10.1515/zpch-1929-14502.
45. Bagley, E.B. End Corrections in the Capillary Flow of Polyethylene. *J. Appl. Phys.* **1957**, *28*, 624–627, doi:10.1063/1.1722814.
46. Spoerk, M.; Sapkota, J.; Weingrill, G.; Fischinger, T.; Arbeiter, F.; Holzer, C. Shrinkage and Warpage Optimization of Expanded-Perlite-Filled Polypropylene Composites in Extrusion-Based Additive Manufacturing. *Macromol. Mater. Eng.* **2017**, *12*, 1700143, doi:10.1002/mame.201700143.
47. Decker, C.; Zahouily, K. Surface modification of polyolefins by photografting of acrylic monomers. *Macromol. Symp.* **1998**, *129*, 99–108, doi:10.1002/masy.19981290109.
48. Cao, Z.; Lei, J.; Zhang, W. Structure and adhesion properties of acrylic acid grafted high-density polyethylene powders synthesized by a novel photografting method. *J. Appl. Polym. Sci.* **2008**, *109*, 2316–2320, doi:10.1002/app.28305.
49. Wang, H.; Brown, H.R. UV grafting of methacrylic acid and acrylic acid on high-density polyethylene in different solvents and the wettability of grafted high-density polyethylene. II. Wettability. *J. Polym. Sci. A Polym. Chem.* **2004**, *42*, 263–270, doi:10.1002/pola.11010.
50. Reddy, C.M.; Weikart, C.M.; Yasuda, H.K. The Effect of Interfacial Tension on the Adhesion of Cathodic E-coat to Aluminum Alloys. *J. Adhes.* **1999**, *71*, 167–187, doi:10.1080/00218469908014847.
51. Liu, W.; Xie, Z.P.; Yang, X.F.; Wu, Y.; Jia, C.; Bo, T.; Wang, L. Surface Modification Mechanism of Stearic Acid to Zirconia Powders Induced by Ball Milling for Water-Based Injection Molding. *J. Am. Ceram. Soc.* **2011**, *94*, 1327–1330, doi:10.1111/j.1551-2916.2011.04475.x.



52. Merle-Méjean, T.; Barberis, P.; Othmane, S.B.; Nardou, F.; Quintard, P.E. Chemical forms of hydroxyls on/in Zirconia: An FT-IR study. *J. Eur. Ceram. Soc.* **1998**, *18*, 1579–1586, doi:10.1016/S0955-2219(98)00080-6.
53. Socrates, G. *Infrared and Raman Characteristic Group Frequencies. Tables and Charts*, 3rd ed.; John Wiley & Sons, Inc.: Chichester, UK, 2001; ISBN 0470093072.
54. D'Amelia, R.P.; Gentile, S.; Nirode, W.F.; Huang, L. Quantitative Analysis of Copolymers and Blends of Polyvinyl Acetate (PVAc) Using Fourier Transform Infrared Spectroscopy (FTIR) and Elemental Analysis (EA). *World J. Chem. Educ.* **2016**, *4*, 25–31, doi:10.12691/wjce-4-2-1.
55. Nasreddine, V.; Halla, J.; Reven, L. Conformation of Adsorbed Random Copolymers: A Solid-State NMR and FTIR-PAS Study. *Macromolecules* **2001**, *34*, 7403–7410, doi:10.1021/ma010833p.
56. Kim, H.-S.; Kim, S.; Kim, H.-J.; Yang, H.-S. Thermal properties of bio-flour-filled polyolefin composites with different compatibilizing agent type and content. *Thermochim. Acta* **2006**, *451*, 181–188, doi:10.1016/j.tca.2006.09.013.
57. Lai, S.-M.; Yeh, F.-C.; Wang, Y.; Chan, H.-C.; Shen, H.-F. Comparative study of maleated polyolefins as compatibilizers for polyethylene/wood flour composites. *J. Appl. Polym. Sci.* **2003**, *87*, 487–496, doi:10.1002/app.11419.
58. Wang, L.; Wang, Z.; Zhang, X.; Shen, J.; Chi, L.; Fuchs, H. A new approach for the fabrication of an alternating multilayer film of poly(4-vinylpyridine) and poly(acrylic acid) based on hydrogen bonding. *Macromol. Rapid Commun.* **1997**, *18*, 509–514, doi:10.1002/marc.1997.030180609.
59. Du, M.; Guo, B.; Lei, Y.; Liu, M.; Jia, D. Carboxylated butadiene–styrene rubber/halloysite nanotube nanocomposites: Interfacial interaction and performance. *Polymer* **2008**, *49*, 4871–4876, doi:10.1016/j.polymer.2008.08.042.
60. Mutsuddy, B.C.; Ford, R.G. *Ceramic Injection Moulding*; Chapman & Hall: London, UK, 1995; ISBN 0412538105.
61. Laghaei, M.; Sadeghi, M.; Ghalei, B.; Shahrooz, M. The role of compatibility between polymeric matrix and silane coupling agents on the performance of mixed matrix membranes: Polyethersulfone/MCM-41. *J. Membr. Sci.* **2016**, *513*, 20–32, doi:10.1016/j.memsci.2016.04.039.
62. Lall, P.; Islam, S.; Dornala, K.; Suhling, J.; Shinde, D. Nano-Underfills and Potting Compounds for Fine-Pitch Electronics. In *Nanopackaging*; Morris, J.E., Ed.; Springer International Publishing: Cham, Switzerland, 2018; pp. 513–574.
63. Venkataraman, N.; Rangarajan, S.; Matthewson, M.J.; Safari, A.; Danforth, S.C.; Yardimci, A.; Guceri, S.I. Mechanical and Rheological Properties of Feedstock Material for Fused Deposition of Ceramics and Metals (FDC and FDMet) and their Relationship to Process Performance. In Proceedings of the Solid Freeform Fabrication Symposium. Solid Freeform Fabrication Symposium, Austin, TX, USA, 9–11 August 1999.

64. Malmberg, A.; Gabriel, C.; Steffl, T.; Münstedt, H.; Löfgren, B. Long-Chain Branching in Metallocene-Catalyzed Polyethylenes Investigated by Low Oscillatory Shear and Uniaxial Extensional Rheometry. *Macromolecules* **2002**, *35*, 1038–1048, doi:10.1021/ma010753l.
65. Liang, X.-K.; Luo, Z.; Yang, L.; Wei, J.-T.; Yuan, X.; Zheng, Q. Rheological properties and crystallization behaviors of long chain branched polyethylene prepared by melt branching reaction. *J. Polym. Eng.* **2018**, *38*, 7–17, doi:10.1515/polyeng-2016-0221.
66. Brito, G.F.; Xin, J.; Zhang, P.; Mélo, T.J.A.; Zhang, J. Enhanced melt free radical grafting efficiency of polyethylene using a novel redox initiation method. *RSC Adv.* **2014**, *4*, 26425, doi:10.1039/c4ra03607g.
67. Ghosh, P.; Dev, D. Reactive processing of polyethylene: Effect of peroxide-induced graft copolymerization of some acrylic monomers on polymer structure melt rheology and relaxation behavior. *Eur. Polym. J.* **1998**, *34*, 1539–1547, doi:10.1016/S0014-3057(97)00278-4.
68. Sharif-Pakdaman, A.; Morshedian, J.; Jahani, Y. Influence of the silane grafting of polyethylene on the morphology, barrier, thermal, and rheological properties of high-density polyethylene/organoclay nanocomposites. *J. Appl. Polym. Sci.* **2012**, *125*, 305–313, doi:10.1002/app.36367.
69. Küçük, I.; Gevgilili, H.; Kalyon, D.M. Effects of dispersion and deformation histories on rheology of semidilute and concentrated suspensions of multiwalled carbon nanotubes. *J. Rheol.* **2013**, *57*, 1491–1514, doi:10.1122/1.4819745.
70. Durmus, A.; Kasgoz, A.; Macosko, C.W. Linear low density polyethylene (LLDPE)/clay nanocomposites. Part I: Structural characterization and quantifying clay dispersion by melt rheology. *Polymer* **2007**, *48*, 4492–4502, doi:10.1016/j.polymer.2007.05.074.
71. Hanemann, T. Nanoparticle surface polarity influence on the flow behavior of polymer matrix composites. *Polym. Compos.* **2013**, *34*, 1425–1432, doi:10.1002/pc.22428.
72. Shang, S.W.; Williams, J.W.; Söderholm, K.-J.M. Work of adhesion influence on the rheological properties of silica filled polymer composites. *J. Mater. Sci.* **1995**, *30*, 4323–4334, doi:10.1007/BF00361512.
73. Fisher, I.; Siegmann, A.; Narkis, M. The effect of interface characteristics on the morphology, rheology and thermal behavior of three-component polymer alloys. *Polym. Compos.* **2002**, *23*, 34–48, doi:10.1002/pc.10410.
74. Spoerk, M.; Savandaiah, C.; Arbeiter, F.; Sapkota, J.; Holzer, C. Optimization of mechanical properties of glass-spheres-filled polypropylene composites for extrusion-based additive manufacturing. *Polym. Compos.* **2017**, *83*, 768, doi:10.1002/pc.24701.
75. Zhang, Q.; Archer, L.A. Poly(ethylene oxide)/Silica Nanocomposites: Structure and Rheology. *Langmuir* **2002**, *18*, 10435–10442, doi:10.1021/la026338j.
76. Carrot, C.; Majesté, J.-C.; Olalla, B.; Fulchiron, R. On the use of the model proposed by Leonov for the explanation of a secondary plateau of the loss modulus in

heterogeneous polymer–filler systems with agglomerates. *Rheol. Acta* **2010**, *49*, 513–527, doi:10.1007/s00397-010-0432-2.

77. McNulty, T.F.; Mohammadi, F.; Bandyopadhyay, A.; Shanefield, D.J.; Danforth, S.C.; Safari, A. Development of a binder formulation for fused deposition of ceramics. *Rapid Prototyp. J.* **1998**, *4*, 144–150.
78. Enneti, R.K.; Onbattuvelli, V.P.; Atre, S.V. Powder Binder Formulation and Compound Manufacture in Metal Injection Molding (MIM). In *Handbook of Metal Injection Molding*; Heaney, D.F., Ed.; Woodhead Publishing: Cambridge, UK, 2012.
79. Miltner, H.E.; Watzeels, N.; Gotzen, N.-A.; Goffin, A.-L.; Duquesne, E.; Benali, S.; Ruelle, B.; Peeterbroeck, S.; Dubois, P.; Goderis, B.; et al. The effect of nano-sized filler particles on the crystalline-amorphous interphase and thermal properties in polyester nanocomposites. *Polymer* **2012**, *53*, 1494–1506, doi:10.1016/j.polymer.2012.01.047.
80. Gopakumar, T.G.; Lee, J.A.; Kontopoulou, M.; Parent, J.S. Influence of clay exfoliation on the physical properties of montmorillonite/polyethylene composites. *Polymer* **2002**, *43*, 5483–5491, doi:10.1016/S0032-3861(02)00403-2.

### **3.7 Summary of the binder development process**

In section 3 the development of a novel feedstock formulation has been conducted through the investigations presented in the publications A, B, C and D. Due to the complexity of the system, the influence of each component has been evaluated separately.

In the work presented in publication A the soluble binder components were selected according to the properties required for the FFF and solvent debinding processes. The binder systems were composed of AA-HDPE as backbone, SA as surfactant and two types of soluble components. SEBS and APO were tested as single soluble components, and the incorporation of PW and EO as second soluble component was also evaluated. The content of the components in the binder systems was kept constant and the different formulations were tested as unfilled binders and as feedstocks with 47 vol.% of zirconia powder. It was found that two types of soluble components are required to meet all the requirements for FFF and solvent debinding: one soluble component with high flexibility and strength is required to produce filaments; the second soluble component must reduce the viscosity and reduce the swelling during solvent debinding. The soluble binder components must be homogeneously dispersed in the feedstock in order to avoid stress concentration and crack propagation during solvent debinding. Based on these findings, SEBS and PW were selected as the soluble binder components. The feedstock filament composed of 47 vol.% powder, 18.55 vol.% AA-HDPE, 5.3 vol.% SA, 14.575 vol.% SEBS and 14.575 vol.% PW could be processed up to the pre-sintering step without defects. However, the low flexibility and brittleness of the material required a careful handling of the filaments.

An statistical evaluation of the effect of the binder components fractions on the properties for FFF and solvent debinding was conducted in publication B. The objective of this investigation was to obtain a better understanding of the feedstock properties and increase the flexibility of the feedstock filaments. Feedstocks with 47 vol.% of zirconia powder and different binder compositions were evaluated using the same procedures as those in publication A. The restrictions imposed in the design of experiments were a backbone content between 35 vol.% and 50 vol.% of the binder, and a PW content equal or lower to the SEBS content. The content of SA was kept constant. Increasing the backbone content increases the strength and stiffness, but also increases the viscosity and reduces the debinding rate. The increase of the SEBS content increases the debinding defects and only increases the flexibility when it is combined in the right proportion with PW. Since the increase of the PW content is the only way to reduce the viscosity and reduce the debinding defects, it was found that the PW to SEBS ratio must be kept in the range  $1 \geq \text{PW/SEBS} \geq 0.6$ .

The influence of the SA on the properties and processability of the feedstock by FFF and solvent debinding was studied in publication C. The feedstock from publication A was compared to a second feedstock with no SA, but both feedstocks having the same relative content of AA-HDPE, PW and SEBS. Incorporating SA in the formulation reduces the viscosity, improves the homogeneity, increases the solvent debinding and reduces the defects in the parts. Nevertheless, it results in a significant decrease of the strength, stiffness and flexibility of the filaments. The reduction of the filament mechanical properties could be caused by the

reduction of the AA-HDPE adhesion to the powder, diminishing the improvements obtained with the acrylic acid grafted backbone.

In fact, since the use of polyolefins grafted with polar groups as backbones in feedstocks is relatively novel, the mechanisms causing the improvement of properties are not fully understood yet. A first step in this direction was taken in publication D by the study of composites of zirconia with HDPE with and without the AA grafting. The interfacial interactions between the grafted backbone and the powder and their effect on the feedstock properties were investigated by means of molecular dynamics simulations and experimental methods. It was observed that the high polarity, the improved interaction with the oxygen atoms in the zirconia surface and the hydrogen bonding with the hydroxyl groups in the powder surface result in a higher powder-binder adhesion for the grafted backbone than for the ungrafted one. Higher powder-adhesion increases the dispersion of the powder in the polymeric binder, and both result in an increase of the filament flexibility and strength. A polymer-filler network is formed for the grafted backbone which results in higher viscosity and shear modulus than for the ungrafted backbone.

Considering the results of publications A, B, C and D, it can be concluded that different types of binder components are necessary to meet the many criteria in the feedstock for the processing by FFF and solvent debinding. Moreover, the fraction of each type of component must be adjusted in order to reach the right combination of properties. The multicomponent binder system composed of AA-HDPE, SA, SEBS and PW developed in this section shows a great potential for the processing of zirconia by FFF and solvent debinding. The results of the feedstock development investigations validated the hypotheses:

1. *By the right combination of binder components, a high strength, stiffness and flexibility, as well as low viscosity could be obtained as required for FFF.*
2. *Solvent debinding requires two types of components. First, a major fraction of the binder must be leached with a solvent. The rest, known as backbone, must maintain the shape of the parts during the process and be removed in the subsequent thermal debinding step. The combination of the right soluble binders and backbones should enable the use of solvent debinding in FFF.*
3. *The use of a polymer grafted with polar groups as backbone should result in an improvement of the adhesion to the polar surface of the zirconia powder. A high powder-binder adhesion should result in a more homogeneous feedstock, with lower viscosity and with higher mechanical properties.*

Nevertheless, the third hypothesis could be only partly validated. The improved powder-binder adhesion for the grafted backbone improved the powder dispersion and increased the mechanical properties. However, it did not reduce the viscosity as was initially expected.

In future investigations, the final adjustment of the content of the binder components must be conducted in order to improve the flexibility of the feedstock filaments while having a low viscosity and no debinding defects. Moreover, the compounding of the feedstocks during the development process was conducted using low shear equipment. The reason to use the low shear equipment was the small amount of material required, which is critical in the

development of binder formulations. However, it is known for PIM feedstocks that the increase of the shear during compounding improves the powder dispersion, especially for small powders like the zirconia used in this PhD thesis [195]. In fact, high shear compounding equipment such as co-rotating twin screw extruders are commonly used for the production at industrial scale of highly filled polymers and feedstocks. Therefore, current investigations are addressing the adjustment of the feedstock composition with high shear compounding equipment and a small number of binder formulations. In the investigations presented in the next sections, a binder developed in previous investigations at the Institute of Polymer Processing [122], composed of a grafted polyolefin as the backbone and a thermoplastic elastomer as the soluble component, was used.

## 4 Influence of the solvent debinding parameters

### 4.1 State of the art

In this section, a brief review of the research performed in the field of solvent debinding of feedstocks is presented. More specifically, in the solvent debinding of feedstocks for Powder Injection Moulding, for which most of the research has been carried out.

#### 4.1.1 Stages and mechanisms of solvent debinding

Three significant phenomena take place during the solvent debinding process: the diffusion of the solvent into the binder, the dissolution of the soluble polymer and the diffusion of the dissolved polymers from the inner regions to the surface [107]. The evolution of the porosity, the dimensional changes, the dissolution mechanisms, and the structure of the parts have been studied for the debinding in water and organic solvents.

Hwang et al. compared the evolution of the pore structure for iron feedstocks containing a binder composed of PP:PW:SA = 30:65:5 wt.% during the thermal and the solvent + thermal debinding. For the solvent debinding at 50 °C in n-heptane, tests at different times were performed, and the mercury porosimetry was measured. The increase in time produced the increase of the median pore diameter, as well as the proportion of smaller powders. The second phenomenon was the increase of the solvent-binder interfaces with the increase of time, which facilitates the penetration of the solvent in more parts. SEM images of the different parts corroborated these results since the increase of the porosity can be observed with the time increase. The weight loss was also measured. At the beginning of the tests, the debinding rate is faster due to the smaller diffusion distance. As the process continues, the pore channels extend to the inner region of the parts, and the solvent and leached polymer need a longer time to diffuse. When comparing the thermal versus the solvent + thermal debinding, the second one proved to be more efficient. The main reason is the formation of a wider distribution of pores, which facilitates the evacuation of the decomposition products in the last thermal debinding stage [106].

The previous authors continued with the analysis of the solvent debinding, including the variation of the length with time. The evolution of PP and feedstock parts in n-heptane was compared. A sharp increase in the length of the samples was measured when the pre-heated solvent was introduced. Following, the parts expanded slowly due to the PP swelling. At the end of the tests, the solvent was taken out, and a drastic contraction was measured. The initial and final changes were produced by the quick penetration and evaporation of the n-heptane in the molecules of PP rather than thermal expansion. As a result, cracks and distortions were observed in the parts. The fast diffusion of the n-heptane in the PP was considered as indicative that the diffusion of the solvent is not the limiting mechanism in the process. Thus, the dissolution of the polymer and the diffusion of the dissolved molecules are the limiting steps in the process [107].

A detailed description of the solvent debinding mechanism in organic solvents was summarized by Westcot et al. [220]. The leaching of the polymer is caused by the combined

action of the solvation and capillary forces. The process starts with the diffusion of the solvent into the binder, together with the diffusion of the soluble components into the solvent. In this initial stage, a swollen gel is produced. If the interaction of the soluble binder with the solvent is stronger than that with the other polymers, a true dissolution takes place. The dissolved molecules diffuse finally to the outer part due to capillary forces. This process is repeated as the dissolved region expands to the interior of the parts. At the beginning of the process, the dissolution is controlling the debinding rate. However, as the process goes further into the parts, the diffusion of the dissolved polymers is the limiting mechanism [220].

Yang et al. performed studies for water-soluble alumina feedstocks with PEwax:PEG:SA=30:65:5 wt.%. Similar results were obtained. However, since in that case the backbone was not affected by the solvent, a different process was proposed. According to the authors, the gradual dimensional change was only produced by the formation of a swollen hydrogel of PEG [230].

The theory of the formation of a PEG gel was refuted by Chen et al. [39]. These authors proved that the gelation process of PEG, produced by crosslinking, can only take place at temperatures above the lower critical solution temperature (LCST). So taking into account that the temperatures used in water debinding processes are considerably lower than that limit, gelation is discarded. A new model was proposed. At low water concentrations, water binds the units of PEG through hydrogen bonding, keeping the initial helix structure of PEG. In the case of high water concentrations, PEG molecules form a new structure where some water molecules form an interface with the polymer, while other molecules are bonded to the PEG chains. When the solvation process finalizes, the hydrated PEG compounds formed through these reactions are transported out of the parts in a diffusion process produced by capillary forces and gradients of composition. Since the molecular weight of hydrated PEG is higher than that of the water, the diffusion of PEG is considerably lower and determines the duration of the process. Finally, the hydrated complexes disperse in the water solution [39].

#### **4.1.2 Effect of the debinding parameters**

The selection of the solvent is determined in most of the cases with the type of binder employed. This selection happens also in the other direction, since the water-soluble feedstocks are selected over wax-based feedstocks in many cases to avoid the use of organic substances. Over the years, many chemicals used originally as solvents have been retired due to their ozone-depleting and carcinogenic effect [13].

For the binders which can be removed with different organic solvents, the right selection of the solvent can lead to significant improvements in the debinding rate. Zaky et al. [236] studied the debinding behaviour in different solvents for a stainless steel PIM feedstock with a binder composed of PW, EVA and SA. The highest debinding rate and maximum amount of dissolved polymer were obtained with n-hexane, followed by n-heptane and isooctane. The difference could be caused by the differences in the carbon number since a higher carbon number could result in lower solubility of the PW and higher solvent viscosity [236]. A similar study was conducted by Ni et al. [155] for Al-Si alloy feedstocks with carnauba wax as the main soluble component. In that case, the debinding in xylene was more efficient than the debinding in hexane, and both were better solvents than heptane [155]. Other approaches



to increase the debinding rate are the increase of the solvent to feedstock ratio [236] and refreshing the solvent [155].

In some cases, an excessive debinding rate and swelling of the binders during solvent debinding can lead to defects in the components. To remove these defects, the use of a swelling inhibitor was investigated by Fan et al. [69] for PIM carbonyl iron parts. The binder system was composed of 40 wt.% of PE, 55 wt.% of PW and 5 wt.% of SA. Heptane was employed as a solvent and different types of alcohols, 1-bromopropane and ethylacetate were tested as inhibitors. Each of the inhibitors had a different solubility parameter. The PW and SA were insoluble in the alcohols, but they could be dissolved by the 1-bromopropane and ethylacetate. The swelling and debinding rate evaluation showed that the alcohols resulted in the most effective reduction of swelling, but also the highest decrease of debinding rate [69].

The temperature of the solvent is another crucial factor in the process. Since solvent debinding is based on dissolution and diffusion mechanisms, the increase of the temperature increases the debinding rate. However, the increase in temperature might lead to softening of the part and to distortions. Therefore, it is necessary to adjust the temperature to the maximum temperature at which the parts preserve the shape. Numerous studies have optimized the solvent debinding temperature for feedstocks for different technologies [8, 29, 43, 86, 160, 236].

The influence of the temperature in the dimensional changes during the immersion in heptane at 40, 50 and 60 °C was studied by Westcot et al. [220]. The dimensional changes of the iron feedstocks containing PP+LDPE+PW+SA were compared to the one of the pure backbones, i.e. PP and LDPE. The thermal expansion of the pure polymers and the filler has a minor role compared to the swelling of the polymers when reacting with the solvent. At the intermediate stage, the swelling is produced by the dissolution of the soluble polymers. A transient swelling peak is observed in this stage. The decrease in the temperature increases the magnitude of the peak. The reason is that the diffusion of the dissolved molecules is lower at lower temperatures. Since most of the defects are originated in this stage, higher temperatures would help to improve the quality of the parts. At the end of the process, the swelling is mostly produced by the swelling of the backbones and the thermal expansion. Higher temperatures produce higher final swelling and increase the probability of distortion of the parts. Thus, it is necessary to reach a trade-off for an efficient process [220].

Another parameter influencing the process is the geometry of the components. It can be stated that the larger the ratio surface area/volume for the components, the faster the debinding process [43, 160]. I.e. as the proportion of polymer close to the surface increases, the diffusion distance for the dissolved molecules is reduced. The influence of the specimen dimensions and geometries in the solvent debinding kinetics has been experimentally studied, and different mathematical models have been proposed for the prediction of this phenomenon [65, 190, 232].

Fan et al. [70] studied in detail the minimum fraction of binder that must be dissolved before the thermal debinding can start for PIM specimens with squared section and thickness of 3, 6 or 8.7 mm. A carbonyl iron feedstock with a binder composed of 40 wt.% polyethylene, 55 wt.% paraffin wax and 5 wt.% stearic acid was employed. For such feedstock with

22.9 vol.% of soluble binder components, a minimum of 59 wt.% of the soluble binders must be removed, which is equivalent to a porosity of 8.5 vol.%. Above that level of porosity, an interconnected structure from the surface to the centre of the specimens is formed, which enables the evacuation of the evaporation and decomposition gases during thermal debinding [70]. Despite these results can be applied for binder systems based in wax, the formation of an open porous structure might not be enough for other binder systems, in which the removal of all the soluble components is required. An example is the FFF stainless steel feedstock employed by Gonzalez-Gutierrez et al. [86]. The dissolution of 94 % of the soluble component was not enough to avoid the apparition of defects in the subsequent thermal debinding, which could be only avoided for a dissolution fraction of 99 % [86].

### 4.1.3 Effect of the powder characteristics

In addition to the properties of the binders, the influence of the geometry of the metallic and ceramic powders might also determine the performance of the feedstocks in solvent debinding, as has been reported in the literature [17, 48, 108, 210, 220].

The effect of the particle size was another of the parameters studied by Westcot et al. [220]. Two feedstocks containing 60 vol% of spherical powder were compared, being one an iron feedstock with a median particle size of 4  $\mu\text{m}$  and the other a 316L stainless steel feedstock with a median particle size 12  $\mu\text{m}$ . The use of smaller particles produced a decrease in the debinding rate and an increase of the dimensional change. The cause of this phenomenon might be the decrease of the pore size and the increase of the contacts between particles with smaller sizes. Therefore, the diffusion of the dissolved molecules is slowed down, increasing the swelling of the parts [220].

Different results were obtained by Hwang et al. [108] when studying the solvent debinding in heptane at 50 °C of stainless steel and iron feedstocks containing PP:PW:SA = 40:55:5 wt.%. Spherical raw powders were air classified in different particle sizes, and feedstocks were elaborated with the different size powders. Some minor differences could be observed at intermediate stages when comparing small and large stainless steel powders. Nevertheless, the debinding rate was practically constant regardless of the size of the particles and of the pores in most of the cases. The reason for this independence could be the considerable difference between the nano-PW molecules and the pores during debinding, which are in the micrometric scale in all the cases [108].

These authors also performed preliminary tests comparing the solvent debinding of the feedstocks containing spherical and small powders, with those of feedstocks containing a 60 vol% of irregular and large powders and a 40 vol% of small and spherical powders. Again, the results showed the invariance with the change of the particle geometry [108].

Nevertheless, similar results to those of Westcot were obtained by Contreras et al. [48] for the solvent debinding in heptane of bronze feedstocks containing a binder of HDPE:PW = 50:50 vol.%. Two irregular powders were employed, with median particles sizes of 13.18  $\mu\text{m}$  and 75.71  $\mu\text{m}$ . The debinding of four feedstocks was compared, two of them only with one of the two powders, and the other two with the combination of both. The results showed an increase of the wax loss with the increase of the particle size, especially at

the first and intermediate stages. As time progressed, the difference disappeared. This trend was kept for the combination of powders, regardless of the increase of the packing density, which would be expected [48].

Contreras et al. also conducted a similar set of tests for determining the influence of the particle morphology. Feedstocks containing the previously mentioned binder and powders with two morphologies were compared. Additionally, two mixtures of the two types of powders were studied. The results clearly showed the increase in the debinding rate with the use of spherical particles, even though the particle concentration was higher for feedstocks containing spherical powders. The reason might be the larger path for the dissolved molecules when the particles are irregular [48].

The changes in solvent debinding behaviour for different powder geometries are of particular importance in the production of multi-material parts. Researchers of the Universiti Kebangsaan Malaysia [17, 210] studied the micro-injection moulding of components combining stainless steel and zirconia. The binder system was composed of 40 vol.% of LDPE and 60 vol.% palm stearin, the second being soluble in acetone. Solvent debinding trials of parts were performed first for single-material parts, obtaining a higher debinding rate for the stainless steel feedstock parts than for those with zirconia. Due to the different debinding rates of the two feedstocks, the temperature of the solvent had to be adjusted for the multi-material parts. An intermediate temperature was selected since a low temperature resulted in excessive swelling of the zirconia feedstock [210], whereas a high temperature could lead to debinding defects [17].

## 4.2 Introduction to publication E

In section 2, the development process of a new feedstock formulation for the FFF and solvent debinding of zirconia has been presented. During that process, the effect of the binder components on the solvent debinding rate and the apparition of defects of FFF feedstocks could be determined.

The influence of the powder chemistry, shape and size on the solvent debinding performance of different metallic and ceramic FFF feedstocks could be observed in previous works to this dissertation [17, 48, 108, 124, 210, 220]. In the introduction of publication E, the results of [124] can be found. In those investigations, it could be observed that the parts with the feedstock of the zirconia powder employed in this thesis had larger defects and lower debinding rates than those containing other powders.

Based on the existing knowledge on solvent debinding of PIM feedstocks previously presented, the investigation in publication E aimed to solve the problems in the debinding of the zirconia feedstock based on the hypothesis:

4. ***The parameters employed in the solvent debinding of FFF feedstocks should determine the debinding rate and the apparition of defects.***

The following parameters were investigated in publication E: the influence of the temperature, the debinding time, the incorporation of stearic acid as a dispersing agent and the use of a swelling inhibitor to reduce the swelling and the associated defects. The binder employed in [124] was a formulation developed in previous investigations at the Institute of Polymer Processing [122], composed of a grafted polyolefin as the backbone and a thermoplastic elastomer as a soluble component.

### 4.3 Publication E

#### ***Debinding behaviour of feedstock for material extrusion additive manufacturing of zirconia***

Christian Kukla, Santiago Cano, Dario Kaylani, Stephan Schuschnigg, Clemens Holzer, Joamin Gonzalez-Gutierrez

**Powder Metallurgy, 62 (2019) 196-204**

**Special Issue *VICNP Ciudad Real, Spain. 2017*, guest-edited by Gemma Herranz**

doi: 10.1080/00325899.2019.1616139

Received: 29.11.2017

Revised: 13.08.2018

Accepted: 03.05.2019

Available online: 15.05.2019

#### **ABSTRACT**

Material extrusion additive manufacturing (MEAM) is mainly used for the production of polymeric components. Using feedstocks similar to those of Powder Injection Moulding (PIM), MEAM of ceramic components is possible. MEAM with filaments is also called Fused Filament Fabrication (FFF). Feedstocks are used as filaments; this imposes new requirements such as flexibility for spooling, stiffness to avoid buckling and constant diameter to ensure a consistent mass flow. Additionally, the binder should be removed without damaging the shaped part. In this paper, the debinding behaviour of MEAM feedstocks with zirconia was investigated. It was observed that higher temperature increases the debinding rate, but cracks occurred; the addition of a surfactant speeds up the debinding rate and reduces cracks; and a mixture of 10 % isopropanol and 90 % cyclohexane initially decreases swelling during debinding, but the debinding rate and the appearance of cracks is unaffected.

*Keywords:* Material extrusion; fused filament fabrication; feedstock; ceramic.

## Introduction

Fused Filament Fabrication (FFF) is a popular Material Extrusion Additive Manufacturing (MEAM) technique. The main reasons of its popularity are its safe and simple fabrication process, low cost and the availability of a great variety of building materials. In FFF, a thermoplastic filament is extruded through a nozzle by the action of two counter rotating feeding wheels and deposited on a plate one layer at a time. The printing chamber and bed are kept at temperatures below the polymer melting point but higher than room temperature to promote adhesion to the printing bed and to reduce thermally induced stresses [1,2].

FFF can be used for the production of metallic or ceramic parts with complex shape, in a process called Shaping, Debinding and Sintering (SDS) [3] or fused deposition of metals (FDMet) [4,5] or ceramics (FDC) [6–8]. Feedstocks used in SDS consist of a polymeric binder and a high load of sinterable powder. After shaping, the binder is removed via solvent extraction and/or thermochemical decomposition. Finally, the powder is sintered together to obtain a solid part. Therefore the content of powders in the feedstock should be equal or higher than 50 vol% to reduce shrinkage and defects during the sintering process. In addition to the requirements of a highly filled system, the processing by FFF imposes further demands on the feedstocks. To be spooled as a filament, high flexibility and strength is required for the feedstock. Since the solid filament must transmit the force from the feeding wheels to the molten feedstock, sufficient stiffness is required to avoid its buckling during the material extrusion process. Furthermore, a low viscosity is necessary to reduce the flow resistance, and a good adhesion is necessary between the already extruded and deposited layers as well as to the building platform. In order to achieve all these properties in a feedstock, multicomponent binder systems are required and the right proportion of the components is needed [7,9].

Our research group developed a binder system consisting of a thermoplastic elastomer for flexibility and a grafted polyolefin for stiffness and tackiness. This relatively simple formulation has been demonstrated to produce filaments processable by FFF with various metallic and ceramic powders such as stainless steel 316L ( $d_{50} = 6.05 \mu\text{m}$ ) [10], titanium alloy Ti6Al4V ( $d_{50} = 14.97 \mu\text{m}$ ) [11], neodymium alloy NdFeB ( $d_{50} = 28.29 \mu\text{m}$ ) [11], strontium ferrite  $\text{SrFe}_{12}\text{O}_{19}$  ( $d_{50} = 1.35 \mu\text{m}$ ) [11,12] and yttria stabilized zirconia YSZ ( $d_{50} = 0.6 \mu\text{m}$ ) [11]. In Figure 1, the mechanical properties of filaments made out of feedstocks containing the developed binder system and 55 vol% of solid content (except for the zirconia feedstock, with a solid content of 50 vol%) are depicted.

As can be seen in Figure 1, the mechanical properties of the filaments are greatly affected by the powder used. For those filaments containing 316L powder a yield stress point followed by strain hardening could be observed. The highest elongation at break ( $\sim 41\%$ ) and maximum stress ( $\sim 12\%$ ) values were measured for this material. Filaments with titanium have a shorter elongation at break ( $\sim 10\%$ ) and no maximum after the onset of plastic deformation. The curve for neodymium alloy filaments has a much shorter elongation at break ( $\sim 3\%$ ) and the stress continuously decays after reaching a maximum. Finally filaments containing ceramic powders (strontium ferrite and zirconia) have very low elongation at break with high stress values, i.e. very brittle filaments were obtained for the feedstocks with these powders.

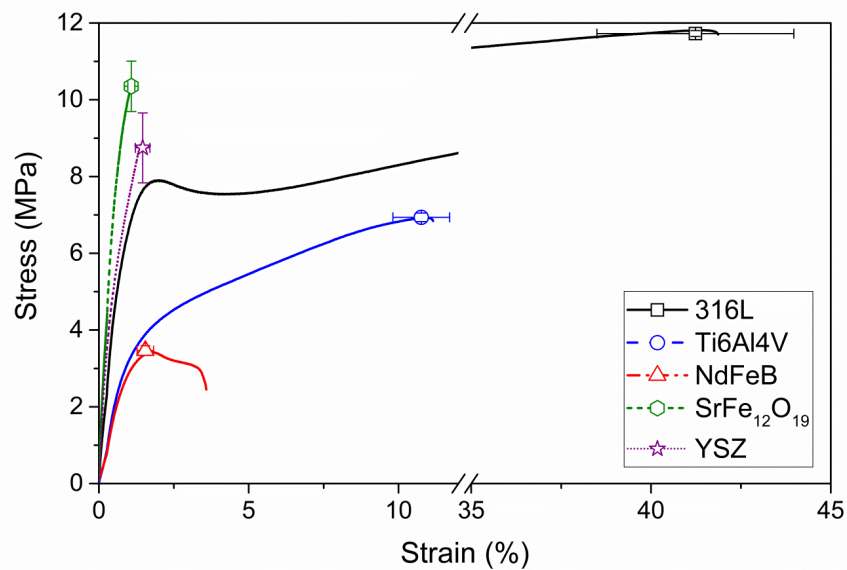


Figure 1. Strain-stress ( $\epsilon - \sigma$ ) curves for filaments containing stainless steel (316L), titanium alloy (Ti6Al4V), neodymium alloy (NdFeB), strontium ferrite ( $\text{SrFe}_{12}\text{O}_{19}$ ) and yttria stabilized zirconia (YSZ) [11].

Despite the big difference in the tensile properties, all filaments were processable by FFF with a Hage3D-140L FFF machine (Hage Sondermaschinenbau GmbH & Co KG, Obdach Austria). Examples of the printed parts are shown in Figure 2.

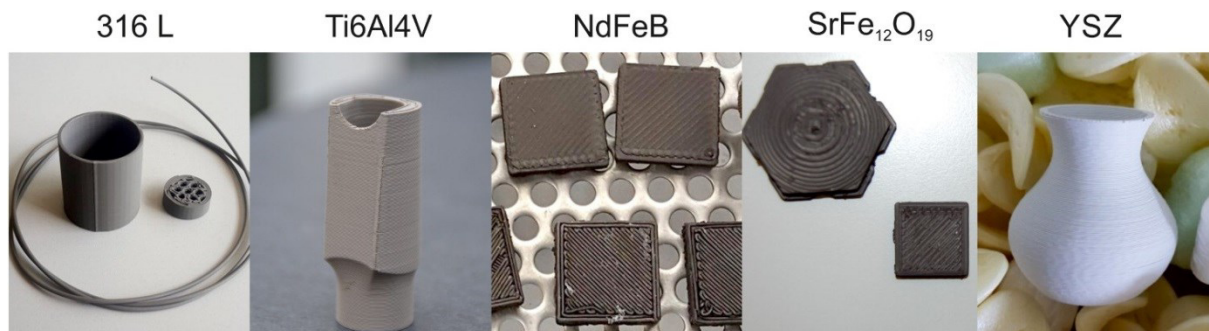


Figure 2. Examples of parts build by FFF with 5 powder types: stainless steel (316L), titanium alloy (Ti6Al4V), neodymium alloy (NdFeB), strontium ferrite ( $\text{SrFe}_{12}\text{O}_{19}$ ) and yttria stabilized zirconia (YSZ) [11].

A two-step debinding process combining solvent and thermal debinding can be conducted for the developed binder. Therefore the solvent debinding behaviour of the feedstock materials was also investigated. In Figure 3a the amount of soluble binder removed in cyclohexane at 60 °C at times up to 12 h is plotted for the different feedstocks. The highest binder loss was obtained for 316L feedstock. For short times (3 and 6 h) a higher debinding rate was obtained for NdFeB than for Ti6Al4V, nevertheless similar values were obtained at 9 and 12 h. The feedstocks with the two ceramic powders showed the lowest values for the leached soluble binders. Figure 3b shows that the filler used in the feedstock not only affect the debinding rate, but also can lead to defects during debinding. All the metal-filled feedstocks could be debound without defects, but the ceramic ones developed cracks [11]. The small particle size of the ceramic powder is most likely responsible for these differences.

In general, feedstocks with small particles have smaller pores between the particles and a higher number of contact points between those particles [13,14]. This creates an intricate network through which the dissolved polymers must be evacuated. In addition, the particles have a high tendency to agglomerate [15], which generates defects during the debinding and sintering steps.

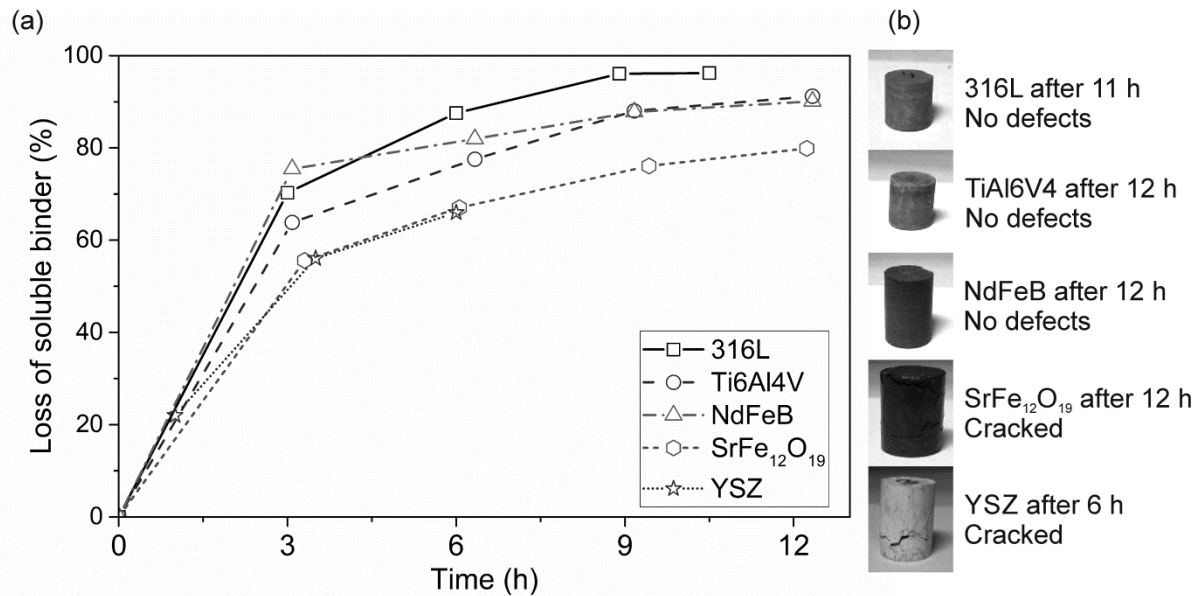


Figure 3. (a) Mass loss of soluble binder component for feedstocks with stainless steel (316L), titanium alloy (Ti6Al4V), neodymium alloy (NdFeB), strontium ferrite (SrFe<sub>12</sub>O<sub>19</sub>) and yttria stabilized zirconia (YSZ); (b) specimens after debinding in cyclohexane at 60 °C at different times[11].

Since zirconia is an important material for industrial and dental applications, it was decided to make a more detailed investigation on the solvent debinding behaviour of zirconia-filled feedstocks. Three main variables were investigated: (i) solvent debinding temperature, (ii) addition of surfactant (stearic acid) to the binder system and (iii) the incorporation of a swelling inhibitor (isopropanol) into the solvent to reduce defects.

The solvent temperature is a major parameter affecting solvent debinding. Three major phenomena occur during the debinding: the diffusion of solvent into the organic components, the dissolution of the soluble binder and the diffusion of the dissolved polymers from the inner regions to the surface [16]. A temperature raise speeds up these phenomena and thus the overall debinding rate. Nevertheless, it could also result in defects and dimensional changes [13].

One reason for adding surfactants to the binder system is the increase of the dispersion of the filler particles ensuring that individual particles are surrounded by binder [17]. Also the surfactant will be removed easily from the binder at the same time as the soluble component, since it has a low melting point, leaving space for more binder to leave without damaging the part.

To conduct the solvent debinding process, a non-polar binder is coupled with a non-polar solvent, which in principle should ensure the dissolution of the main binder component.



However, the solvent could also interact easily with the non-polar polyolefin employed as backbone, producing its swelling [18]. One way to reduce swelling is the incorporation of a swelling inhibitor with higher polarity as observed by Fan et al [19]. According to these authors a significant swelling reduction and defect occurrence is attained while reducing only slightly the debinding rate [19].

### **Experimental procedure**

Tetragonal zirconia powder used to prepare feedstocks in this investigation was TZ-3YS-E grade supplied by the Tosoh Corporation (Tokyo, Japan). The powder is supplied as spray dried granules with a primary particle size of  $d_{50}=0.6 \mu\text{m}$  and a BET (Brunauer–Emmett–Teller) specific surface area of  $7 \pm 2 \text{ m}^2/\text{g}$ .

Feedstocks with a 50 vol% of powder fraction were produced with two types of binders. The first binder investigated consisted of a thermoplastic elastomer TPE (Kraiburg TPE GmbH & Co.KG, Waldkraiburg, Germany) and a grafted polyolefin (Byk Chemie GmbH, Wesel, Germany). To investigate the influence of a surfactant, 5 vol% of the TPE was substituted by stearic acid SA (Merck, KGaA, Darmstadt, Germany). Feedstocks without and with SA will be denoted as feedstock A and B, respectively.

Prior to compounding, the powder was pre-dried at 180 °C for 12 h in order to remove the moisture and reduce its tendency to agglomerate as it is known from the ceramic injection moulding process [15]. Then the material was compounded in an internal mixer Brabender Plasticorder PL 2000 (Brabender GmbH & Co.KG) at 180 °C and 60 rpm. The compounding started with the filling of the binder (including the SA in the compounds in which it was included), followed by the powder, which was introduced in 5 times every 5 minutes. A total compounding time of 90 minutes was employed. After compounding the feedstocks were granulated in a cutting mill having a sieve with square orifices of 2 mm.

Cylinders with a diameter of 8 mm and a length 10 mm were produced by compression moulding in a vacuum press (P200 PV, Dr. Collin GmbH, Ebersberg, Germany). This approach enables the study of the solvent debinding behaviour of small quantities of material on a fast and efficient way. In Table 1 the compression moulding parameters can be found. After the specimens were prepared their mass was recorded.

Table 1. Parameters employed for the production of specimens by compression moulding.

Stage		1	2	3
Time	min	40	5	20
Temperature	°C	175	175	30
Pressure	bar	1	50	50

Cyclohexane (Carl Roth GmbH + Co, KG, Karlsruhe, Germany) was the selected non-polar solvent for the dissolution of the main binder component. Isopropanol (Carl Roth GmbH + Co, KG, Karlsruhe, Germany) was used as a polar solvent and thus swelling inhibitor. A fixed ratio of 20 mL of solvent per gram of feedstock was used. The solvent and specimens were placed in a desiccator DN100 and a recirculating oil bath with heat controllers (Lauda Thermostat, Delran NJ, USA) was employed to control the temperature. A Dimroth condenser was attached to the desiccator lid in order to reflux the solvent and prevent its evaporation. The tests were conducted at temperatures of 50, 60 and 70 °C and times of 1, 3.5 and 6 h. Right after extraction from the solvent, the length of the parts was measured and later the specimens were dried in a vacuum oven (Binder GmbH, Tuttlingen, Germany) at 80 °C for 1 h. The mass loss and defect appearance were studied after the parts were dried.

Using the measured mass loss of the specimens, the loss of soluble binder ( $l_{sb}$ ) was estimated as shown in equation 1:

$$l_{sb} = \frac{m_i - m_f}{m_i} \cdot \frac{1}{\varphi_{sb}} \cdot 100\% \quad (1)$$

where  $m_i$  is the initial mass of the specimen after compression moulding,  $m_f$  is the final mass of the specimen after being in the solvent for either 1, 3.5 or 6 h and after drying for 1 h at 80 °C and  $\varphi_{sb}$  is the mass fraction of soluble binder in the feedstock, which is confidential.

## Results and discussion

The loss of soluble binder, length change and appearance of defects during debinding was investigated as function of: (i) the debinding temperature (ii) the addition of SA to the binder and (iii) the use of isopropanol as swelling inhibitor.

### Effect of the solvent debinding temperature

In Figure 4 the defects observed after the immersion tests at different temperatures are shown. All the specimens had large cracks, independently of the solvent temperature. The cracks can be attributed to the binder softening and swelling, which occur during the solvent debinding process [20,21]. When the specimens are immersed in the hot solvent, a sharp expansion is produced due to the heat [13]. Then the solvent penetrates into the specimens and diffuses between the polymer molecules, producing the swelling of the non-soluble and soluble components. Once the dissolution of the second group occurs, the solved products

are evacuated out of the specimens by capillary forces [13]. As the time progresses, more soluble binder is extracted and the solvent penetrates further into the specimens, causing the increase of the cracks size (Figure 4).

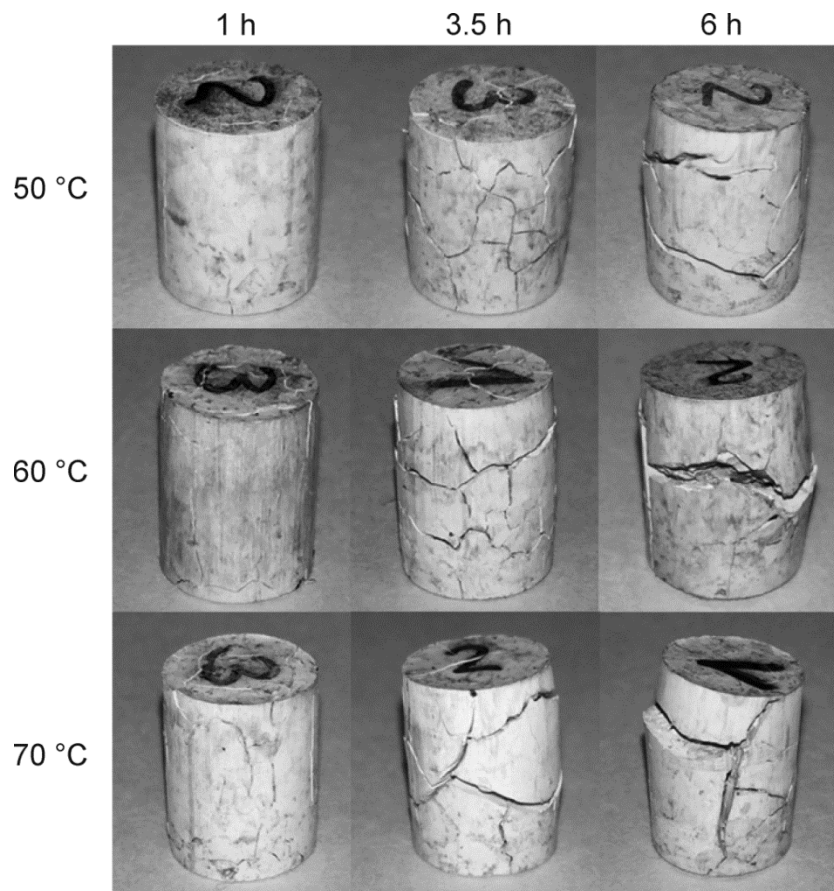


Figure 4. Defects observed in solvent debound specimens at different times and temperatures for feedstock A.

In Figure 5 (a) the loss of soluble binder at different times and temperatures can be observed. The increase of temperature clearly increases the debinding rate. An increase in temperature not only produces an increase in the solubility of the binder, but also facilitates the diffusion of the solvent into the specimen and of the dissolved polymers out to the components [22]. Nevertheless, these results must be evaluated together with the dimensional variation and defects observed in the parts, since these values are also expected to increase with the temperature increase [13].

The maximum length change values at the different evaluated conditions are plotted in Figure 5 (b). A larger dimensional variation occurs when debinding at higher temperature at 1 h, but the opposite trend occurs after 6 h. According to previous studies, a peak of swelling is observed due to the expansion of the soluble components prior to their diffusion out of the specimen [13,23]. Observing Figure 5, it can be stated that the swelling peak is observed at 3.5 h for 70 °C, not being observed for the other temperatures and times. In addition, the highest swelling value at 6 hours is obtained at 50 °C, since a smaller amount of binder could be leached compared to the other temperatures. The improvement of the diffusion rate of the dissolved TPE seems to reduce the dimensional variation.

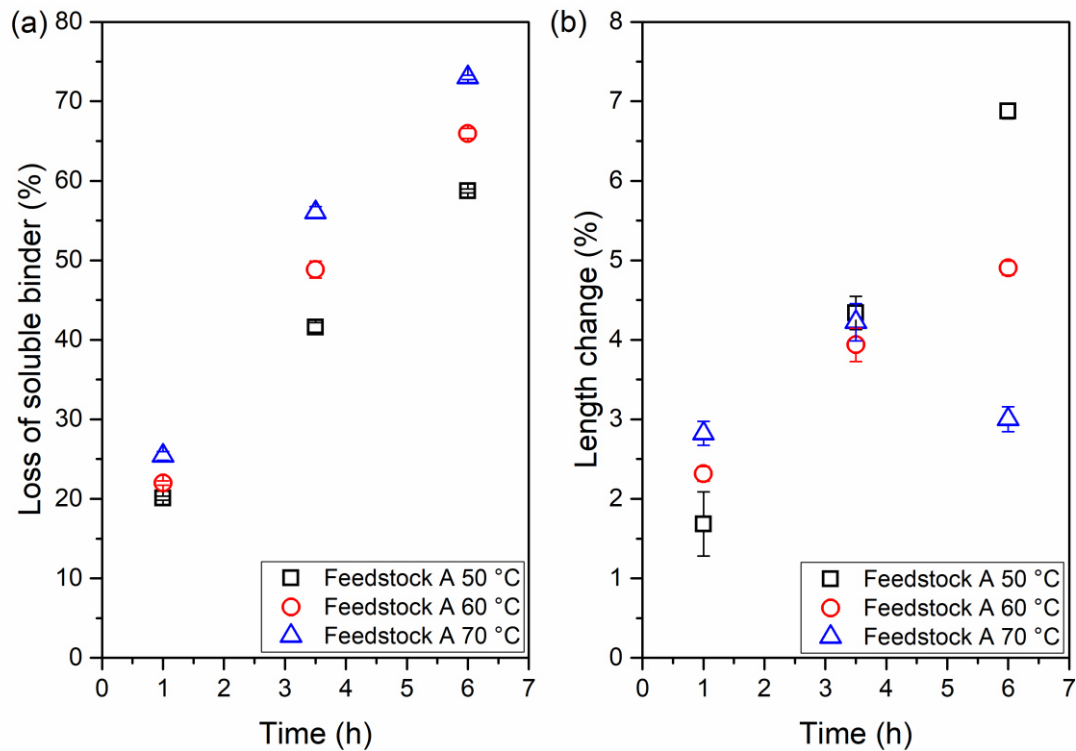


Figure 5. (a) Loss of soluble binder and (b) length change over time at different temperatures for feedstock A.

### Incorporation of SA into binder formulation

In Figure 6 the defects observed in the feedstocks without (Feedstock A) and with SA (Feedstock B) at different times and at 60°C can be observed. The incorporation of SA into the binder formulation resulted in a reduction of the cracks size, especially at longer debinding times. Nevertheless, it did not solve the appearance of cracks. In order to quantify the effect of the stearic acid incorporation, the loss of soluble binder and the length change were determined for both feedstocks.

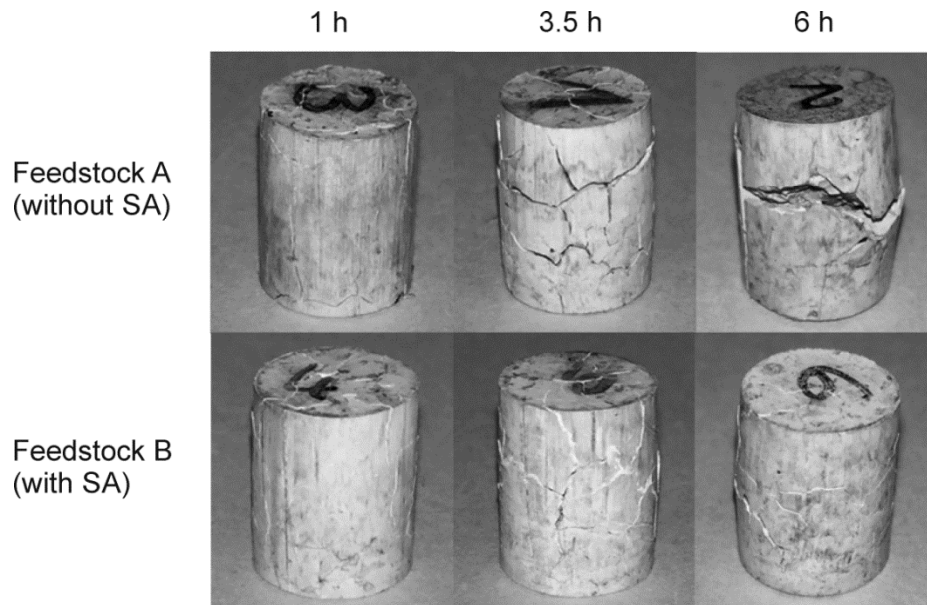


Figure 6. Defects observed in solvent debound specimens for feedstocks without (feedstock A) and with SA (feedstock B).

Figure 7 (a) shows the loss of soluble binder for the tested feedstocks at different times and at 60°C. The fraction of removed binder after the incorporation of SA increases at all measured times. Two phenomena might explain this improvement. First, the stearic acid has a lower molecular weight and a lower melting temperature than the thermoplastic elastomer in the binder, thus enhancing the dissolution and mobility of the dissolved polymer [24,25]. Additionally, the dissolution process might be facilitated by the improvement in the dispersion of the powder, which has been reported for ceramic oxide feedstocks containing SA [26]. The length change of specimens was compared to determine the influence of the surfactant in the dimensional variation. It was observed that the use of SA clearly reduces the length of samples after immersion in cyclohexane (Figure 7 (b)), which results in smaller defects (Figure 6). The small molecular weight of SA not only improves the mobility and dissolution, but results also in less swelling [24,25]. Additionally the improvement of the powder dispersion in the specimens contributes to a further reduction in defects, since the reduced swelling caused by the solvent penetration into the specimen is also homogeneous in the part.

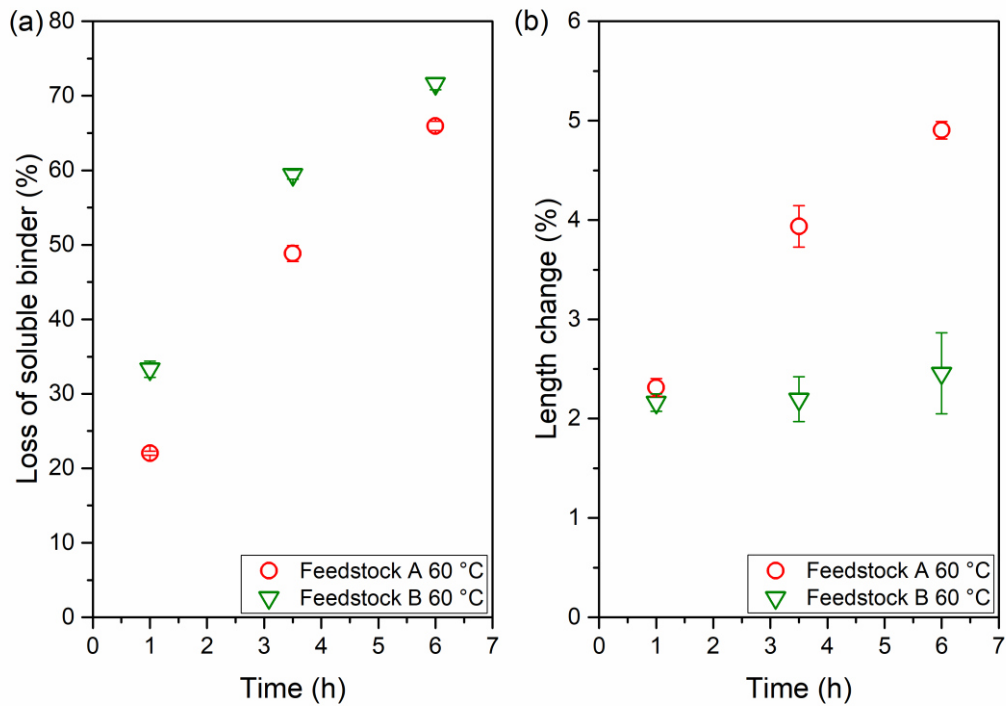


Figure 7. (a) Loss of soluble binder and (b) length change over time at 60 °C for feedstocks without (feedstock A) and with SA (feedstock B).

### Incorporation of isopropanol as swelling inhibitor

Figure 8 shows specimens after the immersion at different times in cyclohexane without and with 10 vol% of isopropanol. No significant changes in the cracks could be observed at any of the immersion times evaluated. Therefore, the use of isopropanol as inhibitor could not be considered as an effective solution for the large defects observed in the tested system.

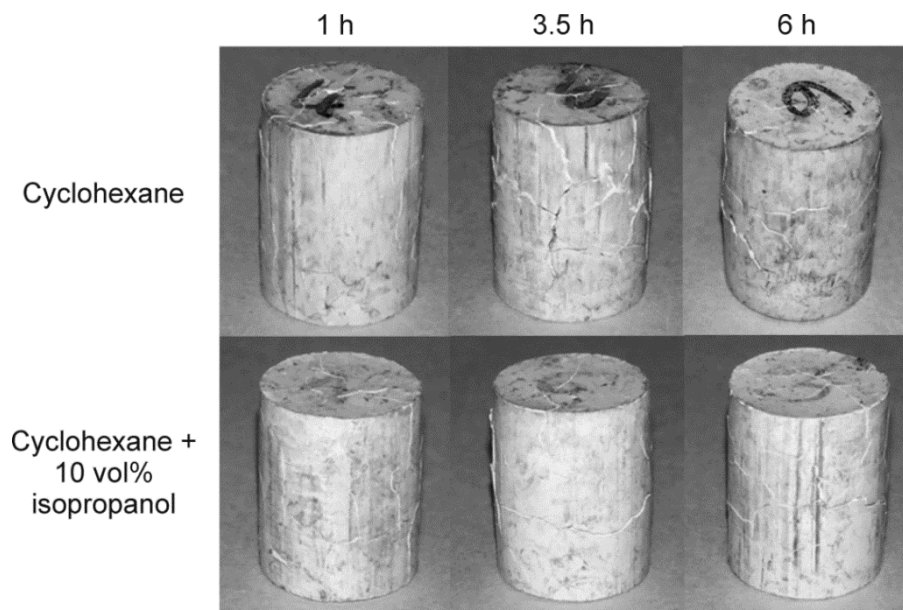


Figure 8. Defects observed in solvent debound specimens after debinding in different solvents at 1, 3.5 and 6 hours.

In Figure 9 (a) the loss of soluble binder ( $l_{sb}$ ) over time for the different solvents is plotted. Only a small binder fraction (around 10% of binder) could be leached out of the specimens with isopropanol. For the tests combining cyclohexane with 10 vol% of isopropanol no significant changes were observed compared to those using only cyclohexane as solvent. The high concentration of solvent per mass of part and the partial solubility of some of the components of the thermoplastic elastomer in isopropanol might explain why no difference was observed.

A different trend was observed by Fan et al. [19] for paraffin wax PIM feedstocks, where a clear reduction in the dissolved fraction was measured when incorporating the swelling inhibitors. The feedstock used in our investigation contains a commercial TPE as soluble component; commercial TPEs are multicomponent compounds. As it can be observed in Figure 10, 10 % of the TPE is soluble in isopropanol, which might be enough to compensate for the replacement of 10 vol% of cyclohexane. Figure 9 (b) shows the change in length with time for different solvents at a temperature of 60 °C. For pure isopropanol, a small length change was measured. The immersion of the specimen into a polar solvent results in a small dimensional variation due to the poor interaction with the binder as observed in the mass loss values. Incorporating 10 vol% of isopropanol only reduced the length change at short times. For the rest of the tested times, the incorporation of the second solvent did not have a significant effect reducing swelling and cracks still developed in all the specimens tested (Figure 12). The partial solubility of the binder in isopropanol can be the reason of the ineffectiveness of this substance as swelling inhibitor. Fan et al. [19] showed that alcohols could be used as swelling inhibitors, while using substances that are able to partially dissolve the binder had no significant effect reducing swelling. In addition, paraffin wax employed by Fan et al. [19] has a smaller molecular weight than TPE and thus less swelling is expected. This might explain the discrepancies observed here.

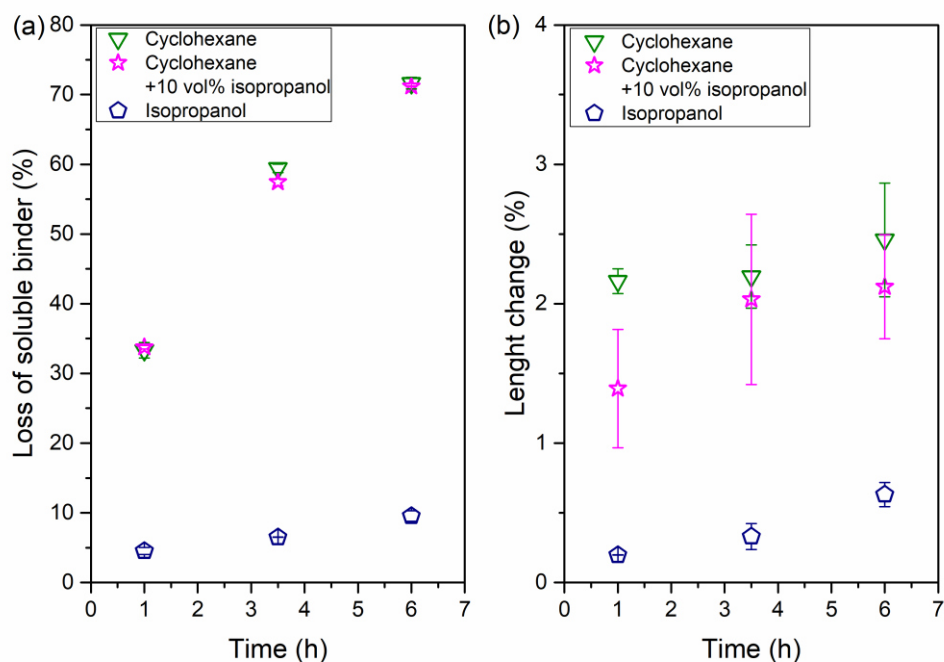


Figure 9. (a) Mass loss of soluble binder and (b) length change over time in different solvents.

### **Conclusions and outlook**

A new binder system has been developed, which allows processing of highly filled filaments by FFF with metal and ceramic particles that later on can be solvent debound and sintered for the production of metal and ceramic parts. Unlike its metallic counterparts, feedstocks containing zirconia experience crack formation during solvent debinding [11]; this has been attributed to the smaller particle size and the use of a binder with a large swelling. Despite the debinding rate could be increased at high temperatures, the large cracks observed in the specimens occurred at all temperatures investigated. The incorporation of SA to the binder in the melt mixing process could improve the debinding rate and contribute to the reduction of defects, but it did not completely eliminate cracks. Incorporating isopropanol as a swelling inhibitor has been also studied here, observing no significant changes in the debinding rate and defects.

For further reduction of the dimensional variation and defects, the modification of other parameters will be studied in further steps. For instance, the improvement of the particle dispersion by using compounding equipment with an increased shear and dispersive mixing, such as co-rotating twin screw extruders and the modification of the binder formulation to reduce swelling and increase the debinding rate.



## References

- [1] A. Boschetto, L. Bottini, and F. Veniali: 'Finishing of Fused Deposition Modeling parts by CNC machining', *Robotics and Computer-Integrated Manufacturing*, 2016, **41**, 92–101, doi: 10.1016/j.rcim.2016.03.004.
- [2] M. Spoerk, J. Gonzalez-Gutierrez, J. Sapkota, S. Schuschnigg, and C. Holzer: 'Effect of the printing bed temperature on the adhesion of parts produced by fused filament fabrication', *Plastics, Rubber and Composites*, 2018, **47**(1), 17–24, doi: 10.1080/14658011.2017.1399531.
- [3] J. Gonzalez-Gutierrez, S. Cano, S. Schuschnigg, C. Kukla, J. Sapkota, and C. Holzer: 'Additive Manufacturing of Metallic and Ceramic Components by the Material Extrusion of Highly-Filled Polymers: A Review and Future Perspectives', *Materials*, 2018, **11**(5), doi: 10.3390/ma11050840.
- [4] G. Wu, N. A. Langrana, S. Rangarajan, R. McCuiston, R. Sadanji, S. C. Danforth, and A. Safari: 'Fabrication of Metal Components using FDMet: Fused Deposition of Metals'. Solid Freeform Fabrication Symposium, Austin, Texas, 9-11 August, 775–782.
- [5] N. Cruz, L. Santos, J. Vasco, and F. M. Barreiros: 'Binder System for Fused Deposition of Metals'. Euro PM2013 Congress & Exhibition, Gothenburg, Sweden, 15-18 September. EPMA, 79–84.
- [6] M. K. Agarwala, V. R. Jamalabad, N. A. Langrana, A. Safari, P. J. Whalen, and S. C. Danforth: 'Structural quality of parts processed by fused deposition', *Rapid Prototyping Journal*, 1996, **2**(4), 4–19, doi: 10.1108/13552549610732034.
- [7] T. F. McNulty, F. Mohammadi, A. Bandyopadhyay, D. J. Shanefield, S. C. Danforth, and A. Safari: 'Development of a binder formulation for fused deposition of ceramics', *Rapid Prototyping Journal*, 1998, **4**(4), 144–150.
- [8] C. M. Pistor: 'Thermal Properties of Green Parts for Fused Deposition of Ceramics (FDC)', *Adv. Eng. Mater.*, 2001, **3**(6), 418–423, doi: 10.1002/1527-2648(200106)3:6<418::AID-ADEM418>3.0.CO;2-Q.
- [9] M. K. Agarwala, R. van Weeren, A. Bandyopadhyay, A. Safari, S. C. Danforth, and W. R. Priedeman: 'Filament Feed Materials for Fused Deposition Processing of Ceramics and Metals'. Solid Freeform Fabrication Symposium, Austin, Texas, United States of America. University of Texas.
- [10] J. Gonzalez-Gutierrez, D. Godec, C. Kukla, T. Schlauf, C. Burkhardt, and C. Holzer: 'Shaping, Debinding and Sintering of Steel Components via Fused Filament Fabrication'. 16th International Scientific Conference on Production Engineering, Zadar, Croatia, 8 -10 June. Croatian Association of Production Engineering, 99–104.
- [11] C. Kukla, J. Gonzalez-Gutierrez, S. Cano, S. Hampel, C. Burkhardt, T. Moritz, and C. Holzer: 'Fused Filament Fabrication (FFF) of PIM Feedstocks'. VI Congreso Nacional de Pulvimetalurgia y I Congreso Iberoamericano de Pulvimetalurgia, Ciudad Real, Castilla La Mancha, Spain. Comité Español de Pulvimetalurgia, 1–6.
- [12] J. Gonzalez-Gutierrez, I. Duretek, C. Holzer, F. Arbeiter, and C. Kukla: 'Filler Content and Properties of Highly Filled Filaments for Fused Filament Fabrication of Magnets'. ANTEC, Anaheim, CA, USA, May 8-10. Society of Plastics Engineers, 1–4.
- [13] E. J. Westcot, C. Binet Andrandall, and R. M. German: 'In situ dimensional change, mass loss and mechanisms for solvent debinding of powder injection moulded components', *Powder Metallurgy*, 2003, **46**(1), 61–67, doi: 10.1179/003258903225010442.

- [14] J. M. Contreras, A. Jiménez-Morales, and J. M. Torralba: 'Fabrication of bronze components by metal injection moulding using powders with different particle characteristics', *Journal of Materials Processing Technology*, 2009, **209**(15-16), 5618–5625, doi: 10.1016/j.jmatprotec.2009.05.021.
- [15] B. C. Mutsuddy and R. G. Ford: 'Ceramic injection moulding'; 1995, London, Chapman & Hall.
- [16] K. S. Hwang, H. K. Lin, and S. C. Lee: 'Thermal, Solvent, and Vacuum Debinding Mechanisms of PIM Compacts', *Materials and Manufacturing Processes*, 1997, **12**(4), 593–608, doi: 10.1080/10426919708935169.
- [17] W. Liu, Z. P. Xie, X. F. Yang, Y. Wu, C. Jia, T. Bo, and L. Wang: 'Surface Modification Mechanism of Stearic Acid to Zirconia Powders Induced by Ball Milling for Water-Based Injection Molding', *Journal of the American Ceramic Society*, 2011, **94**(5), 1327–1330, doi: 10.1111/j.1551-2916.2011.04475.x.
- [18] J. A. Brydson: 'Plastics materials', 7th edn; 1999, Boston, Butterworth-Heinemann.
- [19] Y. L. Fan, K. S. Hwang, and S. C. Su: 'Improvement of the Dimensional Stability of Powder Injection Molded Compacts by Adding Swelling Inhibitor into the Debinding Solvent', *Metall and Mat Trans A*, 2008, **39**(2), 395–401, doi: 10.1007/s11661-007-9351-y.
- [20] S. T. Lin and R. M. German: 'Extraction Debinding of Injection Molded Parts by Condensed Solvent', *International Journal of Powder Metallurgy*, 1989, **21**(5), 19–24.
- [21] H.-K. Lin and K. S. Hwang: 'In situ dimensional changes of powder injection-molded compacts during solvent debinding', *Acta Materialia*, 1998, **46**(12), 4303–4309, doi: 10.1016/S1359-6454(98)00093-7.
- [22] D.-S. Tsai and W.-W. Chen: 'Solvent debinding kinetics of alumina green bodies by powder injection molding', *Ceramics International*, 1995, **21**(4), 257–264, doi: 10.1016/0272-8842(95)99791-9.
- [23] S. C. Hu and K. S. Hwang: 'Length change and deformation of powder injection-molded compacts during solvent debinding', *Metall and Mat Trans A*, 2000, **31**(5), 1473–1478, doi: 10.1007/s11661-000-0265-1.
- [24] M. S. Park, J. K. Kim, S. Ahn, and H. J. Sung: 'Water-soluble binder of cellulose acetate butyrate/poly(ethylene glycol) blend for powder injection molding', *JOURNAL OF MATERIALS SCIENCE*, 2001, **36**, 5531–5536.
- [25] M. D. Hayat, G. Wen, M. F. Zulkifli, and P. Cao: 'Effect of PEG molecular weight on rheological properties of Ti-MIM feedstocks and water debinding behaviour', *Powder Technology*, 2015, **270**, 296–301, doi: 10.1016/j.powtec.2014.10.035.
- [26] S. T. Lin and R. M. German: 'Interaction between binder and powder in injection moulding of alumina', *JOURNAL OF MATERIALS SCIENCE*, 1994, **29**(19), 5207–5212, doi: 10.1007/BF01151118

## 5 Development and study of the FFF process

### 5.1 State of the art

The methodology employed for the preparation of the feedstocks has a strong influence on their homogeneity and the dispersion of the powder, and thus on the properties of the feedstocks and filaments. Powders with a small size ( $<1\ \mu\text{m}$ ) have a high trend to agglomerate [153], and often must be treated prior to compounding. The treatment consists of the breakage of the agglomerates with ball milling in a solution containing a surfactant to coat the powder and prevent re-agglomeration [144, 208, 225]. An additional step of sieving and mixing of the powder results in further removal of the agglomerates [178]. The quantity of agglomerates in the feedstock also depends on the shear during compounding. Fan et al. reported a higher dispersion of the powder in an alumina FFF feedstock produced in a kneader and a twin-roller as compared to the feedstock produced in a single kneading step [67]. The increase of the filament properties when compounding in a co-rotating twin-screw extruder has been observed for a zirconia feedstock in preliminary experiments to this dissertation [1].

As was stated in section 1.3.1.2, the filaments can be produced either in a round die capillary rheometer or in a single or twin screw extruder [4, 125, 193, 213]. The capillary rheometer enables the production of filaments with small quantities of material. Nevertheless, a perfect filling of the cylinder is necessary to avoid the presence of air voids in the melt, whereas with the extruder a continuous melt with no voids is easily obtained. In order to eliminate the agglomerates and debris in the feedstock and to improve the homogeneity of the melt, elements such as a mixing section, a screen and a breaker plate can be used in the extruder [178]. A modified co-extrusion process in which the feedstock filament is coated by one of the binder components has been developed by BASF SE in the last years [185]. The coating of the filament results in an improvement of the stability and mechanical properties of the filament and reduces the requirements on the feedstock.

Once the feedstock filament is spooled, it is shaped in a conventional FFF machine. Due to the high content of particles, the feedstocks have a higher thermal conductivity and viscosity than the conventional thermoplastics [192]. Thus, there is a high trend to buckling between the rollers and the liquefier [213], which can be solved by using a low volumetric feed rate [9]. However, permanent solutions such as the cooling of the solid filament between the rollers to increase the stiffness or the re-design of the nozzle to reduce the extrusion pressure [45] are preferred. The increase of the contact area between the rollers and the filament by, for example, the use of a dual belt feeding system [1], increases the force transmitted into the filament and reduces the possibility of slippage, thus helping to overcome the flow resistance of the material.

The high viscosity of the feedstocks also results in defects such as voids between adjacent strands and in sub-perimeter voids between the inner strands and those in the perimeter [1, 30, 45, 51, 239]. The causes of these defects have been studied in detail during and after the shaping by FFF [3, 45, 71, 114, 127], and can be effectively reduced by a slight overlapping between the extruded strands [3], the over-extrusion of feedstock [80] and by

the alteration of the toolpath [3]. The optimization of the FFF processing parameters is another method to reduce the defects during shaping. The increase of the FFF nozzle temperature results in a reduction of the feedstock viscosity and better bonding between layers [80, 205]. However, the excessive temperature can hinder the deposition of the freshly deposited strands and lead to failure of the process [205]. S. Wu et al. [226] studied the warm isostatic pressing of green parts as another method to reduce FFF defects. Pressing at temperatures above 70 °C resulted in a reduction of the defects, but with no clear improvement of the final sintered parts mechanical properties [226].

A detailed study of the accuracy of the FFF for green 17-4PH stainless steel parts was conducted by G. Wu et al. [225]. The deviation of the green parts from the CAD design was investigated for 3 different geometries, each one produced at different times. An average accuracy of 0.969 % was achieved in the plane parallel to the printing platform (i.e. in the X and Y directions), whereas the accuracy in the Z direction (perpendicular to the building plane and the layers) was 1.556 %, attributed partly to the removal of the support [225]. These authors also suggested that the modification by e.g. machining, of the green parts as a method to improve the surface finish of the final sintered components. Such modification has been conducted recently by Burkhardt et al. [30] for 316L stainless steel parts. Hand-grinding, sandblasting and polishing with a low power laser were the methods evaluated. The melting of the feedstock with the low power laser proved to be the best solution, as it resulted in the redistribution of the material and the reduction of the roughness and defects [30]. Using a nozzle with a small diameter is another method to improve the surface of the FFF parts. By the use of a binder system with low viscosity, Nötzel et al. [156] used nozzle diameters down to 0.15 mm for the production of small ceramic components.

The POM-based feedstock patented by BASF SE [154] for the FFF of stainless steel is so far the only system using a catalytic+thermal debinding, the first step being conducted in a nitric or oxalic acid atmosphere. This method is not discussed here. In section 4.1, the state of the art of solvent debinding for powder-binder based techniques is presented. Therefore, only the thermal debinding process is discussed here.

Thermal debinding is the most common debinding method for FFF. To conduct a progressive removal of the binders and to avoid internal trapped decomposition or evaporation gases, a progressive and long thermal cycle is required in thermal debinding [13]. The embedding of the components in a porous structure such as alumina [6, 49] or a carbon-based paste [55, 224] can be alternatively used. In this process, also known as wick debinding, the molten polymers are partly removed by capillary forces from outside of the part, thus increasing the debinding rate.

The defects generated during shaping influence the debinding behaviour of the FFF parts. The porosity in the green parts results in a faster debinding than for fully dense components produced by the extrusion of profiles in a single screw extruder [11]. Pistor [172] measured an anisotropic thermal expansion of two different feedstocks as a consequence of internal voids in the parts. Furthermore, internal stresses are produced in FFF by the shrinking of the binders when cooling down and by their viscoelastic behaviour [112, 177]. Both the anisotropic thermal expansion and the release of internal stresses result in an anisotropic shrinkage during debinding and thus in warpage of the parts. These phenomena are strongly

related to the build orientation in FFF. For instance, orienting all the strands in the parallel or the perpendicular direction of the main part direction leads to anisotropic shrinkage in the X-Y directions, and thus warpage [112, 177]. However, the X-Y shrinkage is isotropic, and the warpage disappears when the strands angle alternate from  $+45^\circ$  to  $-45^\circ$  in each successive layer [112, 177].

The largest shrinkage of the process occurs in the sintering phase due to the reduction of the porosity and the densification of the components. Due to the generation of the shape in a layer by layer manner, the sintering shrinkage is always anisotropic. The parts shrink in the Z direction between 18 to 23 %, whereas in the X-Y plane, the shrinkage lies typically between 13 to 18 % [81, 112, 177]. Fortunately, this difference can be predicted and included in the design, resulting in parts with the desired geometries.

Due to the sintering approach, the material inside the extruded strands shows isotropic properties [81, 112]. However, the defects generated during the shaping FFF results in anisotropic properties in the parts. The orientation of the roads inside the layers results in different porosity and thus, different mechanical properties, as observed by Damon et al. [51]. The orientation of the parts with respect to the building platform has even a larger effect. Like in other additive manufacturing techniques, the surface defects in between layers act as notches, reducing the properties of the parts if the loads are applied perpendicular to the layer [73]. Weak bonding between layers caused by powder-binder separation promotes this anisotropy, as recently reported by Kurose et al. for stainless steel components [126]. If the processing parameters are optimized to obtain a good bonding between the layers, and the surface defects are removed by polishing, parts with isotropic properties can be obtained as shown by Iyer et al. [112] for silicon nitride bars. Moreover, such FFF parts can even have the same properties as parts produced by conventional processes as isostatic pressing [112].

## 5.2 Introduction to publication F

The last investigations conducted in the frame of this PhD thesis focused on the shaping by FFF. The proposed hypothesis was:

- 5. The defects caused during the shaping step in the FFF of ceramics and their effect on the properties of the final parts could be reduced by the proper adjustment of the parameters during shaping.***

One of the main types of defects generated in the shaping by FFF are the gaps between the extruded strands of material, known as roads. These gaps are an intrinsic defect of FFF and other MEX processes, and different studies have been conducted to reduce them [3, 45, 71, 80, 114, 127, 205]. For polymeric FFF components, the pattern followed by the extrusion head in the shaping of each layer is known to have a strong influence in the size and orientation of the gaps, and thus on the properties of the components. For metallic FFF components, the first studies evaluating this matter have been recently reported [51, 126]. However, no systematic investigation on the effect of the extrusion pattern on the final properties has been conducted for ceramic FFF components. Therefore, the objective of the investigation in publication F was to determine the influence of the extruded roads orientation on the defects and mechanical properties of zirconia FFF parts. For this purpose, the binder system previously developed in [122] was used.

### 5.3 Publication F

#### ***Influence of the infill orientation on the properties of zirconia parts produced by Fused Filament Fabrication***

Santiago Cano, Tanja Lube, Philipp Huber, Alberto Gallego, Juan Alfonso Naranjo, Cristina Berges, Stephan Schuschnigg, Gemma Herranz, Christian Kukla, Clemens Holzer and Joamin Gonzalez-Gutierrez

**Materials, 13 (2020) 3158**

**Special Issue *Additive Manufacturing Materials and Their Applications*, Special Issue Editor Ludwig Cardon**

doi: 10.3390/ma13143158

Received: 22.06.2020

Accepted: 13.07.2020

Available online: 15.07.2020

#### **ABSTRACT**

The fused filament fabrication (FFF) of ceramics enables the additive manufacturing of components with complex geometries for many applications like tooling or prototyping. Nevertheless, due to the many factors involved in the process, it is difficult to separate the effect of the different parameters on the final properties of the FFF parts, which hinders the expansion of the technology. In this paper, the effect of the fill pattern used during FFF on the defects and the mechanical properties of zirconia components is evaluated. The zirconia-filled filaments were produced from scratch, characterized by different methods and used in the FFF of bending bars with infill orientations of  $0^\circ$ ,  $\pm 45^\circ$  and  $90^\circ$  with respect to the longest dimension of the specimens. Three-point bending tests were conducted on the specimens with the side in contact with the build platform under tensile loads. Next, the defects were identified with cuts in different sections. During the shaping by FFF, pores appeared inside the extruded roads due to binder degradation and or moisture evaporation. The changes in the fill pattern resulted in different types of porosity and defects in the first layer, with the latter leading to earlier fracture of the components. Due to these variations, the specimens with the  $0^\circ$  infill orientation had the lowest porosity and the highest bending strength, followed by the specimens with  $\pm 45^\circ$  infill orientation and finally by those with  $90^\circ$  infill orientation.

*Keywords:* Fused filament fabrication; zirconia; material extrusion; infill orientation; raster orientation; fill pattern; rheology; bending strength; printing defects.

## 1. Introduction

Thanks to the considerable efforts and interest of the industry and research institutions, the ceramic additive manufacturing has experienced considerable development and growth that is forecasted to increase in the next years [1]. Among the many technologies that have been developed in the last years [2–6], the four most relevant process categories are [1] vat photopolymerization (VPP), binder jetting (BJT), material jetting (MJT) and material extrusion (MEX). Each additive manufacturing technique has different advantages and disadvantages in terms of speed, dimensional accuracy, properties of the final components and costs [2–7]. Therefore, the feasibility of using one technique or another depends on the application.

The fused filament fabrication (FFF) of ceramics, also known as Fused Deposition of Ceramics (FDC) [8–10], is a MEX process based on the selective extrusion through a nozzle of feedstock in the shape of filament. The feedstock is a multicomponent polymer system highly filled with powder of the desired ceramic material [9,11–13]. Once the so-called green parts are shaped by FFF, the polymer components are removed in the debinding stage by a catalytic reaction [14], dissolution in a solvent [12,15,16] and/or thermal decomposition [9,17–19]. Finally, the parts are sintered to obtain nearly dense components. Some advantages of this technology include the simplicity and the low cost of the equipment required to shape the parts [20], the possibility to produce lightweight structures with closed geometry [19–21], the possibility to combine this technology with a well-established process like ceramic injection molding [22], and the ability to combine various materials in one part by the use of various nozzles [23–25]. Nevertheless, the use of filaments as feed materials requires tight dimensional tolerances of the filaments to ensure proper feeding [8,26,27], which increases its price [28]. Moreover, the roughness in FFF parts and the minimum dimensions achievable are limited by the diameter of the nozzle [29,30].

In FFF and the other MEX techniques [8,14,31–36], the generation of the shape by the extrusion of material strands, known as roads, can result in defects in the gaps between the strands or weak areas if the bonding between the strands is not sufficient [8]. In early investigations, different solutions were proposed to reduce these defects [8,10,37]. However, defects persist and are the cause of anisotropic mechanical properties even for nearly dense ceramics produced by other MEX techniques [38].

These typical FFF shaping defects depend on different factors such as the properties of the material, the processing parameters, the orientation of the parts with respect to the build platform and the pattern followed in the deposition of the material in each layer [39]. In most cases, one or more perimeters are included in each layer following the contour of the part to improve the surface quality, and a raster fill pattern is used in the inner part of the specimens, known as the infill. The orientation of the roads in the infill of the parts is known to have a substantial effect on the properties of polymeric components produced by FFF [37,39,40], and the first studies for metallic FFF components showing similar effects are also available [14]. In the case of FFF ceramic components, the infill orientation is known to have a small effect on the dimensional variations during debinding [17]. However, no detailed investigation is available for ceramic parts on the effect of the infill orientation on the



appearance of defects during the shaping by FFF and the mechanical properties of the final components.

Hence, the objective of this work was to study the influence of the infill orientation on the properties of zirconia FFF components. The feedstock filament was produced from scratch, characterized by different methods and used in the FFF of specimens with infill orientations of  $0^\circ$ ,  $90^\circ$  and  $\pm 45^\circ$  with respect to the longest dimension of the part. The causes of the defects of the final specimens are related to the feedstock properties and the fill pattern used in the FFF with the different infill orientations. Finally, the influence of the defects on the bending properties of the various specimens is discussed.

## 2. Materials and Methods

### 2.1. Materials

The powder used was the tetragonal zirconia ( $ZrO_2$ )—stabilized with 3 mol % yttria ( $Y_2O_3$ ) TZ-3YS-E (Tosoh Europe B.V., Amsterdam, The Netherlands), supplied as spray-dried granules. According to the supplier, the powder has an average particle size of 90 nm and a specific surface area of  $7 \pm 2 \text{ m}^2 \cdot \text{g}^{-1}$  [41]. The powder was mixed with the multicomponent binder system developed at the Institute of Polymer Processing of the Montanuniversitaet Leoben. This system is composed of a commercial thermoplastic elastomer compound (TPE, Kraiburg TPE GmbH & Co. KG, Waldkraiburg, Germany) and polyolefin grafted with a polar component to improve the adhesion to the powder (gPO, BYK Chemie GmbH, Wesel, Germany). The specific polymer grades employed and the fraction of each binder component are confidential.

### 2.2. Feedstock and filament production

The first step in the production of the ceramic filaments was the compounding of the binder system. Pellets of the two components of the binder system were fed together and mixed in the co-rotating twin-screw compounder ZSK 25 (Werner & Pfleiderer GmbH, Stuttgart, Germany). The rotational speed was 270 rpm, and the compounder had a temperature profile from the feed zone to the nozzle of 120, 185, 190, 195 and 200 °C. The material coming out of the nozzle was cooled down with water at room temperature and pelletized using a water bath + pelletizer (Accrapak Systems Ltd., Burtonwood, United Kingdom). An air blade removed most of the water from the surface of the material entering the pelletizer. In order to remove the remaining water, the binder pellets were dried overnight at 60 °C with a hot, dry air drier (Wittmann Kunststoffgeräte GmbH, Vienna, Austria).

The binder system was compounded with the zirconia powder to obtain a feedstock with 47 vol % of powder, which is equivalent to 85.3 wt %. The feedstock was produced in the co-rotating twin-screw compounder Leistritz ZSE 18 HP-48D (Leistritz Extrusionstechnik GmbH, Nuremberg, Germany), equipped with a high-shear screw configuration to ensure the homogeneous dispersion of the ceramic particles in the polymer. The screw speed was set to 600 rpm, and the total mass output (powder + binder) was set to  $6 \text{ kg} \cdot \text{h}^{-1}$ . The binder was introduced in the first zone of the compounder, and the powder was added in the fourth zone using a side feeder consisting of co-rotating screws rotating at 250 rpm. The

temperature of the first zone was set to 25 °C and progressively increased from the second zone to the nozzle with the profile: 180, 200, 205, 205, 210, 210, 210, 210, 210, 210, 220 and 220 °C. Once compounded, the molten feedstock coming out of the nozzle was cooled down on an air-cooled metal conveyor belt and pelletized (Reduction Engineering Scheer, Kent, OH, USA).

The feedstock pellets were then used in the production of filaments in the single screw extruder FT-E20T-MP-IS (Dr Collin GmbH, Ebersberg, Germany) equipped with a die of 1.75 mm diameter. The extrusion temperatures from the feed zone to the nozzle were 230, 235, 240 and 245 °C and the screw rotation speed was set to 19 rpm. A polytetrafluoroethylene (PTFE) conveyor belt collected the extruded filament, which cooled down by natural convection. A self-developed haul-off and spooling unit was used to spool the filaments, whose diameter was measured with the laser measuring device, Diagnostic Laser 2000 (SIKORA AG, Bremen, Germany).

### 2.3. Feedstock evaluation

The morphology of the cryofractured filaments was studied by scanning electron microscopy (SEM, Tescan Vega II, Tescan Brno, s.r.o., Czech Republic). The analyses were performed on gold-sputtered (100 s at 20 mA) specimens at 5 kV using secondary electrons.

Tensile properties of the filaments were measured on 100 mm long straight specimens using the universal testing machine Zwick Z001 (Zwick GmbH & Co.KG, Ulm, Germany) with a 1 kN load cell and pneumatic grips. An initial gauge length of 50 mm was set for all the measurements. The tests, five repetitions each, were performed at standardized conditions (23 °C and 50% relative humidity), at a speed of 10 mm·min<sup>-1</sup> until rupture.

The rheological behavior of the feedstock was characterized using regranulated filaments. The binder obtained in the first compounding step was also evaluated for comparative purposes. Capillary rheology measurements of both materials were conducted in the high-pressure capillary rheometer Rheograph 2002 (Göttfert Werkstoff-Prüfmaschinen GmbH, Buchen, Germany). The tests were conducted at a temperature of 255 °C and apparent shear rates from 75 to 750 s<sup>-1</sup>. Three round dies with a diameter of 1 mm and lengths of 10, 20 and 30 mm were employed. For the binder system, three tests were carried out with each nozzle, whereas five measurements per die were conducted for the feedstock due to the high variations in the recorded pressure. The true shear rate and viscosity values were calculated with the Bagley [42] and Weissenberg–Rabinowitsch [43,44] corrections, respectively.

Thermogravimetric analysis (TGA) of the binder and the feedstock filament were conducted in the TGA/DSC1 (Mettler-Toledo GmbH, Greifensee, Switzerland) under an oxygen atmosphere. The tests were conducted from 25 °C to 600 °C with a heating rate of 10 K·min<sup>-1</sup>. Alumina crucibles were used, and a total of 5 measurements per material were conducted.

## 2.4. Sample production

Prismatic specimens with a length of 40.55 mm, a width of 3.93 mm and a thickness of 3.6 mm were produced using FFF. Figure 1 shows the fill pattern in one layer for each of the infill orientations. This fill pattern is the same in all the layers of the specimens with the 0° and 90° infill orientations. In contrast, in the ±45° infill orientation, the roads of the infill are perpendicular to the roads of the previous layer. Specimen dimensions were set considering a homogeneous shrinkage of 20% and adjusting the length and width so that a whole number of roads were extruded without gaps in the 90° and 0° infill orientations, respectively. The software Simplify3D version 4.1.2 (Simplify3D, Blue Ash, OH, USA) was used to slice the parts and generate the G-Code. In File S1, File S2 and File S3 of the supplementary information the G-Codes for the 0°, ±45° and 90° orientations can be found. The parts were produced using the Duplicator i3 v2 (Wanhao, Jinhua, Zhejiang, China) FFF machine. A brass nozzle with TwinClad® XT coating with a diameter of 0.6 mm and a PTFE tube insert was used. The set layer thickness was 0.15 mm for all the layers, and the printing speed was 5 mm·s<sup>-1</sup> for the first layer and 12.5 mm·s<sup>-1</sup> for the rest of the layers. Independently of the infill orientation, one perimeter was printed with an infill-perimeter overlap of 50% and an extrusion multiplier of 85 %. The build platform was a glass mirror coated with hair spray for better adhesion. The extruder and build platform temperatures were set to 255 °C and 100 °C, respectively. Before starting the specimen production, the build platform and the extruder were preheated for 30 min; the distance of the die to the build platform was calibrated in the printing area. Then, the hair spray coating was applied, and the printing started. The parts were printed in build cycles of 5 specimens per print, with a total of 4 build cycles for the 0° and ±45° infill orientations and 5 build cycles for the 90° infill orientation.



Figure 1. Fill pattern of perimeters (blue) and infills (orange) of one layer for specimens of each of the infill orientations, from top to bottom: 0°, ±45° and 90°.

A two-step debinding process was carried out. First, most of the TPE was dissolved in cyclohexane. Solvent debinding in cyclohexane was performed in the digital thermostatic bath (Ovan B105-DE, Barcelona, Spain). The parts were immersed in cyclohexane at 60 °C for 24 h and 12 mL of fresh solvent per gram of feedstock were used. After 24 h in cyclohexane, the specimens were left to dry in the LAN Technics stove (Labolan, Esparza, Spain) at 50 °C for 24 h. Subsequently, the thermal debinding was conducted in the Hobersal furnace 12PR450/SCH PAD P (Hobersal, Barcelona, Spain) in an air atmosphere. The thermal debinding cycle employed was: heating from room temperature to 175 °C at 150 K·h<sup>-1</sup>; heating to 225 °C at 25 K·h<sup>-1</sup>; heating to 325 °C at 10 K·h<sup>-1</sup>; heating to 440 °C at 5 K·h<sup>-1</sup>, and cooling down of the furnace to room temperature by natural convection. Finally, the parts were sintered in the tubular Hobersal furnace ST 186030 (Hobersal, Barcelona, Spain) under air. The following thermal cycle was used for sintering: room

temperature to 450 °C at 180 K·h<sup>-1</sup>, hold at 450 °C for 1 h; heating to 600 °C at 180 K·h<sup>-1</sup>, hold at 600 °C for 1 h; heating to 1365 °C at 300 K·h<sup>-1</sup>, hold at 1365 °C for 3 h, and cooling down of the furnace by natural convection. During debinding and sintering steps, specimens were placed upside-down so that the face in contact with the build platform during FFF was the air side during sintering, and no further defects were introduced.

### 2.5.Characterization of specimens

After sintering the specimens had dimensions of approximately  $T = 3$  mm,  $W = 2.85$  mm and  $L = 30.75$  mm. There was no significant difference between the sizes of the specimens produced with the different infill orientations. In order to determine the relative density in the green printed specimens, the density of the pelletized feedstock filaments was measured with the helium pycnometer Micrometric Accupyc 1330 (Micromeritics Instrument Corporation, Norcross, GA, USA). For each infill orientation, the five specimens produced in the first build cycle were used to determine the apparent density after printing and after sintering through the simple Archimedes' method.

The face of the specimens in contact with the build platform, corresponding to the first extruded layer, was the side of the specimens evaluated under tensile stress in the bending tests. All the specimens were chamfered to eliminate the influence of edge defects in the perimeter [45]. The two edges of the first layer of the specimens were machined with chamfers of approximately  $0.3 \pm 0.075$  mm.

Three-point bending (3PB) tests were performed following the standard DIN EN 843-1:2008-08 [45]. The support distance was 20 mm; the support and loading rollers had a diameter of 2.5 mm. After applying a preload of 10 N, the tests were conducted on a Zwick Z010 testing machine (Zwick GmbH & Co.KG, Ulm, Germany) at a cross-head speed of 1 mm·min<sup>-1</sup> at 24 °C and approximately 56% relative humidity. The failure occurred within 6 s to 12 s. Nineteen, 22 and 20 specimens were tested for infill orientation of 0°, 90° and ±45°, respectively. The fracture stresses calculated from fracture loads and specimen dimensions were not corrected for the chamfers, leading to an underestimation of the strength values by approximately 4%. For each condition, the obtained fracture strength results were described using a Weibull distribution [46]. The parameters  $\sigma_0$  (characteristic strength) and  $m$  (Weibull modulus) of the distributions were obtained using the maximum likelihood method. No unbiasing correction was applied to the Weibull moduli obtained by this procedure.

The distribution of porosity was measured on polished sections at various locations and orientations with respect to the specimen's long-axis. These samples were prepared from broken bent bars by polishing to a 1 μm diamond suspension finish using a semi-automated Struers RotoForce-4 and RotoPol-25 system (Struers Aps, Ballerup, Denmark). Composite micrographs consisting of six individual images each were taken at each location and orientation using an Olympus BX50 light microscope (Olympus Corporation, Tokyo, Japan) and the image alignment routine implemented in the Olympus Stream Desktop 2.2 image analysis software (Olympus Soft Imaging Solutions GmbH, Münster, Germany)

Polished sections were thermally etched in an air atmosphere for 30 min at 1400 °C to reveal the microstructure of the material. In ceramics, the strength of an individual specimen is related to the size of the most critical defect that is present. The scatter of strength is

related to the size distribution of defects in the entirety of all specimens [47]. Knowledge of the types of failure causing defects that can be gained from fractography [29] can be used to understand the observed trend of strength with infill orientation. Fracture surfaces and polished sections were investigated after gold sputtering using an Olympus SZH10 stereomicroscope (Olympus Corporation, Tokyo, Japan) and a JEOL NeoScope JCM 6000Plus scanning electron microscope (Nikon Corporation, Konan, Japan).

### 3. Results

#### 3.1. Properties of the feedstock

Figure 2 shows the filament diameter over the length of the spool employed for the production of the specimens. Filament dimensions were monitored during production, and extrusion parameters were adjusted to obtain a filament with an average diameter of 1.75 mm and in the range of 1.7 to 1.8 mm. Nevertheless, uncontrolled variations of the pressure in the extruder resulted in a sudden increase or decrease of the filament diameter.

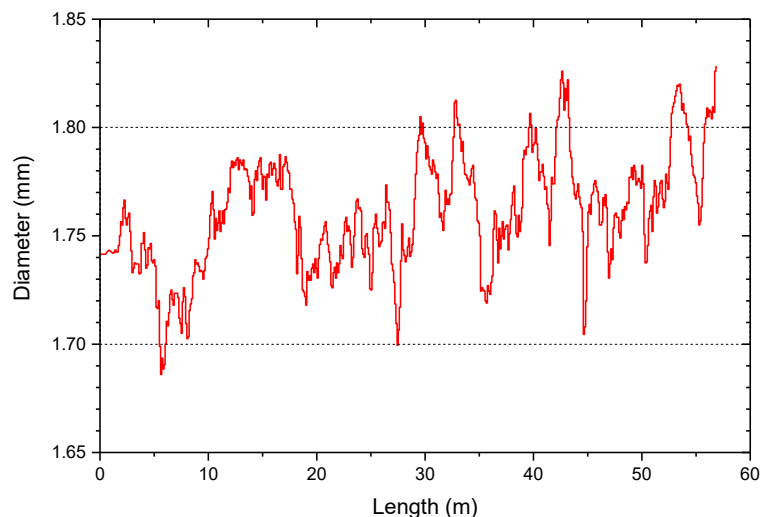


Figure 2. Diameter of the spool employed in the production of the FFF specimens.

Figure 3 shows the cryofracture section of the filaments produced with the feedstock. As can be observed, the powder and binder are homogeneously distributed in a microstructure without large pores. A homogeneous and dense filament is crucial for the successful production of dense FFF components. In our experience, filaments with high porosity or an inhomogeneous microstructure have poor mechanical properties compared to dense and homogeneous filaments. Reduced mechanical properties could lead to the failure of the filament production and spooling, and even complicate the shaping by FFF [9,12,48,49]. The mechanical properties of the filaments were measured by means of tensile tests. The strength and flexibility of the filaments were quantified using the yield stress and the strain at yield, which had values of  $18.8 \pm 0.8$  MPa and  $4 \pm 0.1\%$ , respectively. The filament stiffness was quantified with the secant modulus between 0.1 and 0.3% of strain, obtaining a value of  $1221 \pm 84$  MPa. The properties of another set of filaments produced with a binder developed in our previous study [12] and the same powder fraction and methods described in Section 3.2 were measured as a reference. In that case, the stress and strain at yield are  $19.5 \pm 0.5$  MPa and  $2.9 \pm 0.2\%$ , respectively, and the secant modulus is  $1739 \pm 63$  MPa.

Despite its lower stiffness, the higher flexibility of the filament employed in this study resulted in an easier spooling, handling and FFF processing.

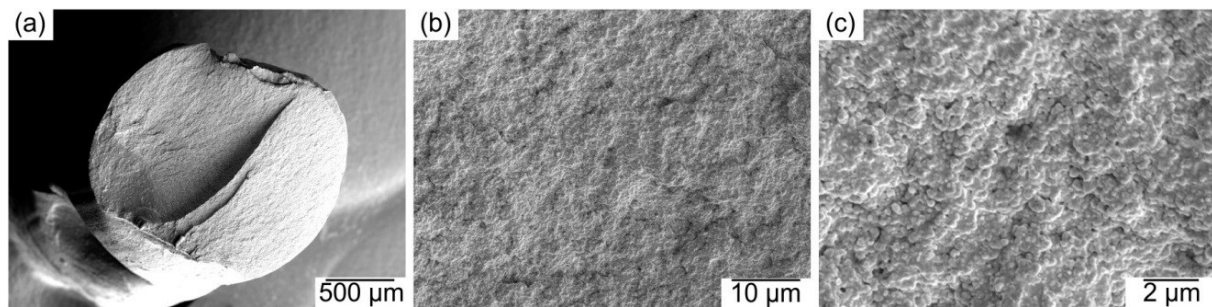


Figure 3. Morphology of the cryofractured feedstock filament at: (a) 100 times magnification; (b) 5000 times magnification and (c) 20000 times magnification.

The flow behavior of the feedstock is another crucial factor for a successful FFF process. The rheological measurements provide further information about the powder–binder interaction and the stability of the flow. A section of the filaments was regranulated and used in the rheological measurements with a high-pressure capillary rheometer to determine its rheological properties. Measurements were also conducted on the binder to determine the influence of the powder addition and further processing. Figure 4a shows representative curves of the pressure at the entrance of the three used dies for the feedstock and the binder.

As can be observed, the pressure increases and reaches a stable value for the binder as the piston speed is increased over time. However, the feedstock showed considerable variations at higher speeds of the piston, or what is the same, as the apparent shear rate increased. These large oscillations of pressure appeared at lower apparent shear rates as the length of the die increased. For the die with a length of 1 mm, the pressure could be measured up to an apparent shear rate of  $500 \text{ s}^{-1}$ , whereas only  $350 \text{ s}^{-1}$  could be reached for the 20 mm die, and  $275 \text{ s}^{-1}$  for the 30 mm die. At those apparent shear rates, the apparent shear stress was 0.25 MPa, 0.25 MPa and 0.24 MPa for die-lengths of 10, 20 and 30 mm, respectively. During the oscillations of pressure, the material came out of the nozzle in a discontinuous periodic manner, with no material coming out of the nozzle for a short time followed by a sudden burst of material. For the binder, the maximum programmed apparent shear rate of  $750 \text{ s}^{-1}$  could be reached for all the dies employed, and the material could be extruded continuously. Due to the pressure variability, the viscosity of the feedstock could only be measured up to intermediate values, as can be observed in Figure 4b. Independently of the nozzle employed, during the measurements bubbles appeared in the extruded feedstock a few millimeters after it left the nozzle. In Figure 4c, an example of the extrudate with such bubbles is shown. Such a phenomenon could not be observed for the binder.

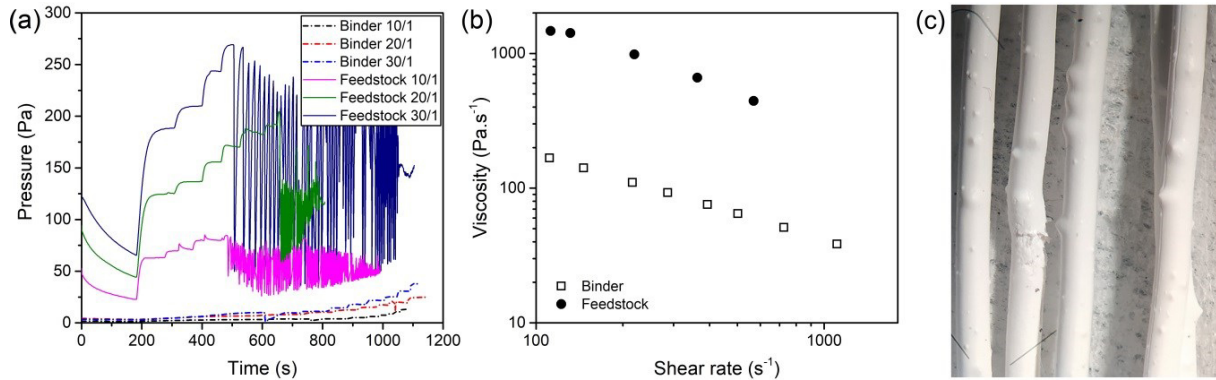


Figure 4. (a) Representative pressure curves measured for the binder and feedstock with the three nozzle geometries; (b) Shear viscosity as a function of the shear rate for the binder and feedstock after applying the Bagley and Weissenberg-Rabinowitsch corrections; (c) Feedstock rods collected during the rheological measurements.

The thermo-oxidation behavior of the binder and the granulated feedstock filament was measured by TGA, obtaining the results shown in Figure 5. In both cases, two decomposition ramps can be observed, a ramp at low temperatures with a pronounced mass loss, and a ramp at higher temperatures with a lower mass loss rate. Each ramp corresponds to the progressive degradation of the polymers in the multicomponent binder system, as has been already observed for zirconia feedstocks for ceramic injection molding [50]. From Figure 5, it can be seen that the slope of all the ramps is more pronounced and the degradation starts at lower temperatures for the feedstock than for the binder.

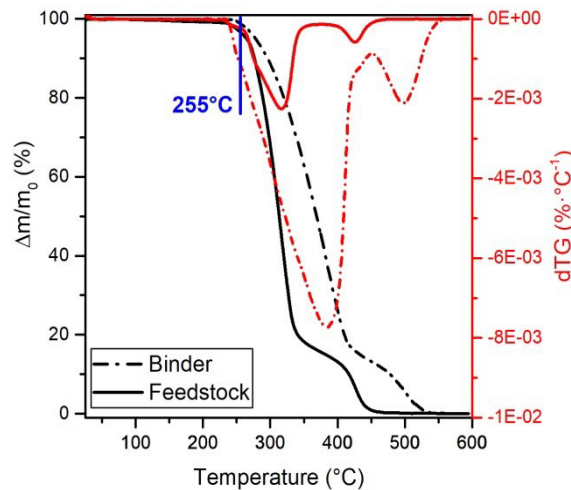


Figure 5. Representative curves of the amount of binder left in samples as temperature increases, and of the derivative of the binder left in the samples at different temperatures for the binder and feedstock. The nozzle temperature (255 °C) used in the FFF shaping is indicated in blue.

### 3.2. Properties of the FFF specimens

Table 1 summarizes the theoretical and actual green mass for all the specimens produced. For the five specimens produced in the control build cycle, the mass, apparent and relative density in the green and sintered state are shown as the “control build cycle” in Table 1. The

theoretical mass was calculated considering a filament with a constant diameter of 1.75 mm, the length indicated in the G-Code of each infill orientation (Files S1–S3 of the Supplementary material) and the density of the feedstock measured in the helium pycnometer ( $3.296 \pm 0.002 \text{ g/cm}^3$ ). The small differences between the theoretical green mass and the actual green mass of the specimens are caused by the variability in the filament diameter (Figure 2), which results in the variability of the mass of the produced specimens. A section of the filament with a diameter higher than 1.75 mm results in overextrusion of material, whereas underextrusion occurs for filament diameters lower than 1.75 mm. Nevertheless, there is no significant difference between the actual green mass of the specimens produced with the different infill orientations.

Due to differences in filament diameter in sections employed to produce the control build cycles, there is overextrusion for the parts from the control build cycle for  $\pm 45^\circ$  and  $0^\circ$  orientations, printed with a filament diameter higher than 1.75 mm, and underextrusion for those of the control build cycle of with  $90^\circ$  orientation, which were produced with a filament diameter smaller than 1.75 mm. The parts for the three control build cycles show the same mass loss of approximately 15 wt % after sintering, which is equivalent to 46.5 vol % of powder in the printed parts, as opposed to 47 vol %. This difference could be caused by the continuous underfeeding of powder during compounding by a small and systematic error in the feeding units in the compounder. The use of a slightly higher feeding rate for the powder could solve it. Still, it would require various iterative cycles that were not possible due to the limited amount of material available.

Since the simple Archimedes' method was used to measure the density of the parts, some water could penetrate the open porosity at the surface of the specimens. Therefore, the density shown in Table 1 is the apparent density, and not the bulk density [7]. The apparent density of the feedstock was also measured, as the helium used in the pycnometer measurements could penetrate the outer pores of the pellets. Nevertheless, since the perimeter was produced with the same procedure independently of the orientation of the infill, a direct comparison of the apparent density can be established. Table 1 shows that the parts produced with  $0^\circ$  infill orientation are denser than those produced with  $\pm 45^\circ$  orientation, and both are denser than those produced with  $90^\circ$  orientation. For the parts produced with  $90^\circ$  orientation, one cause of this difference could be the porosity produced by the underextrusion for this build cycle. Nevertheless, the trend is opposite for the parts produced with  $\pm 45^\circ$  orientation, which were heavier but less dense than the ones with the  $0^\circ$  orientation.

As can be expected, the relative green and sintered density values follow the same trend with the infill as the apparent density. Overall, the relative green density is lower than 100%, and due to the residual porosity caused by incomplete sintering, the relative density after sintering is even lower than after printing. In order to get a better understanding of the type and size of the different pores, and the origin of them, a detailed microscopy evaluation was conducted.

Table 1. Theoretical and actual green mass ( $m_g$ ) for all the specimens produced with the different orientations and for the five parts of a control build cycle for each orientation: green ( $m_g$ ) and sintered mass ( $m_s$ ), mass loss ( $\Delta m$ ), green ( $\rho_g$ ) and sintered ( $\rho_s$ ) apparent



density, and relative green ( $\rho_{rg}$ ) and sintered ( $\rho_{rs}$ ) density. The average and standard deviation values are provided for all the parameters

Infill orientation	Theoretical	Actual		Control build cycle					
	$m_g$ (g)	$m_g$ (g)	$m_g$ (g)	$m_s$ (g)	$\Delta m$ (wt.%)	$^1\rho_g$ (g/cm <sup>3</sup> )	$^1\rho_s$ (g/cm <sup>3</sup> )	$\rho_{rg}$ (%)	$\rho_{rs}$ (%)
0°	1.702	1.706 ±0.029	1.723 ± 0.01	1.464 ± 0.01	15.06 ± 0.07	3.254 ± 0.003	5.943 ± 0.013	98.73 ± 0.08	98.23 ± 0.22
±45°	1.703	1.72 ± 0.041	1.77 ± 0.007	1.487 ± 0.042	15.08 ± 0.03	3.202 ± 0.024	5.878 ± 0.034	97.15 ± 0.71	96.97 ± 0.64
90°	1.694	1.72 ± 0.034	1.642 ± 0.004	1.396 ± 0.003	15 ± 0.06	3.176 ± 0.007	5.797 ± 0.015	96.35 ± 0.21	95.82 ± 0.26

<sup>1</sup>The green apparent density is calculated using the apparent density measured for the feedstock in the helium pycnometer ( $3.296 \pm 0.002$  g/cm<sup>3</sup>), and the sintered density is calculated using the density provided by the powder supplier as reference ( $6.05$  g/cm<sup>3</sup>).

The macroporosity in the sintered and fractured specimens was evaluated for cuts in different directions. In Figure 6, the results of this study are presented. The green and solvent debound specimens showed the same type of defects, as Figure S1 in the supporting information shows. Three types of pores can be observed in Figure 6, each one in a wide variety of sizes: round pores, elongated pores and pores with an irregular shape.

The width and length of pores and their intralayer distribution are shown in the sections xy of Figure 6. These sections were obtained by polishing between 200 and 500  $\mu\text{m}$  of the lower part of the specimens, i.e., the side under tensile loads in the bending tests. In all the cases, the pores shown in these sections follow the fill pattern of the extruder shown in Figure 1. In the outer part of the specimens, the pores follow the perimeter, which is the same for the three infill orientations. In the inner part, the orientation of the pores depends on the infill orientation employed. Pores are aligned in the x-direction for specimens with 0° infill orientation, and in the y-direction for specimens with 90° infill orientation. The pores inside the specimens with the ±45° infill orientation are diagonally aligned to the parts.

The distribution of pores in the different layers can be observed in the sections xz-C, xz-S and xy. These sections show the inhomogeneity in the porosity distribution in all specimens. The most pronounced difference is a reduced porosity in the outer part of the specimens than in the inner part. A low porosity can be seen on the right of the xz-C sections and the sides of the yz sections (Figure 6), and moreover, the sections xz-S have a considerably lower porosity than the xz-C. All these sections correspond to specimen sides, where 50% overlap between perimeter and infill was applied, and thus material overextrusion.

A more subtle difference is the low porosity of the lower part of the specimens compared to the rest, which can be observed in the cuts xz-C, and yz. This area corresponds to the first layers of the specimens, which are closer to the build platform. Before each build cycle, the height of the build platform was adjusted manually relative to the extrusion head. A tight

adjustment was conducted to ensure proper adhesion of the specimens to the platform; this means that the actual height of the first layer was in most of the cases slightly lower than the programmed height of 0.15 mm. In this manner, there is an additional overextrusion of material in the lower part of the specimens that can prevent pores.

The xz and yz sections of Figure 6 show that the infill of the specimens has a different distribution (size and shape) of interlayer porosity depending on the plane orientation of the section with the infill orientation of specimens.

For instance, the sections xz-C are parallel to the infill orientation of the specimens with  $0^\circ$  orientation, which show elongated and thin pores in these sections. For the specimens with  $\pm 45^\circ$  infill orientation, the plane of the section has an alternating orientation of  $+45^\circ$  and  $-45^\circ$  with the infill; in these sections, irregular and large pores are predominant in this case. The infill orientation of  $90^\circ$  is perpendicular to these sections, and small round and irregular pores are predominant.

Since section yz is perpendicular to the infill orientation of  $0^\circ$ , pores inside the parts with this orientation are round and small. The plane of the yz sections is diagonal to the infill orientation of  $\pm 45^\circ$ , and there is an equal amount of irregular and round pores with different sizes. Since the infill orientation of  $90^\circ$  is parallel to the yz section, elongated pores are predominant. However, pores are considerably larger than those of the specimens with a  $0^\circ$  infill orientation in the xz-C sections.

The last phenomenon observed in Figure 6 is the presence of pores inside the extruded roads. These pores are distinguishable as round pores in the right specimen border in the sections xz-C, or in the two side borders of the specimens in the sections yz, which correspond to the perimeter of the specimens. The outer area of the xy sections also corresponds to the perimeter of the specimens, where more pores are distributed. In those areas, some of the pores are round, while some others are elongated and adopt an elliptical shape. For the areas corresponding to the infill of the specimens, it is difficult to determine which of the pores are inside the extruded roads and which are the pores commonly seen in the gaps between roads [8,14].

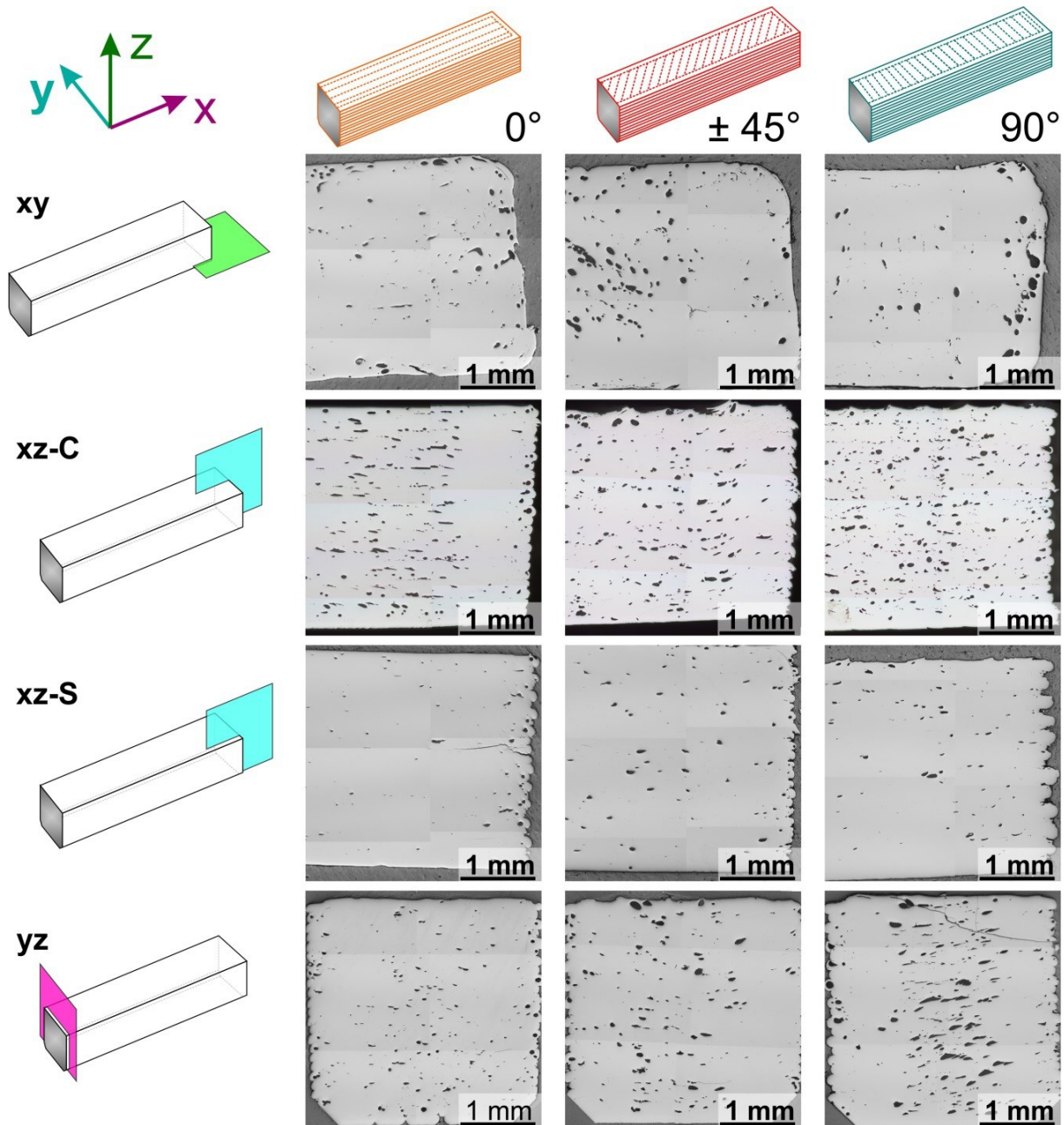


Figure 6. Sections of sintered fractured bars with the three infill patterns. The location and orientation of the imaged plane are indicated in the leftmost column with the directions parallel to the plane used to designate it. The zones studied are the centre (C) or the side (S). The fracture surface is marked with dark grey colour in the schematic representation.

The other potential source of porosity in the specimens is the porosity which could not be removed during sintering. This kind of porosity can be regarded as an intrinsic feature of the material and is also present in similar ceramic components produced by conventional routes [51]. Attempts to remove it by variation of the sintering conditions would lead to oversintering and could cause excessive grain growth that could be detrimental for the mechanical properties [52]. Figure 7 shows the microstructure of a specimen produced with the  $\pm 45^\circ$  infill orientation. Despite some micropores remaining, a homogeneous and dense microstructure can be observed, with small-sized grains (approx. 300 nm to 500 nm).

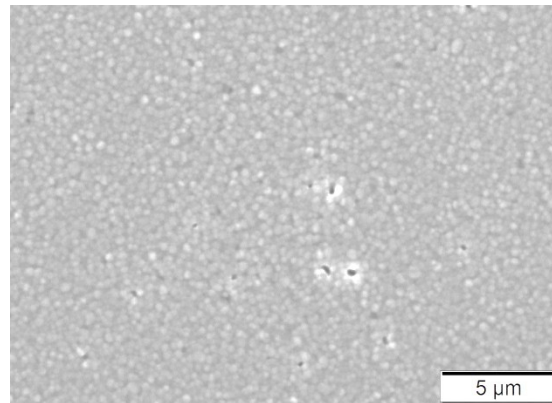


Figure 7. Exemplary microstructure of a sintered specimen.

The infill orientation has a significant effect on the defects in the side of the specimens that were in contact with the build platform, which was the one under tensile loads in the bending tests. Figure 8 shows examples of the defects on this side with the different infill orientations. In the specimens with the  $0^\circ$  infill orientations, thin gaps can be observed between the roads. These gaps become more irregular and broader for the specimens with the  $\pm 45^\circ$  infill orientation, with some large defects in between. For the specimens with the  $90^\circ$  infill orientation, the second type of defects is even more pronounced, and can be easily detected. Moreover, the second type of defects is only found in the inner part, which corresponds to infill roads.

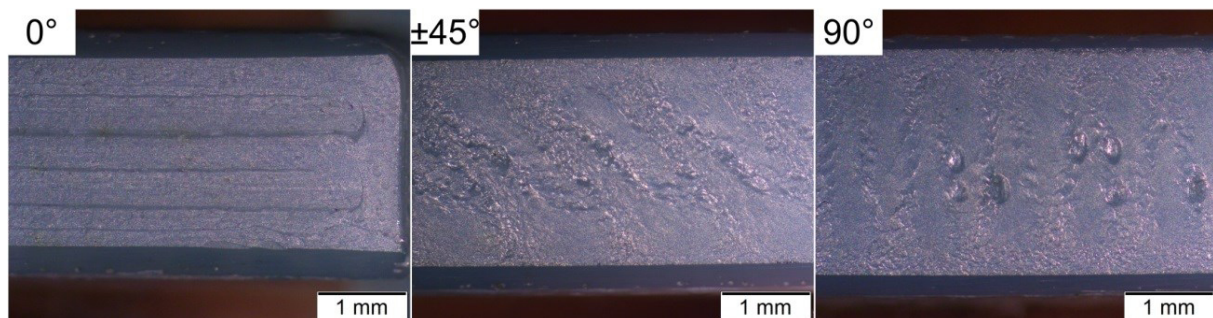


Figure 8. Underside of the sintered specimens produced with the different infill orientations after chamfering.

Figure 9b shows the Weibull plot obtained in the three-point bending tests of the specimens produced with the different infill orientations. Schematics of the bending test configuration are shown in Figure 9a to facilitate the interpretation of the results. Table 2 summarizes the values of the characteristic strength, the average strength and the Weibull modulus. The specimens produced with the  $90^\circ$  infill orientation had a significantly lower characteristic strength than those specimens produced with the other infill orientations. Due to the high variability of the results, no significant difference exists between the characteristic strength of the specimens produced with the  $\pm 45^\circ$  and  $0^\circ$  infill orientations; however, the latter exhibits higher values. When comparing the Weibull moduli of the different specimens, the specimens with the  $0^\circ$  orientation have the highest value, followed by those produced with the  $\pm 45^\circ$  and the specimens with the  $90^\circ$  having the lowest average values. Nevertheless, only the difference between the Weibull modulus of the specimens with  $0^\circ$  orientation and that of the specimens with  $90^\circ$  is statistically significant.

In Table 2, the properties measured in three-point bending tests for 3 mol % yttria-stabilized tetragonal zirconia parts produced by additive manufacturing and conventional methods are shown for comparison. The strength values are higher than MEX-components produced with the same infill orientation [53]. However, the strength values are lower than for VPP and subtractively manufactured components [54]. Moreover, the strength is considerably lower than the typical value of 1200 MPa provided by the supplier [41].

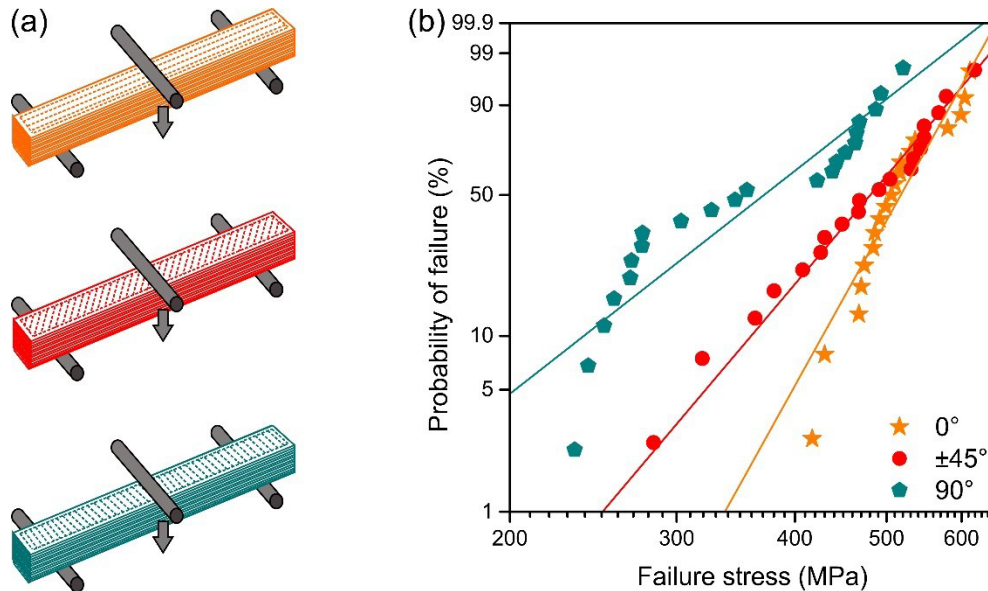


Figure 9. Weibull plot of the specimens produced with the different infill orientations.

Table 2. Weibull modulus ( $m$ ), characteristic bending strength ( $\sigma_0$ ) and average bending strength ( $\sigma$ ) of the specimens produced with the three infill orientations. For comparison, 3 mol% yttria-stabilized tetragonal zirconia parts produced by additive manufacturing material extrusion (MEX), vat photopolymerization (VPP) and subtractive methods are shown. 90% confidence intervals are given in square brackets.

Technology	Infill orientation	$m$ (-) [90% CI]	$\sigma_0$ (MPa) [90% CI]	$\sigma$ (MPa)
FFF (MEX)	0°	9.9 [6.7–12.6]	537 [514–562]	512 ± 55
	±45°	6.5 [4.5–8.3]	508 [477–543]	473 ± 90
	90°	4.3 [3.1–5.5]	404 [368–443]	366 ± 99
3D Gel Printing (MEX) [53]	0°	28 <sup>1</sup>	462 <sup>1</sup>	450 ± 20
Digital Light Processing (VPP) and polishing [54]	-	9.3 [6.7–12.3]	1066 [1031–1101]	1013 ± 126
Subtractive method [54]	-	12 [8.7–15.8]	1206 [1173–1239]	1158 ± 114

<sup>1</sup>Values calculated from the average and standard deviation of the bending strength [55].

Despite a large amount of porosity, the fracture surfaces exhibited fractured mirrors and thus fracture origins could be identified. All specimens failed due to the pores and defects previously described. Figure 10 shows the fracture origin of exemplary specimens with high

and low bending strength. Especially for the specimens with 90° infill orientation, the hackle region which usually shows ridges and grooves radiating away from the failure origin [29] is strongly influenced by the macropores and the layerwise assembly of the specimens. Low strength specimens with 90° infill orientation failed due to defects at the road interfaces which are located on the tensile faces of the specimens (Figure 10). These typical defects are oriented perpendicular to the applied stress and are thus most dangerous. High strength specimens with 90° infill orientation did not show interfacial defects on the tensile sides but failed because of pores located within the volume, see Figure 10. The strong nonlinear trend of the data in the Weibull plot (Figure 9) may also be a hint for the existence of two different defect populations. A similar defect characteristic could be observed for the specimens with ±45° infill orientation. The interfacial defects visible on the tensile sides of the low strength specimens are oriented at an angle to the applied stress (Figure 10). They are therefore less critical than in the case of the 90° infill specimens. For the specimens with 0° infill orientation, interfacial defects which are visible on the tensile sides (see Figure 8 and section yz 0° of Figure 6) are loaded in a longitudinal direction. Failure origins for specimens with 0° infill orientation were pores at some distance from the tensile surface. For several specimens, the size of a critical defect  $a_c$  as calculated from the fracture stress  $\sigma_f$  using the failure criterion from LEFM [56]  $K_{Ic} = \sigma_f Y \sqrt{a_c}$  with a typical fracture toughness of  $K_{Ic} = 4 \text{ MPa}\sqrt{\text{m}}$  for Y-TZP [52] correlates well with the observed defect sizes in Figure 10. A geometry factor,  $Y = 2/\sqrt{\pi}$ , was used for volume defects, and  $Y = 1.12 \sqrt{\pi}$  for surface defects, respectively [56].

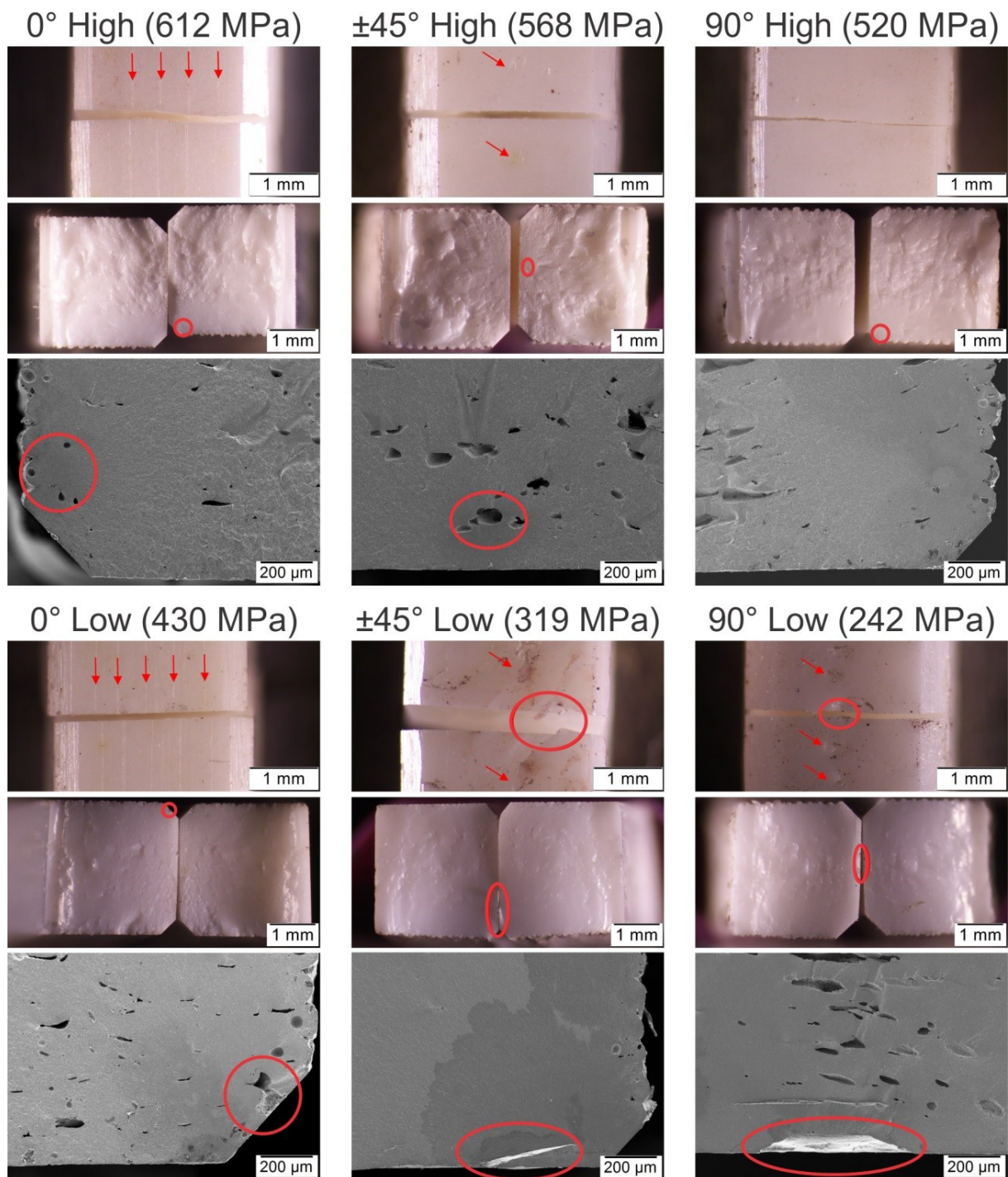


Figure 10. Tensile surfaces and fracture surfaces of specimens with high and low strength and Influence of the defects on the first layer produced during shaping by FFF for the specimens with high and low strength produced with infill orientations of 0°, ±45° and 90°. Periodic defects between the roads produced during FFF are marked by arrows, Locations of the fracture origins are marked with a circles and the defects in the tensile surface are marked with arrows.

## 4. Discussion

Despite the simplicity of the FFF equipment, the processing of ceramics by FFF is a complex process, on which different factors affect the properties and quality of the final ceramic parts. Therefore, all processing steps must be considered to determine the influence of the infill orientation on the properties of final zirconia parts.

The rheological measurements on the binder and the feedstock reveal the notable effect of the zirconia powder in the flow behavior. The expected increase of viscosity after incorporating powder (Figure 4a) is produced by the restricted mobility of the polymeric chains by the solid particles and by the interaction and friction of those particles [57]. The oscillation of the pressure during the rheology of the feedstock shown in Figure 4b has also been observed for unfilled polymers such as polyethylene, highly filled polymers and PIM feedstocks [57–59]. Depending on the nature of the polymeric matrix and filler fraction, different trends have been observed for this oscillation [58]. For multicomponent feedstocks such as the one employed in this study, the pressure oscillations appear only at high concentrations of powder and become more irregular as the powder concentration increases [60,61]. The fact that the oscillations start for all the nozzles at a shear stress of approximately 0.25 MPa could indicate the existence of critical shear stress after which slip of the material in the capillary wall starts [62], leading to the slip-stick effect [59]. Therefore, it can be said that high-shear rates can negatively affect the extrusion process of this material due to flow instabilities. However, it is not expected that the FFF of ceramics reaches those high-shear rates due to the high viscosity of the material, which could lead to problems like buckling or shearing of the filament.

It is also not clear whether the appearance of bubbles of the feedstock coming out of the rheometer (Figure 4c) is related to the pressure oscillations, especially since the bubbles appeared in the whole range of shear rates evaluated, whereas the oscillations started at higher rates. The origin of the bubbles could be related to moisture evaporation at high temperatures [26] or the degradation of binder ingredients at high temperatures catalyzed by moisture, powder, or the combination of both. The polar surface of the zirconia powder and the hydroxyls groups on it [63] could promote the absorption of water [64]. Moreover, water in the feedstock could explain the lower degradation temperatures for the feedstock than for the binder in the TGA (Figure 5) [65]. However, it is surprising that no bubbles appeared in the feedstocks filaments during their production at temperatures up to 245 °C (as shown in Figure 3). Since pelletized feedstock filaments were used in the rheology measurements and the TGA, the additional heating and shearing cycles on the material could contribute to the degradation of the material. At that step of the process, polymers have been melt-mixed to obtain the binder, compounded with the powder to get feedstock, extruded to make filament, and finally extruded during the characterization or the shaping by FFF.

Moreover, the pores inside the extruded roads could be another manifestation of the phenomena described in the previous paragraph. The origin of these pores has been attributed to the existence of previous porosity in the filament [21]. In our case, since the filaments employed in this study have a homogeneous and dense microstructure with no pores (Figure 3), it can be stated that the pores inside the extruded roads appear during the



shaping of the parts by FFF and not in the previous steps of compounding and filament production. Pores inside perimeter roads can be seen as round cavities, which can also be observed in the bulk of specimens, but also as elliptical pores in the perimeters in the xy sections (Figure 6). For the inner region of the specimens, it is not possible to differentiate the pores inside the roads with the gaps between the roads.

The gaps between roads are a direct consequence of the building strategy not only of FFF [8,14,31] but also of other MEX processes such as piston-based [33,34] or screw-based [31,35] systems. These gaps can appear as interroad defects, which are elongated voids in between the extruded roads and parallel to them, or as subperimeter voids, which are produced by the change of direction of the infill when it reaches the perimeter [8,14]. In this study, there is an overlap of 50% between perimeters and infills, which effectively reduces or eliminates the subperimeter voids [8].

In previous studies dealing with the production of metallic and ceramic components, the interroad defects have been detected as long voids running parallel to the roads across the whole section of the parts [14,17]. Such defects cannot be observed in any of the sections evaluated in Figure 6. However, there are small elongated voids observed in the cuts parallel to the road deposition (xz-C for 0° and yz for 90°) and with small size in the cuts of Figure 6 perpendicular to the road deposition (yz for 0° and xz-C for 90°). Nevertheless, some of these voids could be the elliptical pores inside the roads discussed previously. Since the specimens produced with the ±45° infill orientation have roads perpendicular to those of the previous layer, the shape of the interroad defects is different than the shape of these defects for the other orientations, and no direct comparison can be made.

The inconsistency in the filament diameter in this study (Figure 2) could promote the irregularity of the interroad pores in two ways. The direct effect is that a filament section with small or large diameter results in an uncontrolled under- or overextrusion of material [8,26,27]. The second effect is the flow fluctuations by the filament diameter variability, which changes not only the amount of material extruded but also the grip of the rollers on the filament and the force applied on the molten feedstock in the nozzle [8,27,66]. Figure S2 in the supplementary information shows the variation of the mass of the specimens in the different build cycles as a result of the filament diameter; however, no direct correlation between the mass of the specimens and their bending strength could be observed (Figure S2).

Two sources of overextrusion can be found in this study: the programmed overextrusion caused by the perimeter-infill overlap and the uncontrolled overextrusion by the changes in the filament diameter. In principle, the overextrusion of material is an effective way to reduce the porosity in FFF parts [67,68]. Nevertheless, an excessive overextrusion leads to a “flooding” of material between roads and structures such as the one shown in Figure 11a [8,68]. Figure 11b shows the origin of the overextrusion defects, which can eventually result in the apparition of new types of defects, as shown by Costa et al. [68]. The shape and volume of these defects are different depending on the orientation between the roads of consecutive layers, as shown in Figure 11c. With the 0° and 90° infill orientations the roads of the new layer are parallel to those already deposited, resulting in the defects reported by

Costa et al. In the specimens with the  $\pm 45^\circ$  infill orientation, the new roads are perpendicular, which leads to new types of defects.

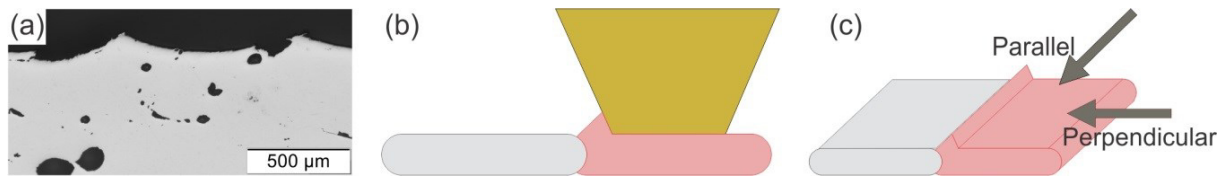


Figure 11. (a) Effect of excessive overextrusion on the top extruded layers; (b) Schematics of the origin of the overextrusion defects by the extrusion of a new road of hot material (in red) over a previously deposited road of cold material (in grey); (c) Schematics of the material deposition on top of a road with overextrusion if the roads of the new layer are parallel or perpendicular to it.

The defects in the lower side of specimens (Figure 8) are directly correlated with the length of the roads for each infill orientation. In Figure 1, it can be observed that long roads are used in the  $0^\circ$  infill orientation, whereas the roads are shorter for the  $\pm 45^\circ$  infill orientation and especially for the  $90^\circ$  infill orientation. Longer roads result in more time for cooling of the material, which in the bulk of the specimens could be detrimental since the bonding between the roads is reduced [8]. However, the situation is different in the first layer of the specimens. If the deposited roads in contact with the build platform are not cold enough, the material could be scrapped away in some areas, resulting in the irregular and large defects observed in the specimens with the  $\pm 45^\circ$  and  $90^\circ$  infill orientations in Figure 8.

In three-point bending tests, all specimens failed due to the pores and defects previously described, which were generated during the FFF of the parts. The FFF-induced defects (Figures 6 and 8) are more prominent and bigger than the intrinsic material defects (Figure 7), which explains the generally low strength compared to traditional and VPP manufactured Y-TZP [41,54,69,70]. In the specimens with the  $90^\circ$  and  $\pm 45^\circ$  infill orientations, different defect types are active. The large defects in the tensile surface (Figure 8) cause the fracture of the low strength specimens, and the origin of the fracture in the high strength specimens are the pores in the core observed in Figure 6. This porosity results in low Weibull moduli and high strength scatter for the specimens with  $\pm 45^\circ$  infill orientation and especially those with  $90^\circ$ . In the specimens with  $0^\circ$  infill orientation, the thin interroad defects on the tensile surface did not cause failure due to the low number of roads used to build the first layer and the favorable orientation of their interfaces concerning the applied stress. In these specimens, only one defect population was responsible for failure: The volume defects (pores) that are equal in size as in other orientations and appear at different locations in the cross-section, in some cases at a rather long distance from the tensile faces of the specimens (Figure 10). As a consequence, it results in higher characteristic strength and a lower scatter of strength for the  $0^\circ$  infill orientation specimens.

## 5. Conclusions

In this study, the influence of the infill orientation on the properties of zirconia parts produced by FFF was evaluated. Bending bars with infill orientations of  $0^\circ$ ,  $\pm 45^\circ$  and  $90^\circ$  were produced, and the properties of ceramic feedstock and sintered parts were measured.

The incorporation of the powder into the organic binder results in significant changes in the rheological properties and thermal degradation behavior. Pressure oscillations appeared during the rheological measurements of the feedstocks at a shear stress of approximately 0.25 MPa, whereas no oscillations were recorded for the binder. Moreover, gases formed during the extrusion process result in pores inside the roads during the shaping by FFF.

FFF shaping causes three defect types: interroad defects, defects due to material under- and overextrusion, and defects caused by the shearing-off by the nozzle of the already deposited material in the first layer. All of these defects are promoted by the variability of the filament diameter, and their shape and orientation are affected by the infill orientation, resulting in different bending strength of the evaluated specimens. The shape of the defects due to excessive overextrusion is different if the roads of the next layer are parallel or perpendicular to the roads of the previous layer. Finally, the shearing-off of the deposited material in the first layer results in defects for the  $\pm 45^\circ$  and  $90^\circ$  orientations.

The strength of the parts was evaluated in the as-sintered state. The bending behavior of the parts is primarily influenced by the quality of the first layer. Interfaces that are oriented normal to the applied stress (as in  $90^\circ$  and to some extent in  $\pm 45^\circ$  infill orientation), bad leveling of the bed, variations of the filament diameter and the shearing-off the deposited material result in high variability of the strength values and low Weibull modulus. The bending strength of parts printed with  $0^\circ$  orientation shows a smaller dependence on these defects than the strength of those parts with  $90^\circ$ . On the other hand, pores inside the specimens are causing failure if the tensile side is free of defects.

Therefore, the loads applied to FFF ceramic parts during their service have to be considered during their production. When possible, the infill roads must be oriented in parallel to the tensile loads. In order to produce dense and strong components by FFF, the defects inside and between the roads must be avoided. The use of filaments with tight dimensional tolerances and the use of controlled overextrusion are known to reduce the interroad defects. In future investigations, the influence of the powder content and the moisture on the degradation of the binder components must be studied to minimize intraroad porosity.

**Author Contributions:** Conceptualization, S.C., T.L., P.H., S.S. and G.H.; methodology, S.C., T.L., P.H., A.G., J.A.N., C.B., S.S. and G.H.; formal analysis, S.C., T.L. and P.H.; investigation, S.C., T.L., P.H., A.G., J.A.N. and C.B.; resources, T.L., G.H. and C.H.; writing—original draft preparation, S.C. and T.L.; writing—review and editing, S.C., T.L., P.H., A.G., J.A.N., C.B., S.S., G.H., C.K., C.H. and J.G.-G.; visualization, S.C. and T.L.; supervision, T.L., S.S., G.H., C.K., C.H. and J.G.-G.; project administration, S.C., T.L., C.B., S.S., G.H. and J.G.-G. ; funding acquisition, C.B., G.H., C.K. and J.G.-G. All authors have read and agreed to the published version of the manuscript.

**Funding:** The research in the Montanuniversitaet Leoben was performed under the projects FlexiFactory3Dp and 3DMultiMat which have received funding from the Austrian Research

Promotion Agency under the program Production of the Future, Grant Agreements No. 860385 and No. 875650. DYPAM group was funded by the FEDER program assigned to the University of Castilla-La Mancha, Grant Agreement No. 2020-GRIN-28850.

**Conflicts of Interest:** The authors declare no conflict of interest. The funders had no role in the design of the study; in the collection, analyses, or interpretation of data; in the writing of the manuscript, or in the decision to publish the results.

### Supplementary Information

Due to the length of the G-Codes employed in publication F, the following files have not been included in this thesis: File S1: G-Code for the specimens with the  $0^\circ$  infill orientation, File S2: G-Code for the specimens with the  $\pm 45^\circ$  infill orientation, File S3: G-Code for the specimens with the  $90^\circ$  infill orientation. However, all these files are available online in the webpage of the journal.

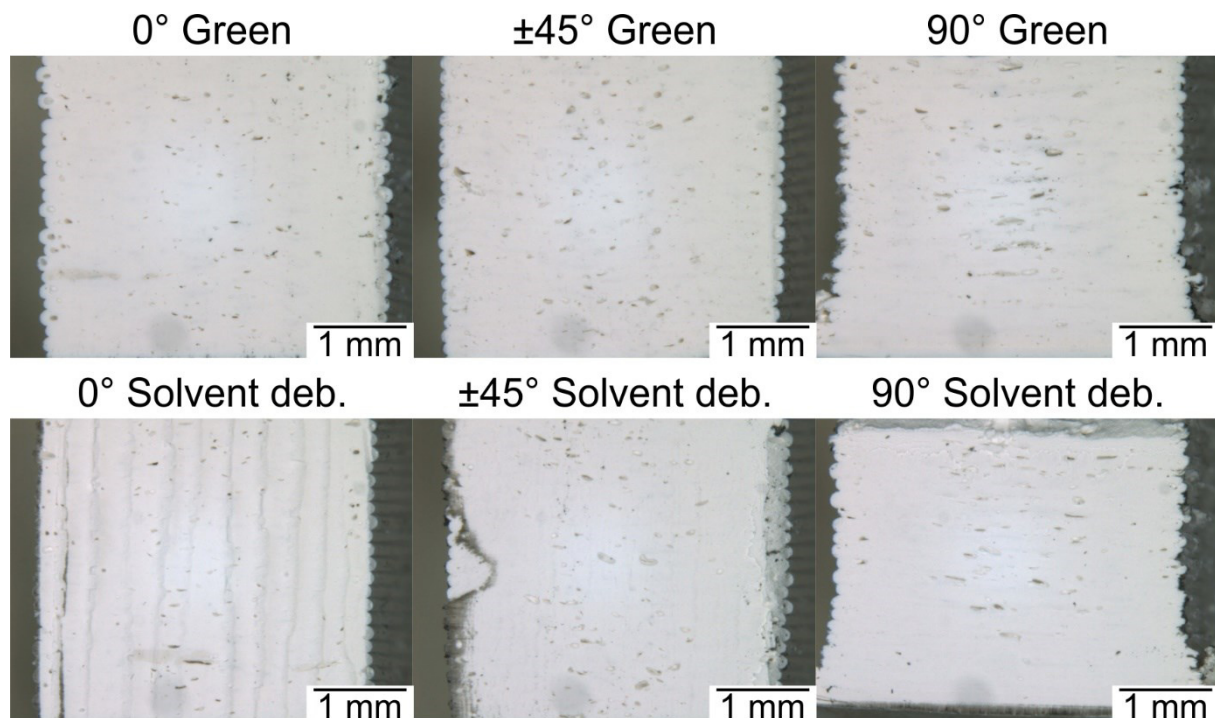


Figure S1: Cross-section of green and solvent debound specimens

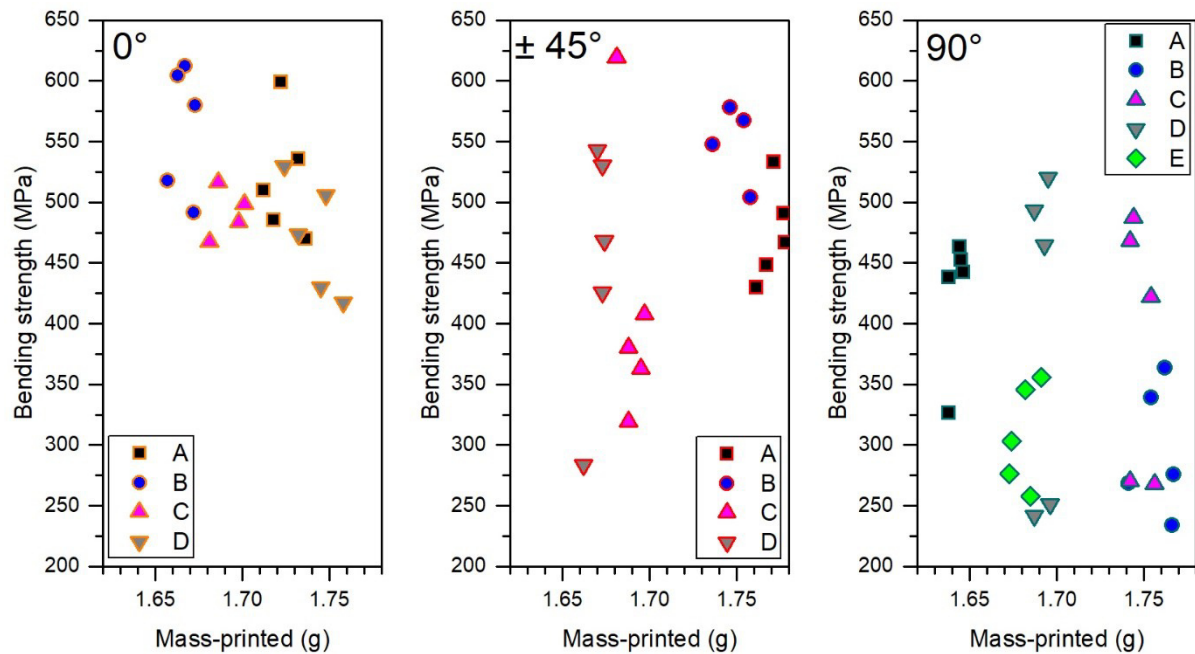


Figure S2: Bending strength and mass of the specimens produced in the different build cycles (A, B, C, D and E) with all the infill orientations

## References

1. SmarTech Analysis. Ceramics Additive Manufacturing Production Markets: Crozet, VA, USA, 2019–2030, 2020.
2. Chen, Z.; Li, Z.; Li, J.; Liu, C.; Lao, C.; Fu, Y.; Liu, C.; Li, Y.; Wang, P.; He, Y. 3D printing of ceramics: A review. *J. Eur. Ceram. Soc.* **2019**, *39*, 661–687, doi:10.1016/j.jeurceramsoc.2018.11.013.
3. Travitzky, N.; Bonet, A.; Dermeik, B.; Fey, T.; Filbert-Demut, I.; Schlier, L.; Schlordt, T.; Greil, P. Additive Manufacturing of Ceramic-Based Materials. *Adv. Eng. Mater.* **2014**, *16*, 729–754.
4. Zocca, A.; Colombo, P.; Gomes, C.M.; Günster, J.; Green, D.J. Additive Manufacturing of Ceramics: Issues, Potentialities, and Opportunities. *J. Am. Ceram. Soc.* **2015**, *98*, 1983–2001.
5. Moritz, T.; Maleksaeedi, S. Additive manufacturing of ceramic components. In *Additive manufacturing: Materials, processes, quantifications and applications*; Zhang, J., Jung, Y.-G., Eds.; Elsevier: Cambridge, MA, USA, 2018, pp. 105–161.
6. Wang, J.-C.; Dommatti, H.; Hsieh, S.-J. Review of additive manufacturing methods for high-performance ceramic materials. *Int J Adv Manuf Technol* **2019**, *103*, 2627–2647.
7. Du, W.; Ren, X.; Pei, Z.; Ma, C. Ceramic Binder Jetting Additive Manufacturing: A Literature Review on Density. *J. Manuf. Sci. Eng.* **2020**, *142*, 1–66.
8. Agarwala, M.K.; Jamalabad, V.R.; Langrana, N.A.; Safari, A.; Whalen, P.J.; Danforth, S.C. Structural quality of parts processed by fused deposition. *Rapid Prototyp. J.* **1996**, *2*, 4–

- 19.
9. McNulty, T.F.; Mohammadi, F.; Bandyopadhyay, A.; Shanefield, D.J.; Danforth, S.C.; Safari, A. Development of a binder formulation for fused deposition of ceramics. *Rapid Prototyp.J.* **1998**, *4*, 144–150.
  10. Fang, T.; Jafari, M.A.; Danforth, S.C.; Safari, A. Signature analysis and defect detection in layered manufacturing of ceramic sensors and actuators. *Mach. Vis. Appl.s* **2003**, *15*, 63–75.
  11. Gorjan, L.; Reiff, L.; Liersch, A.; Clemens, F. Ethylene vinyl acetate as a binder for additive manufacturing of tricalcium phosphate bio-ceramics. *Ceram. Int.* **2018**, *44*, 15817–15823.
  12. Cano, S.; Gonzalez-Gutierrez, J.; Sapkota, J.; Spoerk, M.; Arbeiter, F.; Schuschnigg, S.; Holzer, C.; Kukla, C. Additive manufacturing of zirconia parts by fused filament fabrication and solvent debinding: Selection of binder formulation. *Addit. Manuf.* **2019**, *26*, 117–128.
  13. Nötzel, D.; Hanemann, T. Filament development for the additive manufacturing of ceramic parts via Fused Deposition Modelling (FDM). In Proceedings of the 92nd DKG Annual Meeting and Symposium on High Performance Ceramics, Berlin, Germany, 19–22 March 2017.
  14. Damon, J.; Dietrich, S.; Gorantla, S.; Popp, U.; Okolo, B.; Schulze, V. Process porosity and mechanical performance of fused filament fabricated 316L stainless steel. *Rapid Prototyp.J.* **2019**, *27*, 1319–1327.
  15. Thompson, Y.; Gonzalez-Gutierrez, J.; Kukla, C.; Felfer, P. Fused filament fabrication, debinding and sintering as a low cost additive manufacturing method of 316L stainless steel. *Addit. Manuf.* **2019**, *30*, 100861.
  16. Fan, N.C.; Chen, Y.Y.; Wei, W.C.J.; Liu, B.H.; Wang, A.B.; Luo, R.C. Porous Al<sub>2</sub>O<sub>3</sub> catalyst carrier by 3D additive manufacturing for syngas reforming. *J. Ceram. Process. Res.* **2017**, *18*, 676–682.
  17. Iyer, S.; McIntosh, J.J.; Bandyopadhyay, A.; Langrana, N.A.; Safari, A.; Danforth, S.C.; Clancy, R.B.; Gasdaska, C.J.; Whalen, P.J. Microstructural Characterization and Mechanical Properties of Si<sub>3</sub>N<sub>4</sub> Formed by Fused Deposition of Ceramics. *Int. J. Appl. Ceram. Technol.* **2008**, *5*, 127–137.
  18. Gorjan, L.; Tonello, R.; Sebastian, T.; Colombo, P.; Clemens, F. Fused deposition modeling of mullite structures from a preceramic polymer and  $\gamma$ -alumina. *J. Eur. Ceram. Soc.* **2019**, *39*, 2463–2471.
  19. Conzelmann, N.A.; Gorjan, L.; Sarraf, F.; Poulikakos, L.D.; Partl, M.N.; Müller, C.R.; Clemens, F.J. Manufacturing complex Al<sub>2</sub>O<sub>3</sub> ceramic structures using consumer-grade fused deposition modelling printers. *Rapid Prototyp.J.* **2020**, *26*, 1035–1048,.
  20. de Calan, Guillaume (2020): Benchmark of AM technologies. Nanoe Webinar. Nanoe. Ballainvilliers, France, 5/12/2020. Available online at <https://nanoe.com/en/nanoe/> (accessed on 5/18/2020).

21. Orlovská, M.; Chlup, Z.; Bača, L.; Janek, M.; Kitzmantel, M. Fracture and mechanical properties of lightweight alumina ceramics prepared by fused filament fabrication. *J. Eur. Ceram. Soc.* **2020**, doi:10.1016/j.jeurceramsoc.2020.02.026.
22. Moritz, T.; Müller-Köhn, A.; Abel, J.; Scheithauer, U.; Weingarten, S. Ceramic Injection Moulding and Ceramic Additive Manufacturing side by side: Opportunities and challenges. *Powder Inject. Mould. Int.* **2018**, *12*, 77–84.
23. Abel, J.; Scheithauer, U.; Janics, T.; Hampel, S.; Cano, S.; Müller-Köhn, A.; Günther, A.; Kukla, C.; Moritz, T. Fused Filament Fabrication (FFF) of Metal-Ceramic Components. *JoVE* **2019**, doi:10.3791/57693.
24. Kukla, C.; Cano, S.; Moritz, T.; Müller-Köhn, A.; Courtney, P.; Hampel, S.; Holzer, C. Multimaterial Components by Material Extrusion-Fused Filament Fabrication (ME-FFF) - Production of an Infrared Heater. *Ceram. Forum Int.* **2019**, *96*, 22–27.
25. Jafari, M.A.; Han, W.; Mohammadi, F.; Safari, A.; Danforth, S.C.; Langrana, N.A. A novel system for fused deposition of advanced multiple ceramics. *Rapid Prototyp. J.* **2000**, *6*, 161–175.
26. Fuenmayor, E.; Forde, M.; Healy, A.V.; Devine, D.M.; Lyons, J.G.; McConville, C.; Major, I. Material Considerations for Fused-Filament Fabrication of Solid Dosage Forms. *Pharmaceutics* **2018**, *10*, 44.
27. Turner, B.N.; Gold, S.A. A review of melt extrusion additive manufacturing processes: II. Materials, dimensional accuracy, and surface roughness. *Rapid Prototyp. J.* **2015**, *21*, 250–261.
28. Munsch, M.; Schmidt-Lehr, M.; Wycisk, E. Metal Additive Manufacturing with sinter-based technologies; AM Power Insights No. 4, 2018. Available online: <https://am-power.de/en/insights/additive-manufacturing-sinter-based-technologies/> (accessed on 23 April 2020).
29. Gibson, I.; Rosen, D.; Stucker, B. Additive Manufacturing Technologies. 3D Printing, Rapid Prototyping, and Direct Digital Manufacturing; Springer-Verlag: New York, NY, USA, 2015, ISBN 978-1-4939-2113-3.
30. Nötzel, D.; Eickhoff, R.; Hanemann, T. Fused Filament Fabrication of Small Ceramic Components. *Materials* **2018**, *11*, 1463.
31. Lengauer, W.; Duretek, I.; Fürst, M.; Schwarz, V.; Gonzalez-Gutierrez, J.; Schuschnigg, S.; Kukla, C.; Kitzmantel, M.; Neubauer, E.; Lieberwirth, C.; et al. Fabrication and properties of extrusion-based 3D-printed hardmetal and cermet components. *J. Refract. Hard. Met.* **2019**, *82*, 141–149.
32. Zhang, Y.; Bai, S.; Riede, M.; Garratt, E.; Roch, A. A comprehensive study on Fused Filament Fabrication of Ti-6Al-4V structures. *Addit. Manuf.* **2020**, *34*, 101256.
33. Waalkes, L.; Längerich, J.; Holbe, F.; Emmelmann, C. Feasibility study on piston-based feedstock fabrication with Ti-6Al-4V metal injection molding feedstock. *Addit. Manuf.* **2020**, *35*, 101207.
34. Rane, K.; Petrò, S.; Strano, M. Evolution of porosity and geometrical quality through the

- ceramic extrusion additive manufacturing process stages. *Addit. Manuf.* **2020**, *32*, 101038.
35. Yu, T.; Zhang, Z.; Liu, Q.; Kuliiev, R.; Orlovskaya, N.; Wu, D. Extrusion-based additive manufacturing of yttria-partially-stabilized zirconia ceramics. *Ceram. Int.* **2020**, *46*, 5020–5027.
36. Kurose, T.; Abe, Y.; Santos, M.V.A.; Kanaya, Y.; Ishigami, A.; Tanaka, S.; Ito, H. Influence of the Layer Directions on the Properties of 316L Stainless Steel Parts Fabricated through Fused Deposition of Metals. *Materials* **2020**, *13*, 2493.
37. Ahn, S.-H.; Montero, M.; Odell, D.; Roundy, S.; Wright, P.K. Anisotropic material properties of fused deposition modeling ABS. *Rapid Prototyp.J.* **2002**, *8*, 248–257, doi:10.1108/13552540210441166.
38. Feilden, E.; Blanca, E.G.-T.; Giuliani, F.; Saiz, E.; Vandeperre, L. Robocasting of structural ceramic parts with hydrogel inks. *J. Eur. Ceram. Soc.* **2016**, *36*, 2525–2533.
39. Goh, G.D.; Yap, Y.L.; Tan, H.K.J.; Sing, S.L.; Goh, G.L.; Yeong, W.Y. Process–Structure–Properties in Polymer Additive Manufacturing via Material Extrusion: A Review. *Crit. Rev. Solid State Mater. Sci.* **2020**, *45*, 113–133, doi:10.1080/10408436.2018.1549977.
40. Koch, C.; van Hulle, L.; Rudolph, N. Investigation of mechanical anisotropy of the fused filament fabrication process via customized tool path generation. *Addit. Manuf.* **2017**, *16*, 138–145.
41. Tosoh Corporation. Advanced Ceramics: Zirconia Powders. Available online: <https://www.tosoh.com/our-products/advanced-materials/zirconia-powders> (accessed on 4 July 2020).
42. Bagley, E.B. End Corrections in the Capillary Flow of Polyethylene. *J. Appl. Phys.* **1957**, *28*, 624–627.
43. Eisenschitz, R.; Rabinowitsch, B.; Weissenberg, K. Zur Analyse des Formveraenderungswiderstandes. Mitteilungen der deutschen Materialspruefungsanstalten **1929**, *9*, 91–94.
44. Rabinowitsch, B. Über die Viskosität und Elastizität von Solen. *Z. Phys. Chem.* **1929**, *145A*, 1–26.
45. DIN EN 843-1:2008-08, Hochleistungskeramik—Mechanische Eigenschaften monolithischer Keramik bei Raumtemperatur—Teil\_1: Bestimmung der Biegefestigkeit; Deutsche Fassung EN\_843-1:2006; Beuth Verlag GmbH: Berlin, Germany, 2008.
46. DIN EN 843-5 Hochleistungskeramik - Mechanische Eigenschaften monolithischer Keramik bei Raumtemperatur - Teil 5: Statistische Auswertung; Deutsche Fassung EN 843-5:2006; Beuth Verlag GmbH: Berlin, Germany, 2006.
47. Danzer, R.; Lube, T.; Supancic, P.; Damani, R. Fracture of Ceramics. *Adv. Eng. Mater.* **2008**, *10*, 275–298.
48. Rangarajan, S.; Qi, G.; Venkataraman, N.; Safari, A.; Danforth, S.C. Powder Processing, Rheology, and Mechanical Properties of Feedstock for Fused Deposition of Si<sub>3</sub>N<sub>4</sub> Ceramics. *J. Am. Ceram. Soc.* **2000**, *83*, 1663–1669.



49. Venkataraman, N.; Rangarajan, S.; Matthewson, M.J.; Safari, A.; Danforth, S.C.; Yardimci, A.; Guceri, S.I. Mechanical and Rheological Properties of Feedstock Material for Fused Deposition of Ceramics and Metals (FDC and FDMet) and their Relationship to Process Performance. In Proceedings of the Solid Freeform Fabrication Symposium. Laboratory for Freeform Fabrication, University of Texas, Austin, TX, USA, 9–11 August 1999.
50. Xie, H.; Jiang, J.; Yang, X.; He, Q.; Zhou, Z.; Xu, X.; Zhang, L. Theory and practice of rapid and safe thermal debinding in ceramic injection molding. *Int. J. Appl. Ceram. Technol.* **2019**, *44*, 2718.
51. Mutsuddy, B.C.; Ford, R.G. *Ceramic injection moulding*; Chapman & Hall: London, UK, 1995, ISBN 0412538105.
52. Eichler, J.; Rödel, J.; Eisele, U.; Hoffman, M. Effect of Grain Size on Mechanical Properties of Submicrometer 3Y-TZP: Fracture Strength and Hydrothermal Degradation. *J. Am. Ceram. Soc.* **2007**, *90*, 2830–2836.
53. Shao, H.; Zhao, D.; Lin, T.; He, J.; Wu, J. 3D gel-printing of zirconia ceramic parts. *Ceram. Int.* **2017**, *43*, 13938–13942.
54. Lu, Y.; Mei, Z.; Zhang, J.; Gao, S.; Yang, X.; Dong, B.; Yue, L.; Yu, H. Flexural strength and Weibull analysis of Y-TZP fabricated by stereolithographic additive manufacturing and subtractive manufacturing. *J. Eur. Ceram. Soc.* **2020**, *40*, 826–834.
55. Munz, D.; Fett, T. *Ceramics: Mechanical Properties, Failure Behaviour, Materials Selection*; Springer International Publishing: Cham, Switzerland, 1999, ISBN 978-3-642-58407-7.
56. Lawn, B. *Fracture of Brittle Solids*. Cambridge University Press: Cambridge, UK, 1993, ISBN 9780511623127.
57. Rueda, M.M.; Auscher, M.-C.; Fulchiron, R.; Périé, T.; Martin, G.; Sonntag, P.; Cassagnau, P. Rheology and applications of highly filled polymers: A review of current understanding. *Prog. Polym. Sci.* **2017**, *66*, 22–53.
58. Hausnerova, B. Rheological characterization of powder injection molding compounds. *Polimery* **2010**, *55*, 3–11.
59. Kukla, C.; Duretek, I.; Gonzalez-Gutierrez, J.; Holzer, C. Rheology of Highly Filled Polymers. In *Rheology of Highly Filled Polymers*; Rivera-Armenta, J.L., Cruz, B.A.S., Kukla, C., Duretek, I., Gonzalez-Gutierrez, J., Holzer, C., Eds.; InTechOpen Limited, London, UK, 2018, ISBN 978-1-78984-001-8.
60. Hausnerová, B.; Sába, P.; Kubát, J.; Kitano, T.; Becker, J. Rheological Behaviour of Hard-Metal Carbide Powder Suspensions at High Shear Rates. *Polym. Eng. Sci.* **2000**, *20*, 4.
61. Hausnerová, B.; Sába, P.; Kubát, J. Capillary Flow of Hard-Metal Carbide Powder Compounds. *IPP* **1999**, *14*, 254–260.
62. Birinci, E.; Kalyon, D.M. Development of extrudate distortions in poly(dimethyl siloxane) and its suspensions with rigid particles. *J Rheol.* **2006**, *50*, 313–326.
63. Cano, S.; Gooneie, A.; Kukla, C.; Rieß, G.; Holzer, C.; Gonzalez-Gutierrez, J. Modification of Interfacial Interactions in Ceramic-Polymer Nanocomposites by Grafting: Morphology

- and Properties for Powder Injection Molding and Additive Manufacturing. *Appl. Sci.* **2020**, *10*, 1471.
64. Semakina, O.K.; Phomenko, A.N.; Leonteva, A.A.; Rymanova, I.E. Research of Surface Properties of Fillers for Polymers. *Procedia Chem.* **2015**, *15*, 79–83.
65. Chao, F.; Bowler, N.; Tan, X.; Liang, G.; Kessler, M.R. Influence of adsorbed moisture on the properties of cyanate ester/BaTiO<sub>3</sub> composites. *Compos. Part A Appl. Sci. Manuf.* **2009**, *40*, 1266–1271.
66. Gilmer, E.L.; Miller, D.; Chatham, C.A.; Zawaski, C.; Fallon, J.J.; Pekkanen, A.; Long, T.E.; Williams, C.B.; Bortner, M.J. Model analysis of feedstock behavior in fused filament fabrication: Enabling rapid materials screening. *Polymer* **2018**, *152*, 51–61.
67. Godec, D.; Cano, S.; Holzer, C.; Gonzalez-Gutierrez, J. Optimization of the 3D Printing Parameters for Tensile Properties of Specimens Produced by Fused Filament Fabrication of 17-4PH Stainless Steel. *Materials (Basel)* **2020**, *13*, 774.
68. Costa, A.E.; Ferreira da Silva, A.; Sousa Carneiro, O. A study on extruded filament bonding in fused filament fabrication. *Rapid Prototyp. J.* **2019**, *25*, 555–565.
69. Kosmač, T.; Oblak, C.; Jevnikar, P.; Funduk, N.; Marion, L. The effect of surface grinding and sandblasting on flexural strength and reliability of Y-TZP zirconia ceramic. *Dent Mater.* **1999**, *15*, 426–433.
70. Harrer, W.; Schwentenwein, M.; Lube, T.; Danzer, R. Fractography of zirconia-specimens made using additive manufacturing (LCM) technology. *J. Eur. Ceram. Soc.* **2017**, *37*, 4331–4338.

## 6 Conclusions and research outlook

### 6.1 Conclusions

The AM of ceramics enables the production of short series of components and opens new possibilities for the production of light weight products and highly complex geometries. In this manner, the AM technologies are complementary techniques to the conventional processes for ceramics. Depending on the characteristics of the process such as building speed, dimensional accuracy, attainable geometries and cost, each AM technology will find its applications in the years to come. The FFF of ceramics is one of the AM technologies with the higher potential due to the low cost and simplicity of the processing equipment, the large knowledge existing for the FFF of polymeric components and the possibility to process a wide variety of materials. Nevertheless, many challenges have to be addressed before FFF is an industrial feasible process for the thermoplastic based manufacturing of ceramic components. In order to overcome the current limitations of the FFF of ceramics, a deeper knowledge on the employed materials and the phenomena occurring in the process is required.

The main objective of this PhD thesis was to develop a better understanding of one of the most influencing factors of the FFF process, the ceramic feedstock. More specifically, of the feedstocks for FFF and solvent debinding, which are the main type of materials used commercially, but for which little information exists in the literature.

A novel feedstock formulation was developed in a systematic manner by evaluating the influence of each type of component separately. The feedstock is composed of acrylic acid-grafted high density polyethylene (AA-HDPE), stearic acid (SA), paraffin wax (PW) and styrene-ethylene/butylene-styrene copolymer (SEBS). In the first step, the influence of the solvent debinding components was investigated. It was found that two types of soluble components are required to meet all the requirements for FFF and solvent debinding. One soluble component with high flexibility and strength, such as SEBS, is required to produce filaments. A second soluble component must reduce the viscosity and the swelling during solvent debinding, such as the PW used in this thesis. The soluble binder components must be homogeneously dispersed in the feedstock in order to avoid stress concentration and crack propagation during solvent debinding. For instance, if an extender oil is used instead of the PW, the feedstock is more heterogeneous, resulting in heterogeneous swelling and defects.

The statistical evaluation of the effect of the binder components fractions on the properties for FFF and solvent debinding enabled to obtain a better insight in the function of each component. Increasing the backbone (AA-HDPE) content increased the strength and stiffness, but reduced the debinding rate and increased the viscosity. However, the largest increase of viscosity was obtained with the increase of the SEBS fraction. The increase of the SEBS fraction increased the swelling during debinding and thus the defects, but improved the flexibility if combined in the right proportion with PW. Therefore, a PW to SEBS ratio of  $1 \geq \text{PW/SEBS} \geq 0.6$  is necessary for a good combination of properties.

To determine the influence of the SA on the feedstock properties and processability, a separate study was conducted comparing a feedstock with this surfactant versus another feedstock without it. Incorporating SA reduced the viscosity, improved the homogeneity, increased the solvent debinding and reduced the defects in the parts. Furthermore, the reduction of the defects during solvent debinding with the incorporation of SA could be observed for the two feedstock compositions evaluated in this thesis. Nevertheless, the SA incorporation decreased significantly the strength, stiffness and flexibility of the filaments.

The last component studied was the AA-HDPE used as backbone. Molecular dynamic simulations and experimental characterization of composites of zirconia with HDPE with and without the AA grafting were conducted. It was observed that the high polarity, the improved interaction with the oxygen atoms of the oxide and the hydrogen bonding with the hydroxyl groups in the powder surface resulted in a higher powder-binder adhesion for the AA-HDPE than for the HDPE. Higher powder-adhesion increased the dispersion of the powder in the AA-HDPE, and both resulted in an higher filament flexibility and strength for the AA-HDPE composites. A polymer-filler network was formed for the AA-HDPE which resulted in a higher viscosity and shear modulus than for the HDPE.

The results of the feedstock development investigations validated the first and second hypotheses:

1. *By the right combination of binder components, a high strength, stiffness and flexibility, as well as low viscosity could be obtained as required for FFF.*
2. *Solvent debinding requires two types of components. First, a major fraction of the binder must be leached with a solvent. The rest, known as backbone, must maintain the shape of the parts during the process and be removed in the subsequent thermal debinding step. The combination of the right soluble binders and backbones should enable the use of solvent debinding in FFF.*

Nevertheless, the third hypothesis was only partly validated, since a higher viscosity was measured for the AA-HDPE than for the HDPE:

3. *The use of a polymer grafted with polar groups as backbone should result in an improvement of the adhesion to the polar surface of the zirconia powder. A high powder-binder adhesion should result in a more homogeneous feedstock, with lower viscosity and with higher mechanical properties.*

The multicomponent binder system composed of AA-HDPE, SA, SEBS and PW developed in this thesis shows a great potential for the processing of zirconia by FFF and solvent debinding. Current investigations are addressing the final adjustment of the content of the binder components in the feedstock to improve the flexibility of the feedstock filaments while having a low viscosity and no debinding defects. Based on the results obtained in this thesis, a small number of formulations have been selected to be produced in larger amounts using compounding equipment with high shear rate and to be evaluated through all the steps of the FFF process.

In addition to the investigations of the feedstock compositions for the processing by FFF and solvent debinding, the effect of the processing parameters on the processability of this type of feedstocks was investigated. More specifically, the effect of the solvent debinding and FFF shaping parameters on the processing of a zirconia feedstock with a binder composed of a grafted polyolefin as the backbone and a thermoplastic elastomer as the soluble component [122] was investigated.

The effect of the solvent debinding parameters on the defects and debinding rate of compression moulded cylinders was studied first with immersion trials in cyclohexane. The increase of the solvent temperature improved the debinding rate by the improvement of the polymer dissolution and the diffusion of the dissolved polymers out of the specimens. However, it did not influence the formation of cracks. No changes in the debinding rate and defect apparition could be observed when isopropanol was incorporated as a swelling inhibitor. In fact, the feedstock composition was the most influencing factor in the solvent debinding performance, since the use of SA in the feedstock improved the debinding rate and reduced the solvent debinding defects. Therefore, it can be stated that the results of this investigation cannot validate the hypothesis:

4. *The parameters employed in the solvent debinding of FFF feedstocks should determine the debinding rate and the apparition of defects.*

Surprisingly, the large defects in the compression moulded cylinders used in the publication E could not be observed for the parts shaped by FFF in publication F with the same feedstock. Therefore, residual stresses in the compression moulded cylinders could promote the apparition of defects. Thus, despite compression moulded cylinders can be employed in the development of new feedstocks for the comparison of the debinding performance of different formulations, the magnification of the debinding defects must always be considered.

In the last part of this PhD thesis, the influence of the FFF shaping parameters on the defects and bending properties of zirconia bars was evaluated. More specifically, the parameter studied was the orientation of the extruded roads of the infill with respect to the longest dimension of the bending specimens. Specimens with infill orientations of  $0^\circ$ ,  $\pm 45^\circ$  and  $90^\circ$  were produced and characterized. This study was complemented with the characterization of the feedstock filament employed in the FFF shaping. The formation of gases during the feedstock extrusion resulted in voids inside the extruded strands. Gaps between the extruded roads, the over- and underextrusion of material and the scrapping-off by the nozzle of the material in the first layer resulted in defects during the shaping by FFF. The variability of the filament diameter promoted the apparition of the FFF-defects. Moreover, the shape and orientation of these defects was influenced by the infill orientation, which resulted in higher mechanical properties for the specimens produced with the  $0^\circ$  orientation than for the  $90^\circ$  orientation. On this manner, the fifth hypothesis of the thesis has been validated:

5. *The defects caused during the shaping step in the FFF of ceramics and their effect on the properties of the final parts could be reduced by the proper adjustment of the parameters during shaping.*

The results obtained in this PhD thesis provide a deeper understanding of the polymeric binder components required for the combination of FFF and solvent debinding. Furthermore, the influence of the processing parameters on the processability of this type of compounds and on the properties of the final ceramic parts is determined. The results of the conducted investigations can facilitate the development and optimization of binder formulations for the processing of ceramics and metals not only by FFF, but also by other conventional and additive manufacturing technologies requiring of similar feedstocks. Moreover, the developed binder was made publically available for further studies. Finally, a better understanding of the phenomena occurring during the shaping by FFF and the solvent debinding of ceramic feedstocks has been gained.

### 6.2 Research outlook

Despite most of the initial questions have been answered, the obtained results arise many new questions that must be addressed in future investigations. For instance, the effect of the compounding shear forces on the dispersion of the zirconia particles could be different depending on the binder formulations. The roller rotors mixers are commonly used in the feedstock development since they require only small amounts of feedstock, which enables the production of many different formulations without a large waste of material. However, high shear equipment such as co-rotating twin screw extruders or shear rollers enable a better dispersion of the ceramic particles [195] and are the preferred option for the large scale production of feedstocks. Therefore, future studies must address the effect of the compounding shear on the properties of feedstocks with different characteristics, especially with different viscosity.

The use of polyolefins grafted with polar components as backbone shows a great potential not only for FFF [68, 87, 122], but also for Powder Injection Moulding (PIM) [223], in which similar multicomponent feedstocks are used. The results in publication D provide a first insight into the interfacial interactions between the zirconia powder and the grafted polyolefin. However, feedstocks are complex multicomponent systems in which the other binder components can interact with the backbone and the powder. Therefore, future studies must determine the nature of the interactions occurring in feedstocks with grafted components and the effect on the properties and processability of these feedstocks. Moreover, the effect of the backbone grafting on the thermal debinding behaviour must be investigated, especially for metallic powders. If the grafted backbone with high adhesion to the powder is not completely removed, the residual carbon could deteriorate the properties of components made by metals such as stainless steels.

In publication C, the effect of the surface area to volume ratio and the processing method of compression moulding and FFF specimens could be observed. Parts with a higher surface area to volume ratio have a faster debinding due to the shorter diffusion length [43, 160]. Moreover, at the beginning of the solvent debinding of thick components, the solvent enters in contact with the outer part of the components and produces the swelling. Since there is no swelling in the inner part of the components, internal stresses could appear in the components. These internal debinding stresses could result in delamination between the layers [49], especially when there is a poor inter-layer bonding [3]. Therefore, future studies

should investigate the maximum thickness that can be produced for the defect-free production by FFF and solvent debinding. Furthermore, the effect of the inter-layer bonding in the apparition of solvent debinding defects should be a matter of future investigations.

The causes of the gases during the FFF shaping in publication F must be determined in order to reduce the porosity inside the extruded roads. As was discussed in publication F, some possible causes are trapped moisture inside the feedstock, the catalytic degradation of the binder by the water or the powder, the combination of both or the many processing cycles on the feedstock. Current investigations are addressing this question by the comparison of the rheological and thermal properties and the processing by FFF of feedstocks dried at different time spans. Furthermore, feedstocks with different powder concentrations are being used in these investigations in order to determine the role of the powder content in the formation of gases during the extrusion of the feedstock. The increase of powder content could promote the densification during sintering and reduce the intrinsic sintering porosity observed in publication F. However, increasing the powder content could result in a significant increase of viscosity and reduction of the mechanical properties, promoting the apparition of the FFF shaping defects observed in publication F.

## 7 Acronyms

3DP	Three-dimensional printing
3PB	Three-point bending tests
AA	Acrylic acid
AA-HDPE	Acrylic-acid grafted high density polyethylene
AAPE	Acrylic acid polyethylene
AM	Additive manufacturing
APO	Amorphous polyolefin
ATR	Attenuated reflection spectroscopy
BET	Brunauer-Emmett-Teller
BJT	Binder jetting
CAB	Cellulose acetate butyrate
CAD	Computer assisted design
CIM	Ceramic injection moulding
CM	Compression moulded
CNC	Computer numerical control
DMD	Digital micromirror device
DOE	Design of experiments
DPD	Dissipative particle dynamics
DSC	Differential scanning calorimetry
EO	Extender oil
EVA	Ethylene vinyl acetate
FDC	Fused deposition of ceramics
FDM	Fused deposition modeling
FDMet	Fused deposition of metals
FEF	Freeze-form extrusion fabrication
FFF	Fused filament fabrication
gP	Grafted polyolefin
HDPE	High density polyethylene
ISOBAM	Isobutylene and Maleic Anhydride
LCST	Lower critical solution temperature



LDPE	Linear density polyethylene
LENS	Laser engineered net shaping
LSB	Loss of soluble binder
MC	Monte Carlo
MD	Molecular dynamics
MEAM	Material extrusion additive manufacturing
MEX	Material extrusion
MFR	Melt flow rate
MJT	Material jetting
MVR	Melt volume rate
OWRK	Owens, Wendt, Rabel and Kaelble
PAA	Polyacrylic acid
PE	Polyethylene
PEG	Polyethylene glycol
PIM	Powder injection molding
PM	Powder metallurgy
PMMA	Poly(methyl methacrylate)
POM	Polyoxymethylene
PP	Polypropylene
PTFE	Polytetrafluoroethylene
PVA	Polyvinyl alcohol
PVB	Polyvinyl butyral
PVOH	Polyvinyl alcohol
PVP	Polyvinylpyrrolidone
PW	Paraffin wax
SA	Stearic acid
SDS	Shaping debinding and sintering
SEBS	Styrene-ethylene/butylene-styrene
SEM	Scanning electron microscopy
SLA	Stereolithography
SLM	Selective laser melting
SLS	Selective laser sintering

SM	Secant modulus
STL	Standard tessellation language
TGA	Thermogravimetric analysis
TPE	Thermoplastic elastomer
UTS	Ultimate tensile stress
UV	Ultraviolet
VPP	Vat photopolymerization

## 8 Literature

- [1] Abel, J.; Scheithauer, U.; Janics, T.; Hampel, S.; Cano, S.; Müller-Köhn, A.; Günther, A.; Kukla, C.; Moritz, T.: Fused Filament Fabrication (FFF) of Metal-Ceramic Components, *Journal of Visualized Experiments* (143), 2019
- [2] Abolhasani, H.; Muhamad, N.: A new starch-based binder for metal injection molding, *Journal of Materials Processing Technology* 210 (6-7), 2010, pp. 961–968
- [3] Agarwala, M.K.; Jamalabad, V.R.; Langrana, N.A.; Safari, A.; Whalen, P.J.; Danforth, S.C.: Structural quality of parts processed by fused deposition, *Rapid Prototyping Journal* 2 (4), 1996, pp. 4–19
- [4] Agarwala, M.K.; Weeren, R. van; Bandyopadhyay, A.; Safari, A.; Danforth, S.C.; Priedeman, W.R.: Filament Feed Materials for Fused Deposition Processing of Ceramics and Metals, In: Bourell D.L.;Berger C.;Marcus H.L.;Crawford R.H.; Barlow J.W. (Ed.), *Proceedings of the Solid Freeform Fabrication Symposium, The University of Texas at Austin, 1996*
- [5] Agarwala, M.K.; Weeren, R. van; Bandyopadhyay, A.; Whalen, P.J.; Safari, A.; Danforth, S.C.: Fused Deposition of Ceramics and Metals: An Overview, In: Bourell D.L.;Berger C.;Marcus H.L.;Crawford R.H.; Barlow J.W. (Ed.), *Proceedings of the Solid Freeform Fabrication Symposium, The University of Texas at Austin, 1996*
- [6] Agarwala, M.K.; Weeren, R. van; Vaidyanathan, R.; Bandyopadhyay, A.; Carrasquillo, G.; Jamalabad, V.R.; Langrana, N.A.; Safari, A.; Garofalini, S.H.; Danforth, S.C.; Burlew, J.; Donaldson, R.; Whalen, P.J.; Ballard, C.: Structural Ceramics by Fused Deposition of Ceramics, In: Marcus H.L. (Ed.), *Proceedings of the Solid Freeform Fabrication Symposium, 1995*
- [7] AIM3D GmbH: Edelstahl, Germany, 2017, <http://www.aim3d.de/materialien/edelstaehle/> (Accessed on: 07.07.2017)
- [8] Aini Wahab, N.; Nasiruddin Ahmad, I.; Afian Omar, M.; Sauti, R.; Saedon, J.: Determination of optimised solvent debinding parameters of injection moulded 316L stainless steel using Taguchi approach, *Materials Today: Proceedings* 16, 2019, pp. 2357–2366
- [9] Allahverdi, M.; Danforth, S.C.; Jafari, M.A.; Safari, A.: Processing of advanced electroceramic components by fused deposition technique, *Journal of the European Ceramic Society* 21, 2001, pp. 1485–1490
- [10] Atisivan, R.; Bose, S.; Bandyopadhyay, A.: Porous Mullite Preforms via Fused Deposition, *Journal of the American Ceramic Society* 84 (1), 2001, pp. 221–223
- [11] Bandyopadhyay, A.; Danforth, S.C.; Safari, A.: Effects of processing history on thermal debinding, *JOURNAL OF MATERIALS SCIENCE* 35 (16), 2000, pp. 3983–3988
- [12] Bandyopadhyay, A.; Das, K.; Marusich, J.; Onagoruwa, S.: Application of fused deposition in controlled microstructure metal - ceramic composites, *Rapid Prototyping Journal* 12 (3), 2006, pp. 121 - 128

- [13] Banerjee, S.; Joens, C.J.: Debinding and sintering of metal injection molding (MIM) components, In: Heaney D.F. (Ed.): Handbook of metal injection molding, Woodhead Publishing in materials, Vol. 70, Woodhead Publishing, Cambridge UK, Philadelphia PA, 2012, pp. 133–180
- [14] Barrière, T.; Hutton, J.F.; Walters, K.: An introduction to rheology, Rheology series, vol. 3, Elsevier; Distributors for the U.S. and Canada, Elsevier Science Pub. Co, Amsterdam, New York, 1989
- [15] Bartolo, P.J.; Gaspar, J.: Metal filled resin for stereolithography metal part, CIRP Annals - Manufacturing Technology 57 (1), 2008, pp. 235–238
- [16] BASF AG: Ultrafuse 316L, Technical Data Sheet, 2019, [https://www.basf.com/global/images/about-us/locations/europe/german-companies/b3dps/documents/metals/Ultrafuse\\_316L\\_Technical\\_Data\\_Sheet\\_TDS.pdf](https://www.basf.com/global/images/about-us/locations/europe/german-companies/b3dps/documents/metals/Ultrafuse_316L_Technical_Data_Sheet_TDS.pdf) (Accessed on: 14.05.2020)
- [17] Basir, A.; Sulong, A.B.; Jamadon, N.H.; Muhamad, N.: Bi-Material Micro-Part of Stainless Steel and Zirconia by Two-Component Micro-Powder Injection Molding: Rheological Properties and Solvent Debinding Behavior, Metals 10 (5), 2020, pp. 595
- [18] Bellini, A.; Shor, L.; Gucerì, S.I.: New developments in fused deposition modeling of ceramics, Rapid Prototyping Journal 11 (4), 2005, pp. 214–220
- [19] Beran, T.; Mulholland, T.; Henning, F.; Rudolph, N.; Osswald, T.A.: Nozzle clogging factors during fused filament fabrication of spherical particle filled polymers, Additive Manufacturing 23, 2018, pp. 206–214
- [20] Berger, C.; Abel, J.; Pötschke, J.; Moritz, T.: Properties of Additive Manufactured Hardmetal Components Produced by Fused Filament Fabrication (FFF), In: EPMA (Ed.), Euro PM2018 Proceedings, European Powder Metallurgy Association (EMPA), Shrewsbury, United Kingdom, 2018
- [21] Berman, B.: 3-D printing: The new industrial revolution, Business Horizons 55 (2), 2012, pp. 155–162
- [22] bin Suleiman Ahmad, M.J.; binti Johari, N.; bin Ahmad, M.A.; bin Ibrahim, R.; bin Abu Talib, A.B.D.R.; bin Harmin, M.Y.: Solvent Debinding of Inconel 718 Fabricated via Metal Injection Molding, Advanced Materials Research 1133, 2016, pp. 275–279
- [23] Blanchart, P.: Extraction, Properties and Applications of Zirconia, In: Pawłowski L.; Blanchart P. (Ed.): Industrial Chemistry of Oxides for Emerging Applications, John Wiley & Sons Ltd, Chichester, UK, 2018, pp. 165–209
- [24] Bose, A.; Schuh, C.A.; Tobia, J.C.; Tuncer, N.; Mykulowycz, N.M.; Preston, A.; Barbati, A.C.; Kernan, B.; Gibson, M.A.; Krause, D.; Brzezinski, T.; Schroers, J.; Fulop, R.; Myerberg, J.S.; Sowerbutts, M.; Chiang, Y.-M.; John, H.A.; Sachs, E.M.; Lomeli, E.E.; Lund, A.C.: Traditional and additive manufacturing of a new Tungsten heavy alloy alternative, International Journal of Refractory Metals and Hard Materials 73, 2018, pp. 22–28

- [25] Bose, S.; Vahabzadeh, S.; Ke, D.; Bandyopadhyay, A.: Additive Manufacturing of Ceramics, 2015, pp. 143–184
- [26] Brans, K.: 3D Printing, a Maturing Technology, IFAC Proceedings Volumes 46 (7), 2013, pp. 468–472
- [27] Brennan, R.E.; Turcu, S.; Hall, A.; Hagh, N.M.; Safari, A.: Fabrication of Electroceramic Components by Layered Manufacturing (LM), *Ferroelectrics* 293 (1), 2003, pp. 3–17
- [28] Bresciani, A.: Shaping in Ceramic Technology – an Overview, In: Händle F. (Ed.): *Extrusion in ceramics, Engineering materials and processes*, Springer, Berlin, New York, 2007
- [29] Buggakupta, W.; Chuankrerkkul, N.; Surawattana, J.: Effects of Water Temperatures on Water-Soluble Binder Removal in Ceramic Materials Fabricated by Powder Injection Moulding, *Key Engineering Materials* 659, 2015, pp. 90–95
- [30] Burkhardt, C.; Freigassner, P.; Weber, O.; Imgrund, P.; Hampel, S.: Fused Filament Fabrication (FFF) of 316L Green Parts for the MIM process, In: EPMA (Ed.), *World PM2016 Proceedings, European Powder Metallurgy Association (EMPA)*, 2016, pp. 1–7
- [31] Butt, J.; Mebrahtu, H.; Shirvani, H.: Microstructure and mechanical properties of dissimilar pure copper foil/1050 aluminium composites made with composite metal foil manufacturing, *Journal of Materials Processing Technology* 238, 2016, pp. 96–107
- [32] Camargo, A.; Rodrigues, D.; Tschiptschin, A.P.: Debinding Kinetics of Injection Molding Samples - The Effects of the Binder Melt Index Flow, *Key Engineering Materials* 189-191, 2001, pp. 604–609
- [33] Cano, S.; Cajner, H.; Gonzalez-Gutierrez, J.; Sapkota, J.; Kukla, C.; Arbeiter, F.; Schuschnigg, S.; Holzer, C.: Optimization of material properties for highly-filled thermoplastic polymers used in fused filament fabrication of ceramics, *AIP Conference Proceedings* 2065, 2019
- [34] Cano, S.; Gonzalez-Gutierrez, J.; Sapkota, J.; Spoerk, M.; Arbeiter, F.; Schuschnigg, S.; Holzer, C.; Kukla, C.: Additive manufacturing of zirconia parts by fused filament fabrication and solvent debinding, Selection of binder formulation, *Additive Manufacturing* 26, 2019, pp. 117–128
- [35] Cano, S.; Gooneie, A.; Kukla, C.; Rieß, G.; Holzer, C.; Gonzalez-Gutierrez, J.: Modification of Interfacial Interactions in Ceramic-Polymer Nanocomposites by Grafting: Morphology and Properties for Powder Injection Molding and Additive Manufacturing, *Applied Sciences* 10 (4), 2020, pp. 1471
- [36] Cano, S.; Lube, T.; Huber, P.; Gallego, A.; Naranjo, J.A.; Berges, C.; Schuschnigg, S.; Herranz, G.; Kukla, C.; Holzer, C.; Gonzalez-Gutierrez, J.: Influence of the Infill Orientation on the Properties of Zirconia Parts Produced by Fused Filament Fabrication, *Materials* 13 (14), 2020, pp. 3158
- [37] Castro Martínez, L.; Rincón Rincón, E.; Levenfeld Laredo, B.; Torralba Castelló, J.M.: Moldeo por inyección de metales. Estado actual, *Tecnología@ y Desarrollo. Revista de Ciencia, Tecnología y Medio Ambiente* III, 2005

- [38] Checot-Moinard, D.; Rigollet, C.; Lourdin, P.: Powder injection moulding PIM of feedstock based on hydrosoluble binder and submicronic powder to manufacture parts having micro-details, *Powder Technology* 208 (2), 2011, pp. 472–479
- [39] Chen, G.; Cao, P.; Wen, G.; Edmonds, N.: Debinding behaviour of a water soluble PEG/PMMA binder for Ti metal injection moulding, *Materials Chemistry and Physics* 139 (2-3), 2013, pp. 557–565
- [40] Chen, K.Y.; Chen, Y.Y.; Wei, W.C.J.: 3D printed ZnO absorbent for desulfurization of syngas fuel, In: SICE (Ed.), *Proceedings of the 2017 IEEE/SICE International Symposium on System Integration*, 2017, pp. 115–120
- [41] Chen, Z.; Li, Z.; Li, J.; Liu, C.; Lao, C.; Fu, Y.; Liu, C.; Li, Y.; Wang, P.; He, Y.: 3D printing of ceramics: A review, *Journal of the European Ceramic Society* 39 (4), 2019, pp. 661–687
- [42] Cho, H.; Park, J.M.; Rho, J.; Park, S.J.: Warpage of Powder Injection Molded Copper Structure, *Metals and Materials International* 56, 2019, pp. 11
- [43] Chomsirigul, N.; Khuanthong, O.; Sooksaen, P.; Chuankrerkkul, N.: Influence of Specimen Dimensions and Temperature on the Debinding Behavior of Alumina Feedstock, *Key Engineering Materials* 608, 2014, pp. 170–174
- [44] Chuankrerkkul, N.; Davies, H.A.; Messer, P.F.: Application of PEG/PMMA Binder for Powder Injection Moulding of Hardmetals, *Materials Science Forum* 561-565, 2007, pp. 953–956
- [45] Clancy, R.B.; Jamalabad, V.R.; Whalen, P.J.; Bhargava, P.; Dai, C.; Rangarajan, S.; Wu, S.; Danforth, S.C.; Langrana, N.A.; Safari, A.: Fused Deposition of Ceramics: Progress Towards a Robust and Controlled Process for Commercialization, In: *Laboratory for Freeform Fabrication; University of Texas at Austin (Ed.), Proceedings of the Solid Freeform Fabrication Symposium*, 1997
- [46] Clemens, F.: Thermoplastic Extrusion for Ceramic Bodies, In: Händle F. (Ed.): *Extrusion in ceramics, Engineering materials and processes*, Springer, Berlin, New York, 2007
- [47] Colombo, P.; Mera, G.; Riedel, R.; Sorarù, G.D.: Polymer-Derived Ceramics: 40 Years of Research and Innovation in Advanced Ceramics, *Journal of the American Ceramic Society* 73 ([9]), 2010, no-no
- [48] Contreras, J.M.; Jiménez-Morales, A.; Torralba, J.M.: Fabrication of bronze components by metal injection moulding using powders with different particle characteristics, *Journal of Materials Processing Technology* 209 (15-16), 2009, pp. 5618–5625
- [49] Conzelmann, N.A.; Gorjan, L.; Sarraf, F.; Poulikakos, L.D.; Partl, M.N.; Müller, C.R.; Clemens, F.J.: Manufacturing complex Al<sub>2</sub>O<sub>3</sub> ceramic structures using consumer-grade fused deposition modelling printers, *Rapid Prototyping Journal* 26 (6), 2020, pp. 1035–1048

- [50] Cruz, N.; Santos, L.; Vasco, J.; Barreiros, F.M.: Binder System for Fused Deposition of Metals, In: EPMA (Ed.), Euro PM2013 Proceedings, European Powder Metallurgy Association (EMPA), Bellstone, 2013, pp. 79–84
- [51] Damon, J.; Dietrich, S.; Gorantla, S.; Popp, U.; Okolo, B.; Schulze, V.: Process porosity and mechanical performance of fused filament fabricated 316L stainless steel, *Rapid Prototyping Journal* 27 (7), 2019, pp. 1319–1327
- [52] Daute, P.; Jaeckel, M.; Waldmann, J.: Sinterable feedstock for use in 3D printing devices, WO002016004985A1, 2014
- [53] de Calan, G.: Benchmark of AM technologies, Nanoe Webinar, Ballainvilliers, France, 2020
- [54] Deckers, J.; Vleugels, J.; Kruth, J.P.: Additive Manufacturing of Ceramics: A Review, *Journal of Ceramic Science and Technology* 5 (4), 2014, pp. 245–260
- [55] Dehdari Ebrahimi, N.; Ju, Y.S.: Thermal conductivity of sintered copper samples prepared using 3D printing-compatible polymer composite filaments, *Additive Manufacturing* 24, 2018, pp. 479–485
- [56] Della Bona, A.; Pecho, O.E.; Alessandretti, R.: Zirconia as a Dental Biomaterial, *Materials (Basel, Switzerland)* 8 (8), 2015, pp. 4978–4991
- [57] Deng, L.; Qiao, L.; Zheng, J.; Ying, Y.; Yu, J.; Li, W.; Che, S.; Cai, W.: Injection molding, debinding and sintering of ZrO<sub>2</sub> ceramic modified by silane coupling agent, *Journal of the European Ceramic Society* 40 (4), 2020, pp. 1566–1573
- [58] Derby, B.: Inkjet printing ceramics, From drops to solid, *Journal of the European Ceramic Society* 31 (14), 2011, pp. 2543–2550
- [59] Derby, B.; Reis, N.: Inkjet Printing of Highly Loaded Particulate Suspensions, *MRS Bulletin* 28 (11), 2003, pp. 815–818
- [60] Dimopoulos Eggenschwiler, P.; Papetti, V.; Lucci, F.; Ortona, A.: Additive manufactured open cell structures: Promising substrates for automotive catalysts, pp. 279–290
- [61] Du, W.; Ren, X.; Pei, Z.; Ma, C.: Ceramic Binder Jetting Additive Manufacturing: A Literature Review on Density, *Journal of Manufacturing Science and Engineering*, 2020, pp. 1–66
- [62] EAMG: Introduction to Additive Manufacturing Technology, A guide for Designers and Engineers, 2015
- [63] Enneti, R.K.; Onbattuvelli, V.P.; Atre, S.V.: Powder binder formulation and compound manufacture in metal injection molding (MIM), In: Heaney D.F. (Ed.): Handbook of metal injection molding, Woodhead Publishing in materials, Vol. 70, Woodhead Publishing, Cambridge UK, Philadelphia PA, 2012
- [64] Enneti, R.K.; Onbattuvelli, V.P.; Atre, S.V.: Powder binder formulation and compound manufacture in metal injection molding (MIM), In: Heaney D.F. (Ed.): Handbook of metal injection molding, Woodhead Publishing in materials, Woodhead, Oxford, 2012, pp. 64–92

- [65] Enneti, R.K.; Shivashankar, T.S.; Park, S.J.; German, R.M.; Atre, S.V.: Master debinding curves for solvent extraction of binders in powder injection molding, *Powder Technology* 228, 2012, pp. 14–17
- [66] ExOne, [www.exone.com/Resources/Materials](http://www.exone.com/Resources/Materials) (Accessed on: 30.09.2016)
- [67] Fan, N.C.; Chen, Y.Y.; Wei, W.C.J.; Liu, B.H.; Wang, A.B.; Luo, R.C.: Porous Al<sub>2</sub>O<sub>3</sub> catalyst carrier by 3D additive manufacturing for syngas reforming, *Journal of Ceramic Processing Research* 18 (9), 2017, pp. 676–682
- [68] Fan, N.C.; Wei, W.C.J.; Liu, B.H.; Wang, A.B.; Luo, R.C.: Ceramic feedstocks for additive manufacturing, In: ICIT (Ed.), *Proceedings, 2016 IEEE International Conference on Industrial Technology (ICIT)*, The Howard Plaza Hotel Taipei, Taipei, Taiwan, 14-17 March, 2016, IEEE, Piscataway, NJ, 2016, pp. 1147–1151
- [69] Fan, Y.L.; Hwang, K.S.; Su, S.C.: Improvement of the Dimensional Stability of Powder Injection Molded Compacts by Adding Swelling Inhibitor into the Debinding Solvent, *Metallurgical and Materials Transactions A* 39 (2), 2008, pp. 395–401
- [70] Fan, Y.L.; Hwang, K.S.; Wu, S.H.; Liao, Y.C.: Minimum Amount of Binder Removal Required during Solvent Debinding of Powder-Injection-Molded Compacts, *Metallurgical and Materials Transactions A* 40 (4), 2009, pp. 768–779
- [71] Fang, T.; Jafari, M.A.; Danforth, S.C.; Safari, A.: Signature analysis and defect detection in layered manufacturing of ceramic sensors and actuators, *Machine Vision and Applications* 15 (2), 2003, pp. 63–75
- [72] Ford, S.; Despeisse, M.: Additive manufacturing and sustainability, An exploratory study of the advantages and challenges, *Journal of Cleaner Production* 137, 2016, pp. 1573–1587
- [73] Gasdaska, C.J.; Clancy, R.; Jamalabad, V.; Dalfonzo, D.: Solid Freeform Fabrication of Silicon Nitride Ceramics, *MRS Proceedings* 542, 1998, pp. 60
- [74] Gausemeier, J.; Echterhoff, N.; Kokoschka, M.; Wall, M.: *Thinking ahead the Future of Additive Manufacturing - Analysis of Promising Industries*, 2011
- [75] Gebler, M.; Schoot Uiterkamp, A.J.M.; Visser, C.: A global sustainability perspective on 3D printing technologies, *Energy Policy* 74, 2014, pp. 158–167
- [76] German, R.M.: *Powder injection molding*, Metal Powder Industries Federation, Princeton N.J. USA, 1990
- [77] Giberti, H.; Strano, M.; Annoni, M.; Yuan, Y.; Menon, L.; Xu, X.: An innovative machine for Fused Deposition Modeling of metals and advanced ceramics, *MATEC Web of Conferences* 43, 2016, pp. 3003
- [78] Gibson, I.; Rosen, D.; Stucker, B.: *Additive Manufacturing Technologies, 3D Printing, Rapid Prototyping, and Direct Digital Manufacturing*, 2. Ed., Springer-Verlag, New York, 2015
- [79] Gill, D.: *Laser Engineered Net Shaping*, 2002



- [80] Godec, D.; Cano, S.; Holzer, C.; Gonzalez-Gutierrez, J.: Optimization of the 3D Printing Parameters for Tensile Properties of Specimens Produced by Fused Filament Fabrication of 17-4PH Stainless Steel, *Materials (Basel, Switzerland)* 13 (3), 2020
- [81] Gong, H.; Crater, C.; Ordonez, A.; Ward, C.; Waller, M.; Ginn, C.; Chang, G.: Material Properties and Shrinkage of 3D Printing Parts using Ultrafuse Stainless Steel 316LX Filament, *MATEC Web of Conferences* 249, 2018, pp. 1001
- [82] Gonzalez, P.; Schwarzer, E.; Scheithauer, U.; Kooijmans, N.; Moritz, T.: Additive Manufacturing of Functionally Graded Ceramic Materials by Stereolithography, *Journal of Visualized Experiments* (143), 2019
- [83] Gonzalez-Gutierrez, J.; Arbeiter, F.; Schlauf, T.; Kukla, C.; Holzer, C.: Tensile properties of sintered 17-4PH stainless steel fabricated by material extrusion additive manufacturing, *Materials Letters* 248, 2019, pp. 165–168
- [84] Gonzalez-Gutierrez, J.; Cano, S.; Schuschnigg, S.; Kukla, C.; Sapkota, J.; Holzer, C.: Additive Manufacturing of Metallic and Ceramic Components by the Material Extrusion of Highly-Filled Polymers: A Review and Future Perspectives, *Materials* 11 (5), 2018
- [85] Gonzalez-Gutierrez, J.; Duretek, I.; Holzer, C.; Arbeiter, F.; Kukla, C.: Filler Content and Properties of Highly Filled Filaments for Fused Filament Fabrication of Magnets, In: *Society of Plastics Engineers (Ed.), ANTEC 2017, Proceedings, Society of Plastics Engineers*, 2017, pp. 1–4
- [86] Gonzalez-Gutierrez, J.; Godec, D.; Kukla, C.; Schlauf, T.; Burkhardt, C.; Holzer, C.: Shaping, Debinding and Sintering of Steel Components via Fused Filament Fabrication, In: *Abele E.; Udijak T.; Ciglar D. (Ed.), CIM 2017 Computer Integrated Manufacturing and High Speed Machining, Croatian Association of Production Engineering, Zagreb, Croatia*, 2017, pp. 99–104
- [87] Gooneie, A.; Gonzalez-Gutierrez, J.; Holzer, C.: Atomistic Modelling of Confined Polypropylene Chains between Ferric Oxide Substrates at Melt Temperature, *Polymers* 8 (10), 2016, pp. 361
- [88] Gorjan, L.; Reiff, L.; Liersch, A.; Clemens, F.: Ethylene vinyl acetate as a binder for additive manufacturing of tricalcium phosphate bio-ceramics, *Ceramics International* 44 (13), 2018, pp. 15817–15823
- [89] Griffin, E.A.; McMillin, S.: Selective Laser Sintering and Fused Deposition Modeling Processes for Functional Ceramic Parts, In: *Marcus H.L. (Ed.), Proceedings of the Solid Freeform Fabrication Symposium*, 1995
- [90] Guo, N.; Leu, M.C.: Additive manufacturing: technology, applications and research needs, *Frontiers of Mechanical Engineering* 8 (3), 2013, pp. 215–243
- [91] Hajek, K.: Ceramic Injection Moulding: Binder innovations and Additive Manufacturing open up new opportunities, *Powder Injection Moulding International* 12 (1), 2018, pp. 67–72

- [92] Harrer, W.; Schwentenwein, M.; Lube, T.; Danzer, R.: Fractography of zirconia-specimens made using additive manufacturing (LCM) technology, *Journal of the European Ceramic Society* 37 (14), 2017, pp. 4331–4338
- [93] Harun, M.R.; Muhamad, N.; Sulong, A.B.; Nor, N.H.M.; Jamaludin, K.R.; Ibrahim, M.H.I.: Solvent Debinding Process for ZK60 Magnesium Alloy Mim Compact, *Jurnal Teknologi* 59 (2), 2012, pp. 159–168
- [94] Hausnerova, B.; Kuritka, I.; Bleyan, D.: Polyolefin backbone substitution in binders for low temperature powder injection moulding feedstocks, *Molecules* 19 (3), 2014, pp. 2748–2760
- [95] Hausnerova, B.; Novak, M.: Environmentally Efficient 316L Stainless Steel Feedstocks for Powder Injection Molding, *Polymers* 12 (6), 2020
- [96] Hayat, M.D.; Wen, G.; Zulkifli, M.F.; Cao, P.: Effect of PEG molecular weight on rheological properties of Ti-MIM feedstocks and water debinding behaviour, *Powder Technology* 270, 2015, pp. 296–301
- [97] Heaney, D.F.: Powders for metal injection molding (MIM), In: Heaney D.F. (Ed.): *Handbook of metal injection molding*, Woodhead Publishing in materials, Vol. 70, Woodhead Publishing, Cambridge UK, Philadelphia PA, 2012, pp. 50–63
- [98] Herranz, G.; Levenfeld, B.; Varez Alvarez, A.; Torralba, J.M.: Development of new feedstock formulation based on high density polyethylene for MIM of M2 high speed steels, *Powder Metallurgy* 48 (2), 2005, pp. 134–138
- [99] Hidalgo, J.; Abajo, C.; Jiménez-Morales, A.; Torralba, J.M.: Effect of a binder system on the low-pressure powder injection moulding of water-soluble zircon feedstocks, *Journal of the European Ceramic Society* 33 (15-16), 2013, pp. 3185–3194
- [100] Hidalgo, J.; Jiménez-Morales, A.; Torralba, J.M.: Torque rheology of zircon feedstocks for powder injection moulding, *Journal of the European Ceramic Society* 32 (16), 2012, pp. 4063–4072
- [101] Hinczewski, C.; Corbel, S.; Chartier, T.: Ceramic suspensions suitable for stereolithography, *Journal of the European Ceramic Society* 18 (6), 1998, pp. 583–590
- [102] Hu, S.C.; Hwang, K.S.: Length change and deformation of powder injection-molded compacts during solvent debinding, *Metallurgical and Materials Transactions A* 31 (5), 2000, pp. 1473–1478
- [103] Huang, M.-S.; Hsu, H.-C.: Effect of backbone polymer on properties of 316L stainless steel MIM compact, *Journal of Materials Processing Technology* 209 (15-16), 2009, pp. 5527–5535
- [104] Huang, S.H.; Liu, P.; Mokeddar, A.; Hou, L.: Additive manufacturing and its societal impact, A literature review, *The International Journal of Advanced Manufacturing Technology* 67 (5-8), 2013, pp. 1191–1203
- [105] Hund, D.: Metal AM in the automotive industry: New vehicle structures, series components for the luxury market and beyond, *Metal Additive Manufacturing* 2 (2), 2016, pp. 63–75

- [106] Hwang, K.S.; Hsieh, Y.M.: Comparative study of pore structure evolution during solvent and thermal debinding of powder injection molded parts, *Metallurgical and Materials Transactions A* 27 (2), 1996, pp. 245–253
- [107] Hwang, K.S.; Lin, H.K.; Lee, S.C.: Thermal, Solvent, and Vacuum Debinding Mechanisms of PIM Compacts, *Materials and Manufacturing Processes* 12 (4), 1997, pp. 593–608
- [108] Hwang, K.S.; Shu, G.-J.; Lee, H.J.: Solvent debinding behavior of powder injection molded components prepared from powders with different particle sizes, *Metallurgical and Materials Transactions A* 36 (1), 2005, pp. 161–167
- [109] Ibrahim, M.; Mohd Amin, A.; Asmawi, R.; Mustafa, N.: Influences of Restaurant Waste Fats and Oils (RWFO) from Grease Trap as Binder on Rheological and Solvent Extraction Behavior in SS316L Metal Injection Molding, *Metals* 6 (2), 2016, pp. 19
- [110] ÖNORM EN ISO/ASTM 52900:2017-01: ISO/ASTM 52900:2015 Additive manufacturing - General principles - Terminology, February 2017
- [111] ISO/ASTM 52915:2016: Standard Specification for Additive Manufacturing File Format (AMF) Version 1.2, 2016
- [112] Iyer, S.; McIntosh, J.J.; Bandyopadhyay, A.; Langrana, N.A.; Safari, A.; Danforth, S.C.; Clancy, R.B.; Gasdaska, C.J.; Whalen, P.J.: Microstructural Characterization and Mechanical Properties of Si<sub>3</sub>N<sub>4</sub> Formed by Fused Deposition of Ceramics, *International Journal of Applied Ceramic Technology* 5 (2), 2008, pp. 127–137
- [113] Jafari, M.A.; Han, W.; Mohammadi, F.; Safari, A.; Danforth, S.C.; Langrana, N.A.: A novel system for fused deposition of advanced multiple ceramics, *Rapid Prototyping Journal* 6 (3), 2000, pp. 161–175
- [114] Jamalabad, V.R.; Chard, J.A.; Gasdaska, C.J.; Clancy, R.B.: Topology Driven Improvement of FDC Build Parameters, In: *Laboratory for Freeform Fabrication; University of Texas at Austin (Ed.), Proceedings of the Solid Freeform Fabrication Symposium*, 1998
- [115] Johnson, A.; Bingham, G.A.; Wimpenny, D.I.: Additive manufactured textiles for high - performance stab resistant applications, *Rapid Prototyping Journal* 19 (3), 2013, pp. 199 - 207
- [116] Kazmer, D.O.; Coogan, T.; Mead, J.; Barry, C.; Johnston, S.; Malloy, R.; Sobkowicz-Kline, M.; Vangness, J.; Casey, P.; Rondeau, D.; Moshe, A.: A Protocol for Filament Production and Use in Fused Deposition Modeling, In: *ANTEC 2016*, 2016, pp. 881–886
- [117] Krauss, V.A.; Oliveira, A.A.M.; Klein, A.N.; Al-Qureshi, H.A.; Fredel, M.C.: A model for PEG removal from alumina injection moulded parts by solvent debinding, *Journal of Materials Processing Technology* 182 (1-3), 2007, pp. 268–273
- [118] Kukla, C.; Cano, S.; Holzer, C.; Gonzalez-Gutierrez, J.: Influence of stearic acid in feedstocks for FFF and PIM, In: *EPMA (Ed.), Euro PM2019 Proceedings*, European Powder Metallurgy Association (EMPA), Shrewsbury, UK, 2019

- [119] Kukla, C.; Cano, S.; Kaylani, D.; Schuschnigg, S.; Holzer, C.; Gonzalez-Gutierrez, J.: Debinding behaviour of feedstock for material extrusion additive manufacturing of zirconia, *Powder Metallurgy* 62 (3), 2019, pp. 196–204
- [120] Kukla, C.; Cano, S.; Moritz, T.; Müller-Köhn, A.; Günther, A.; Hampel, S.; Holzer, C.: Production of Multimaterial Components by Material Extrusion -Fused Filament Fabrication (ME-FFF), In: EPMA (Ed.), Euro PM2018 Proceedings, European Powder Metallurgy Association (EMPA), Shrewsbury, United Kingdom, 2018, pp. 1–6
- [121] Kukla, C.; Duretek, I.; Gonzalez-Gutierrez, J.; Holzer, C.: Rheology of PIM feedstocks, *Metal Powder Report* 72 (1), 2017, pp. 39–44
- [122] Kukla, C.; Duretek, I.; Schuschnigg, S.; Gonzalez-Gutierrez, J.; Holzer, C.: Properties for PIM Feedstocks Used in Fused Filament Fabrication, In: EPMA (Ed.), World PM2016 Proceedings, European Powder Metallurgy Association (EMPA), 2016
- [123] Kukla, C.; Gonzalez-Gutierrez, J.; Burkhardt, C.; Weber, O.; Holzer, C.: The Production of Magnets by FFF - Fused Filament Fabrication, In: EPMA (Ed.), Euro PM2017 Proceedings, European Powder Metallurgy Association (EMPA), Bellstone, 2017, pp. 1–6
- [124] Kukla, C.; Gonzalez-Gutierrez, J.; Cano, S.; Hampel, S.; Burkhardt, C.; Moritz, T.; Holzer, C.: Fused Filament Fabrication (FFF) of PIM Feedstocks, In: Herranz G.; Ferrari B.; Cabrera J.M. (Ed.), *Actas del VI Congreso Nacional de Pulvimetalurgia y I Congreso Iberoamericano de Pulvimetalurgia*, Asociación ManchaArte, 2017, pp. 1–6
- [125] Kukla, C.; Gonzalez-Gutierrez, J.; Duretek, I.; Schuschnigg, S.; Holzer, C.: Effect of Particle Size on the Properties of Highly-Filled Polymers for Fused Filament Fabrication, In: Polymer Processing Society (Ed.), *Proceedings of 32nd Annual Meeting of the Polymer Processing Society*, 2016, pp. 274–277
- [126] Kurose, T.; Abe, Y.; Santos, M.V.A.; Kanaya, Y.; Ishigami, A.; Tanaka, S.; Ito, H.: Influence of the Layer Directions on the Properties of 316L Stainless Steel Parts Fabricated through Fused Deposition of Metals, *Materials* 13 (11), 2020
- [127] Langrana, N.A.; Qiu, D.; Bossett, E.; Danforth, S.C.; Jafari, M.A.; Safari, A.: Virtual simulation and video microscopy for fused deposition methods, *Materials & Design* 21 (2), 2000, pp. 75–82
- [128] Lee, S.H.; Jeung, W.Y.: Anisotropic injection molding of strontium ferrite powder using a PP/PEG binder system, *Journal of Magnetism and Magnetic Materials* 226-230, 2001, pp. 1400–1402
- [129] Lengauer, W.; Duretek, I.; Schwarz, V.; Kukla, C.; Kitzmantel, M.; Neubauer, E.; Lieberwirth, C.; Morrison, V.: Preparation and properties of extrusion-based 3D-printed hardmetal and cermet parts, pp. 1–8
- [130] Leu, M.C.; Liu, Q.; Bryant, F.D.: Study of Part Geometric Features and Support Materials in Rapid Freeze Prototyping, *CIRP Annals - Manufacturing Technology* 52 (1), 2003, pp. 185–188

- [131] Lewis, J.A.: Colloidal Processing of Ceramics, *Journal of the American Ceramic Society* 83 (10), 2000, pp. 2341–2359
- [132] Lim, T.K.: *Edible Medicinal and Non-Medicinal Plants*, Springer Netherlands, Dordrecht, 2012
- [133] Lin, H.-K.; Hwang, K.S.: In situ dimensional changes of powder injection-molded compacts during solvent debinding, *Acta Materialia* 46 (12), 1998, pp. 4303–4309
- [134] Lineberry, D.: *Electron Beam Freeform Fabrication* (Accessed on: 04.10.2016)
- [135] Liu, S.; Ye, F.; Liu, L.; Liu, Q.: Feasibility of preparing of silicon nitride ceramics components by aqueous tape casting in combination with laminated object manufacturing, *Materials & Design* (1980-2015) 66, 2015, pp. 331–335
- [136] Liu, W.; Cai, Q.-S.; Ma, Y.; Huang, Q.; Zhang, J.: Fabrication of 93W–Ni–Fe alloy large-diameter rods by powder extrusion molding, *International Journal of Refractory Metals and Hard Materials* 42, 2014, pp. 233–239
- [137] Liu, W.; Yang, X.F.; Xie, Z.P.; Jia, C.; Wang, L.: Novel fabrication of injection-moulded ceramic parts with large section via partially water-debinding method, *Journal of the European Ceramic Society* 32 (10), 2012, pp. 2187–2191
- [138] Lombardi, J.L.; Hoffman, R.A.; Waters, J.A.; Popvich, D.: Issues Associated with EFF & FDM Ceramic Filled Feedstock Formulation, In: *Laboratory for Freeform Fabrication; University of Texas at Austin* (Ed.), *Proceedings of the Solid Freeform Fabrication Symposium*, 1997, pp. 457–464
- [139] Lyons, B.: *Additive Manufacturing in Aerospace, Examples and Research Outlook*, *The Bridge* 42 (1), 2012, pp. 13–19
- [140] Mak, L.; Sneijders, H.: Making the business case: How sinter-based Additive Manufacturing can compete with Powder Injection Moulding, *Powder Injection Moulding International* 14 (2), 2020, pp. 77–84
- [141] Markforged Inc.: *Markforged Products*, <https://markforged.com/product-category/materials/> (Accessed on: 13.06.2020)
- [142] Maziero Volpato, C.A.; Altoe Garbelotto, L.G.D.; Celso, M.; Bondioli, F.: Application of Zirconia in Dentistry: Biological, Mechanical and Optical Considerations, In: *Sikalidis C. (Ed.): Advances in Ceramics - Electric and Magnetic Ceramics, Bioceramics, Ceramics and Environment*, InTech, 2011
- [143] McNulty, T.F.; Mohammadi, F.; Bandyopadhyay, A.; Shanefield, D.J.; Danforth, S.C.; Safari, A.: Development of a binder formulation for fused deposition of ceramics, *Rapid Prototyping Journal* 4 (4), 1998, pp. 144–150
- [144] McNulty, T.F.; Shanefield, D.J.; Danforth, S.C.; Safari, A.: Dispersion of Lead Zirconate Titanate for Fused Deposition of Ceramics, *Journal of the American Ceramic Society* 82 (7), 1999, pp. 1757–1760
- [145] Mcor webpage (Accessed on: 25.10.2016)

- [146] Melocchi, A.; Parietti, F.; Maroni, A.; Foppoli, A.; Gazzaniga, A.; Zema, L.: Hot-melt extruded filaments based on pharmaceutical grade polymers for 3D printing by fused deposition modeling, *International journal of pharmaceutics* 509 (1-2), 2016, pp. 255–263
- [147] Ming, C.L.; Garcia, D.A.: Development of Freeze-Form Extrusion Fabrication with use of sacrificial material, In: *Solid Freeform Fabrication Symposium*, 2013
- [148] Miranda, P.; Saiz, E.; Gryn, K.; Tomsia, A.P.: Sintering and robocasting of beta-tricalcium phosphate scaffolds for orthopaedic applications, *Acta biomaterialia* 2 (4), 2006, pp. 457–466
- [149] Moballegh, L.; Morshedean, J.; Esfandeh, M.: Copper injection molding using a thermoplastic binder based on paraffin wax, *Materials Letters* 59 (22), 2005, pp. 2832–2837
- [150] Moritz, T.; Maleksaeedi, S.: Additive manufacturing of ceramic components, In: Zhang J.; Jung Y.-G. (Ed.): *Additive manufacturing, Materials, processes, quantifications and applications*, Elsevier, Cambridge, Massachusetts, 2018, pp. 105–161
- [151] Moritz, T.; Müller-Köhn, A.; Abel, J.; Scheithauer, U.; Weingarten, S.: Ceramic Injection Moulding and Ceramic Additive Manufacturing side by side, *Opportunities and challenges, Powder Injection Moulding International* 12 (4), 2018, pp. 77–84
- [152] Munsch, M.; Schmidt-Lehr, M.; Wycisk, E.: *Metal Additive Manufacturing with sinter-based technologies*, AM Power Insights, Nr. 4, Hamburg, Germany, 2018
- [153] Mutsuddy, B.C.; Ford, R.G.: *Ceramic injection moulding*, Chapman & Hall, London, 1995
- [154] Nestle, N.; Hermant, M.-C.; Schmidt, K.: Mixture for use in a fused filament fabrication process, WO 2016/012486 A1, 2016
- [155] Ni, J.; Yu, M.; Han, K.: Debinding and Sintering of an Injection-Moulded Hypereutectic Al-Si Alloy, *Materials (Basel, Switzerland)* 11 (5), 2018
- [156] Nötzel, D.; Eickhoff, R.; Hanemann, T.: Fused Filament Fabrication of Small Ceramic Components, *Materials* 11 (8), 2018, pp. 1463
- [157] Nötzel, D.; Hanemann, T.: Filament development for the additive manufacturing of ceramic parts via Fused Deposition Modelling (FDM), In: DKG (Ed.), *92nd DKG Annual Meeting and Symposium on High Performance Ceramics*, 2017
- [158] Novichenko, D.; Marants, A.; Thivillon, L.; Bertrand, P.H.; Smurov, I.: Metal Matrix Composite Material by Direct Metal Deposition, *Physics Procedia* 12, 2011, pp. 296–302
- [159] Olakanmi, E.O.; Cochrane, R.F.; Dalgarno, K.W.: A review on selective laser sintering/melting (SLS/SLM) of aluminium alloy powders, *Processing, microstructure, and properties, Progress in Materials Science* 74, 2015, pp. 401–477
- [160] Oliveira, R.V.B.; Soldi, V.; Fredel, M.C.; Pires, A.T.N.: Ceramic injection moulding, Influence of specimen dimensions and temperature on solvent debinding kinetics, *Journal of Materials Processing Technology* 160 (2), 2005, pp. 213–220

- [161] Omar, M.A.; Davies, H.A.; Messer, P.F.; Ellis, B.: The influence of PMMA content on the properties of 316L stainless steel MIM compact, *Journal of Materials Processing Technology* 113 (1-3), 2001, pp. 477–481
- [162] Onagoruwa, S.; Bose, S.; Bandyopadhyay, A.: Fused Deposition of Ceramics (FDC) and Composites, In: Bourell D.L.; Berger C.; Crawford R.H.; Marcus H.L.; Wood K.L.; Barlow J.W. (Ed.), *Proceedings of the Solid Freeform Fabrication Symposium*, 2001
- [163] Orlovská, M.; Chlup, Z.; Bača, L.; Janek, M.; Kitzmantel, M.: Fracture and mechanical properties of lightweight alumina ceramics prepared by fused filament fabrication, *Journal of the European Ceramic Society*, 2020
- [164] Park, M.S.; Kim, J.K.; Ahn, S.; Sung, H.J.: Water-soluble binder of cellulose acetate butyrate/poly(ethylene glycol) blend for powder injection molding, *Journal of Materials Science* 36 (23), 2001, pp. 5531–5536
- [165] Pekin, S.; Bukowski, J.; Zangvil, A.: A Study on Weight Loss Rate Controlled Binder Removal From Parts Produced by FDC, In: *Laboratory for Freeform Fabrication; University of Texas at Austin (Ed.)*, *Proceedings of the Solid Freeform Fabrication Symposium*, 1998
- [166] Pekin, S.; Zangvil, A.; Ellingson, W.: Binder Formulation in EVA-wax system for Fused Deposition of Ceramics, In: *Laboratory for Freeform Fabrication; University of Texas at Austin (Ed.)*, *Proceedings of the Solid Freeform Fabrication Symposium*, 1998
- [167] Pelanconi, M.; Barbato, M.; Zavattoni, S.; Vignoles, G.L.; Ortona, A.: Thermal design, optimization and additive manufacturing of ceramic regular structures to maximize the radiative heat transfer, *Materials & Design* 163, 2019, pp. 107539
- [168] Petrovic, V.; Vicente Haro Gonzalez, J.; Jordá Ferrando, O.; Delgado Gordillo, J.; Ramón Blasco Puchades, J.; Portolés Griñan, L.: Additive layered manufacturing: Sectors of industrial application shown through case studies, *International Journal of Production Research* 49 (4), 2011, pp. 1061–1079
- [169] Petzoldt, F.: Standards for metal Additive Manufacturing: A global perspective, *Metal Additive Manufacturing* 2 (2), 2016, pp. 45–54
- [170] Pham, D.T.; Gault, R.S.: A comparison of rapid prototyping technologies, *International Journal of Machine Tools and Manufacture* 38 (10-11), 1998, pp. 1257–1287
- [171] Pilipović, A.; Raos, P.; Šercer, M.: Experimental testing of quality of polymer parts produced by Laminated Object Manufacturing - LOM, *Technical Gazette* 18 (2), 2011, pp. 253–260
- [172] Pistor, C.M.: Thermal Properties of Green Parts for Fused Deposition of Ceramics (FDC), *Advanced Engineering Materials* 3 (6), 2001, pp. 418–423
- [173] Pollard, D.; Herrmann, G.; Ward, C.; Etches, J.; Detand, J.; Ruxu, D.: A Comparison of FDM Structural Layouts and Implementation of an Open-Source Arm-Based System, *MATEC Web of Conferences* 167, 2018, pp. 3002

- [174] Qu, X.; Gao, J.; Qin, M.; Lei, C.: Application of a wax-based binder in PIM of WC–TiC–Co cemented carbides, *International Journal of Refractory Metals and Hard Materials* 23 (4-6), 2005, pp. 273–277
- [175] Rahaman, M.N.: Ceramic processing and sintering, *Materials engineering*, Vol. 23, 2. Ed., M. Dekker, New York, 2003
- [176] Rane, K.; Strano, M.: A comprehensive review of extrusion-based additive manufacturing processes for rapid production of metallic and ceramic parts, *Advances in Manufacturing* 5 (4), 2019, pp. 245
- [177] Rangarajan, S.; Pozsgai, I.; McIntosh, J.J.; McCuiston, R.C.; Harper, B.L.; Langrana, N.A.; Safari, A.; Danforth, S.C.; Clancy, R.B.; Gasdaska, C.J.; Whalen, P.J.: Homogeneity, Anisotropy, and Texture In Si<sub>3</sub>N<sub>4</sub> Ceramics made by Fused Deposition, *MRS Proceedings* 542, 1998
- [178] Rangarajan, S.; Qi, G.; Banyopadhyay, A.; Dai, C.; Han, J.H.; Bhargava, P.; Wu, S.; Safari, A.; Danforth, S.C.: The Role of Materials Processing Variables in the FDC Process, In: *Laboratory for Freeform Fabrication; University of Texas at Austin (Ed.), Proceedings of the Solid Freeform Fabrication Symposium*, 1997, pp. 431–440
- [179] Rangarajan, S.; Qi, G.; Venkataraman, N.; Safari, A.; Danforth, S.C.: Powder Processing, Rheology, and Mechanical Properties of Feedstock for Fused Deposition of Si<sub>3</sub>N<sub>4</sub> Ceramics, *Journal of the American Ceramic Society* 83 (7), 2000, pp. 1663–1669
- [180] Riecker, S.; Clouse, J.; Studnitzky, T.; Andersen, O.; Kieback, B.: Fused Deposition Modeling - Opportunities for cheap metal AM, In: *EPMA (Ed.), World PM2016 Proceedings*, European Powder Metallurgy Association (EMPA), 2016
- [181] Rivers, R.D.: Method of injection molding metal parts, US 4113480 A, 1978
- [182] Roberjot, S.; Auzene, D.; Iordache, L.; Popot, J.; Boulanger, T.; Beeckam, E.; Emmerechts, C.; Monnoye, D.; Baraldi, U.: Water solvent debinding for PIM parts, In: *World PM2010 Proceedings*, 10th - 14th October 2010, Fortezza da Basso, Florence, Italy, Shrewsbury, 2010
- [183] Robocasting webpage, <https://www.robocasting.net/> (Accessed on: 20.10.2016)
- [184] Royer, A.; Barrière, T.; Gelin, J.C.: The degradation of poly(ethylene glycol) in an Inconel 718 feedstock in the metal injection moulding process, *Powder Technology* 284, 2015, pp. 467–474
- [185] Schaaf, P. Van der; Inderbitzin, B.; Hermant, M.-C.; Schoemer, M.: Filaments based on a coated core material, US 2018/0202076 A1, 2016
- [186] Scheithauer, U.; Schwarzer, E.; Moritz, T.; Michaelis, A.: Additive Manufacturing of Ceramic Heat Exchanger: Opportunities and Limits of the Lithography-Based Ceramic Manufacturing (LCM), *Journal of Materials Engineering and Performance* 27 (1), 2018, pp. 14–20
- [187] Schlacher, J.; Lube, T.; Harrer, W.; Mitteramskogler, G.; Schwentenwein, M.; Danzer, R.; Bermejo, R.: Strength of additive manufactured alumina, *Journal of the European Ceramic Society*, 2020



- [188] Schlieper, G.: Tooling for metal injection molding (MIM), In: Heaney D.F. (Ed.): Handbook of metal injection molding, Woodhead Publishing in materials, Vol. 70, Woodhead Publishing, Cambridge UK, Philadelphia PA, 2012, 93-109e
- [189] Setasuwon, P.; Bunchavimonchet, A.; Danchaivijit, S.: The effects of binder components in wax/oil systems for metal injection molding, Journal of Materials Processing Technology 196 (1-3), 2008, pp. 94–100
- [190] Shivashankar, T.S.; German, R.M.: Effective Length Scale for Predicting Solvent-Debinding Times of Components Produced by Powder Injection Molding, Journal of the American Ceramic Society 82 (5), 1999, pp. 1146–1152
- [191] Sigmund, W.M.; Bell, N.S.; Bergström, L.: Novel Powder-Processing Methods for Advanced Ceramics, Journal of the American Ceramic Society 83 (7), 2000, pp. 1557–1574
- [192] Singh, P.; Shaikh, Q.; Balla, V.K.; Atre, S.V.; Kate, K.H.: Estimating Powder-Polymer Material Properties Used in Design for Metal Fused Filament Fabrication (DfMF3), JOM 11 (5), 2019, pp. 840
- [193] Singh, R.; Ranjan, N.: Experimental investigations for preparation of biocompatible feedstock filament of fused deposition modeling (FDM) using twin screw extrusion process, Journal of Thermoplastic Composite Materials 31 (11), 2018, pp. 1455–1469
- [194] SmarTech Analysis: Ceramics Additive Manufacturing Production Markets: 2019-2030, 2020
- [195] Sommer, F.; Walcher, H.; Kern, F.; Maetzig, M.; Gadow, R.: Influence of feedstock preparation on ceramic injection molding and microstructural features of zirconia toughened alumina, Journal of the European Ceramic Society 34 (3), 2014, pp. 745–751
- [196] Sotomayor Lozano, M.E.: Desarrollo de los procesos de moldeo por inyección y extrusión para la obtención de piezas de aceros inoxidables dúplex y ferríticos, Doctoral Thesis an der University Carlos III of Madrid, Leganés, 2010
- [197] Spectrum Filaments: Filament catalog, [https://spectrumfilaments.com/data/include/cms/Spectrum\\_Catalogue\\_2019.pdf](https://spectrumfilaments.com/data/include/cms/Spectrum_Catalogue_2019.pdf) (Accessed on: 13.06.2020)
- [198] Spoerk, M.; Arbeiter, F.; Cajner, H.; Sapkota, J.; Holzer, C.: Parametric optimization of intra- and inter-layer strengths in parts produced by extrusion-based additive manufacturing of poly(lactic acid), Journal of Applied Polymer Science 134 (41), 2017, pp. 45401
- [199] Spoerk, M.; Sapkota, J.; Weingrill, G.; Fischinger, T.; Arbeiter, F.; Holzer, C.: Shrinkage and Warpage Optimization of Expanded-Perlite-Filled Polypropylene Composites in Extrusion-Based Additive Manufacturing, Macromolecular Materials and Engineering 12, 2017, pp. 1700143
- [200] Stratasy's webpage, <http://www.stratasy.com/> (Accessed on: 20.10.2016)

- [201] Syed, W.U.H.; Pinkerton, A.J.; Li, L.: Combining wire and coaxial powder feeding in laser direct metal deposition for rapid prototyping, *Applied Surface Science* 252 (13), 2006, pp. 4803–4808
- [202] Tari, M.J.; Bals, A.; Park, J.; Lin, M.Y.; Thomas Hahn, H.: Rapid prototyping of composite parts using resin transfer molding and laminated object manufacturing, *Composites Part A: Applied Science and Manufacturing* 29 (5-6), 1998, pp. 651–661
- [203] Thavanayagam, G.; Pickering, K.L.; Swan, J.E.; Cao, P.: Analysis of rheological behaviour of titanium feedstocks formulated with a water-soluble binder system for powder injection moulding, *Powder Technology* 269, 2015, pp. 227–232
- [204] The Virtual Foundry Inc.: The Virtual Foundry Products, <https://www.thevirtualfoundry.com/> (Accessed on: 13.06.2020)
- [205] Thompson, Y.; Gonzalez-Gutierrez, J.; Kukla, C.; Felfer, P.: Fused filament fabrication, debinding and sintering as a low cost additive manufacturing method of 316L stainless steel, *Additive Manufacturing* 30, 2019, pp. 100861
- [206] Tourneroché, P.; Gelin, J.C.; Sahli, M.; Barrière, T.: Development and Thermo-physical Characterization of Polymers/Metallic Powder Mixtures for MIM Application, *Procedia Engineering* 81, 2014, pp. 2530–2536
- [207] Travitzky, N.; Bonet, A.; Dermeik, B.; Fey, T.; Filbert-Demut, I.; Schlier, L.; Schlordt, T.; Greil, P.: Additive Manufacturing of Ceramic-Based Materials, *Advanced Engineering Materials* 16 (6), 2014, pp. 729–754
- [208] Trunec, M.; Dobšák, P.; Cihlář, J.: Effect of powder treatment on injection moulded zirconia ceramics, *Journal of the European Ceramic Society* 20 (7), 2000, pp. 859–866
- [209] TU Wien: Two photon polymerisation (2PP), [http://amt.tuwien.ac.at/projects/two\\_photon\\_polymerization/](http://amt.tuwien.ac.at/projects/two_photon_polymerization/) (Accessed on: 25.10.2016)
- [210] Ukwueze, B.E.; Sulong, A.B.; Muhamad, N.; Sajuri, Z.: Solvent De-Binding of Bi-Material Green Component of Two-Component Powder Injection Moulded Stainless Steel and Zirconia, *International Journal of Mechanical & Mechatronics Engineering* 18 (3), 2018, pp. 96–104
- [211] Urtekin, L.; Uslan, I.; Tuc, B.: Investigation of Properties of Powder Injection-Molded Steatites, *Journal of Materials Engineering and Performance* 21 (3), 2012, pp. 358–365
- [212] Valkenaers, H.; Vogeler, F.; Ferraris, E.; Voet, A.; Kruth, J.P.: A Novel Approach to Additive Manufacturing: Screw Extrusion 3D-Printing, In: Azcarate S.; Dimov S. (Ed.): *Proceedings of the 10th International Conference on Multi-Material Micro Manufacture*, Research Publishing, San Sebastian, Spain, 2013, pp. 235–238
- [213] Venkataraman, N.; Rangarajan, S.; Matthewson, M.J.; Harper, B.L.; Safari, A.; Danforth, S.C.; Wu, G.; Langrana, N.A.; Gucer, S.I.; Yardimci, A.: Feedstock material property – process relationships in fused deposition of ceramics (FDC), *Rapid Prototyping Journal* 6 (4), 2000, pp. 244–253

- [214] von Karsa-Wilberforce, S.; Müller, C.; Kerber, A.; Jaeckel, M.; Grimmer, P.; Turzynski, F.: The production and evaluation of alumina sinter supports for Metal Injection Moulding by ceramic Additive Manufacturing, *Powder Injection Moulding International* 14 (2), 2020
- [215] Vurpillat, J.: 3D Demonstrators Designed for Bigger, Lighter Auto and Aerospace Parts, 2016, <http://blog.stratasys.com/2016/08/24/infinite-build-robotic-composite-3d-demonstrator/> (Accessed on: 07.10.2016)
- [216] Wahab, N.A.; Omar, M.A.; Sauti, R.; Nordin, N.A.; Ahmad, I.N.: Rapid Debinding of Injection Moulded M2 High Speed Steel Using Palm Stearin/Waste Rubber Binder, *Advanced Materials Research* 879, 2014, pp. 112–118
- [217] Weller, C.; Kleer, R.; Piller, F.T.: Economic implications of 3D printing: Market structure models in light of additive manufacturing revisited, *International Journal of Production Economics* 164, 2015, pp. 43–56
- [218] Wen, G.; Cao, P.; Gabbitas, B.; Zhang, D.; Edmonds, N.: Development and Design of Binder Systems for Titanium Metal Injection Molding, An Overview, *Metallurgical and Materials Transactions A* 44 (3), 2013, pp. 1530–1547
- [219] Wen, J.; Liu, W.; Xie, Z.P.; Lou, C.; Yang, X.F.: Effects of the binder compositions on the homogeneity of ceramic injection molded compacts, *Ceramics International* 44 (3), 2018, pp. 3218–3225
- [220] Westcot, E.J.; Binet Andrandall, C.; German, R.M.: In situ dimensional change, mass loss and mechanisms for solvent debinding of powder injection moulded components, *Powder Metallurgy* 46 (1), 2003, pp. 61–67
- [221] Wiech, R.E.: Manufacture of parts from particulate material, US 4197118 A, 1976
- [222] Wohlers, T.; Gornet, T.: History of Additive Manufacturing. Wohlers Report 2016, Wohlers Associates, 2016
- [223] Wongpanit, P.; Khanthasri, S.; Puengboonsri, S.; Manonukul, A.: Effects of acrylic acid-grafted HDPE in HDPE-based binder on properties after injection and debinding in metal injection molding, *Materials Chemistry and Physics* 147 (1-2), 2014, pp. 238–246
- [224] Wu, G.; Langrana, N.A.; Rangarajan, S.; Sadangi, R.; Safari, A.; Danforth, S.C.: Feasibility of Fabricating Metal Parts from 17-4PH Stainless Steel Powder, In: Laboratory for Freeform Fabrication; University of Texas at Austin (Ed.), *Proceedings of the Solid Freeform Fabrication Symposium*, 1998
- [225] Wu, G.; Langrana, N.A.; Sadanji, R.; Danforth, S.C.: Solid freeform fabrication of metal components using fused deposition of metals, *Materials & Design* 23 (1), 2002, pp. 97–105
- [226] Wu, S.; Rangarajan, S.; Dai, C.; McCuiston, R.; Langrana, N.A.; Safari, A.; Danforth, S.C.; Clancy, R.B.; Whalen, P.J.: Warm isostatic pressing (WIP'ing) of GS44 Si<sub>3</sub>N<sub>4</sub> FDC parts for defect removal, *Materials & Design* 24 (8), 2003, pp. 681–686

- [227] XERION BERLIN LABORATORIES GmbH: Fusion Factory Brochure, <https://www.xerion.de/fusionfactory/Fusion-Factory-Brochure.pdf> (Accessed on: 13.06.2020)
- [228] Yang, L.; Zhang, S.; Oliviera, G.; Stucker, B.: Development of a 3D Printing Method for Production of Dental Application, In: Solid Freeform Fabrication Symposium, 2012
- [229] Yang, W.-W.; Hon, M.-H.: In situ evaluation of dimensional variations during water extraction from alumina injection-moulded parts, *Journal of the European Ceramic Society* 20 (7), 2000, pp. 851–858
- [230] Yang, W.-W.; Yang, K.-Y.; Wang, M.-C.; Hon, M.-H.: Solvent debinding mechanism for alumina injection molded compacts with water-soluble binders, *Ceramics International* 29 (7), 2003, pp. 745–756
- [231] Yang, X.; Petcavich, R.J.: Powder and binder systems for use in metal and ceramic powder injection molding, US 6008281 A, 1999
- [232] Yang, X.F.; Xie, Z.P.; Liu, G.W.; Huang, Y.: Dynamics of water debinding in ceramic injection moulding, *Advances in Applied Ceramics* 108 (5), 2009, pp. 295–300
- [233] Yang, Y.; Zhang, C.; Wang, D.; Nie, L.; Wellmann, D.; Tian, Y.: Additive manufacturing of WC-Co hardmetals: a review, *The International Journal of Advanced Manufacturing Technology* 64 (11), 2020, pp. 219
- [234] Ye, Y.; Qiao, L.; Zheng, J.; Ying, Y.; Li, W.; Yu, J.; Che, S.; Jiang, L.: Effect of microcrystalline wax on the solvent debinding of the Sr-ferrite ceramics prepared by powder injection molding, *Journal of the European Ceramic Society* 37 (5), 2017, pp. 2105–2114
- [235] Yoo, J.; Cima, M.J.; Khanuja, S.; Sachs, E.M.: Structural Ceramic Components by 3D Printing, In: Solid Freeform Fabrication Symposium, 1993
- [236] Zaky, M.T.: Effect of solvent debinding variables on the shape maintenance of green molded bodies, *JOURNAL OF MATERIALS SCIENCE* 39 (10), 2004, pp. 3397–3402
- [237] Zaky, M.T.; Soliman, F.S.; Farag, A.S.: Influence of paraffin wax characteristics on the formulation of wax-based binders and their debinding from green molded parts using two comparative techniques, *Journal of Materials Processing Technology* 209 (18-19), 2009, pp. 5981–5989
- [238] Zanardini, M.; Bacchetti, A.; Zanoni, S.; Ashourpour, M.: Additive Manufacturing Applications in the Domain of Product Service System, An Empirical Overview, *Procedia CIRP* 47, 2016, pp. 543–548
- [239] Zhang, Y.; Bai, S.; Riede, M.; Garratt, E.; Roch, A.: A comprehensive study on Fused Filament Fabrication of Ti-6Al-4V structures, *Additive Manufacturing*, 2020, pp. 101256
- [240] Zhao, M.; Qiao, L.; Zheng, J.; Ying, Y.; Yu, J.; Li, W.; Che, S.: Investigation of the solvent debinding in the injection molding of ZrO<sub>2</sub> ceramics using LDEP, HDPE and wax binders, *Ceramics International* 45 (3), 2019, pp. 3894–3901

- [241] Zocca, A.; Colombo, P.; Gomes, C.M.; Günster, J.; Green, D.J.: Additive Manufacturing of Ceramics, Issues, Potentialities, and Opportunities, *Journal of the American Ceramic Society* 98 (7), 2015, pp. 1983–2001
- [242] Zu, Y.S.; Lin, S.T.: Optimizing the mechanical properties of injection molded W-4.9%Ni-2.1%Fe in debinding, *Journal of Materials Processing Technology* 71 (2), 1997, pp. 337–342